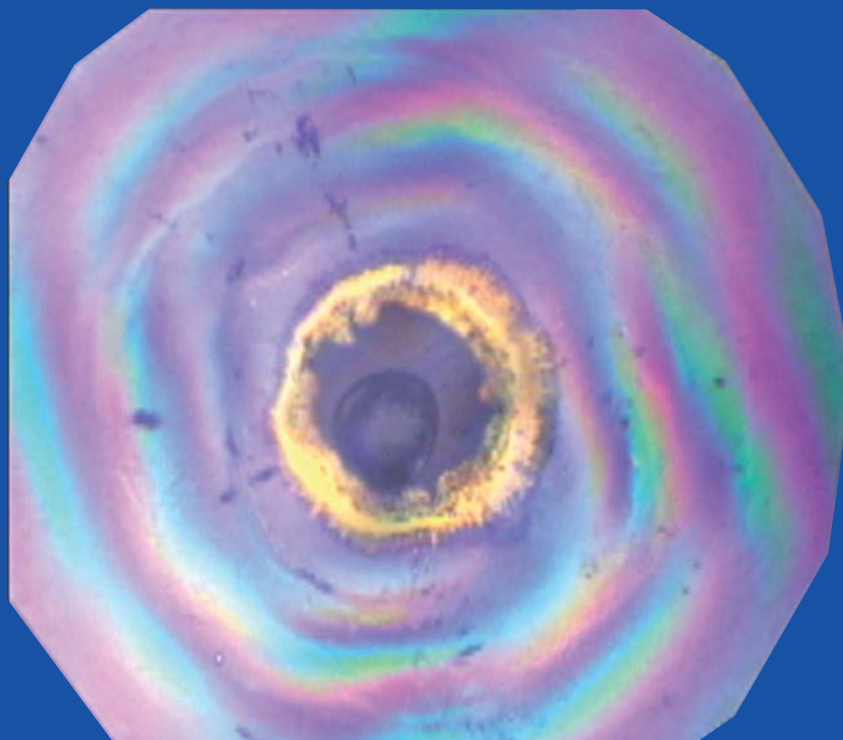
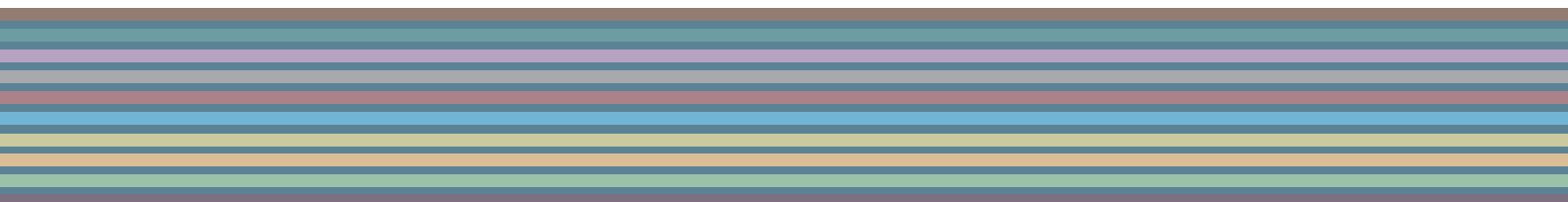


# SCIENTIFIC REPORT 2005-2006



## LABORATOIRE LÉON BRILLOUIN





## DIRECTOR'S INTRODUCTION

STRUCTURES AND PHASE TRANSITIONS

7

SUPERCONDUCTIVITY AND MAGNETISM

31

MATERIALS SCIENCES & APPLICATIONS

59

SOFT MATTER

83

LIFE SCIENCE

111

INSTRUMENTATION

131

THEORY

151

**EXPERIMENTAL PROGRAMME AND USER ACTIVITIES**

**159**

**PRESENTATION OF LLB**

**171**

**PUBLICATIONS**

**179**

# Director's Introduction

The “Laboratoire Léon Brillouin“ is a Mixed Research Unit (UMR12) shared and funded jointly by the “Commissariat à l’Energie Atomique” (CEA) and the “Centre National de la Recherche Scientifique” (CNRS) . It uses the neutrons produced by the Research Reactor ORPHEE.

The recent confirmation of the LLB as the national French neutron source occurs in a changing European landscape. Several small facilities are closing whereas medium and world-class ones have either been recently commissioned (FRMII, SINQ) or are benefiting from major upgrades (ILL, HMI, ISIS). The near future will see the opening of several new megawatt spallation sources: SNS in the United States, JPARC in Japan and probably later ESS in Europe.

Neutron scattering is undoubtedly in a phase of expansion, and the demand for measurement time is increasing. In a complex world which is facing critical challenges in health, environment, energy, transport, communication and food, neutron scattering is a unique tool which can answer many questions in condensed matter science that no other technique can address.

Because efficient use of this technique requires a significant commitment of resources and time, a tiered structure of the neutron facilities and the scientific community is necessary. In addition, there is no way to perform neutron scattering in a standard laboratory as neutrons are only available at medium- and large-scale facilities. The European network is well organized with the ILL as the European Source and national sources located in the main countries. NMI3\* is a very efficient structure, and the Heads of the European facilities meet regularly to share information. LLB is one of its cornerstones. It serves as a base for the French neutron community and provides access to many European users who are supported by the European Access program. It also fosters the education of PhD students and supports instrument and method development.

LLB is a laboratory in which teams have the mission to carry out their own research programs. For this reason each team member is involved in the national and international scientific community in order to enrich the community with results obtained from neutron techniques, attract new users and provide a link between the laboratories and the professionals who use neutron methods. The work described in this report is that performed and/or initiated by the researchers of LLB and that of close users. The results of experiments led by the other external users, often with the help and the expertise of LLB scientists, are beyond the scope of this report. These efforts are evidenced by the many publications in which the contribution of the LLB is acknowledged. The statistics for these external studies may be found in the last section of this report.

In order to provide users with special expertise that spans the broad spectrum of topics accessible using neutron methods, the research groups are rather small and tackle very different problems. The report is presented in seven sections: Structure and Phase Transitions, Superconductivity and Magnetism, Materials Science and Applications, Soft Matter, Life Science, Instrumentation and Theory. Each section is introduced by an overview of the work accomplished and a discussion of future prospects. The details of the experiments are described in subsequent highlights (referred to as  $Hn$ ) or short clips (referred to as  $Cn$ ).

## SUPERCONDUCTIVITY AND MAGNETISM

The LLB team is recognized as a leader in the physics of strongly-correlated electron systems whose properties include unconventional superconductivity as well as the unusual magnetic behaviour of manganites and ruthenates. Significant progress has recently been achieved with the detection of magnetic moments, probably due to orbital current, in the pseudo-gap region of YBaCuO. Beyond the particulars of each system, the aim of this research is to elucidate more general parameters that govern their behaviour: inhomogeneities, quantum critical points, orbital degrees of freedom, etc. The other research topics of the group are frustrated magnetism, surface magnetism and photomagnetism.

## STRUCTURE AND PHASE TRANSITIONS

Smart materials are solving engineering problems and providing opportunities for new innovative products. Since their properties are linked to structural details, it is essential to carefully determine their structure and control their phase transitions. This drive has stimulated strong activity by the LLB team, which takes advantage of the unique properties of the neutron to see light atoms and resolve magnetic structures. The activity is further enriched by strong interactions with the French community of chemistry of solids. The main research on phase transitions concerns confined mediums, pressure effects, effects of magnetic frustration, and transitions in electrolytic medium. The structure studies are focused on new materials such as nanotubes, hydrides, manganites and biomaterials and on materials under combined, extreme conditions of pressure and/or field and/or temperature.

The tools developed at the LLB (improved diffractometers, world-class sample environments and new methods for structure analysis) and the emergence of new functional and multifunctional materials foretells a bright future for this research activity.

## MATERIALS SCIENCE AND APPLICATIONS

While a much of neutron activity is still devoted to the study of model systems, there is a simultaneous move towards the resolution of technological problems. Extensive research focused on energy problems, information technology and structural materials has been developed at the LLB during the last two years. The diversity of the research on key elements of energy systems is quite impressive and it includes the dynamics of water in Nafion membranes, structure and dynamics in solid oxide fuel cells, relaxation processes in polymer electrolytes for Li-batteries, porous alumina membranes, water-oil macroemulsions for heavy oil extraction, advanced materials for the nuclear industry.

The scientific activity in the field of metallurgy is focused on the development of new alloys and on the microstructural evolution of materials submitted to external loadings. These fields involve much industrial collaboration, and efforts are underway to improve the diffractometers devoted to texture and strains.

The study of the magnetism of surfaces and of thin layers is a key part of the research program at LLB and is driven by the spintronics and recording media technology.

\* NMI3 : Integrated Infrastructure Initiative for Neutron Scattering and Muon Spectroscopy of the European Union 6<sup>th</sup> Framework Programme.

## SOFT MATTER

LLB has a long history in soft matter. Some of the currently accepted models of polymers were confirmed at LLB, in large part because the interaction between the internal team and the external user community is strong and very professional. This example typifies the proliferation within the national community of a strong research activity that was established at the LLB. The group has many ongoing activities including determination of the structure and behaviour of new polymers, study of systems under constraints (mechanic, magnetic etc...), investigation of the effects of confinement, and study of complex ternary mixed systems. This research takes advantage of small angle scattering, reflectivity and quasi-elastic neutron scattering techniques as well as of contrast matching from selective deuteration, which allows one to independently highlight different parts of a complex system.

The research in the area of soft matter is very rich and encompasses a diverse set of systems. It is driven by the underlying applications that include mechanic reinforcement, pharmacology, food, oil, transportation etc.

## LIFE SCIENCE

Water is the major constituent of living matter, and it obviously plays a key role in the dynamics of proteins. In this research area, the vast, specialized experience of the LLB team is fully exploited. The research at LLB is directed towards the shape and dynamics of the proteins and their correlation with biological functions. Special attention is focused on the folding and unfolding mechanism of the proteins, on the translocation process and on the dynamics of photo-excited proteins.

In life science, probably more than in any other systems, the objects (such as proteins in the cells) interact, form and move in crowded environments. Measurements of samples in similar environments have been initiated, and it is a new step forward for the biology community and food industry which are confronted by such complex situations. Also here, small angle neutron scattering and quasi-elastic scattering are well-adapted tools for such studies. The implementation of the deuteration laboratory on the ILL-ESRF site should give a new boost to life science research at LLB as well.

## THEORY

A small group of theoreticians support the experimental activities, especially in the areas of superconductivity and biology.

For superconductivity, they have provided theoretical support for the asymmetry between the hole-doped and electron-doped cuprates, and performed calculations on the mechanism responsible for superconductivity based on spectra obtained with neutron scattering. They recently reproduced quantitatively the parameters of superconductivity.

In biology the activity is focused on the calculation of Brownian and fractional Brownian dynamics of proteins in relation to quasi-elastic neutron scattering.

## INSTRUMENTATION

In the changing landscape of neutron scattering, the LLB faces a serious challenge of instrumentation maintenance and upgrades in order to maintain the high standards of a national source. The current effort is insufficient for the LLB to retain its current status as a medium source competitive with "sister facilities" such as FRMII in Munich or NIST in the United States. The ongoing CAP 2010 program must only be viewed as a first step to provide momentum for a more complete renewal of the instrumentation. It is now urgent to adopt an ambitious policy for instrumentation improvements and upgrades which involves increased funding as well as increased manpower devoted to this mission. It is only under these conditions that the best scientists will be attracted to the LLB, the brightest students will choose our laboratory to prepare their PhD, the users will continue to submit proposals to LLB, and the French community will be strong enough to put effort into the emerging new facilities. The Board of Directors wishes to make this message very clear.

## OTHER ACTIVITIES OF ORPHEE

The commercial activities of neutron radiography and silicon doping are run by DEN (Direction of Nuclear Energy of CEA), and activation analysis is performed by LPS (Pierre Sue Laboratory). While these are important activities of ORPHEE, they are beyond the scope of this report which is devoted to LLB.

With its triple mission of (1) offering neutron instrumentation, technical support and expertise to the users, (2) teaching the neutron technique to young scientists and new users, (3) carrying out its own research, the LLB is at the heart of many research efforts and is active in the specific research communities working on subjects developed in the laboratory.

Each year, LLB organises a tutorial "les FAN du LLB" based on practical training and hosts the students of The European HERCULES training program. LLB also participates in and contributes to the thematic school of the "French Neutron Society" (SFN), and LLB team members teach in doctoral schools in several French universities via the "itinerant chair" of the SFN.

In 2006 LLB hosted two thematic (GDR) meetings. It is involved in national and international research networks as the RTRA "triangle de la physique" (Triangle of Physics) on the ("plateau de Saclay"); C-Nano or the European Network of Excellence: Functionalized Advance Materials and Engineering Hybrids and Ceramics (FAME).

With the synchrotron SOLEIL at walking distance from LLB, new horizons are opening. Saint Aubin LLB/SOLEIL meetings (the next one scheduled in March 2007) and their joint organization of the tenth International Conference on Surface X-ray and Neutron Scattering (SXNS10) in 2008 are the witness to a fruitful scientific collaboration. We also expect to share technical support and some infrastructure.

The immersion of LLB in scientific communities, the professionalism of its members, and the number and quality of the users are ingredients for a strong neutron community that utilizes the best current and emerging neutron sources to tackle scientific problems which will address the challenges of the 21<sup>st</sup> century.









# STRUCTURE AND PHASE TRANSITIONS

# STRUCTURE AND PHASE TRANSITIONS

## Introduction

The field of structure and phase transitions grows and evolves. The possibility to synthesize new materials, or to study model systems in a peculiar state, like in confined media or under extreme conditions of pressure, temperature or magnetic field, opens a wide variety of interesting phenomena. It also stimulates new concepts and theoretical approaches.

Neutron is a privileged probe to investigate condensed matter at a microscopic level, thanks to its unique characteristics. Among others, one can mention the simultaneous study of magnetic and crystalline orders, the possibility to play with isotopic contrast (H-D substitution for instance), to vary easily the physical parameters, the non destructive study of “precious compounds”. As a general trend, neutrons are combined with other probes, not only for standard characterization, but in fully common analysis, allowing one to better understand the complex states of matter, their stability and the connection with their physical properties. Synchrotron X ray diffraction is the most prominent example, and common fields of research are expected to grow with the collaboration LLB-Soleil. Local probes are also involved (like EPR,  $\alpha$ SR), as well as a large variety of macroscopic probes. We briefly review in the next sections the trends in phase transitions and structure studies which appeared in LLB for the last two years, and introduce some highlights and clips which illustrate them. At the end, we present some emergent fields, which might grow in the next years.

## Recent trends in phase transitions

Many studies are devoted to states of matters in which phase transitions have to be described with new concepts, well beyond the classical approaches like Landau's mean field theory. We will successively present four points:

- Materials confined in a restricted geometry, where confinement could either suppress or strongly modify the transitions observed in the bulk material.
- By changing interatomic distances, pressure allows one to tune the energy balance and the physical properties. It induces new phases, changes transition temperatures, or induces  $T=0$  transitions. Applied pressure is often compared with chemical substitution, considered as “chemical pressure”. Experiments under pressure are a strong point in LLB, as shown by several examples.
- Geometrical frustration provides nice examples of materials with ground state entropy, like spin liquids or spin ices, without transition down to  $T=0$ . In such materials, perturbations may induce new transitions, yielding a large variety of magnetic states often sensitive to applied pressure or magnetic field.
- An original study of an electrochemical oxidation allows one to tune oxygen composition and finely investigate the phase diagram.

### PHASE TRANSITIONS IN CONFINED MEDIA

---

The synthesis of materials in mesoporous matrices, like the MCM-matrix with regular system of monodisperse nano-channels and their potential application stimulated works by several groups. A full understanding of the systems requires the knowledge of their atomic and mesoscopic structures together with their dynamics. Therefore studies were done by combining neutron diffraction, small angle neutron scattering, X ray synchrotron diffraction and inelastic neutron scattering.

In a **smectic crystal** confined in one dimensional nanopores of porous silicon films, the smectic transition is completely suppressed, and short range order settles in, while the molecular dynamics slows down. This spectacular effect is attributed to random fields coupling with the smectic order parameter. This is developed in the thesis work of R. Guégan. [*H1*, R. Guégan].

In magnetic and dielectric materials, confinement can lead to a suppression of the phase transitions, a change in the critical exponents, or even to a new reentrant transition. These effects were studied in detail in model antiferromagnets or ferrimagnets such **MnO**, CoO,  $\text{Fe}_2\text{O}_3$ ,  $\text{Fe}_3\text{O}_4$ , confined in different media (porous glass, nanochannels, twinned channels). These studies were performed through an INTAS project coordinated by the LLB (2003-2006) in which seven West and East European laboratories were involved, which led to more than ten publications [*H2*, I. Golosovsky].

The influence of confinement on the crystallization and vitreous transitions was studied in **liquid Toluene** confined in nanoporous matrix. The studies allowed an Orsay team<sup>1</sup> to follow the structure and dynamics of the confined fluid, as well as its density, which can be controlled by applied pressure. It will be developed in the thesis work of F. Audonnet.

## STRUCTURE AND PHASE TRANSITIONS

### PRESSURE INDUCED TRANSITIONS

A very nice example of a pressure induced transition in a confined medium is provided by the **Urea-alkane** crystals under pressure. Urea inclusion compounds form solid 1D channels via host urea hydrogen bonds, which can accommodate guest alkane molecules. Pressure induces in the guest system a transition from incommensurate to commensurate structure, opening the possibility of tuning 1D structure of confined materials and therefore to manipulate their tribological properties at a molecular level [C1, B. Toudic].

The manganites  $\text{LaCaMnO}_3$  with colossal magnetoresistance show a strong coupling between electric and magnetic properties. In these compounds the insulating metal transition temperature  $T_{\text{IM}}$  is sensitive to pressure. The study of the magnetic order in  $\text{La}_{0.75}\text{Ca}_{0.25}\text{MnO}_3$  under pressure performed at LLB by an Italian team of Rome, showed that the Curie temperature  $T_{\text{C}}$  and the insulating-metal temperature  $T_{\text{IM}}$  scale with pressure, yielding a unique transition line from a paramagnetic insulator to a ferromagnetic metal up to 8 GPa [C2, M. Baldini].

The geometrically frustrated  $\text{R}_2\text{Mo}_2\text{O}_7$  pyrochlores undergo a threshold transition from an insulating spin glass to a ferromagnetic metal depending on the rare earth ionic radius. The study of the new system  $(\text{Tb}_{1-x}\text{La}_x)_2\text{Mo}_2\text{O}_7$  where the lattice constant is suitably adjusted, allows one to cross the threshold in both ways, by tuning interatomic distances. So, starting from the spin glass  $\text{Tb}_2\text{Mo}_2\text{O}_7$ , with only short range magnetic order, the dilution by non magnetic La ion expands the lattice and induces long range magnetic order, which can be destroyed by pressure. By combining neutron techniques, muons and X ray synchrotron at ambient pressure and under pressure, one can follow the evolution of magnetic order and spin fluctuations in the crossover region. It is a part of the thesis work of A. Apetrei [H3, A. Apetrei].

### GEOMETRICAL MAGNETIC FRUSTRATION

In some frustrated ferromagnets situated just above a magnetic threshold, the huge sensitivity of itinerant d electrons to pressure combined with the geometrical frustration allows one to tune the magnetic state with pressure and induces order-disorder transitions. Long term studies of  $\text{GdMn}_2$  with a threshold from localized to itinerant magnetism<sup>2</sup>, and  $\text{Gd}_2\text{Mo}_2\text{O}_7$  with a threshold from ferromagnetic metal to insulating spin glass<sup>3</sup>, were performed in LLB. They involved extended collaborations with ESRE, ILL and PSI muon source. They revealed non trivial pressure effect in itinerant magnets, which could either suppress the frustration ( $\text{GdMn}_2$ ) or induce it ( $\text{Gd}_2\text{Mo}_2\text{O}_7$ ).

Geometrically frustrated systems can stabilize exotic magnetic states such as spin liquids, spin ices or chemically ordered spin glasses. In  $\text{Tb}_2\text{Sn}_2\text{O}_7$ , where Tb ions occupy a pyrochlore lattice of corner sharing tetrahedra, a two steps transition towards a new type of order was observed. This magnetic structure was called “**ordered spin ice**” since it possesses a local spin ice order inside a tetrahedron and a long range ferromagnetic order. (C3, I. Mirebeau).

Other unusual phase transitions are observed in frustrated **Laves hydrides** due to the coupling of the magnetic and the hydrogen lattices. Hexagonal hydrides  $\text{RMn}_2\text{H}_x$  (R=rare earth), including new compounds obtained at high pressures, show intricate magneto-structural transitions. In some cases, a transition to a chemically *less* ordered state yields a *more* ordered magnetic sublattice, showing a rare example of an “order by disorder” transition. In such systems, hydrogen insertion can be used as a gentle way to tune the magnetic properties<sup>4</sup>.

Geometrical frustration is also involved in  $\text{Sr}_3\text{HoCrO}_6$  where the spin chains are triangularly arranged. The ground state shows partial disorder as expected for 1D frustrated compounds, and an applied field induces puzzling steps in the magnetization [C4, V. Hardy]. Such steps recall the magnetization plateaus observed in other systems with ground state degeneracy, like spin ices, quantum dimer systems, or molecular magnets with quantum tunnelling.

### IN SITU SUCCESSION OF PHASE TRANSITIONS IN AN ELECTROCHEMICAL MEDIUM

Electrochemical oxidation of antiferromagnetic  $\text{SrCO}_{2.5}$  was studied in situ, combining neutron diffraction and X-ray absorption spectroscopy at the Co absorption edge. It allowed to characterize two intermediate phases and to follow the evolution of the Co valence state during the reaction [C5, R. Le Toquin]. This thesis work received the prize of the Société Française de Neutronique (SFN 2005 prize).

## Recent trends in structures

Many efforts are currently devoted to the synthesis of new materials, requiring high accuracy in the structure determination in order to improve their physical properties. On the other hand emerging studies of biomaterials (like kidney stones) or archeomaterials (like Etruscan weapons) find in neutron scattering a unique technique to answer some specific questions. More and more, the analysis yielded the development of sophisticated structural models to account for the experimental data. Finally, several studies were performed under extreme pressure conditions, confirming the LLB leader role in this field. One can mention the determination of the phase diagrams of  $H_2$  and  $O_2$ , the study of FeO and MnO antiferromagnets, and of compounds of geological interest.

### NEW MATERIALS

---

**Laves hydrides** have been synthesized by two groups under high pressure conditions, leading to new compounds stable at ambient pressure. Magnetic and hydrogen orders were studied by neutron diffraction.  $RMn_2D_6$  ( $R=Y, Ho, Dy, Er$ ) compounds show only short range or partial magnetic orders, attributed to the chemical Mn or R disorder. [C6, V. Paul-Boncour]. The  $TbMn_2D_{2.9}$  compound at the verge of a transition from itinerant to localized magnetism, was studied in both hexagonal and cubic crystal structures, leading to different types of magnetic order. This study showed that the Mn-Mn distance is not the only parameter which governs the itinerant-localized transition, but that the lattice topology plays an important role [C7, O. Makarova].

The study of ternary compounds with alkali, tetrahydrofuran and carbon **nanotubes** revealed the very interesting possibility of *tuning the intertube spacing* through the alkali cations, which form a single layer surrounding the nanotubes. This study is a part of the thesis work of J. Cambedouzou [C8, J. Cambedouzou].

The magnetic structure of the **manganese sulfides** or chlorosulfides compounds with 1D or 2D crystalline structuration was solved, showing 3 dimensional magnetic order but with an incommensurate modulation coexisting in some cases with 1D magnetic correlations. This study belongs to the thesis work of C. Doussier-Brochard [C9, C. Doussier-Brochard].

In a series of new hydrothermally synthesized  $M^{II}$ -hydroxysulfates, the possibility to choose the 3d element from Mn to Cu allows one to change progressively the magnetic interactions and the geometrical frustration caused by  $\alpha$ -3-OH bridges, resulting in various canted antiferromagnetic structures [C10, S. Vilminot].

In the **manganite** field, M. Giot (LLB-CRISMAT thesis), studied in detail the complex charged ordered  $Bi_xCa_{1-x}MnO_3$  ( $0.5 < x < 0.64$ ) series, confirming nicely the Zener polaron ordering model. She determined a classical CE-type magnetic structure for  $x = 0.5$ , evolving towards a ferromagnetic coupling for higher  $x$  [C11, M. Giot].

In **life science** a collaboration with D. Bazin (LPS, Orsay) and M. Daudon (Necker Hospital, Paris) has started focusing on the specific structural information available from powder neutron diffraction on biological materials like kidney stones. Such biomaterials can differ from each other in composition, structure and microstructure, revealing a large variety of specific diseases. Thanks to the high penetration depth of the neutron beam, it is possible to study, in a non-destructive way, the whole sample (of a few mm typical size) obtaining a quantitative phase analysis of the kidney stone together with the average crystallites size. This information is complementary with the results obtained by other techniques (synchrotron radiation,  $\alpha$ -X-ray fluorescence, X-ray absorption spectroscopy). These data are compared with the macroscopic morphologies of the calculi and their medical classification and pathologies [C12, D. Bazin].

### NEW TOOLS FOR STRUCTURE ANALYSIS

---

The structural models developed to simulate the structure factors of the nanotube bundles, have inspired simulations in the nanoporous channels. The precise description of the bundle geometry allowed one to ascertain the position of the alkali metal with respect to the nanotubes, as well as the ribbon/wire shape of the MnO confined in the nanochannels. [C8, J. Cambedouzou and H2, I. Golosovsky].

The interplay between crystal structure and rotational dynamics of methyl groups which has been nicely established in the 4-methylpyridine-N-oxide molecule. Rotational dynamics cannot be described by the quantum sine-Gordon model in 1D. The obtained structure shows the existence of eight distinct molecular sites suggesting that the four tunnelling transitions observed with inelastic neutron scattering could correspond to different effective potentials for the methyl rotors. [C13, F. Damay].

## STRUCTURE AND PHASE TRANSITIONS

## MODEL MATERIALS UNDER EXTREME CONDITIONS

A structural transition was observed under pressure in solid D<sub>2</sub>, and the structure of the pressure induced quantum phase was solved by combining X ray synchrotron and neutron diffraction on a single crystal. The study, which involved the development of a hybride pressure cell, was performed at the extreme conditions of 38 GPa and 1.5K. An orientational order of the D<sub>2</sub> molecules showing topological frustration was suggested. The result of this study was published in Nature (2005) (*H4, I. Goncharenko*).

FeO and MnO antiferromagnets were studied under high pressure. The neutron study was combined with synchrotron X ray diffraction, ultrasonic interferometry (elastic constants), Mössbauer effect (Fe hyperfine field). It allowed one to determine the pressure dependence of the magnetic and structural transitions. The two transitions do not occur systematically at the same temperature and could be decoupled under pressure [*CI4, L. Dubrovinsky*].

## Perspectives

Studies of elementary molecular crystals such as H<sub>2</sub> and O<sub>2</sub> under pressure have shown spectacular effects in the last years and will be continued. In particular, quantum effects on orientational ordering in hydrogen isotopes will be studied. Another objective is to search for weak magnetism in O<sub>8</sub> clusters in the epsilon phase of solid O<sub>2</sub> at pressures above 10 GPa. The recently developed technique combining neutron and synchrotron studies on the same sample brings new possibilities to study crystal and magnetic structures under pressure. Among others things, it opens a route to the exact determination of crystal structures of light hydrides under pressure.

Geometrically frustrated systems keep being a hot topic of solid state physics, attracting an increasing number of scientists, as shown by the recent creation of a European GDR, and the onset of devoted conferences. By yielding complex magnetic structures, geometrical frustration is a tool allowing one to tune specific properties, like the giant abnormal Hall effect in R<sub>2</sub>Mo<sub>2</sub>O<sub>7</sub> pyrochlores, the magneto-striction in spinels, or the coupling between piezoelectric, ferroelectric and magnetic properties in multiferroic materials. Neutron scattering has a prominent role to play here.

The confinement of materials is an open door to many new behaviours, and studies of materials in confined media (including nanotubes) will certainly develop. These studies are performed through close collaborations of LLB scientists with external groups. Several theses are being starting (at Orsay, Rennes, Montpellier) which will include experiments in LLB.

The synthesis of functional materials with dedicated properties related to energy constitutes a challenge for humanity. The contribution of neutrons should be essential. Among them, let us cite the synthesis and study of new hydrides developed by external groups (Kurchatov, Thiais) in collaboration with LLB. They offer a potential interest for hydrogen storage. On thermoelectricity and magnetic refrigeration, S. Tencé is starting thesis work (LLB/ICMCB-Bordeaux).

Materials combining several functional properties are very attractive, like for example manganites and multiferroics. Their study should develop as well as the investigation of ionic and protonic conductors (collaboration LLB/CIRIMAT-Toulouse).

The high penetration of neutron beam and its non-destructive ability to explore massive or precious samples should trigger specific studies on biological materials and archeological pieces (teams of Florence-Milan).

Experimental geosciences and mineral physics now focus on in-situ investigations under high pressures and high temperatures rather than on quenched samples to model real processes inside earth or other planets. Here again, the combination of neutron and synchrotron studies should be very useful. In LLB high pressure studies of geological samples are already developed in collaboration with a geophysical laboratory in Bayreuth.

<sup>1</sup>C. Alba-Simionesco, N. Brody, F. Audonnet. Laboratoire de Chimie Physique, Univ. Paris Sud Orsay.

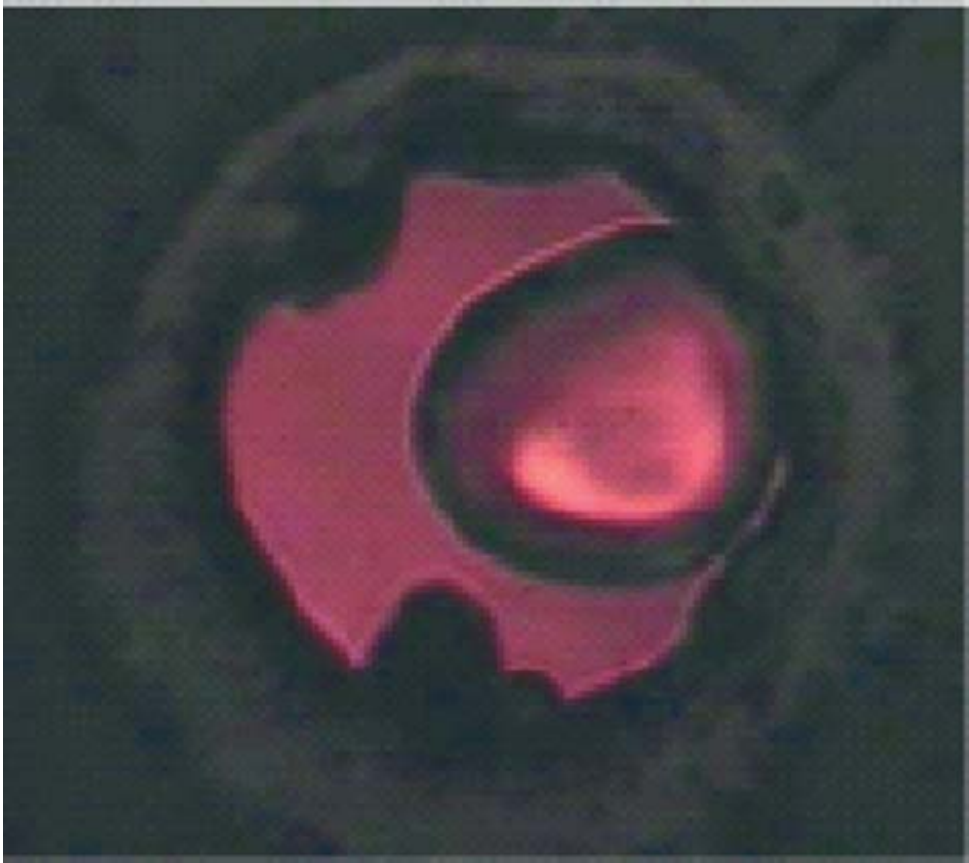
<sup>2</sup>Pressure induced magnetic transitions in the frustrated laves compound GdMn<sub>2</sub>, I. Goncharenko et al. Phys. Rev. B 72, 014420 (2005).

<sup>3</sup>Ferromagnetic spin glass transition induced by pressure in Gd<sub>2</sub>Mo<sub>2</sub>O<sub>7</sub>, I. Mirebeau et al. condmat 06006420, to appear in Phys. Rev. B (2006).

<sup>4</sup>Oscillating dependence between magnetic and chemical ordering in the frustrated Laves hydrides RMn<sub>2</sub>D<sub>2</sub>, O. Makarova et al Phys. Rev B 67, 134418, (2003); article in preparation.



# STRUCTURE AND PHASE TRANSITIONS



- H1. Anisotropic quenched disorder effects on a liquid crystal confined into nanochannels**  
R. Guégan, R. Lefort, M. Guendouz, I. Mirebeau, D. Morineau
- H2. Diffraction studies of MnO confined in nanochannels of mesoporous matrices**  
I.V. Golosovsky, I. Mirebeau, G. André, D. A. Kurdyukov, Yu. A. Kumzerov, V. P. Sakhnenko
- H3. Pressure induced ferromagnetic spin glass transition in the geometrically frustrated pyrochlore  $(\text{Tb}_{1-x}\text{La}_x)_2\text{Mo}_2\text{O}_7$**   
A. Apetrei, I. Mirebeau, I. Goncharenko, D. Andreica, P. Bonville, W. A. Crichton, A. Forget, D. Colson
- H4. Neutron diffraction study of the broken symmetry phase in solid deuterium at the pressure of 38 GPa**  
I.N. Goncharenko, P. Loubeyre
- [C1. **B. Toudic**] First evidence of a pressure induced lock-in in an aperiodic composite crystal
- [C2. **M. Baldini**] Pressure effects in  $\text{La}_{0.75}\text{Ca}_{0.25}\text{MnO}_3$  studied by neutron and optical methods
- [C3. **I. Mirebeau**] Ordered spin ice state and magnetic fluctuations in  $\text{Tb}_2\text{Sn}_2\text{O}_7$
- [C4. **V. Hardy**] Magnetism of the geometrically frustrated spin-chain compound  $\text{Sr}_3\text{HoCrO}_6$ : Magnetic and heat capacity measurements and neutron powder diffraction.
- [C5. **R. Le Toquin**] Time-resolved in situ studies of oxygen intercalation into  $\text{SrCoO}_{2.5}$ , performed by neutron diffraction and X-ray absorption spectroscopy
- [C6. **V. Paul-Boncour**] Structural and magnetic properties of  $\text{RMn}_2\text{D}_6$  compounds (R=Y, Dy, Er) synthesized under high deuterium pressure
- [C7. **O.L. Makarova**] Role of topology on magneto-structural coupling in new Laves hydrides
- [C8. **J. Cambedouzou**] Tunable intertube spacing in single-walled carbon nanotubes
- [C9. **C. Doussier-Brochard**] Magnetic structure of an antimony manganese chlorosulfide  $\text{MnSbS}_2\text{Cl}$
- [C10. **S. Vilminot**] Magnetic structures of the synthetic magnetic minerals based on hydroxysulfates of divalent metals,  $\text{Co}_3(\text{OD})_2(\text{SO}_4)_2$ ,  $\text{Co}_5(\text{OD})_6(\text{SO}_4)_2(\text{H}_2\text{O})_4$ ,  $\text{Cu}_4(\text{OD})_6\text{SO}_4$
- [C11. **M. Giot**] Magnetic structure of the charge ordered  $\text{Bi}_x\text{Ca}_{1-x}\text{MnO}_3$  manganites
- [C12. **D. Bazin**] Structural study of pathological calcification : the case of kidney stones
- [C13. **F. Damay**] Synchrotron and neutron diffraction structural study of 4-methylpyridine-N-oxide (4MPNO) at 10K
- [C14. **L. S. Dubrovinsky**] High-pressure magnetism in geophysically important materials FeO and MnO

# H1. ANISOTROPIC QUENCHED DISORDER EFFECTS ON A LIQUID CRYSTAL CONFINED INTO NANOCANNELS

R. GUÉGAN<sup>1</sup>, R. LEFORT<sup>1</sup>, M. GUENDOZ<sup>2</sup>, I. MIREBEAU<sup>3</sup> AND D. MORINEAU<sup>1</sup>

<sup>1</sup> Groupe Matière Condensée et Matériaux, UMR-CNRS 6626, Université de Rennes 1, 35042 Rennes, France

<sup>2</sup> Laboratoire d'Optronique, FOTON, UMR-CNRS 6082, 22302 Lannion, France

<sup>3</sup> Laboratoire Léon Brillouin (CEA-CNRS), CEA, Saclay, 91191 Gif-sur-Yvette Cedex

Intense experimental and theoretical efforts have focused on quenched disorder effects in condensed matter as they bring about some most challenging questions of modern statistical physics. Most universal features of quenched disorder effects can be envisaged in the frame of random field theories.

From this standpoint, liquid-crystals (LC) confined in random porous materials are definitively recognized as paradigm systems, which allows one to address experimentally general questions on phase transitions, critical scaling and non-ergodicity in the presence of quenched random fields [1].

LC present many different phase transitions in bulk conditions, involving a variety of universality classes and the breaking of continuous symmetries. They offer unique opportunities to test some general theoretical predictions. The smectic transition has retained a special interest because it is predicted to be unstable towards the presence of an arbitrarily weak quenched disorder. A positionally disordered but topologically ordered "smectic Bragg glass" (SBG) is even predicted in the case of anisotropic random media [2]. However, this new thermodynamically distinct low-temperature phase remains enigmatic experimentally. LC are elastically soft materials and may directly couple to the surface of the porous matrix, which acts as an external field. Confinement in strongly disordered porous materials can be used as an experimental way to introduce an external random field coupling to the LC order parameters. Primary studies have been carried out with random porous silica (aerogels) and aerosil LC-dispersions [1,3], which lead to an almost spatially homogeneous random pinning of the LC. In the present contribution, we prove that it is possible to introduce anisotropic random fields in one-dimensional (1D) conditions of confinement [4]. These new openings rely on the use of aligned nanochannels formed in porous silicon films (PSi) [5].

Anodization of heavily p+-doped (100) oriented silicon leads to a parallel arrangement of unconnected channels (diameter: ~30 nm, length: 30 μm) running perpendicular to the surface wafer (called columnar form of the PSi). The aspect ratio of each channel exceeds 1000:1 and induces a low dimensionality (quasi 1D) to the system (cf. Fig. 1). The preferential alignment of all the channels perpendicularly to the silicon surface prevents powder average limitations when measuring anisotropic observables of unidimensional nanoconfined systems.

Under these conditions of confinement, anisotropic quenched disorder is introduced by the highly corrugated inner surface of the 1D pores, which has been proved to be strongly irregular at the microscopic length scales i.e., ~1 nm.

Fully hydrogenated octylcyanobiphenyl (8CB) has been chosen as a reference LC. It undergoes with increasing temperature the following sequence of phases: crystal (K), Smectic A (A), Nematic (N) and isotropic (I) with the following transition temperatures:  $T_{KA}=294.4$  K,  $T_{NA}=305.8$  K and  $T_{NI}=313.5$  K.

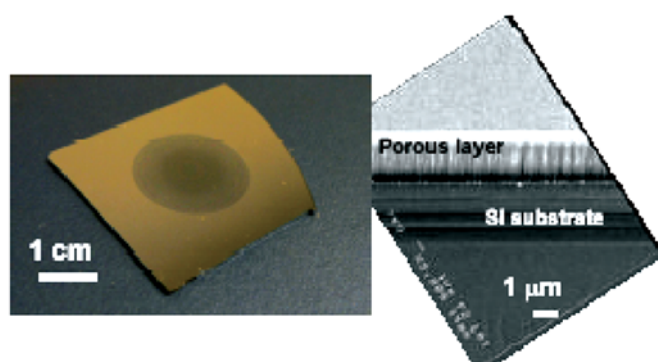


**Figure 1.** Top view of the porous silicon wafer (left). Side view of the porous layer by scanning electron microscopic (right)

A spontaneous alignment of the mesophases and crystalline phases has been observed in confinement. It corresponds to a preferential orientation of the nematic and smectic orderings along the pore axis, as revealed by spectroscopic ellipsometry, polarized microRaman and small angle neutron scattering (PAXY, LLB) [6]. This direct consequence of confinement has been related to the unidirectional character of the porous geometry. The nature of the surface interaction (anchoring) is not prevailing here, since changing the interaction from hydrophilic to hydrophobic by surface chemical treatment (silanization) does not affect qualitatively the overall structure and phase behaviour of 8CB in PSi [5].

A precise structural description of the confined phases requires an improved q-resolution, which can be achieved with a monochromatic cold-source double-axis neutron diffractometer (G6.1). The macroscopic parallel alignment of the porous nanochannels allows one to investigate the effects of anisotropic quenched disorder on the structure of the mesophases by selecting peculiar incidence angles so that the transfer of momentum  $q$  is practically parallel or perpendicular to the pores axis. An extreme alteration of the phase diagram of 8CB in PSi has been observed (cf. Fig. 2). Crystallization is strongly depressed on cooling and leads to two crystalline phases below 250 K, which do not correspond to any stable phase of bulk 8CB.

## STRUCTURE AND PHASE TRANSITIONS

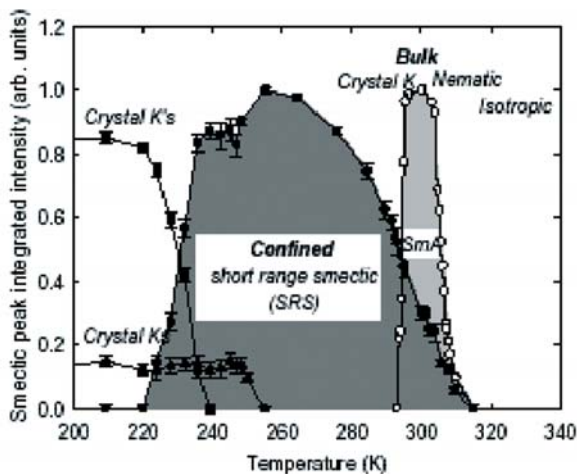


**Figure 2.** Phase behaviour of bulk and confined 8CB, revealed by the temperature variation of the Bragg peaks characteristic of the different phases.

More remarkable is the absence of a nematic-smectic transition, which is replaced by a reversible and gradual increase of a short-range translational order. This short range ordered smectic phase (SRS) is stable and evolves on an extremely wide temperature range down to 50 K below the bulk crystallization. Its structure factor is characterized by a single broad diffraction peak at  $q = 0.2\text{\AA}^{-1}$ , which corresponds to the location of the smectic Bragg peak in the bulk. A lineshape analysis of this peak has revealed the existence of two components, which agrees with recent random fields theoretical predictions. The first term (of Lorentzian type) dominates at high temperature and reflects the smectic thermal fluctuations also observed in the bulk. An additional term is required in the presence of quenched disorder and prevails in the SRS phase at low temperature. The fitting of the structure factor with this theoretical expression provides a smectic correlation length, which increases continuously from 3 nm at the bulk nematic-smectic transition temperature up to 12 nm at 250K (cf. Fig. 3). This variation strongly differs from what is expected for more usual nanoconfinement effects in terms of surface interaction and finite size effects. These latter effects are exemplified by the case of 8CB confined in alumina nanochannels of the same size (30 nm), which are known to present a fairly regular wall structure. In this case, the signature of a sharp transition from the nematic to the smectic phase is maintained although it is slightly rounded and depressed (about 2 K). The variation of the smectic fluctuations correlation length follows the critical behavior of the bulk, although the smectic domains are ultimately spatially limited at the transition by finite size effects. An additional independent proof of the primacy of quenched disorder effects for 8CB in PSi is the apparent linear dependence between  $\kappa_{si}$  and the smectic susceptibility obtained by

integration of the pseudo- Bragg peak intensity. Such a relationship, which has been predicted theoretically, points up the origin of the SRS phase. The gradual increase of short-range correlation length is resulting from the competition between the elasticity of the smectic layers and the strength of disorder introduced by the porous solid.

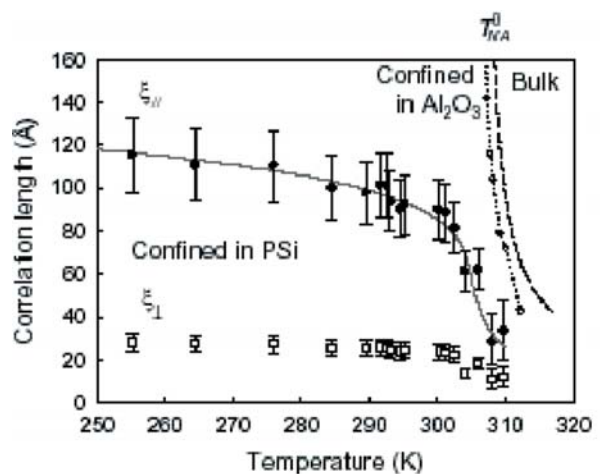


**Figure 3.** The temperature variation of the smectic correlation length for bulk 8CB (dashed line), for 8CB confined in porous alumina (dotted line) and for 8CB confined in porous silicon (filled circles).

The confinement of LC in PSi has opened new perspectives in the unexplored regime of anisotropic and strong quenched disorder, which may inspire future investigations. Our results already imply that much of the scenario expected for weak disorder is retained in the regime obtainable with PSi. Additional crucial aspects related to the ergodicity of the system and the occurrence of a glassy dynamics resulting from quenched disorder remain to be explored [7,8].

Financial supports from the *Centre de Compétence C.Nano Nord-Ouest*, *CNRS* and *Rennes Metropole* are expressly acknowledged.

- [1] T. Bellini, L. Radzihovsky, J. Toner, and N. A. Clark, *Science* **294**, 1074 (2001).
- [2] B. Jacobsen, K. Saunders, L. Radzihovsky, and J. Toner, *Phys. Rev. Lett.* **83**, 1363 (1999); L. Chen and J. Toner *Phys. Rev. Lett.* **94**, 137803 (2005).
- [3] R. L. Leheny, S. Park, R. J. Birgeneau, J.-L. Gallani, C. W. Garland, and G. S. Iannacchione, *Phys. Rev. E* **67**, 011708 (2003).
- [4] R. Guégan, D. Morineau, C. Loverdo, W. Béziel, and M. Guendouz, *Phys. Rev. E* **73**, 011707 (2006).
- [5] R. Guégan, *PhD Thesis dissertation*, University of Rennes, France (2006).
- [6] R. Lefort, D. Morineau, R. Guégan, A. Moréac, C. Ecolivet and M. Guendouz, *Philos. Mag.* (in press); *cond-mat/0605112* (2006).
- [7] M. Marinelli, F. Mercuri, S. Paoloni and U. Zammit, *Phys. Rev. Lett.* **95**, 237801 (2005).
- [8] R. Guégan, R. Lefort, W. Béziel, D. Morineau, M. Guendouz and B. Frick, (submitted); *cond-mat/0604353* (2006).

## H2. DIFFRACTION STUDIES OF MnO CONFINED IN NANOCANNELS OF MESOPOROUS MATRICES.

I.V. GOLOSOVSKY<sup>1</sup>, I. MIREBEAU<sup>2</sup>, G. ANDRÉ<sup>2</sup>, D. A. KURDYUKOV<sup>3</sup>, YU. A. KUMZEROV<sup>3</sup>, V. P. SAKHNENKO<sup>4</sup>

<sup>1</sup> St. Petersburg Nuclear Physics Institute, 188350, Gatchina, St. Petersburg, Russia

<sup>2</sup> Laboratoire Léon Brillouin, CE-Saclay, F-91191, Gif-sur-Yvette, France

<sup>3</sup> A. F. Ioffe Physico-Technical Institute, 194021, St. Petersburg, Russia

<sup>4</sup> Rostov State University, 344090, Rostov/Don, Russia

The properties of magnetics confined in nanometer scale cavities drastically differ from those in the bulk material. The investigation of model materials in the unusual conditions of a so-called “restricted geometry” is of fundamental interest since the confined geometry and the influence of the surface yield unusual properties.

During the past years, we carried out systematic studies of 3d-oxides in confinement, first in MnO confined in a vycor glass matrix with a random network of pores [1] then in MnO confined in MCM-41 or SBA matrix with a regular system of nanochannels [2,3,4] and MnO confined in MCM-48 matrix with a gyroidal channel system [5]. These amorphous silica matrices known as molecular sieves were discovered in 1992 and attracted much attention. They do not produce Bragg reflections and are very suitable to diffraction studies. Oxides within the matrix cavities were synthesized from solutions by the “bath deposition method”. The high specific surface of the matrices and the good wetting of the channel walls by the liquid solution ensure that MnO predominantly occupies the channel voids.

Since the discovery of antiferromagnet order in MnO in 1949, this oxide has been the subject of intense experimental and theoretical interest. In MnO the antiferromagnetic order, which appears at 117 K by a first order phase transition, is accompanied by a rhombohedral contraction of the cubic lattice. In the magnetic structure, which consists of ferromagnetic sheets stacked antiferromagnetically along the (111) axis, the moments in the first coordination sphere are frustrated. Greenwald and Smart in the early 50's suggested that the distortion removes the frustration. So the structural distortion and the magnetic ordering in MnO are mutually dependent.

### Shape of the nanoparticles.

Neutron diffraction and x-ray synchrotron experiments showed that, in contrast within the porous glass where MnO forms isotropic aggregates, inside the channel type matrices MnO forms nanowires or nanoribbons. In the latter, the two-dimensional character of the diffracting objects leads to a specific lineshape known as a “saw-tooth” profile and to a specific shift from the Bragg position towards larger diffraction angles. This yields an “effective” lattice parameter which is systematically lower than the corresponding lattice parameter of the three-dimensional lattice.

The profiles measured at the synchrotron source LURE were compared with those calculated numerically for objects of different dimensions using the Debye formula (Figure 1,2). This analysis allowed us to estimate the dimensions of the

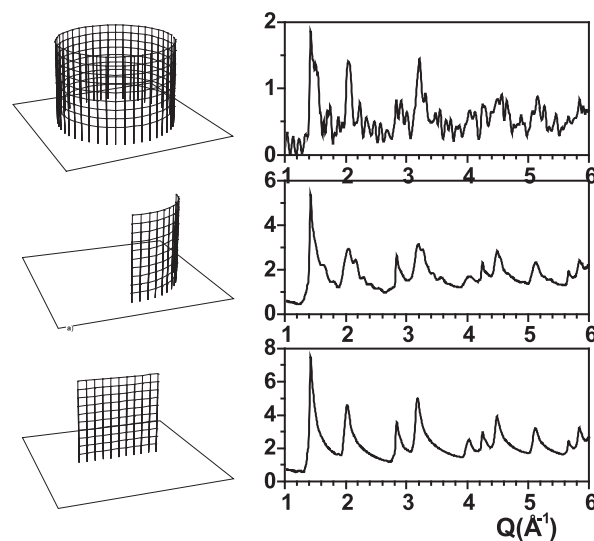


**Figure 1.** Numerical simulation of diffraction patterns from diffracting objects of different shapes.

nanoparticles, which appear to be thin ( $\sim 10$  Å) ribbon or wire-like structures. In all cases, the nanoparticle lengths are in the interval of 180–260 Å, increasing with the channel diameter [2].

### Magnetic order and phase transition.

Neutron diffraction studies of confined MnO, performed at the diffractometer G6-1 showed that the magnetic structure is similar to the structure in the bulk.

However, the volume-averaged magnetic moment of confined MnO appears to be noticeably smaller than the moment in the bulk. This is a well known phenomenon in confined magnets, which is explained by the disorder of the magnetic moments at the surface.

In all type of matrices, the magnetic transition in confined MnO becomes continuous with a Néel temperature  $T_N$  enhanced with respect to the bulk [1,3]. Such behavior is well known as a finite-size “rounding” of the phase transition and results from the limitation of the correlation length by the nanoparticle size.

The observation of an enhanced Néel temperature is surprising, since a common effect expected in all nanostructured material is the decrease of  $T_N$  when the correlation length becomes limited by the nanoparticle size. In the present case, the magnetic disorder and the violation of the translation symmetry at the nanoparticle surface result in a small surface ferromagnetic moment whereas the core remains antiferromagnetically ordered. Taking into account the

## STRUCTURE AND PHASE TRANSITIONS

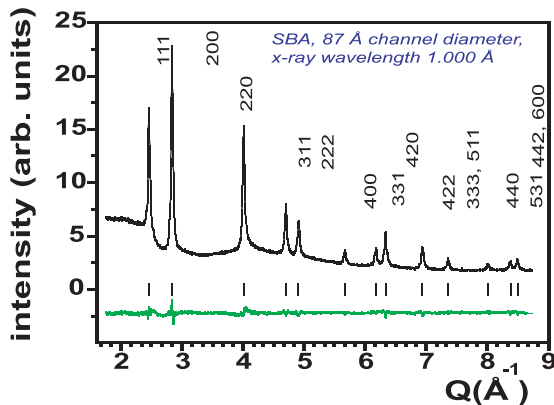


**Figure 2.** Observed x-ray diffraction pattern of MnO confined in SBA matrix with 87 Å channel diameter; in green, the difference pattern

ternary interaction of the non-critical ferromagnet, a critical antiferromagnetic behavior and the associated structural order parameters, the enhanced  $T_N$  can be explained within the framework of the Landau theory [3].

In MnO within channels of MCM-41 matrices, the critical exponent in the temperature dependence of the magnetic moment decreases with decreasing the channel diameter. We attribute the observed change of the magnetic transition to the increasing anisotropy and the change in the dimensionality of the magnetic system to a quasi-one-dimensional case (Figure 3).

### Néel temperature (K) Exponent( $\beta$ )

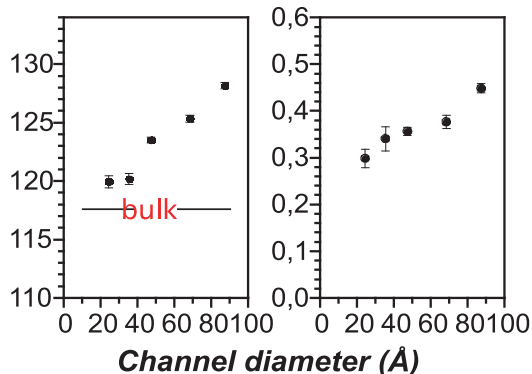


**Figure 3.** Dependences of the Néel temperature and critical exponent  $\beta$  with the channel diameter, as calculated by fitting the data with a power law.

### Structural distortion and magnetic order.

According to conventional theory, antiferromagnetism in MnO is stabilized by the structural distortion. However, in the case of nanoparticles, the high anisotropy and the inner stresses add new terms to the free energy, which could drastically change the energy balance.

Interestingly, low temperature high-resolution x-ray diffraction experiments, performed in ESRF on nanoparticles of MnO confined in MCM-41 matrix with 35 Å channel diameter, showed a new structural transition at about 60 K, well below

the Néel transition which occurs at about 120 K. At this second transition, the structural distortions which appeared below  $T_N$  suddenly disappear and the structure becomes cubic as in the paramagnetic region. This "reentrant" transition is accompanied by an increase of the lattice parameter, of the amplitude of atomic motion and the appearance of inner stresses (Figure 4). Surprisingly, there is no change in the temperature dependence of the magnetic moment associated with the low temperature transition. Such behavior drastically differs from the behavior known for the bulk.

### Loss of long-range atomic order in MnO confined in MCM-48 matrix with a gyroidal system of channels.

The matrix MCM-48 is marvelous because the channels piercing in its amorphous silica body comply with the symmetry of the cubic space groups. The channel wall surface exactly follows the so-called "periodic minimal surface", forming a gyroidal structure with a three-dimensional network of channels.

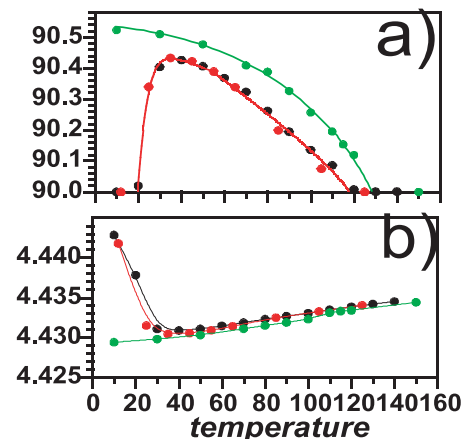


**Figure 4.** Temperature dependences of the angle of rhombohedral distortion ( $\alpha$ ) and the unit cell parameter.

Synchrotron X-ray experiments performed at ESRF showed that the nanoparticles of MnO have a ribbon-like shape with a length of about 50 Å and do not show long-range atomic ordering. In spite of the disordered atomic structure, a phase transition from the cubic structure accompanied with a rhombohedral distortion was observed, like in the bulk material. The parameters of the phase transition appear to be similar to the parameters of the transition observed in MnO within the MCM-41 matrix, where atomic ordering extends over much longer length scales [5].

1. I. V. Golosovsky, I. Mirebeau, G. André, et al., Phys. Rev. Lett., **86**, 5783, 2001.
2. I. V. Golosovsky, I. Mirebeau, E. Elkaim, D. A. Kurdyukov and Y. A. Kumzerov. Eur. Phys. Journ. B, **47**, 55, 2005.
3. I. V. Golosovsky, I. Mirebeau, V. P. Sakhnenko, D. A. Kurdyukov and Y. A. Kumzerov. PRB, **72**, 1444091, 2005.
4. I. V. Golosovsky, I. Mirebeau, F. Fauth, D. A. Kurdyukov and Yu. A. Kumzerov. PRB, **74**, 05443315, 2006.
5. I. V. Golosovsky, I. Mirebeau, F. Fauth, et al., accepted by PRB, 2006.

# H3. PRESSURE INDUCED FERROMAGNETIC SPIN GLASS TRANSITION IN THE GEOMETRICALLY FRUSTRATED PYROCHLORE $(\text{Tb}_{1-x}\text{La}_x)_2\text{Mo}_2\text{O}_7$

A. APETREI<sup>1</sup>, I. MIREBEAU<sup>1</sup>, I. GONCHARENKO<sup>1</sup>, D. ANDREICA<sup>2</sup>, P. BONVILLE<sup>3</sup>, W. A. CRICHTON<sup>4</sup>, A. FORGET<sup>3</sup> AND D. COLSON<sup>3</sup>

<sup>1</sup> Laboratoire Léon Brillouin (CEA-CNRS), CEA – Saclay, 91191 Gif-sur-Yvette France

<sup>2</sup> Laboratory for Muon spectroscopy, Paul Scherrer Institute, 5232 Villigen-PSI, Switzerland

<sup>3</sup> Service de physique de l'Etat Condensé CEA-CNRS, CE-Saclay, 91191 Gif sur Yvette France

<sup>4</sup> European Synchrotron Radiation facility, BP 220, 38043 Grenoble, France

In the pyrochlore compounds  $\text{R}_2\text{Mo}_2\text{O}_7$ , both rare earth  $\text{R}^{3+}$  and  $\text{M}^{4+}$  transition metal ions form a three-dimensional network of corner sharing tetrahedra. The pyrochlore lattice is geometrically frustrated both for antiferromagnetic (AF) and ferromagnetic (F) nearest-neighbour exchange interactions, leading to intriguing magnetic states such as spin liquids, spin ices or chemically ordered spin glasses. Pyrochlores are extensively studied since their electrical and magnetic properties strongly depend on the rare earth ionic radius  $r$ . Compounds with small ionic radius Y, Dy and Tb are spin glass (SG) insulators, whereas those with Gd, Sm and Nd are ferromagnetic metals.  $(\text{R},\text{R}')_2\text{Mo}_2\text{O}_7$  series with different substitutions on the  $\text{R}^{3+}$  site show a universal dependence of the transition temperature versus  $r$  [1], suggesting that Mo-Mo interactions change sign at a critical value  $r_c$ , which controls the SG-F threshold. Band structure calculations and photoemission experiments [2] point out that the concomitant changes of the transport and magnetic properties come from strong electron correlations in the Mo  $t_{2g}$  band nearby the Fermi level. Up to now, there has been no microscopic investigation of the SG/F threshold, so as to follow the changes in the magnetic correlations and spin fluctuations. To understand the role of interatomic distances in this transition, the most direct way is to combine applied pressure and chemical pressure. We studied the  $(\text{Tb}_{1-x}\text{La}_x)_2\text{Mo}_2\text{O}_7$  system, allowing us to cross the critical threshold by both chemical and applied pressure. By using three microscopic probes, namely neutron diffraction,  $\mu\text{SR}$  and synchrotron X ray diffraction, this study provides the first and complete characterization of the SG-F threshold [3].

Magnetic diffraction patterns were recorded on the powder diffractometers G61 and G41 of the Laboratoire Léon Brillouin (LLB) at ambient pressure, and under pressure on G61. Starting from the spin glass  $\text{Tb}_2\text{Mo}_2\text{O}_7$ , the dilution by *non magnetic* La ion expands the lattice, inducing long range magnetic order (LRO), which is further destroyed under pressure (Fig.1). Clearly, negative chemical pressure and applied pressure have reversed effects on the magnetic order. The magnetic structure (Fig.2) was solved by a systematic search, using the program BasReps and symmetry-representation analysis combined with Fullprof. We searched for a solution in the in the space group  $I41/amd$ , the highest subgroup of the  $Fd\text{-}3m$  space group allowing F and AF components simultaneously. In the ordered structure with  $\mathbf{k}=0$  propagation vector, the four tetrahedra of the cubic unit cell are

equivalent, for both Tb and Mo lattices. In a given Tb tetrahedron, the  $\text{Tb}^{3+}$  moments orient in the local spin ice (2in-2out)

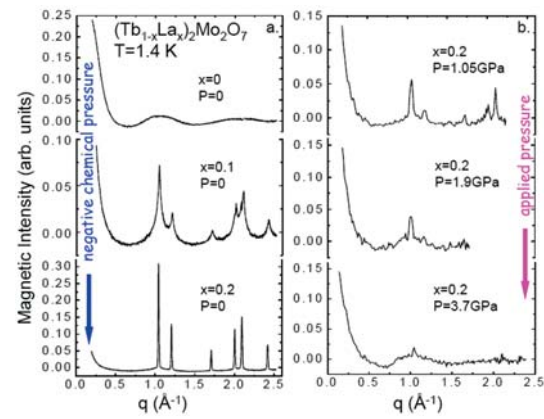


**Figure 1.** Magnetic intensity of  $(\text{Tb}_{1-x}\text{La}_x)_2\text{Mo}_2\text{O}_7$  at 1.4 K versus the scattering vector  $q=4\pi\sin\theta/\lambda$ . The neutron wavelength is  $\lambda=4.741 \text{ \AA}$ . A spectrum in the paramagnetic phase (70 K) was subtracted and the magnetic intensity was scaled to the (222) nuclear peak intensity.

structure, with a small angle  $qt$  with the local  $\langle 111 \rangle$  anisotropy axes. Their F component orders along a  $[001]$  axis. The Mo moments align close to a  $[001]$  axis, with a slight tilting  $\theta_m$  towards the local  $\langle 111 \rangle$  axis (inset Fig. 2). Mo and Tb moments are F coupled.

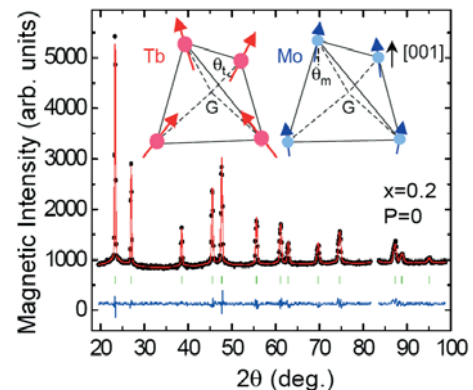


**Figure 2.** Magnetic intensity for  $x=0.2$  at 1.5 K versus the scattering angle  $2q$ ,  $\lambda=2.426 \text{ \AA}$ . A 70 K spectrum was subtracted. Solid lines show the best refinement and the difference spectrum (bottom). In inset: magnetic structure of the Tb- and Mo- tetrahedra.

## STRUCTURE AND PHASE TRANSITIONS

As a striking feature, the long range order (LRO) is induced by diluting the Tb lattice with a non magnetic ion. It proves that the main effect of dilution is the lattice expansion. From the variation of the lattice constant, a small La content ( $x=0.06$ ) is expected to induce the SG-F transition. The SG-F transition is mostly determined by the change in sign of the Mo-Mo exchange interactions and the onset of F interactions like in  $\text{Nd}_2\text{Mo}_2\text{O}_7$  [4]. We notice that Tb magnetism should still play a role since  $(\text{Y}_{1-x}\text{La}_x)_2\text{Mo}_2\text{O}_7$  compounds do not show LRO. The non collinear structure for both  $\text{Tb}^{3+}$  and  $\text{Mo}^{4+}$  comes from the uniaxial anisotropy of the  $\text{Tb}^{3+}$  ion, which brings spin ice frustration in the ferromagnetic region. The ground state moments are strongly reduced with respect to the free ion values.

Under pressure, the ordered moments ( $x=0.2$ ) decrease and reorient. At 1.05 GPa, LRO and SRO phases coexist. The ordering temperature decreases under pressure. At 3.7 GPa the Bragg peaks disappear (see Fig. 3a). When fitting the 3.7 GPa data with a SRO model [5] involving correlation parameters up to the fourth neighbours, we find short range F Tb-Tb spin correlations and AF Tb-Mo spin correlations. So the Tb-Mo correlations change sign at the threshold. The strong intensity at small angles, not taken into account by the SRO model was fitted by a Lorentzian, yielding a mesoscopic correlation length between Tb moments of  $18(7)$  Å. All parameters are close to the values in  $\text{Tb}_2\text{Mo}_2\text{O}_7$  spin glass.

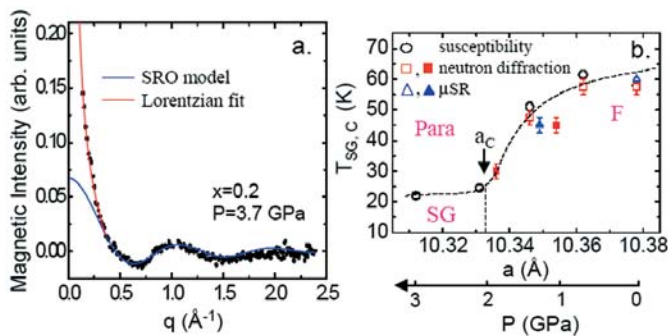


**Figure 3.** a. Magnetic intensity for  $x=0.2$  sample at 1.4 K and 3.7 GPa. Lines are fits using SRO model and Lorentzian fit respectively. b. Phase diagram for  $(\text{Tb}_{1-x}\text{La}_x)_2\text{Mo}_2\text{O}_7$  in the threshold region: ambient pressure (open symbols) and under pressure (full symbols).

$\mu$ SR measurements (Fig. 4) shed a new light on the magnetic order by probing the spin fluctuations and the static local field below  $T_C$ . We measured the  $x=0.2$  sample at ambient pressure on GPS and GPD at the Paul Scherrer Institute (PSI) and at 1.3 GPa on GPD. Data analysis allows us to separate the dynamic term  $\lambda_z$  and static terms  $\langle B_{loc} \rangle$  and  $\lambda_T$  (see [3] for a complete description). The longitudinal relaxation rate  $\lambda_z$  which reflects the spin fluctuations shows a critical peak at  $T_C$  then a broad maximum at a lower temperature  $T^*$ . The static

terms reflecting the static local field “seen” by the muon spin, scale with the Tb moment measured by neutrons. The dynamical anomaly at  $T^*$ , akin to that observed in  $\text{Sm}_2\text{Mo}_2\text{O}_7$  and re-entrant spin glasses, suggest a freezing of short range correlated moments. It occurs without any anomaly in the static terms, which means that it does not break the LRO.

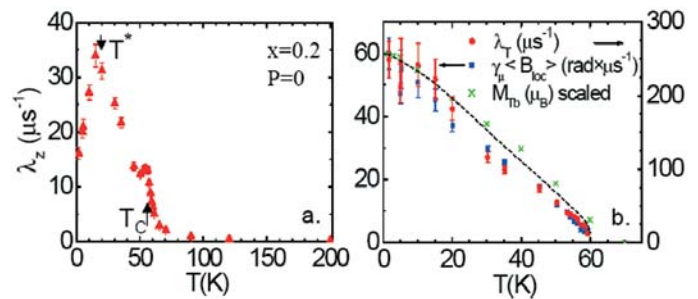


**Figure 4.**  $\mu$ SR ambient pressure results for  $x=0.2$ . Temperature dependence of: a.  $\lambda_z$ . b.  $\langle B_{loc} \rangle$ ,  $\lambda_T$  and  $M_{Tb}$  (scaled).

The phase diagram (Fig. 3b) shows the transition temperatures determined by all probes versus the lattice constant. The equation of state  $a(P)$  measured by X ray synchrotron diffraction at ID31 (ESRF) allowed us to combine ambient pressure data on compounds with different  $x$ , with high pressure data for  $x=0.2$ . The critical lattice constant agrees with previous determinations [1].

The fact that high pressure and ambient pressure data merge in a single curve supports a dominant mechanism induced by a change in the Mo-Mo interactions. But our microscopic study also shows important features not taken into account by current theories: i) the role of rare earth magnetism at the threshold should be taken into account. ii) the mechanism by which Mo-Mo interactions change sign should be different under chemical pressure and applied pressure. In the first case, it reflects the aperture of a Mott-Hubbard gap, yielding an insulating spin glass. In the second case, it is likely connected with the increase of the Mo bandwidth, yielding a metallic spin glass. iii) the role of Tb anisotropy in the spin correlations and fluctuations is clarified thanks to a comparative study in  $\text{Gd}_2\text{Mo}_2\text{O}_7$ . In  $\text{Gd}_2\text{Mo}_2\text{O}_7$ , with isotropic Gd ion, the ferromagnetic ground state is collinear and the transition at  $T^*$  is strongly suppressed [6]. The rare earth anisotropy also plays a role on the conductivity, leading to a giant abnormal Hall effect in the ferromagnetic region.

- [1] T. Katsufuji et al., Phys. Rev. Lett. **84**, 1998 (2000).
- [2] I. V. Solovyev, Phys. Rev. B **67**, 174406 (2003); J. S. Kang et al., Phys. Rev. B **65**, 224422 (2002).
- [3] A. Apetrei et al., cond-mat/0604627, to appear in Phys. Rev. Lett (2006).
- [4] Y. Taguchi et al., Science **291**, 2573 (2001).
- [5] J. E. Greedan et al., Phys. Rev. B **43**, 5682 (1991).
- [6] I. Mirebeau et al., cond-mat/0606420, to appear in Phys. Rev. B (2006).

# H4. NEUTRON DIFFRACTION STUDY OF THE BROKEN SYMMETRY PHASE IN SOLID DEUTERIUM AT THE PRESSURE OF 38 GPa

I.N. GONCHARENKO<sup>1</sup> AND P. LOUBEYRE<sup>2</sup>

<sup>1</sup> Laboratoire Léon Brillouin (CEA-CNRS), CEA – Saclay, 91191 Gif-sur-Yvette, France

<sup>2</sup> Département Physique Théorique et Applications, CEA, 91680 Bruyères-le-Châtel, France

The solid hydrogen H<sub>2</sub>, HD and D<sub>2</sub> exhibit intricate quantum phenomena, which have been the subject of numerous experimental and theoretical studies. Studying these phenomena is considered as essential to understand the quantum many-body effects of density. Various exciting scenarios have been suggested for high-pressure dense hydrogens, for example, room temperature superconductivity in monoatomic hydrogen or quantum melting at T=0K at the onset of the transition to the monoatomic state [1]. Despite enormous theoretical and experimental efforts, there was no unambiguous information on nature of the pressure induced phases in solid hydrogen. Optical probes detected a phase transition in solid D<sub>2</sub> at the pressure of 25 GPa and low temperatures [2]. A similar transition occurs in H<sub>2</sub> at much higher pressures of 70-100 GPa [3]. The giant isotopic effect reveals the quantum nature of the pressure-induced phase. The transition was interpreted as a transition to a rotationally ordered state. In the ground state at low temperature and low pressure, hydrogen molecules are in the J=0 spherical rotational states and exhibit a rotational disorder down to T=0 K. At high pressures, a trade-off between two tendencies, going higher in kinetic energy (that is, to J≠0 rotational levels) and gaining a negative potential energy through a orientational ordering that minimizes electric quadrupole–quadrupole energy might lead to a breaking of the spherical symmetry and the stabilization of an orientationally ordered state (the so-called broken symmetry phase or BSP). In H<sub>2</sub>, the contribution of the kinetic energy is higher than in D<sub>2</sub>, which explains the isotopic effect on the pressure of the transition. The crystal structure of the quantum pressure-induced phases in solid hydrogen is a challenge for modern density-functional theory (DFT) and molecular dynamic simulations (MD). Various theoretical models proposed different crystal structures, most of them suggesting an orthorhombic lowering of symmetry in the basal plane of the initial h.c.p. lattice (see, for example Refs. 4,5). Until the present study, there was no direct evidence of the structural transition in high-pressure solid hydrogen, neither proof of its crystal structure. The optical data on vibron modes provides only indirect information on crystal structure. X-rays are scattered by electronic shells, and therefore almost insensitive to the orientations of hydrogen molecules having no internal electronic orbitals. Contrarily, neutrons are scattered by nuclei and therefore can “see” the orientations of the molecules. While the advantages of neutron techniques in studies of high-pressure hydrogen are obvious, such study is a challenge from an experimental point of view. At pressures above 25 GPa the sample volume is measured in small fraction (10<sup>-3</sup>) of cubic millimetre. It seemed almost

impossible to obtain high-quality structural information from such a small sample at the pressure of 38 GPa (the pressure was chosen well above the phase boundary) and low (down to 1.5K) temperatures. To carry out the study, we used a new approach, based on a combination of neutron and synchrotron probes. A high-quality single-crystal of D<sub>2</sub> was grown from He-D<sub>2</sub> mixture (Fig. 1). The crystal was surrounded by He pressure transmitting medium, which preserved it from shattering as pressure was increased to 38 GPa.



**Figure 1.** Single crystal of solid D<sub>2</sub> surrounded by He pressure transmitting medium.

New pressure cells (Fig.2) allowed to combine neutron and X-ray diffraction on the same sample. The quality and orientation of the crystal were checked at the ESRF (ID27 and ID9 beamlines) by X-ray diffraction. This saved many weeks of neutron time. Then the pressure cell was brought to the LLB and installed on the lifting-counter diffractometer 6T2, equipped by a He-flow cryostat. The neutron data on (100), (0-10), (-110), (110), (-210), (1-20) and (101) reflections were collected in the temperature range 1.5-70 K. The present study sets a new record for the maximal pressure in single-crystal neutron measurements.

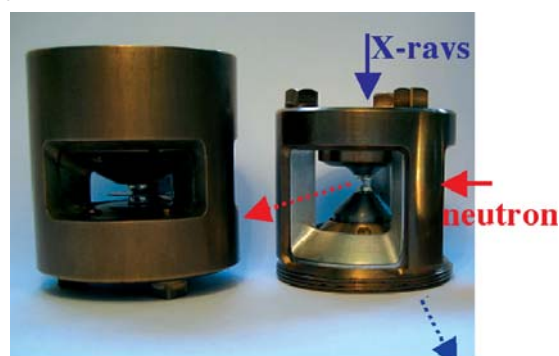


**Figure 2.** New “hybrid” low-temperature cells compatible with neutron and X-ray scattering at the LLB.

## STRUCTURE AND PHASE TRANSITIONS

Fig. 3 and 4 show the first direct diffraction evidence of the BSP transition in solid  $D_2$  under pressure. As temperature decreases, a small ( $\sim 5\%$ ) decrease in intensity indicates a pressure-induced structural transition. The temperature ( $\sim 45$  K) of the transition exactly coincides with the temperature at which a shift in vibron modes was detected by optical spectroscopy and a tiny change in  $c/a$  ratio by X-ray scattering. The analysis of the obtained data revealed rather surprising results [6]. Firstly, we did not observe any significant difference ( $>5\%$ ) in the measured intensities from the reflections which are linked by the P-3 symmetry (and therefore equivalent) in the initial h.c.p. structure, but should become different in the orthorhombic cells predicted by theory. Secondly, the observed variation of intensities at the phase transition are much smaller than those predicted by the theoretical models [4,5].

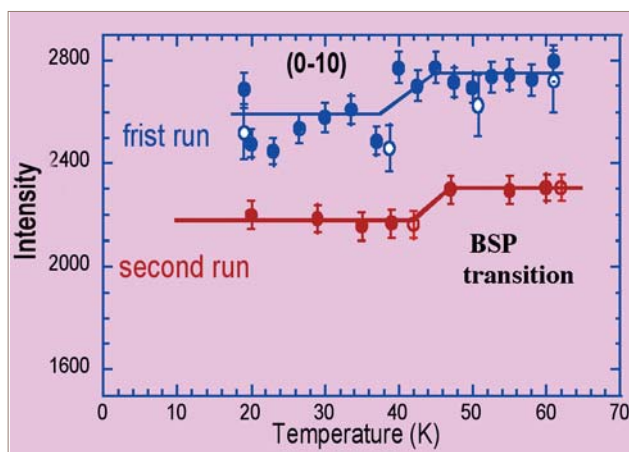


**Figure 3.** Integrated intensity of the (0-10) reflection versus temperature at the pressure of 38 GPa. Another interesting feature is the presence of incommensurate satellites (1-x, 0 0) in neutron and X-ray diffraction patterns.

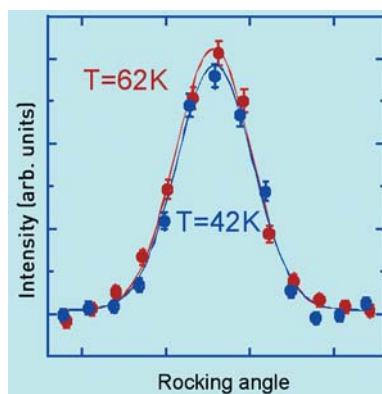


**Figure 4.** Rocking curves of the (0-10) reflection measured at different temperatures.

Based on our observations, and a proposition of local ordering from a MD simulation by Cui et al [7], we suggest

another type of orientational ordering with is similar to that in metastable ortho-para mixtures having cubic f.c.c. structure (so called Pa3 structure). This structure minimises the electric quadrupole-quadrupole energy. It has P-3 symmetry. If developing in a h.c.p. structure, it exhibits a topological frustration (Fig. 5): the molecules have to choose 3 orientations from 6 possible directions along the body diagonals in a bi-pyramid. Stacking faults between different possible orientations might result in a short-range ordered structure or a long-range incommensurate modulation, similar to that observed experimentally. The obtained results should stimulate further theoretical works on orientational ordering and quantum phenomena in dense hydrogen.

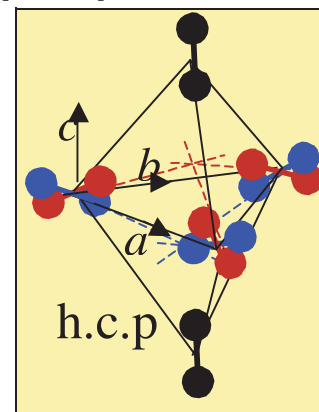


**Figure 5.** Two possible "frustrated" types of orientational ordering in the BSP phase. The orientations shown in red and blue colours have the same quadrupole-quadrupole energy.

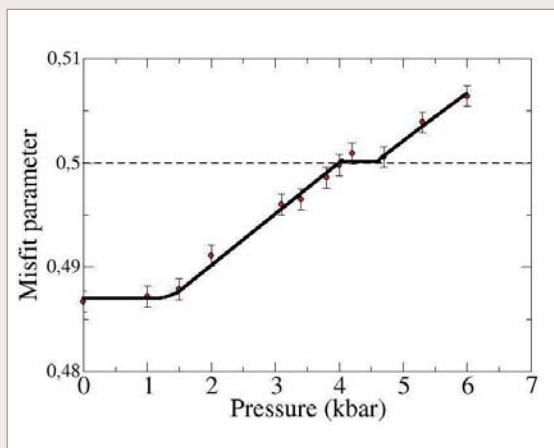
Finally, by a combination of state-of-art synchrotron and neutron techniques, we carried out the first direct diffraction study of the quantum BSP phase in solid  $D_2$ , which was a mystery for about 25 years. Forthcoming neutron experiments in an extended  $q$  range and also similar measurements in solid  $H_2$  at the pressure of 70 GPa should help to improve the understanding of the crystal structure of the BSP phase and to study the isotopic effect on the structure.

Authors thank A. Goukasov and O. Makarova for help in neutron experiments and R. Le Toullec, F. Occelli, M. Hanfland and M. Mezouar for help in X-ray experiments.

- [1] E. Babaev, A. Sudbo and N. Ashcroft, *Phys. Rev. Lett.* **95**, 105301 (2005).
- [2] I.F. Silvera, R.J. Wijngaarden, *Phys. Rev. Lett.* **47**, 39-42 (1981).
- [3] H.E. Lorenzana, I.F. Silvera, K.A. Goettel, *Phys. Rev. Lett.* **63**, 2080 (1989).
- [4] H. Kitamura, Sh. Tsuneyuki, O. Tadashi, T. Miyake, *Nature* **404**, 259 (2000).
- [5] K. A. Johnson, N. W. Ashcroft, *Nature* **403**, 632 (2000).
- [6] I. Goncharenko, P. Loubeyre, *Nature* **435**, 1206 (2005).
- [7] T. Cui, E. Cheng, B. J. Alder, K. B. Whaley, *Phys. Rev. B* **55**, 12253 (1997)

**[C1. B. Toudic] First evidence of a pressure induced lock-in in an aperiodic composite crystal**

Nanometer-sized containers have huge potential for use in molecular manipulation and chemical reactions. In the frame of this work, we report the first pressure-induced lock-in in an aperiodic nanoporous crystal [1]. This result is based on the concept of free sliding applied to aperiodic materials, allowing striking nanotribologic properties. The studied compound, urea-alkane, is a self-assembled nanoporous crystal made of a host urea lattice with hydrogen bonds and a confined guest sublattice non-covalently bounded, like in many biophysical model systems. Neutron diffraction measurements performed on a triple axis spectrometer with cold neutron, 4F, give a unique opportunity to get very high spatial resolution with the precise hydrostatic environment to very carefully measure the different lattice parameters. The retained urea-hexadecane has the period of the guest just slightly larger than twice the one of the host.



Colossal Magneto resistance (CMR) compounds

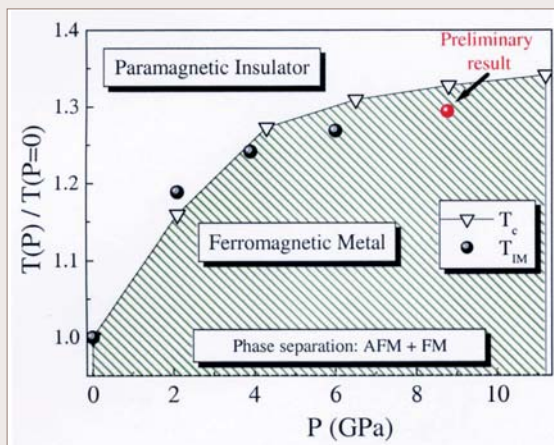
Selective compressibility allowed a commensurate lock-in at the value . Then, the two sub-systems are 'attached' as in normal crystals giving a direct proof of a lock-in energy term in such self-assembled supramolecular crystals. The continuous control of the guest repeat gives a unique tool for tuning one-dimensional properties of confined compounds. These results open a broad field of scientific subjects that can be tackled combining the low friction of incommensurate nanoporous materials with the conformational, optic and electronic properties of guest molecules.

[1] B. Toudic, F. Aubert, C. Ecolivet, P. Bourges and T. Brezewski *Physical Review Letters* **96**, 145503 (2006)

[Collaboration: B. Toudic, F. Aubert, C. Ecolivet, GMCM Rennes 1; P. Bourges, LLB; T. Brezewski, Bilbao]

**[C2. M. Baldini] Pressure effects in  $\text{La}_{0.75}\text{Ca}_{0.25}\text{MnO}_3$  studied by neutron and optical methods**

CMR compounds exhibit a close relation between magnetic and electronic properties [1]. Optical studies revealed a rapid increase of temperature of insulator-metal transition in the prototypical CMR manganite  $\text{La}_{0.75}\text{Ca}_{0.25}\text{MnO}_3$ . In order to establish the relation between the insulator-metal transition and the magnetic ordering, we studied the magnetic structure of  $\text{La}_{0.75}\text{Ca}_{0.25}\text{MnO}_3$  by neutron diffraction. We obtained the magnetic phase diagram and the  $T_C(P)$  line over a wide pressure range (0-8 GPa). The  $T_C(P)$  and the  $T_{IM}(P)$  [2] behaviour under hydrostatic pressure is the same up to (at least) 8 GPa. This result provides the important evidence that the Double Exchange mechanism, responsible for the close connection between magnetic and electronic transition, still holds in the high pressure regime. On the other hand, an antiferromagnetic peak was observed at pressure above 4 GPa and T 100 K, revealing the onset of a phase separation between FM and AFM. This result gives an unambiguous answer to the hypothesis of a reinforced role of the SE coupling between the  $t_{2g}$  core spins and explains the  $T_C(P)$  and the  $T_{IM}(P)$  saturation observed at higher pressure [3].



[1] A.J. Millis, *Nature* **392**, (1998)

[2] A. Congeduti, P. Postorino, E. Caramagno, M. Nardone, A. Kumar, D. D. Sarma, *Phys. Rev. Lett.* **86**, 1251 (2001)

[3] A Sacchetti, P Postorino and M. Capone, *New J. of Phys.* **8**, 3 (2006)

[Collaboration: M. Baldini, E.Arcangeletti, P. Postorino, Universita di Perugia Italy, L. Capogna CNR-OGG Grenoble, I. Goncharenko, LLB.]

Magnetic pressure-temperature phase diagram of  $\text{La}_{0.75}\text{Ca}_{0.25}\text{MnO}_3$

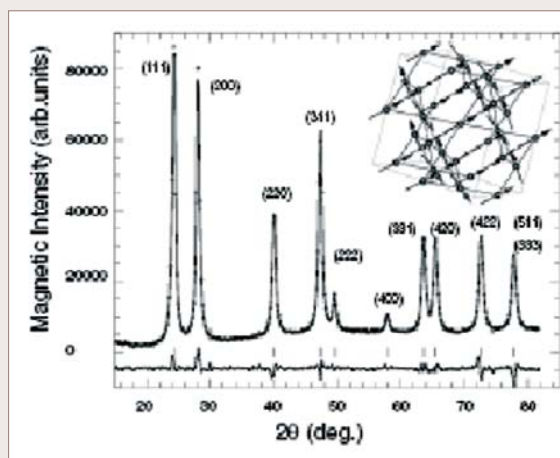
## STRUCTURE AND PHASE TRANSITIONS

**[C3. I. Mirebeau] Ordered spin ice state and magnetic fluctuations in  $Tb_2Sn_2O_7$** 

$Tb_2Sn_2O_7$  is a geometrically frustrated pyrochlore showing antiferromagnetic liquid like correlations down to 4 K. Below 1.3 K we have observed by neutron diffraction a “two steps” transition towards a new magnetic structure, with both ferromagnetic and antiferromagnetic character [1]. The local structure in a Tb tetrahedron is akin to a spin ice [2], but the four tetrahedra of the unit cell are identical, yielding ferromagnetic component. The ordered ground state, previously predicted by theory [3] but not observed before, seems to result from the combined influence of dipolar interactions and finite anisotropy. We have also indirectly observed *fluctuations of the ordered moments* below  $T_c$ , by comparing the ordered moment measured by neutron diffraction to that derived from specific heat. These abnormal fluctuations were recently probed by muons, at such extend that they completely wash out the static field felt by the muon spin [4]. Their precise nature and the way how they coexist with the ordered state remains a mystery, opening a new field of investigation for both experiment and theory.

[1] I. Mirebeau, A. Apetrei et al *Phys. Rev. Lett.* **94**, 246402, (2005).; [2] S. T. Bramwell and M. J. P. Gingras, *Science* **299**, 1495, (2001); [3] J. D. M. Champion et al *Europhys. Lett.* **57**, 93, (2002). ; [4] P. Dalmas et al *Phys Rev. Lett.* **96**, 127202, (2006); F. Bert et al condmat 0603434 to appear in PRL (2006).

[Collaboration: I. Mirebeau, A. Apetrei ( LLB); P. Bonville, D. Colson, A. Forget (SPEC); V. Glazkov, J. P. Sanchez (CEA-Grenoble) ; O. Isnard, E. Suard (ILL)].



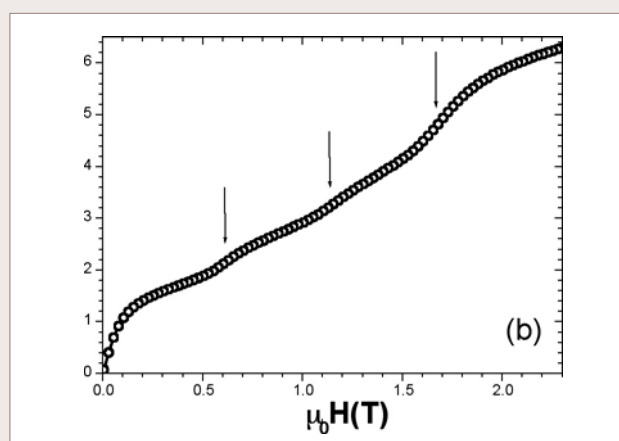
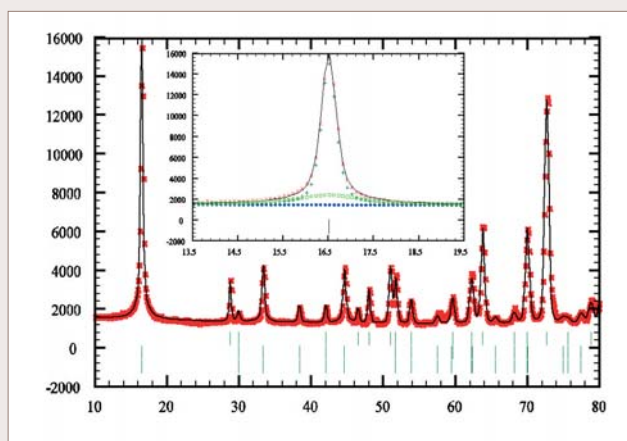
Magnetic neutron diffraction spectrum at 0.10 K, with the ordered spin ice structure in inset. From ref. [1]

**[C4. V. Hardy] Magnetism of the geometrically frustrated spin-chain compound  $Sr_3HoCrO_6$ : Magnetic and heat capacity measurements and neutron powder diffraction**

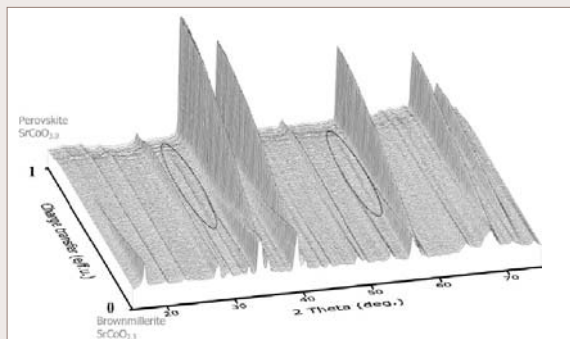
$Sr_3HoCrO_6$  has been investigated versus temperature by combining magnetic and specific heat capacity measurements, as well as neutron powder diffraction, by using the G4.1 diffractometer. The structure, refined in R-3c with  $a=9.78$  and  $c=11.30$  Å, can be described as a triangular lattice that consists of chains, running along the c-axis, alternating face-shared  $HoO_6$  prisms and  $CrO_6$  octahedra, the Sr cations lying between the chains. Long-range antiferromagnetic order occurs around 1 K but this magnetic state has features consistent with partially disorder antiferromagnetism, a state theoretically expected in quasi-1D compounds experiencing geometrical frustration. Two of the three chains on the triangular lattice are found ferromagnetic along c, with an antiferromagnetic coupling between them, the third chain remaining incoherent (Fig. a). This leads to unusual temperature dependence of the magnetic Bragg peaks, with a maximum of intensity at 9K, and a broadening at lower temperature. It also gives rise to puzzling behaviours as exemplified with the pattern of steps on the  $M(H)$  curves at low temperature (Fig.b).

V. Hardy et al, *Physical Review B* **74**, 064413 (2006)

[Collaboration: C. Martin and V. Hardy, CRISMAT, UMR6508, CAEN ; G. André, LLB]



**[C5. R. Le Toquin] Time-resolved in situ studies of oxygen intercalation into SrCoO<sub>2.5</sub>, performed by neutron diffraction and X-ray absorption spectroscopy**



Evolution of the neutron powder diffraction pattern obtained in situ during the electrochemical oxidation of SrCoO<sub>2.5</sub> vs charge transfer. The diffractogram of the brownmillerite SrCoO<sub>2.5</sub> is represented at the bottom, whereas that of the perovskite SrCoO<sub>3.0</sub> is shown at the top. The dotted ellipsoids show the positions of the superstructure reflections.

reaction product (SrCoO<sub>3.0</sub>) does not proceed continuously but gives evidence for the formation of O<sup>-</sup> species for stoichiometries corresponding to SrCoO<sub>2.82</sub>(0.07)[1]. The use of neutrons (vs X-rays) in the diffraction experiments and the choice of the transmission (vs fluorescence) mode in the XAFS experiment guarantee that the obtained data well represent bulk and not just surface properties.

[1] R. Le Toquin, W. Paulus, A. Cousson, C. Prestipino, C. Lamberti, JACS 128 (2006) 13161-13174

[Collaboration : R. Le Toquin, W. Paulus, Université de Rennes 1, A. Cousson, LLB, C. Prestipino, C. Lamberti, Université de Turin]

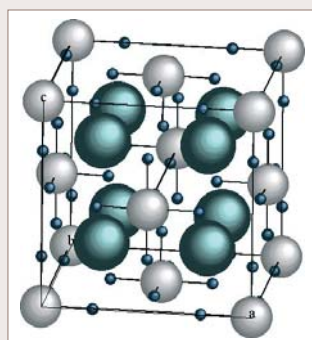
**[C6. V. Paul-Boncour] Structural and magnetic properties of RMn<sub>2</sub>D<sub>6</sub> compounds (R=Y, Dy, Er) synthesized under high deuterium pressure**

Hydrogen absorption in RMn<sub>2</sub> Laves Phases (R= Rare Earth) modifies significantly their magnetic properties. For x ≈ 4.5, the RMn<sub>2</sub>H<sub>x</sub> hydrides crystallize in a structure derived from that of the parent intermetallic, with H atoms in tetrahedral interstitial sites. Applying a hydrogen pressure of several MPa to YMn<sub>2</sub> led to the formation of YMn<sub>2</sub>H<sub>6</sub> [1]. According to X-ray (XRD) and neutron powder (NPD) diffraction experiments, YMn<sub>2</sub>D<sub>6</sub> crystallizes in a disordered fluorite structure (K<sub>2</sub>PtCl<sub>6</sub> type) with a = 6.709(1) Å at 300 K (Fig. 1). In the Fm3m space group, the Y and half of the Mn atoms (Mn1) occupy randomly the 8c site whereas the remaining Mn atoms (Mn<sub>2</sub> in 4a site) are surrounded by 6 H atoms (24e site). This structure is not derived from that of the C15 YMn<sub>2</sub> and the H atoms form covalent bonding with Mn atoms. RMn<sub>2</sub>D<sub>6</sub> phases, isostructural to YMn<sub>2</sub>D<sub>6</sub>, were also obtained starting either from C15 (R =Dy, Ho) or C14 (R=Er) Laves phases. YMn<sub>2</sub>D<sub>6</sub> displays a modified Curie Weiss behaviour and the NPD study shows the absence of long range magnetic order. The M(H) curves of the RMn<sub>2</sub>D<sub>6</sub> compounds (R=Ho, Dy and Er) at 4.2 K show a ferromagnetic behaviour but the saturation magnetization is only half that of the parent compound. NPD studies on ErMn<sub>2</sub>D<sub>6</sub> [2] revealed only local magnetic order of Er moment below 5 K, with ferro and antiferromagnetic correlations (Fig. 2). This has been related to the chemical disorder of R and Mn atoms on the 8c site.

[1] V. Paul-Boncour, S. M. Filipek, M. Dorogova, et al. J. Sol. State Chem., 178 (2005) 356

[2] V. Paul-Boncour, S. M. Filipek, G. André, F. Bourée et al., J. Phys. : Cond. Mat., 18 (2006) 6409

[Collaboration: V. Paul-Boncour, LCMTR Thiais; S.M. Filipek (Poland), G. André, LLB ; F. Bourée LLB]



Mn2

D

Mn1.R

**Figure 1:** Structure of the RMn<sub>2</sub>D<sub>6</sub> compound

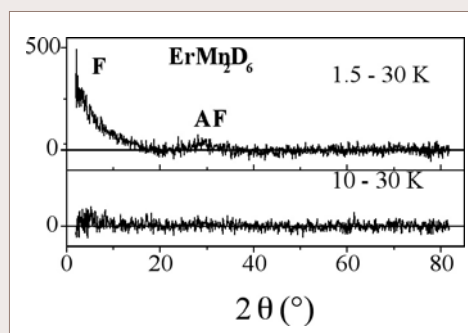


**Figure 2:** Difference NPD patterns of ErMn<sub>2</sub>D<sub>6</sub>

## STRUCTURE AND PHASE TRANSITIONS

**[C7. O.L. Makarova] Role of topology on the magneto-structural coupling in new Laves hydrides**

Intricate magnetic and structural phenomena in the Laves phases ( $\text{RMn}_2$ ) and their hydrides come from the magnetic instability (transition from localized to itinerant states) in the Mn sublattice, which is governed by the value of the first-neighbor Mn-Mn distance. On the other hand, the topological frustration in the Mn sublattice could contribute to an unusually strong magneto-structural coupling [1-5]. Recently, progress in high-pressure high-temperature synthesis offered the opportunity to study the magnetic and crystal structures of the same chemical compounds, having the same Mn-Mn distances, but different crystal structures: cubic or hexagonal. Our results show that topology plays a dominant role in the formation of the magnetic ordering (short-range or long-range) and also affects the transition from the localized to the magnetic itinerant state.

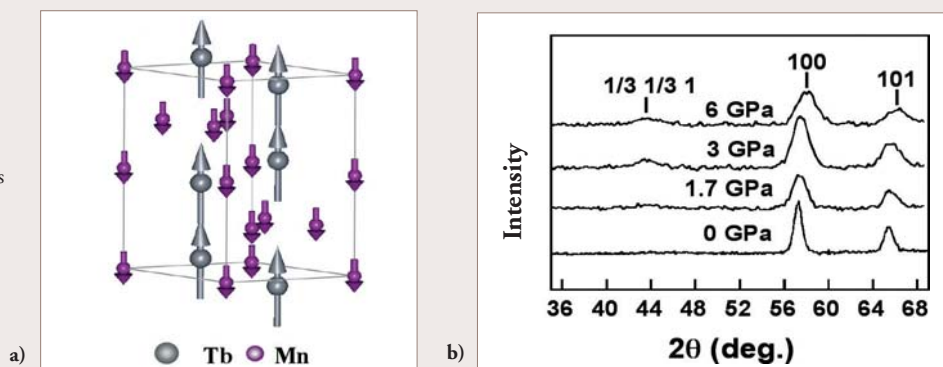
[1] I.N. Goncharenko et al Phys. Rev. B, **56**, 2580, (1997) ; [2] I.N. Goncharenko et al Phys. Rev. B, **59**, 9324, (1999)

[3] O.L. Makarova et al Phys. Rev. B, **66**, 104423, (2002) ; [4] O.L. Makarova et al Phys. Rev. B, **67**, 134418, (2003)

[5] O. L. Makarova et al Solid State Com., **132**, 329, (2004)

[Collaboration: O.L. Makarova, RRC « Kurchatov Institute », Moscow, Russia ; I.N. Goncharenko, I. Mirebeau, F. Bourée, LLB ; A.V. Tsvyaschenko, IHPP, Troitsk, Russia ; L.N. Fomicheva, IHPP, Troitsk, Russia]

**Figure:** a) Magnetic structure of the hexagonal hydride  $\text{TbMn}_2\text{H}_{2.9}$ .  
b) Magnetic neutron diffraction spectra of  $\text{TbMn}_2\text{D}_{2.9}$  measured at different pressures and  $T=1.4\text{K}$  at the G6.1 diffractometer. The presence of the  $(1/3\ 1/3\ 1)$  reflection indicates a pressure-induced long-range antiferromagnetic component.

**[C8. J. Cambedouzou] Tunable intertube spacing in single-walled carbon nanotubes**

The structure of ternary compounds made of alkali, tetrahydrofuran (THF) and single-walled carbon nanotubes (SWNT) have been investigated using the G6-1 powder diffractometer at LLB [1]. Hydrogen-deuterium substitution in THF allows a layered structure around the nanotubes to be determined. The important changes in the neutron diffraction profile of ternary compounds by comparison with pristine SWNT (figure a) can be understood and simulated assuming that the alkali cations form a monolayer surrounding each tube of the bundle, while THF molecules intercalate between the decorated tubes and at the surface of the bundles (figure b). The structural model we propose also allows to state that the vanishing of the diffraction feature at  $0.6\ \text{\AA}^{-1}$  in the  $\text{LiC}_{5.88}$ -TDF compound is integrally due to isotopic contrast effects, the structure of both hydrogenated and deuterated compounds remaining exactly the same. In spite of this insertion, the triangular bundle structure is preserved, albeit with a much larger lattice parameter, which depends on the size of the inserted cation.

[1] J. Cambedouzou et al., Phys. Rev. B 72 (2005), 041404(R)

[Collaboration : J. Cambedouzou, S. Rols, N. Bendiab, R. Almairac and J.L. Sauvajol (LCVN Montpellier), P. Petit and C. Mathis (ICS Strasbourg), I. Mirebeau (LLB Saclay), M. Johnson (ILL Grenoble)]

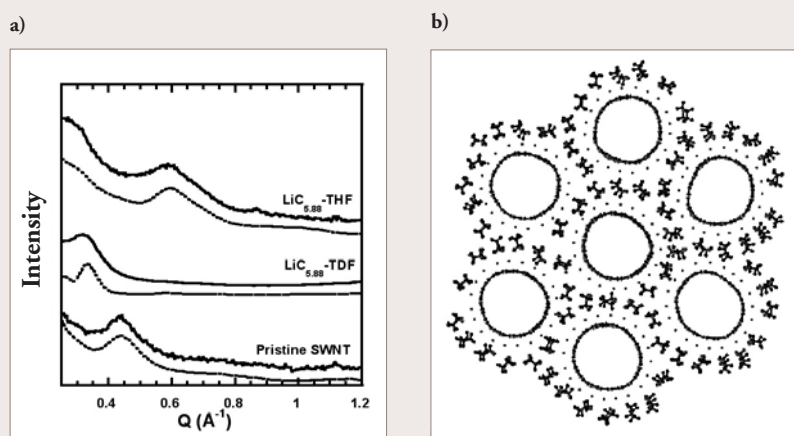


**Figure :** a) Experimental (plain lines) and calculated (dotted lines) neutron diffraction profiles of hydrogenated (top) and deuterated (center) ternary compounds, and pristine SWNT (bottom). b) Representation of a  $\text{LiC}_6$ -THF bundle of seven tubes.

**[C9. C. Doussier-Brochard] Magnetic structure of an antimony manganese chlorosulfide MnSbS<sub>2</sub>Cl**

Relatively to chalcogenides or halogenides, mixed compounds of the halogeno-chalcogenide type have been poorly studied up to now. Among them, quaternary compounds combining a transition metal *TM* with another cation are of special interest for their physical properties, due to the dilution of *TM* in the crystal matrix and the competition of the two types of cations versus the two ligands.

The crystal structure of MnSbS<sub>2</sub>Cl can be described as edge-sharing MnS<sub>4</sub>Cl<sub>2</sub> octahedra along the *b*-axis, and corner-sharing along the *a*-axis, forming waved layers separated by Bi atoms. The magnetic susceptibility versus temperature, shows a large maximum, around 39 K, characteristic of a low-dimensional anti-ferromagnetic behaviour, following by an increase at 27K.

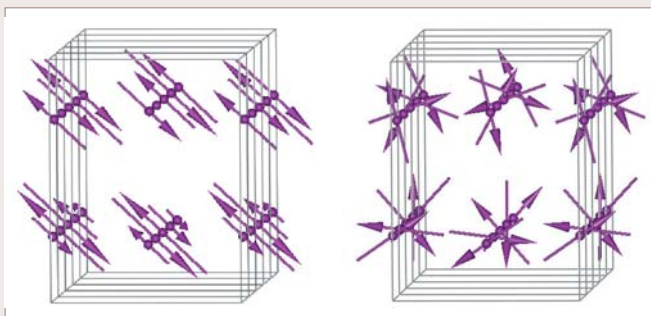
To elucidate this magnetic behaviour, powder neutron diffraction experiments were performed on the multi-detector G4.1 and allowed us to solve the magnetic structure and its thermal evolution [1]. Below T<sub>N</sub>=35 K, a complex 3D long-range antiferromagnetic ordering takes place, characterized by an incommensurate 1D propagation wave-vector along the *b*-axis, equal to  $k = [0, 0.3838, 0]$ . The Rietveld refinements give two possible modulation models, sinusoidal and helicoidal, with similar magnetic reliability factors and a moment of 4.5 μ<sub>B</sub> on Mn at 1.5 K.

MnSb<sub>2</sub>S<sub>4</sub> and MnPb<sub>4</sub>Sb<sub>6</sub>S<sub>14</sub>, which present chains of MnS<sub>4</sub> octahedra separated respectively by 6 and 16 Å, have been also studied to show the evolution of magnetic structure versus 2D or 1D organization [2].

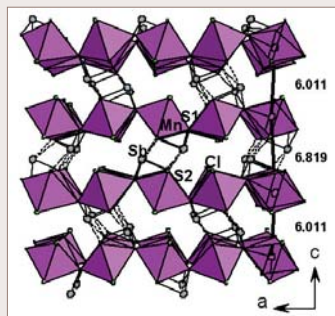
[1] C. Doussier, G. André, P. Léone, E. Janod, Y. Moëlo, Journal of Solid State Chemistry, 179 (2006) 486

[2] C. Doussier, thesis, Université de Nantes (2006)

[Collaboration : C. Doussier, P. Léone, E. Janod, Y. Moëlo Université de Nantes, G. André, LLB]



Magnetic structure with sinusoidal (left) or helicoidal (right) modulation



Crystal structure of MnSbS<sub>2</sub>Cl

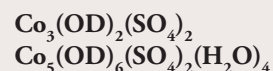
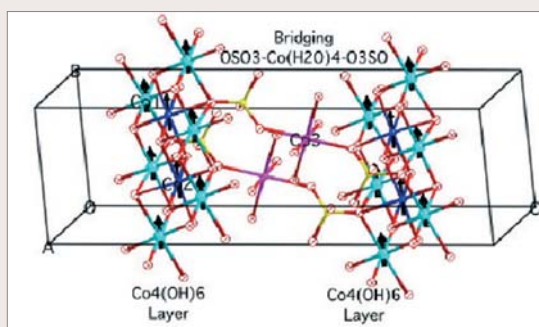
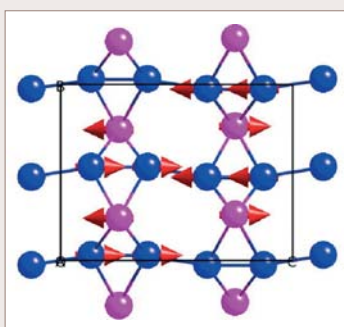
**[C10. S. Vilminot] Magnetic structures of the synthetic magnetic minerals based on hydroxysulfates of divalent metals, Co<sub>3</sub>(OD)<sub>2</sub>(SO<sub>4</sub>)<sub>2</sub>, Co<sub>5</sub>(OD)<sub>6</sub>(SO<sub>4</sub>)<sub>2</sub>(H<sub>2</sub>O)<sub>4</sub>, Cu<sub>4</sub>(OD)<sub>6</sub>SO<sub>4</sub>**

High-resolution (3T2) and high-flux (G4.1) neutron powder diffraction (NPD) data have been used to determine the nuclear and magnetic structures of a series of M<sup>II</sup>-hydroxysulfates, M = Mn, Co, Ni and Cu, as part of an ongoing project to understand short-range (SRO) and long-range (LRO) magnetic ordering and geometrical frustration caused by μ<sub>3</sub>-OH bridges. For the M<sub>3</sub>(OD)<sub>2</sub>(SO<sub>4</sub>)<sub>2</sub> series which are canted antiferromagnets [T<sub>N</sub> = 42 (Co), 26 (Mn) and 29 K (Ni)], the Ni exhibits collinear moments along *b* while for Co and Mn the moments lie in the *ac*-plane with a rare co-existence of SRO and LRO.[1]

Co<sub>5</sub>(OD)<sub>6</sub>(SO<sub>4</sub>)<sub>2</sub>(H<sub>2</sub>O)<sub>4</sub> consists of triangular Co<sup>II</sup>-OH layers pillared by ...O<sub>3</sub>SO-Co<sup>II</sup>(H<sub>2</sub>O)<sub>4</sub>-OSO<sub>3</sub>...and it behaves as a ferromagnet below 14 K.[2] Extensive magnetization by varying temperature, field and pressure and heat capacity measurements and NPD reveal an easy-plane XY-magnet where the moment of the pillaring Co remains random. Due to slight anisotropy in the layer the moments are oriented along *b*. These results demonstrate, for the first time, the existence of LRO in a single layer.

Cu<sub>4</sub>(OD)<sub>6</sub>SO<sub>4</sub> has a complex corrugated layered structure and it behaves as a canted AF. NPD was modelled with the moments oriented collinearly perpendicular to the corrugated planes with alternation along ±*a* for neighbouring chains within double chains building up the planes [3].

[Collaboration : S. Vilminot, IPCMS, Strasbourg; G. André, F. Bourée-Vigneron, LLB; M. Kurmoo, ULP, Strasbourg]



[1] M. Ben Salah *et al.*, Chem. Mater. 17 (2005) 2612-2621.

[2] M. Ben Salah *et al.*, J. Am. Chem. Soc. 128 (2006) 7972-7981.

[3] S. Vilminot *et al.*, Dalton Trans., (2006) 1455-1462.

## STRUCTURE AND PHASE TRANSITIONS

**[C.11. M. Giot] Magnetic structure of the charge ordered  $\text{Bi}_x\text{Ca}_{1-x}\text{MnO}_3$  manganites.**

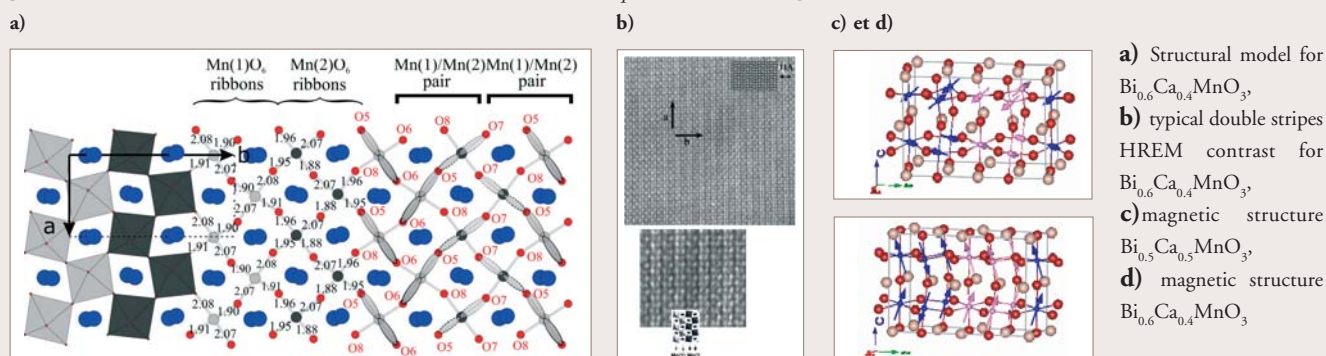
Within the thesis of M. Giot [1], crystals and polycrystalline sample were synthesized to study the magnetic and nuclear structure of the charge ordered  $\text{Bi}_x\text{Ca}_{1-x}\text{MnO}_3$   $0.5 \leq x \leq 0.64$  manganites. The “Zener polaron ordering” model based on the  $P2_1nm$  space group and the “classical  $\text{Mn}^{3+}/\text{Mn}^{4+}$  ordering” model based on  $P2_1/m$  space group were refined from single crystal X-Ray diffraction [2]. For the three crystals ( $x = 0.55, 0.60, 0.64$ ) the  $P2_1nm$  space group allowed the best fitting. A common model for the charge ordered structure (Fig. a) was proposed: the two Mn site have a valence equal to 3.5 and the structure consists on the alternation of double ribbons of  $\text{Mn}(1)\text{O}_6$  and  $\text{Mn}(2)\text{O}_6$  octahedra. The HREM images were well simulated with this model (Fig. b). The evolution of the anti-ferromagnetic structure with the Bi/Ca ratio study was performed on the powder diffractometer G4.1 at LLB. The data can be refined with different physical models, in particular the classical CE-type model is one of the solutions for  $\text{Bi}_x\text{Ca}_{1-x}\text{MnO}_3$  manganites with  $x = 0.5$  (Fig. c). The moments tend to establish a ferromagnetic coupling with increasing  $x$  (Fig. d).

[1] « Etudes structurales et magnétiques de manganites  $\text{Bi}_x\text{Ca}_{1-x}\text{MnO}_3$  présentant des mises en ordre complexes »

co-financed by CEA and Region BASSE-NORMANDIE : performed between LLB CEA Saclay and CRISMAT Caen.

[2] M. Giot et al Chem. Mat. 18 (14): 3225-3236 (2006).

[Collaborations : LLB, CRISMAT-Caen, M. Nevřiva and K. Knize-Czech Republic, P. Roussel-Lille]

**[C12. D. Bazin] Structural study of pathological calcification : the case of kidney stones**

Urolithiasis constitutes a serious health problem that affects 3 to 20% of the population. Calculi may be composed of various inorganic and/or organic compounds. Ca oxalate (70% of the cases), Ca and Mg phosphates (15%) and uric acid (10%) are the main common components. A site of initial crystallization has been described in the 1930's by Randall. Due to their contribution to the pathogenesis of calcium urinary stones, Randall's plaques (fig. 1) have been the subject of numerous researches. The aim of this study was to determine the structural characteristics of kidney stones which have similar chemical formula i.e. the carbonate apatite. Powder Neutron Diffraction (P.N.D.) indicates that apatite crystallites contain a very small number of units cells in which Ca and phosphate groups have the spatial arrangement of apatite (fig. 2). Moreover, a significant anisotropy in the morphology of these entities is observed. Then, these "nanobiocrystals" may constitute needles-like and finally spherical objects as observed by Scanning Electronic Microscopy (S.E.M.) (fig. 3). The complete set of data give thus major structural information on these biological entities which lead to an understanding of the first steps of the genesis of the Randall's plaques.

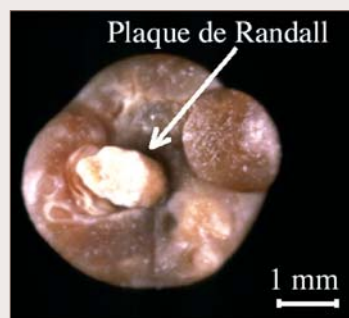


Figure 1. "Giant" Randall's plaque

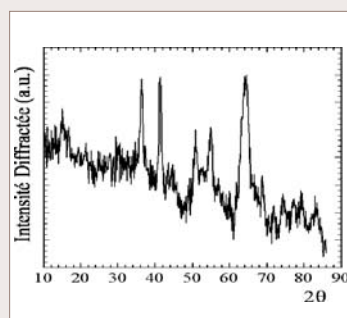


Figure 2. P.N.D. of an urinary stone

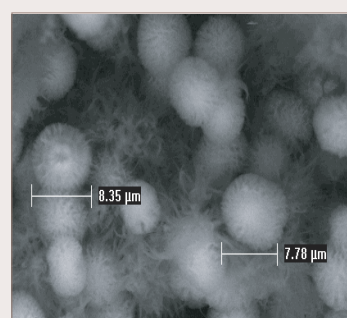


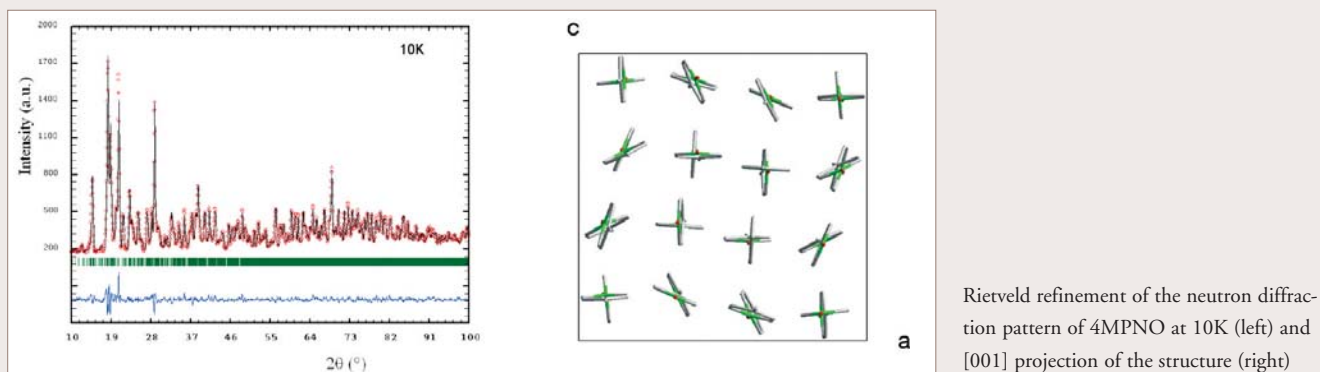
Figure 3. S.E.M. micrograph of an urinary stone

D. Bazin et al. Ann Biol Clin 2006 ; 64 (2) : 125-39. [Collaboration M. Daudon (AP-HP, Necker), D. Bazin (LPS), A. Mazouyes (Ecole Centrale Paris, LPS), P.A. Albouy, A. Thiaville, S. Rouzière, O. Stephan, A. Glotter (LPS), G. André, A. Cousson (LLB), E. Foy, P. Chevalier (Lab. P. Sue), G. Matzen, E. Veron (CRMHT), E. Elkaim, D. Thiaudiere (Soleil)].

**[C13. F. Damay] Synchrotron and neutron diffraction structural study of 4-methylpyridine-N-oxide (4MPNO) at 10K**  
 Combined synchrotron and neutron powder diffraction have been used to solve the structure of fully deuterated 4MPNO at 10 K. Using a simulated annealing algorithm on the synchrotron data, we were able to propose a structural model for 4MPNO, which involves a tetragonal cell with space group  $P4_1$  ( $a = b = 15.410(2)\text{\AA}$ ,  $c = 19.680(3)\text{\AA}$ ). This model gives an excellent fit to both sets of diffraction data (Figure 1, left), even though it is impossible to rule out entirely other molecular arrangements. In our model, the asymmetric unit contains 8 molecules exhibiting a complex pattern of reorientations around the three cell axes (Figure 1, right). Along  $c$ , two columns of roughly perpendicular molecules alternate with two columns of molecules tilted by about  $40^\circ$ . This pattern is actually reminiscent of a combination of the 250 K and 100 K structures of 4MPNO, respectively [1]. Moreover, in sharp contrast with the simpler structure of parent compound 4-methylpyridine (4MP) at 10 K, the fourfold symmetry for methyl pairs and the translational invariance of the methyl sites are destroyed, as the molecular site symmetry in  $P4_1$  is 1. The thermal ellipsoids calculated from the TLS matrix also show that the methyl groups are now largely localised. As a consequence, unlike 4MP, rotational dynamics in 4MPNO cannot be described by the quantum sine-Gordon model in 1D. Our results suggest two kinds of methyl-methyl interaction: along infinite chains parallel to  $a$  and  $b$  on the one hand, and between perpendicular chains through pairs of face to face methyl groups along  $c$  on the other [1].

[1] F. Damay et al, Acta Crystallogr. B 62, 627-633 (2006).

[Collaborations: F. Damay, A. Carretero-Genevri, A. Cousson, J. Rodriguez-Carvajal, LLB, F. Fillaux, LADIR, W. Van Beek, ESRF].



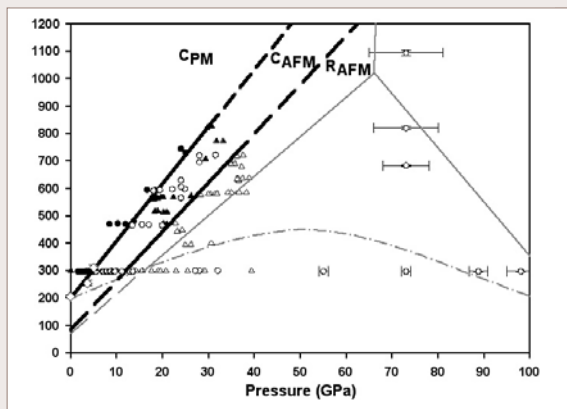
**[C14. L. S. Dubrovinsky] High-pressure magnetism in geophysically important materials FeO and MnO**

Magnetic ordering influences the density, bulk modulus, and elastic constants of materials. Developments of models of the Earth and analysis of the acoustic data, which provide the main experimental information on the Earth's interior, require direct information on magnetic properties of geophysical materials. Wüstite (FeO), the end-member of the magnesiowüstite MgO-FeO solid solution and the second abundant mineral in the Earth's lower mantle, is a good example of such a "geomaterial". Our combined Mössbauer, acoustic and neutron diffraction studies [1] show that the magnetic ordering temperature rapidly increases with pressure (Figure) and that pressure results in a considerable softening of the elastic modulus. The study established the existence of a magnetically ordered cubic phase of wüstite (Figure). This behavior differs from the other prototype antiferromagnetic oxide, MnO [2]. Below 3.5 GPa the magnetic ordering transition coincides with the structural transition, whereas at higher pressures the two transitions decouple, and the lattice distortion occurs at higher temperatures than the magnetic transition. Our results show that the structural transition (rhombohedral distortion) in transition metal monoxides is not directly coupled with the long-range magnetic ordering.

[1] A. P. Kantor, S. D. Jacobsen, I. K. Kantor, L. S. Dubrovinsky, C. A. Mc. Cammon, H. J. Reichman, I. N. Goncharenko, Phys. Rev. Lett. 93, 215502 (2004).

[2] A.P. Kantor, L. S. Dubrovinsky, N. A. Dubrovinskaia, I. Y. Kantor, I. Goncharenko, J Alloys Compounds 401, 42-45 (2005).

[Collaboration : L.S. Dubrovinsky, I.Yu. Kantor, A.P. Kantor, (Bayerisches Geoinstitut), N. A. Dubrovinskaia (Lehrstuhl für Kristallographie, Universität Bayreuth), I.N. Goncharenko (LLB)]



Phase diagram of non-stoichiometric wüstite. Black lines – phase boundaries between cubic paramagnetic ( $C_{PM}$ ), cubic antiferromagnetic ( $C_{AFM}$ ), and rhombohedral antiferromagnetic ( $R_{AFM}$ ) phases obtained in this study. Circles – Mössbauer spectroscopic runs: solid circles – paramagnetic phase, open circles – magnetically ordered phase. Triangles – X-ray diffraction studies: solid triangles – cubic phase, open triangles – rhombohedral phase. Diamonds are  $T_N$  values obtained from neutron diffraction studies. The structural phase boundary of Fei and Mao (Fei and Mao, 1994) and the magnetic phase boundary proposed by Badro et al. (Badro et al., 1999) are also shown for comparison in gray color. Letters C, R, and B8 designate cubic, rhombohedral and NiAs-like hexagonal phases, PM and AFM – paramagnetic and antiferromagnetic phases, respectively.







# SUPERCONDUCTIVITY AND MAGNETISM

# SUPERCONDUCTIVITY AND MAGNETISM

Over the years, neutron scattering has imposed itself as a prominent tool for studying the microscopic mechanisms of magnetism in solids. In the context of the emergence of powerful new techniques such as real-space imaging, high-field NMR, or magnetic x-ray scattering, its contribution remains central because, as problems of growing complexity can be tackled, it becomes essential to fully exploit complementarities between different probes. Indeed, the installation of the new synchrotron source SOLEIL in the close neighborhood of LLB is stimulating projects for future collaborations in the field of magnetism. The comparison of spin and charge excitation spectra, for example, can be expected to be one of the keys to understanding the properties of strongly correlated electrons and the occurrence of unconventional superconductivity. Even before the first x-ray beams have been produced, two joint LLB-SOLEIL workshops in this field, *Magnetism and Nanostructures* (May 2005) and *Strongly Correlated Electrons* (June 2006), have already been held.

This part of the Report describes recent neutron work of magnetism and superconductivity in different classes of materials, from transition-metal oxides and lanthanide compounds with strong electron correlations to frustrated magnetic systems, molecular magnets and photomagnetism (other aspects of magnetism, more closely related to structures or phase transitions, are covered in the corresponding chapter). After giving an overview of the salient results, and placing them in perspective with the current trends of research in each field, selected studies are presented in the form of self-contained “highlights”, followed by shorter contributions (“clips”) intended to give a snapshot at one particularly interesting piece of data.

Whereas a majority of these results have been obtained on the pool of neutron spectrometers available in Saclay, a growing number of LLB scientists frequently carry out experiments on other neutron sources (ILL, FRMII, ISIS, PSI, NIST, etc.) as part of their own research programs, in order to make optimal use of the specificities of each instrument.

## A - Strongly correlated electrons

Several families of  $3d$  element oxides are known to exhibit most unusual electronic and magnetic properties, among which “colossal” magnetoresistance (CMR) in manganites or unconventional superconductivity in quasi-2D systems such as in high- $T_c$  cuprates, ruthenates or hydrated cobaltates. In all these systems, strong electronic correlations, as well as the complex interplay between different degrees of freedom (charge, spin, orbital moment, lattice vibrations,...) seem to play a crucial role. Neutron scattering techniques are unique in their ability to reveal spin or orbital magnetic order, to measure spin excitation spectra, or to trace anomalies in lattice dynamics. It is therefore no surprise that the properties of those systems, either static or dynamic, constitute one of the most active fields of research at LLB, like in many other neutron centers.

Heterogeneity in charge distributions, such as charge segregation or charge ordering, is one of the key aspects for understanding the new properties of several families of oxides exhibiting colossal magnetoresistance (CMR), “stripe” structures, etc. In other systems, like  $\text{Sr}_2\text{RuO}_4$ , the electronic and magnetic properties are more indicative of a homogeneous charge distribution (itinerant models), but strong correlations among the carriers remain central to their low-temperature properties, including superconductivity. In the case of high- $T_c$  cuprates, the validity of approaches based on stripes or, alternatively, on a homogeneous itinerant spin-exciton picture, remains controversial. Important new results make it possible to assess the implications of each model in greater detail. Studies on oxides with exotic electronic properties reinforce the interest for the physics taking place close to quantum critical points, which has long been a recurrent question in heavy-fermion systems. The comparison of properties in electron- and hole-doped cuprates is an important aspect of this problem. In relation with the central role played by orbital order in transition metal oxides, quadrupolar degrees of freedom of  $4f$  electron states are now being recognized as a main source of novel physical phenomena in rare-earth compounds, among which a number of unconventional long-range order and fluctuations, possibly providing a novel route to superconductivity.

It is worth noting that many of the studies described in this section concern new compounds, for which the possibility to work on large, high-quality single crystals has been crucial. This clearly reflects the key role assumed by material synthesis and crystal growth, and emphasizes the urgent need to reinforce those activities as a basis for the development of forefront programs in solid-state physics at neutron sources and other large facilities.

### INHOMOGENEOUS CHARGE STATES : FROM MANGANITES TO CUPRATES

In the 3D manganites  $\text{La}_{1-x}(\text{Sr,Ca})_x\text{MnO}_3$ , recent measurements have brought to light the existence of nanoscopic ferromagnetic platelets, which, as can be deduced from their anisotropic coupling, are associated with a low hole density. The magnetic excitations in these nano-objects take the form of stationary waves, which have been observed by inelastic neutron scattering [H4, S. Petit]. For the particular composition  $x = 1/8$  and for  $x = 0.15$ , these ferromagnetic clusters become self-organized, leading to a rearrangement of both spin and charge textures. The evolution of the platelets through the metal-insulator transition occurring at  $x = 0.175$  is still under study.

## SUPERCONDUCTIVITY AND MAGNETISM

Replacing La by Pr in  $\text{Pr}_{1-x}\text{Ca}_x\text{MnO}_3$  suppresses the ferromagnetic metallic region in the phase diagram, so that the compound remains insulating at all  $x$ . There, the interesting evolution is that observed under an applied field of a few tesla, which restores a metallic state. Quantitative analysis of small-angle magnetic neutron scattering in CMR  $\text{Pr}_{1-x}\text{Ca}_x\text{MnO}_3$  crystals (for  $x$  near 0.33) has shown that the magnetic heterogeneities take place at different scales (thesis of D. Sorel, Crismat–LLB)<sup>[1]</sup>. Applying a field close to the value where the CMR effect is observed causes mesoscopic (200 nm) inhomogeneities of (conducting) ferromagnetic phase to grow within the insulating phase. Nanoscopic inhomogeneities are also present (both as small ferromagnetic clusters inside the antiferromagnetic (AFI) phase and as small *paramagnetic* ones inside the ferromagnetic phase), but they do not exhibit any change under the application of the field.

In the layer compound  $\text{La}_{2-x}\text{Sr}_x\text{MnO}_4$  [H5, D. Senff], which does not exhibit giant magnetoresistance properties and remains insulating, a complex spin excitation spectrum has been observed close to the concentration  $x = 1/2$ . It can be perfectly described by the appearance of zigzag charge lines, resulting from the competition between spin and charge degrees of freedom. The appearance of coupled spin and charge arrangement into stripes has been recognized for quite a long time in another layered system,  $\text{La}_{2-x}\text{Sr}_x\text{NiO}_4$ . In order to achieve a better understanding of the different parameters controlling spin and charge ordering, neutron scattering studies have been extended to isostructural systems with different transition metals, for instance  $\text{La}_{2-x}\text{Sr}_x\text{CoO}_4$  (Ph. D. thesis of M. Zwick, Univ. Cologne).

It has been proposed that stripes could also play a crucial role in the anomalous electronic properties of high-temperature superconductors. There is experimental evidence, based on neutron studies, that static stripes can indeed exist in  $\text{La}_{2-x}\text{Ba}_x\text{CuO}_4$  close to  $x = 1/8$ . Since lattice vibrations involving oxygen atoms can be extremely sensitive to the formation of charge lines, neutron scattering has been used to track phonons anomalies in order to reveal the existence of stripes. Evidence has indeed been found for a softening of the Cu–O bond-stretching mode in the latter compound, but also in superconducting  $\text{La}_{2-x}(\text{Ba},\text{Sr})_x\text{CuO}_4$  and  $\text{YBa}_2\text{Cu}_3\text{O}_{6+x}$ . This result suggests the possible existence of *dynamic* stripes, which might be essential to the physics of cuprates and to their superconductivity [H3, D. Reznik].

## ITINERANT VIEW OF UNCONVENTIONAL SUPERCONDUCTORS, QUANTUM CRITICALITY, HIDDEN ORDER

In  $\text{Sr}_2\text{RuO}_4$ , a superconducting compound isostructural to  $\text{La}_{2-x}\text{Sr}_x\text{CuO}_4$ , itinerant magnetic models can capture the main characteristics of the spin excitation spectra. Recent inelastic neutron scattering measurements have therefore focused on a quantitative description of the spin susceptibility, which can then be implemented into spin-exchange models proposed to account for *p*-wave superconductivity in this system (Ph. D. thesis of P. Steffens, Univ. of Cologne).

Unusual spin-triplet collective excitations developing only in the superconducting state of high- $T_c$  cuprates have raised a great deal of interest. Recent inelastic neutron scattering studies of the dispersion of these modes (Ph. D. thesis of S. Pailhès, LLB) and their anisotropy (thesis of V. Hinkov, MPI Stuttgart) suggest that they have mainly quasi-2D character — aside from an energy-dependent 1D anisotropy, and can be quite well described as a triplet spin exciton. This picture implies a homogeneous electronic liquid, in contrast to the alternative (inhomogeneous) stripe picture also proposed to account for the physics of cuprates. Quantitative theoretical calculations carried out by F. Onufrieva and P. Pfeuty using Eliashberg equations, try to precisely estimate the role played by those collective modes in the appearance of unconventional superconductivity.<sup>[2]</sup>

The phase diagram of superconducting cuprates, plotted as a function of charge density, is asymmetric with respect to electron and hole doping. It has been theoretically argued that this asymmetry could correspond to the existence of two topological quantum critical points (QCPs).<sup>[2]</sup> Neutron scattering measurements on electron-doped cuprates  $(\text{Nd},\text{Ce})_2\text{CuO}_4$  indicate that the spin gap closes linearly in applied magnetic fields, without the appearance of in-gap states, at variance with the behavior reported for hole-doped materials [H2, E. M. Motoyama].

From a more general point of view, when the QCP corresponds to the end point of an ordered phase, the strong fluctuations associated with the broken symmetry of the ordered phase could be responsible for anomalous electronic properties. This idea, commonly used in connection with superconducting heavy-fermion systems, has also been proposed to be applicable to high-temperature superconductivity. Recently, polarized neutron experiments (thesis of B. Fauqué, LLB) carried out in the elusive pseudo-gap phase of cuprates, have shown that this phase is actually characterized by long-range magnetic order, which may be associated with an array of circulating currents [H1, B. Fauqué]. Interestingly, this circulating-current phase may disappear close to the doping level where the superconducting temperature is maximum.

When superconductivity develops close to a QCP, the appearance of the associated ordered phase can also turn out to be detrimental to superconductivity. The compound  $\text{Sr}_2\text{RuO}_4$  is known to be close to a quantum critical point, which can be

approached by Ti substitution (thesis of O. Schuman, Univ. of Cologne). Neutron scattering has been used to study how the magnetic order is stabilized around the impurity, but the observed order does not seem to play the leading role in the superconducting pairing. In the isoelectronic compound  $(\text{Sr,Ca})_2\text{RuO}_4$ , the substitution of Ca for Sr, leads to a tilt and a rotation of the oxygen octahedra, which are accompanied by a re-organization of the electronic structure. Inelastic neutron scattering studies are crucial here because, by tracing changes in the spin excitation spectrum, they can reveal how the evolution of the electronic band structure relates to the appearance of metamagnetism and provide useful insight into the new class of QCP, known as “metamagnetic QCP” or “magnetically tuned QCP”, which has recently been suggested for the bilayer compound  $\text{Sr}_3\text{Ru}_2\text{O}_7$ .

## QUADRUPOLAR PHENOMENA IN F-ELECTRON SYSTEMS

Neutron diffraction results on light-rare-earth hexaboride alloys ( $\text{Ce}_x\text{Pr}_{1-x}\text{B}_6$  and  $\text{Ce}_x\text{Nd}_{1-x}\text{B}_6$ ) reflect the effects of competing interactions between atoms carrying different types of quadrupole moments, while shedding light on the complex pattern of commensurate and incommensurate structures occurring in an applied magnetic field. Comparison of the neutron data with synchrotron results obtained in Japan on the same materials gives a clue to separating the dependences of magnetic and quadrupole order parameters [H6, J.-M. Mignot]. This work will be extended to alloys with different compositions, as well as to compounds from the skutterudite family, in which even more exotic (hexadecapole) order parameters have been conjectured.

## B - Frustrated magnetism

Geometrically frustrated magnetism is characterized, in a classical approach, by a highly degenerate ground state. It gives rise to unusual phase transitions and exotic spin excitations from a novel ground state, whose study by elastic and inelastic neutron scattering is essential for testing theoretical models.

The simplest example of a frustrated magnet is the Ising triangular antiferromagnet, a good realization of which is provided by  $\text{CuFeO}_2$  (N. Terada, Tokyo Univ. of Science, with A. Gukasov and D. Petitgrand, LLB). The magnetic excitation spectra have been determined in the low-temperature commensurate phase of this compound, where they were found to consist of three branches with a gap, as well as in the “partially disordered” incommensurate state at intermediate temperatures. One to two per cent aluminum doping in  $\text{CuFeFe}_{1-x}\text{Al}_x\text{O}_2$  produces a total of four different new phases depending on temperature. Simultaneously magnetic excitations show a dramatic change with the appearance of a new gapless branch. The next step will be to study the effects of magnetic fields on both magnetic structures and magnetic excitations.

A more involved case of geometric frustration is found in the highly-frustrated 2D Kagome-lattice systems, exemplified by Nd-langasite ( $\text{Nd}_3\text{Ga}_5\text{SiO}_{14}$ ). This compound is a good candidate in the search for a spin-liquid state because no magnetic order is found down to 1.5 K despite the existence of strong antiferromagnetic fluctuations. The broad, slightly dispersive excitation around 1 meV observed by a team from Grenoble [3] in triple-axis experiments is in qualitative agreement with theoretical calculations for a classical Heisenberg antiferromagnet on a Kagome lattice. Future studies will be extended to related systems like  $\text{Pr}_3\text{Ga}_5\text{SiO}_{14}$ . “Buckled” Kagome lattices, where a lifting of the ground state degeneracy is expected to take place as a result of the distortion, provide an elegant example of order from subleading interactions in a highly frustrated system. In the staircase-distorted 2D Kagome lattice  $\text{Ni}_3\text{V}_2\text{O}_8$ , no less than four different ordered magnetic phases (two incommensurate and two commensurate) have been reported to occur below 9 K. Single-crystal experiments have now succeeded in identifying three nearly non-dispersive magnetic excitation modes below 1.5 THz in the lowest commensurate phase (thesis of N. Wilson, Univ. of Warwick).

## C - Molecule-based magnetism and photomagnetism

In the field of molecule-based magnetism, classical spin-density studies of the ground state of paramagnetic molecules based on flipping-ratio polarized-neutron measurements are still in high demand. Progress in neutron instrumentation opens unmatched opportunities for studying novel effects in photomagnetism

Recently, experiments have been devoted to an asymmetric end-to-end azido double-bridged Cu(II) dinuclear complex [C4, C. Aronica] and that of an AF bidimensional Mn(II) compound in the paramagnetic phase [C5, J. Manson]. This work has been supplemented by a thorough investigation of the magnetic phase diagram of this compound in an external magnetic field. A very original application of this same technique is demonstrated in the mapping of spin-redistribution due to quantum entanglement in a pure organic magnet (spin tetramer) [H7, A. Zheludev].

Progress made in photomagnetism encompasses the first successful observation of a photoexcited state by neutron powder diffraction on a FeII spin-crossover system [C6, A. Goujon]. Future evolutions of this experimental approach will strongly depend on its applicability to compounds displaying strong photoabsorption. Different possibilities to overcome this problem are now being tested.

It is generally accepted, on the basis of static susceptibility and XANES absorption results, that the photoinduced and thermally quenched high-spin (HS) states are nearly the same. Therefore, the study of thermally quenched states makes it possible to anticipate the properties of the photoinduced HS state. In the thermally quenched state of the (Co-Fe) Prussian-blue analogue and in  $(\text{Co}^{\text{III}}, \text{W}^{\text{VI}})$  octacyanotungstate, SQUID magnetization measurements suggest the existence of magnetic order.

## SUPERCONDUCTIVITY AND MAGNETISM

Neutron diffraction measurements have been carried out in both phases but no evidence for a magnetic order could be found. On the other hand, recent measurements on  $[\text{Fe}(\text{ptz})_6(\text{BF}_4)_2]$  under pressure<sup>[4]</sup> have evidenced that the ferroelastic transition can be dissociated from the spin transition, with the appearance of a new intermediate distorted high-spin state.

New insight in photoexcitation processes in spin-crossover systems has been gained from single-crystal Laue neutron diffraction measurements performed at the ILL. The results demonstrate a gradual homogeneous photoexcitation of  $\text{Fe}^{II}$  ions under light irradiation at low temperature, in contrast to the nucleation and growth of high-spin domains (denoted “like-spin”), implying a coexistence between the LS and HS phases [C7, A. Goujon]. Further studies of the photo-transformation process and of the subsequent relaxation in a single crystal close to the light-induced instability are now in progress.

Rapid developments can be expected in the next few years as a result of the enhanced data acquisition rates provided by the freshly renovated SUPER-6T2 neutron diffractometer [Instrumentation –H1, A. Gukasov]. Photoexcitation effects will be observable with greatly improved sensitivity, making it possible to address the conditions of the nucleation and growth process at the initial stage of the separation into like-spin phases. More generally, enhanced data collection speed for very small samples will open up new perspectives for powder and single-crystal diffraction on this instrument.

## D - Magnetic surface scattering

The LLB offers a large panel of surface scattering techniques, which users can combine in order to fit their needs. Even more flexible experimental conditions are expected from the implementation of new sample environments.

Studies of magnetic thin films structures have expanded tremendously over the last decade, encompassing an ever-growing variety of materials, from 3d metals (Fe, Co, Ni) and oxides (manganites, ferrites) to semiconductors (GaMnAs, ZnO:Co) and rare-earth elements (Dy, Er, etc.). Polarized neutron reflectivity is applied routinely in experiments on PRISM. Small angle scattering is used both in a normal scattering geometry (regular SANS) or at grazing incidence (PAPYRUS). Magnetic diffraction studies can also be performed on films down to 20 nm in thickness, using either unpolarized (3T1, 4F1) or polarized (6T2) neutron beams.

In the last two years, about twelve studies have benefited from such combined measurements. The topics were quite diverse: effects of epitaxial strains, modified or suppressed magnetic order in thin films, magnetization surface effects, magnetic micro-structures and nanostructures, etc. Materials studied include MnAs thin films, in which there is a coexistence of ferromagnetic and paramagnetic phases [C11, V. Garcia], multiferroic materials such as  $\text{BiFeO}_3$ , exhibiting both ferromagnetic and ferroelectric properties (H. Béa, CNRS/Thalès, Palaiseau), ultrashort-period Fe/Co superlattices (M. Bjork and G. Andersson, University of Uppsala), FePt/FePt films mixing in-plane and normal-to-plane materials (W. Szuszkiewicz, Polish Acad. of Sciences), and  $[\text{YBCO/LSMO}]_n$  superlattices for probing the interaction between magnetic and superconducting materials (G. Beutier, CEA/Grenoble).

The above measurements do not require any special sample preparation, nor extensive measuring times, and can now be performed routinely. On the other hand, inelastic scattering measurements in thin films, whose feasibility was demonstrated previously,<sup>[5]</sup> remain restricted to very specific samples. In the future, efforts will focus on increasing the versatility of the spectrometers, as well as improving the sample environments provided to users. A new polarizing bender is presently being installed on 4F1 in response to requests for polarized neutron diffraction measurements. For reflectivity and SANS, new technological materials, with  $T_c$  much in excess of 300 K, will require high-temperature studies. We therefore plan to implement a new device allowing magnetic fields above 1 T to be applied at temperatures up to 400°C. A dedicated magnet system capable of producing fields of several kilogauss for diffraction experiments would also be desirable.

[1] Co-funded by the CEA and the “Région Basse-Normandie”.

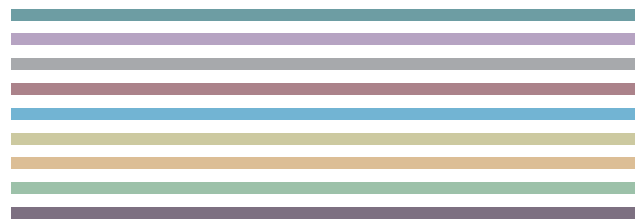
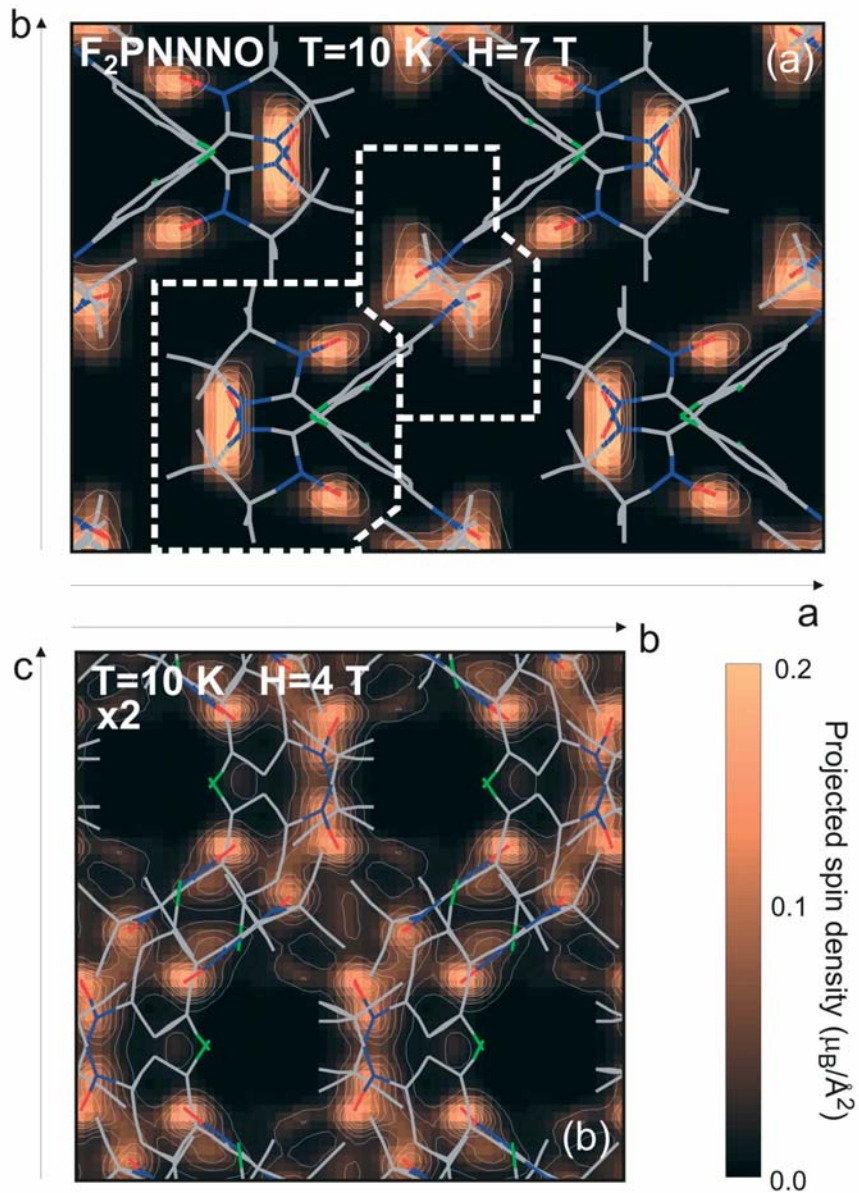
[2] Chapter “Theory” in this report

[3] R. Balou, J. Robert, V. Simonet, B. Canals, Laboratoire Louis Néel, CNRS Grenoble, K. Marty, P. Bordet, Laboratoire de Cristallographie, CNRS Grenoble, with D. Petitgrand, LLB.

[4] M.-H. Lemée-Cailleau, C. Ecolivet, B. Ouladdiaf, F. Moussa, J. Jetic, J. F. Létard, International Conference on Magnetism ICM'2006, J. Magn. Magn. Mater., in press.

[5] LLB Scientific Report 2003-2004.

# SUPERCONDUCTIVITY AND MAGNETISM



## SUPERCONDUCTIVITY AND MAGNETISM

- H1. Magnetic order in the pseudogap phase of high- $T_c$  superconductors**  
B. Fauqué, Y. Sidis, V. Hinkov, S. Pailhès, C.T. Lin, X. Chaud, Ph. Bourges
- H2. Spin-gap Closing under magnetic field in the electron doped high- $T_c$  superconductor**  
E.M. Motoyama, D. Petitgrand, M. Greven
- H3. Bond-stretching phonon anomaly reflecting dynamic charge inhomogeneity in copper-oxide superconductors**  
D. Reznik, L. Pintschovius, M. Ito, S. Iikubo, M. Sato, H. Goka, M. Fujita, K. Yamada, G. D. Gu, J.M. Tranquada
- H4. A 2D stripe superstructure revealed by spin waves in cubic ferromagnetic  $\text{La}_{1-x}\text{Sr}_x\text{MnO}_3$  ( $x = 0.125$  and  $x = 0.15$ )**  
S. Petit, M. Hennion, F. Moussa, P. Reutler, A. Revcolevskii, Y. M. Mukovskii
- H5. Spin-wave dispersion in orbitally ordered  $\text{La}_{0.5}\text{Sr}_{1.5}\text{MnO}_4$**   
D. Senff, F. Krüger, S. Scheidl, M. Benomar, Y. Sidis, F. Demmel, M. Braden
- H6. Competing order parameters in light-rare-earth hexaborides**  
J.-M. Mignot, G. André, M. Sera, and F. Iga
- H7. Spin redistribution by entanglement in an organic magnet**  
A. Zheludev, V. O. Garlea, S. Nishihara, Y. Hosokoshi, A. Cousson, A. Gukasov, K. Inoue

**[C1. S. P. Bayrakci]**Magnetic Ordering and SpinWaves in  $\text{Na}_{0.82}\text{CoO}_2$ **[C2. O. Mentré]**Spin gap in the one-dimensional  $S = 1/2$  spin-ladder compound  $\text{Bi}_2\text{Cu}(\text{P}_{1-x}\text{V}_x)\text{O}_6$ **[C3. S.M. Yusuf]**Two- and three-dimensional magnetic ordering in the bilayer manganite  $\text{Ca}_{2.5}\text{Sr}_{0.5}\text{GaMn}_2\text{O}_8$ **[C4. C. Aronica]**

Ferromagnetic Interaction in an Asymmetric End-to-End Azido Double-Bridged Copper(II) Dinuclear Complex

**[C5. J. Manson]**Neutron diffraction study of a molecule-based 2-dimensional magnetic compound  $\text{Mn}(\text{dca})^2(\text{pym})(\text{H}_2\text{O})$ : spin density and magnetic phase diagram.**[C.6. A. Goujon]**

Photoswitchable molecular compounds studied by neutron powder diffraction

**[C7. A. Goujon]**Neutron Laue diffraction on the spin crossover crystal  $[\text{Fe}(\text{ptz})_6](\text{BF}_4)_2$  showing continuous photo-induced transformation**[C8. A. Tamion]**

Magnetization depth profile of (Fe/Dy) multilayers

**[C9. M. Delalande]**

Polarized SANS studies of FePt Magnetic Nanoparticles.

**[C10. G. Viau]**

Small Angle polarised neutrons studies of dispersed magnetic Co-Ni nanowires

**[C11. V. Garcia]**

Magneto-structural phase transition in MnAs epilayers grown on GaAs(111)B substrates

# H1. MAGNETIC ORDER IN THE PSEUDOGAP PHASE OF HIGH-TC SUPERCONDUCTORS

B. FAUQUÉ<sup>1</sup>, Y. SIDIS<sup>1</sup>, V. HINKOV<sup>2</sup>, S. PAILHÈS<sup>1,3</sup>, C.T. LIN<sup>2</sup>, X. CHAUD<sup>4</sup>, PH. BOURGES<sup>1</sup>

<sup>1</sup> Laboratoire Léon Brillouin, CEA-CNRS, CEA/Saclay, 91191 Gif sur Yvette, France

<sup>2</sup> MPI für Festkörperforschung, Heisenbergstr. 1, 70569 Stuttgart, Germany

<sup>3</sup> LNS, ETH Zurich and Paul Scherrer Institute, CH-5232 Villigen PSI, Switzerland

<sup>4</sup> CRETA/CNRS, 25 Avenue des Martyrs, BP 166, 38042 Grenoble cedex 9, France.

In the optimally doped and underdoped regimes, high- $T_c$  copper oxide superconductors (SC) exhibit a pseudogap state with anomalous magnetic, transport, thermo-dynamic, and optical properties below a temperature,  $T^*$ , which is large in comparison to the superconducting transition temperature,  $T_c$ . The origin of the pseudogap is a challenging issue as it might eventually lead to identify the superconducting mechanism. Two major classes of theoretical models attempt to describe the pseudogap state: in the first case, it represents a precursor of the superconducting  $d$ -wave gap with preformed pairs below  $T^*$ , which would acquire phase coherence below  $T_c$ . In a second approach, the pseudogap is associated either with an ordered or with a disordered phase competing with the SC state. The order parameter associated with these competing phases may involve charge- and spin- density waves, or charge currents flowing around the  $\text{CuO}_2$  square lattice, such as D-charge density wave (DDW) or orbital circulating currents (CC) as proposed by C. M. Varma [1].

Most of the above phases break the translation symmetry of the lattice (TSL). Therefore, they may induce charge, nuclear or magnetic superstructures that can be probed by neutron or x-ray diffraction techniques. In contrast, the novel CC phases preserve the TSL as they correspond to 4 or 2 current loops per unit cell [1]. The charge currents could be identified by virtue of the pattern of ordered orbital magnetic moments pointing perpendicularly to the  $\text{CuO}_2$  planes (*i.e.*, along  $c^*$ ). These orbital magnetic moments should be detectable by neutron diffraction. Although the TSL is preserved, the magnetic signature of the CC phase does not reduce to ferromagnetism: the loops are staggered within each unit cell which corresponds to a zero magnetic propagation wavevector,  $\mathbf{Q} = 0$ , but with no net magnetization. In neutron diffraction, the magnetic intensity is superimposed on the nuclear Bragg peak, meaning that these experiments are very delicate as the magnetic intensity, proportional to the squared magnetic moment  $M^2$ , is expected to be very small as compared to the nuclear Bragg intensity. In order to detect this hidden magnetic response, polarized neutron experiments, which allow us to separate magnetic and nuclear cross sections, are therefore required.

Motivated by this theoretical work, we have studied the possibility of a magnetic order associated to these circulating current phases. Polarized neutron measurements were performed on the triple-axis spectrometer 4F1, using full polarization analysis. We have reported the first successful observation of a magnetic order in the pseudogap state of the cuprate  $\text{YBa}_2\text{Cu}_3\text{O}_{6+x}$  [2]. Since this type of phase does not break the translational symmetry, the magnetic contribution occurs only on top of the nuclear Bragg peaks, and we thus measured the magnetic signal on the weakest Bragg peak: the (011) reflection provides the best compromise between the magnetic scattering amplitude and the leakage of the Bragg scattering into the spin-flip channel. For the neutron polarization  $\mathbf{P} // \mathbf{Q}$ , where one expects the magnetic scattering to be strongest, the spin-flip (SF) intensity increases notably at low temperature, in contrast of the non-spin-flip (NSF) intensity which is essentially flat (Fig. 1). To assess the reproducibility of our observation, we have studied a large variety of samples from the underdoped part of the phase diagram of the high- $T_c$  compound family  $\text{YBa}_2\text{Cu}_3\text{O}_{6+x}$  with  $T_c$  ranging from to 54 K in underdoped samples to 75 K in an overdoped sample.

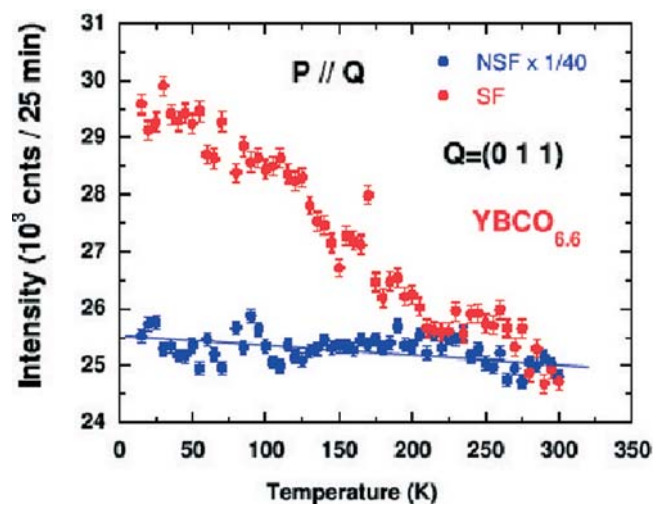


**Figure 1.** Raw polarized-neutron intensity : the full red points show the spin-flip (SF) scattering and the blue ones the non-spin-flip (NSF) scattering. A signal occurs below  $\oplus 220$  K only in the SF channel.

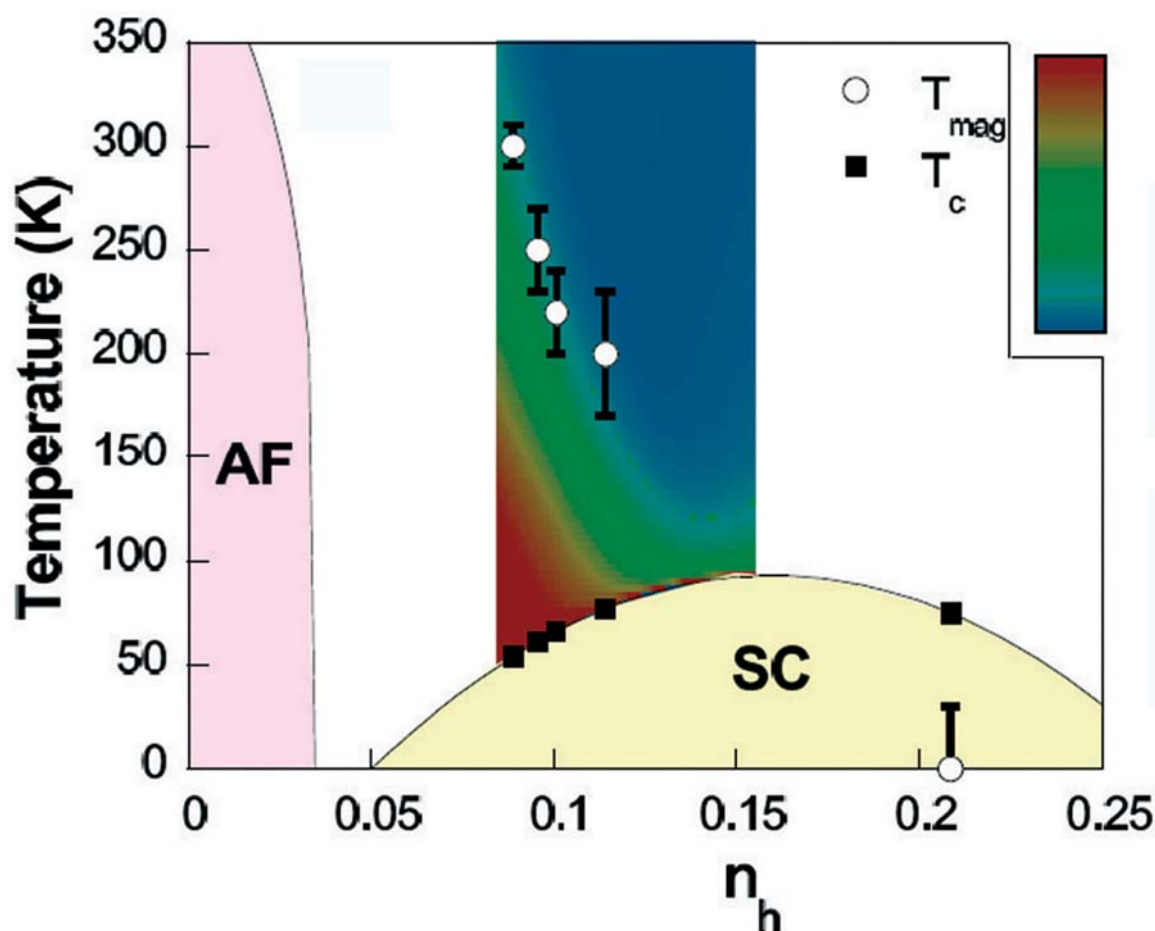


**Figure 2.** High- $T_c$  phase diagram as a function of the hole doping. The coloured area (blue=0) shows the pseudogap phase as measured by resistivity.  $T_{\text{mag}}$  is the temperature where the magnetic order occurs.

The results demonstrate the appearance of a magnetic scattering in the SF channel below a temperature  $T_{\text{mag}}$ , that matches quite well the pseudogap temperature  $T^*$  as defined by the resistivity measurement (Fig. 2). The magnitude of the observed signal changes with the neutron polarization as is expected for a magnetic intensity. This definitively rules out any experimental artefact.

The typical cross section of the magnetic order is  $\oplus 10^{-4}$  of the strongest Bragg peaks. This explains why such a magnetic order was not detected before using unpolarized neutron diffraction. Using the observed magnetic cross section and assuming a weakly momentum-dependent form factor, one can deduce a typical magnitude for the ordered magnetic moment of about 0.05 to 0.1  $\mu_B$ , with a moment decreasing with increasing doping. This is about the magnitude expected from current loops in the CC phase. However, such an orbital moment is expected to lie perpendicular to the  $\text{CuO}_2$  planes, whereas, in our case, the moments are not purely along the  $c^*$  axis. Combining the data for all measured

polarizations in the different samples, one can estimate the mean angle between the direction of the moments (assumed to be collinear) and the  $c^*$  axis to be  $\approx 45^\circ \pm 20^\circ$ , valid for all samples. In summary, we have reported the first signature of an unusual magnetic order in several  $\text{YBa}_2\text{Cu}_3\text{O}_{6+x}$  samples matching the pseudogap behaviour in underdoped high- $T_c$  cuprates [2]. Such an observation points towards the existence of a hidden order parameter for the pseudogap phase in high- $T_c$  superconductors. Importantly, our experiment reveals a 3D long-range order which does not break the translational symmetry of the lattice and, therefore, implies a decoration of the unit cell with staggered spin or orbital moments. The symmetry of the observed order corresponds to that expected for orbital moments associated with a circulating current state [1].

[1] C.M. Varma, Phys. Rev. B 55, 14554 (1997); *ibid.* 73, 155113 (2006).

[2] B. Fauqué et al, Phys. Rev. Lett. 96, 197001 (2006).

# H2. SPIN-GAP CLOSING UNDER MAGNETIC FIELD IN THE ELECTRON-DOPED HIGH-TC SUPERCONDUCTOR: $\text{Nd}_{1.85}\text{Ce}_{0.15}\text{CuO}_4$

E.M. MOTOYAMA<sup>1</sup>, D. PETITGRAND<sup>2</sup>, M. GREVEN<sup>1</sup>

<sup>1</sup> Department of Physics, Stanford University, Stanford, California 94305, USA

<sup>2</sup> Laboratoire Léon Brillouin (CEA-CNRS), CEA/Saclay, 91191 Gif sur Yvette Cedex

Understanding the nature of superconductivity in high- $T_c$  superconductors requires the characterization of the various phases (antiferromagnetic insulating, spin-density wave, charge-density wave...) that may compete with the superconducting state.

Up to now, this has been achieved mainly by studying the properties of these compounds upon varying external parameters such as the carrier concentration or the temperature. However, the effect of a strong magnetic field has been much less studied. As a consequence, the nature of the field-induced ground state is still an open question.

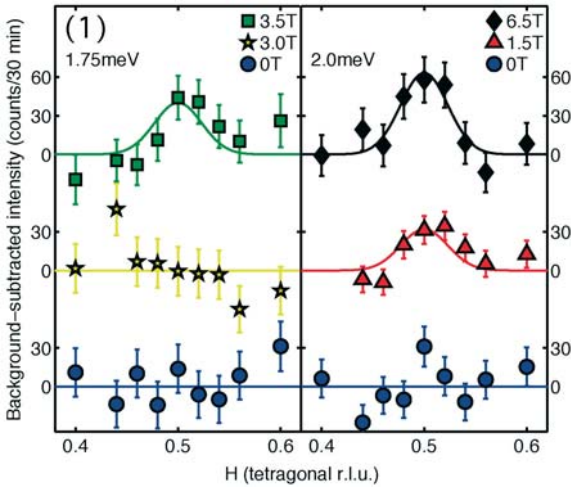


**Figure 1.** Transverse scans ( $b$   $1$ - $b$   $0$ ) through the AF zone center  $(1/2, 1/2, 0)$  at an energy transfer of  $\varepsilon = 1.75$  meV (left) and  $\varepsilon = 2.0$  meV (right). Before each scan, the sample was field-cooled from above  $T_c$  to  $T = 1.8$  K. Typical counting time is 30 min. per point.

In this study, we use inelastic neutron scattering to determine the magnetic-field effect on the superconducting spin-gap of  $\text{Nd}_{2-x}\text{Ce}_x\text{CuO}_4$ , the prototype of electron-doped high- $T_c$  superconductors. A detailed report of the results was published in Ref. [1]. The dynamic susceptibility  $\chi''(\mathbf{q}_0, \varepsilon)$  near the antiferromagnetic (AF) point  $\mathbf{q}_0 = (1/2, 1/2, 0)$  has been measured as a function of energy for different magnetic fields using the same method as used in our previous zero-field study [2].

In Fig.1, showing a typical  $q$  scan at constant energy for different fields, one sees how an applied magnetic field can cause the signal, which was initially suppressed by the spin-gap opening, to reappear. Before each scan, the sample

was first heated above  $T_c$  and then cooled down in the new field back to  $T = 1.8$  K; this procedure was followed in order to ensure a macroscopically uniform internal field. At an energy transfer of  $\varepsilon = 1.75$  meV [Fig. 1(a)], the magnetic excitations are completely suppressed up to  $H = 3$  T, and reappear at 3.5 T. A similar behavior is seen at the slightly higher energy transfer of  $\varepsilon = 2.0$  meV [Fig. 1(b)]. In this case, the peak is seen to reappear at a lower field of  $H = 1.5$  T

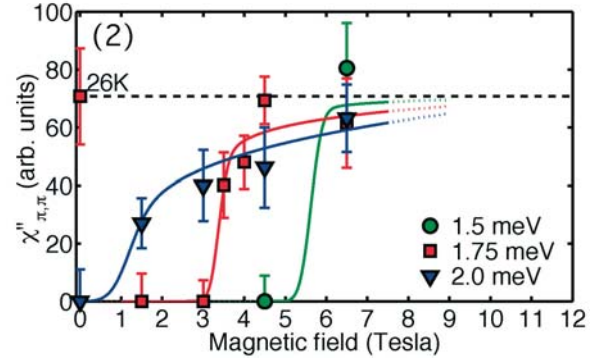


**Figure 2.** Dynamic susceptibility  $\chi''(\mathbf{q}_0, \varepsilon)$  at  $\mathbf{q}_0 = (1/2, 1/2, 0)$  as a function of field at several energies. All data are taken at  $T = 1.8$  K except the zero-field point at  $T = 26$  K.

Figs. 2 to 4 summarize the experimental results obtained on the triple-axis spectrometer 4F2 at LLB.

For hole-doped materials, the upper critical field at which superconductivity is completely destroyed is  $\sim 50$  T or larger [3], prohibitively large for neutron scattering experiments. For the electron-doped materials, on the other hand,  $H_{c2}$  is relatively lower ( $\sim 10$  T) [3], which has allowed us to observe a field effect on the superconducting magnetic gap in  $\text{Nd}_{2-x}\text{Ce}_x\text{CuO}_4$  up to high values of the relative magnetic-field strength.

Fig. 2 shows the evolution of the magnetic signal with magnetic field for energies within the zero field gap. The signal remains zero up to a threshold field which depends on energy. Then the signal increases with field, which is a first indication that the gap decreases. The horizontal dashed line represents the signal measured above  $T_c$  ( $T = 26$  K) showing that the dynamical susceptibility at high  $H$  and low  $T$  is essentially the same as above  $T_c$  in zero field.

## SUPERCONDUCTIVITY AND MAGNETISM

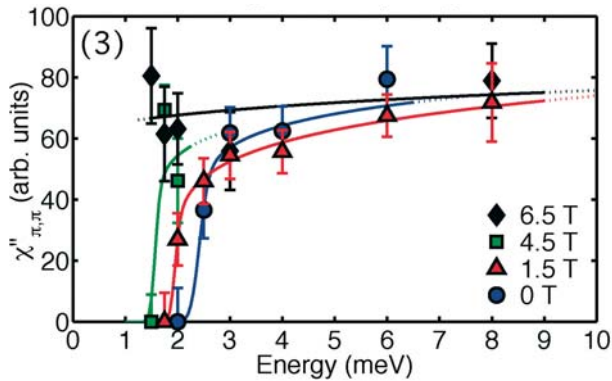


**Figure 3.** Field dependence of the magnetic excitation spectrum  $\chi''(\mathbf{q}_0, \epsilon)$  as a function of energy at  $T = 1.8$  K. Curves are guides to the eye.

Fig. 3 shows the dynamical susceptibility  $\chi''(\mathbf{q}_0, \epsilon)$  for several fields up to 6.5 T. The zero-field gap energy in our sample is 2.5 meV, slightly smaller than in a previous work [2], in accordance with our somewhat lower  $T_c$ . It decreases down to 1.5 meV at 5 T. At  $H = 6.5$  T, we have not been able to measure the gap because of the dominating magnetic excitations of Nd at low energies. These results can be interpreted as a rigid down shift of the gap profile with field.

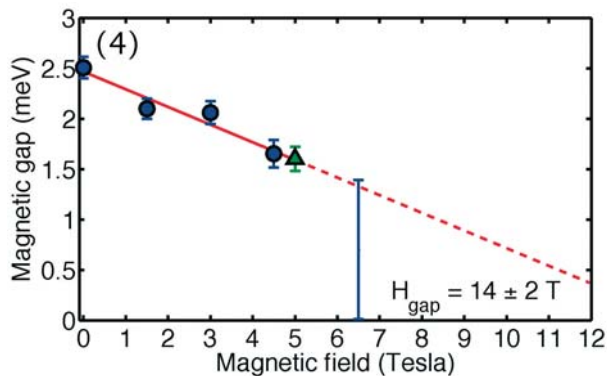


**Figure 4.** Evolution of the magnetic gap (half-maximum energy) as a function of field. The dependence is linear and extrapolates to zero at  $H_{\text{gap}} \sim 14.2$  T. The vertical bar reflects the fact that the gap energy is less than 1.5 meV.

Our results do not show any field-induced excitation in the gap as reported for the  $\text{La}_{2-x}\text{Sr}_x\text{CuO}_4$  compound [4-6].

In Fig. 4, the gap energy is plotted as a function of field. The magnetic gap decreases linearly with field, and collapses completely at an extrapolated value of  $H_{\text{gap}} \sim 14.2$  T, consistent with an upper critical field of  $H_{c2} \sim 10-12$  T [3]. The gapped spectrum of  $\text{Nd}_{2-x}\text{Ce}_x\text{CuO}_4$  undergoes a rigid

shift towards lower energies as the magnetic field is increased, which is in strong contrast to the formation of in-gap states in optimally doped and slightly overdoped  $\text{La}_{2-x}\text{Sr}_x\text{CuO}_4$  [4-6]. Because measurements below 1.5 meV were not possible, it is natural to ask whether the formation of some in-gap states in  $\text{Nd}_{2-x}\text{Ce}_x\text{CuO}_4$  could be hidden below this energy. However, we emphasize that the signal strength at 1.5 meV remains zero up to 4.5 T. Since our energy resolution is 1.3 meV (full width at half maximum), the experiment is sensitive to any in-gap intensity down to very low energies.

The results point to a picture in which the non-superconducting ground state at fields above  $H_{c2}$  does not possess magnetic order, but is a paramagnet with AF fluctuations. The first piece of evidence is that, in  $\text{Nd}_{1.85}\text{Ce}_{0.15}\text{CuO}_4$ , applying a magnetic field and increasing temperature have similar effects, and the gap does not appear to close until superconductivity is completely suppressed [7]. Moreover, the signal strength seen at high magnetic fields equals that in the normal state just above  $T_c$ . All of this indicates that the non-superconducting ground state beyond  $H_{c2}$  resembles the paramagnetic normal state above  $T_c$ . The absence of magnetic-field-induced in-gap states in  $\text{Nd}_{1.85}\text{Ce}_{0.15}\text{CuO}_4$  and the likely absence of field-induced magnetic order imply an important difference between the electron-doped and hole-doped cuprates; the competing spin- (and charge-) density wave order (often referred to as “stripes”) observed in hole-doped superconductors, especially in materials derived from the high- $T_c$  parent compound  $\text{La}_2\text{CuO}_4$ , hinders an unobstructed study of the AF-correlated superconductor due to the presence of a nearby quantum critical point. This complication appears to be avoided by the electron-doped materials, which possess the additional experimental advantage of a relatively low upper critical field.

[1] E.M. Motoyama, P.K. Mang, D. Petitgrand, G. Yu, O.P. Vajk, I.M. Vishik and M. Greven Phys. Rev. Lett., **96**, 137002 (2006)

[2] D. Petitgrand, K. Yamada, M. Fujita, and T. Uefuji, Physica C **408-410**, 778 (2004).

[3] Y. Wang et al., Science **299**, 86 (2003).

[4] B. Lake et al., Science **291**, 1759 (2001).

[5] J. M. Tranquada et al., Phys. Rev. B **69**, 174507 (2004).

[6] R. Gilardi et al., Europhys. Lett. **66**, 840 (2004).

[7] K. Yamada et al., Phys. Rev. Lett. **90**, 137004 (2003).

# H3. BOND-STRETCHING PHONON ANOMALY REFLECTING DYNAMIC CHARGE INHOMOGENEITY IN COPPEROXIDE SUPERCONDUCTORS

D. REZNIK<sup>1,2</sup>, L. PINTSCHOVIOUS<sup>1</sup>, M. ITO<sup>3</sup>, S. IIKUBO<sup>3</sup>, M. SATO<sup>3</sup>, H. GOKA<sup>4</sup>, M. FUJITA<sup>4</sup>, K. YAMADA<sup>4</sup>, G. D. GU<sup>5</sup>, AND J.M. TRANQUADA<sup>5</sup>

<sup>1</sup> Forschungszentrum Karlsruhe, Institut für Festkörperphysik, P.O.B. 3640, D-76021 Karlsruhe, Germany

<sup>2</sup> Laboratoire Léon Brillouin, CE Saclay, F-91191 Gif-sur-Yvette Cedex, France

<sup>3</sup> Department of Physics, Division of Materials Science, Nagoya University, Furo-cho, Chikusa-ku, Nagoya 464-8602, Japan

<sup>4</sup> Institute for Material Research, Tohoku University, Katahira, Aoba-ku, Sendai, 980-8577, Japan.

<sup>5</sup> Condensed Matter Physics and Materials Science Department, Brookhaven National Laboratory, Upton, New York 11973-5000, USA

While many believe that antiferromagnetism is important for the high-temperature superconductivity, there has been resurgent interest in the role of electron-lattice coupling. The Karlsruhe group, in collaboration with others, has been investigating electron-phonon coupling due to charge inhomogeneities in copper oxide superconductors. This work focused on detailed measurements of optic oxygen modes believed to couple most strongly to dynamic charge inhomogeneity. The IT spectrometer is ideally suited for such a study, as its performance is optimized for the high energies of these phonons. A collaboration with the theory group in Karlsruhe (K-P. Bohnen and R. Heid), made it possible to compare experimental results to predictions of band theory and thus separate the conventional Fermi-liquid physics from still poorly understood correlation effects. Band theory works remarkably well for predicting electron-phonon effects in the recently studied conventional superconductors MgB<sub>2</sub> and YNi<sub>2</sub>B<sub>2</sub>C. They have a very

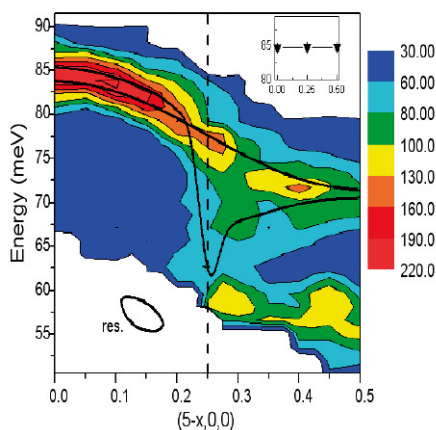


**Figure 1.** Color-coded contour plot of the intensities observed on La<sub>1.875</sub>Ba<sub>0.125</sub>CuO<sub>4</sub> at T = 10 K. The intensities above and below 60 meV are associated with plane-polarized Cu-O bond-stretching vibrations and bond-bending vibrations, respectively. Black lines are dispersion curves evaluated from two-peak fits to the data. The white area at the lower left corner of the diagram was not accessible in this experiment. The ellipse illustrates the instrumental resolution. The inset shows the dispersion in the [110]-direction. The dashed line represents the charge-ordering wavevector.

strong electron-lattice coupling involving a particular phonon that was predicted by band theory and confirmed quantitatively by experiment. Our inelastic neutron scattering measurements showed that there is a similarly strong anomaly in the Cu-O bond-stretching phonon in cuprate superconductors La<sup>2-x</sup>Sr<sub>x</sub>CuO<sub>4</sub> (x = 0.07, 0.15) and in YBa<sub>2</sub>Cu<sub>3</sub>O<sub>6+x</sub> (x = 0.6, 0.95); however, this behavior is completely absent in band theory calculations. Instead, the anomaly is strongest in La<sub>1.875</sub>Ba<sub>0.125</sub>CuO<sub>4</sub> and La<sub>1.48</sub>Nd<sub>0.4</sub>Sr<sub>0.12</sub>CuO<sub>4</sub>, compounds that exhibit spatially modulated long-range charge and magnetic order, often called stripe order. It occurs at a wave vector corresponding to the charge order.

Stripe order is known to result from strong electron-electron correlations due to Mott physics. While the static stripe compounds are not superconductors, many believe that dynamic stripes play a crucial role in the physics of the cuprates and, possibly, in the mechanism of high T<sub>c</sub> superconductivity. Existence of dynamic stripes is still controversial. Observation of a very similar anomaly in compounds with and without static stripes suggests that they may be present throughout the doping range associated with superconductivity (the anomaly is absent in undoped and overdoped non-superconductors).

More importantly, the phonon measurements conclusively demonstrated that a strong charge fluctuation, not predicted by band theory, is present in copper oxide superconductors and that it strongly couples to phonons. It follows that electron-phonon coupling may be important to understanding the superconductivity although its contribution to the mechanism is likely indirect.

[1] D. Reznik, L. Pintschovius, M. Ito, S. Iikubo, M. Sato, H. Goka, M. Fujita, K. Yamada, G.D. Gu, and J.M. Tranquada, Nature 440, 1170 (2006).

[2] L. Pintschovius, D. Reznik, and K. Yamada, to appear in Phys. Rev. B

## H4. A 2D STRIPE SUPERSTRUCTURE REVEALED BY SPIN WAVES IN CUBIC FERROMAGNETIC $\text{La}_{1-x}\text{Sr}_x\text{MnO}_3$ ( $x = 0.125$ and $x = 0.15$ )

S. PETIT<sup>1</sup>, M. HENNION<sup>1</sup>, F. MOUSSA<sup>1</sup>, P. REUTLER<sup>2</sup>, A. REVCOLEVSKII<sup>2</sup> AND Y. M. MUKOVSKII<sup>3</sup>

<sup>1</sup> Laboratoire Léon Brillouin CEA-CNRS, CE Saclay, 91191, Gif-sur-Yvette Cedex, France

<sup>2</sup> Laboratoire de Physico-Chimie des Solides, Université Paris-Sud, 91405 Orsay Cedex, France

<sup>3</sup> Moscow State Steel and Alloys Institute, Moscow 119991, Russia

Manganites  $\text{La}(\text{Ca,Sr})\text{MnO}_3$  belong to a large class of compounds in which the strong correlations among electrons are suspected to be responsible for nanoscale charge segregation effects. In these oxides, the hole concentration can be tuned by substituting Ca or Sr on the La-sites. At zero doping, the spins of Mn form ferromagnetic ( $a,b$ ) planes stacked antiferro-magnetically along the  $c$  axis. Upon doping, a new ferromagnetic coupling resulting from the double-exchange mechanism becomes effective and stabilizes a ferromagnetic, metallic state beyond  $x \sim 0.2$ . However, the way this compound evolves towards the new phase is very peculiar, emphasizing the role of charge segregation. We have shown previously [1] that at low doping, *hole-rich* platelets embedded in a *hole-poor* matrix are formed within the ( $a,b$ ) planes. Neutron scattering experiments enabled us to determine their size ( $\sim 16 \text{ \AA}$ ) and their liquid-like distribution. As  $x$  increases, these platelets grow and percolate for  $x = 0.12$ , while the antiferromagnetic coupling along  $c$  concomitantly becomes zero. Beyond this concentration, inelastic neutron scattering experiments show that the magnetic excitation spectrum consists of a dispersed branch at small  $q$ , and several discrete modes at larger  $q$ . The former indicates long-range ferromagnetically coupled spins, while the latter are attributed to standing spin waves within small ferromagnetic domains. Moreover, recent experiments

carried out as a function of temperature in  $\text{La}_{7/8}\text{Sr}_{1/8}\text{MnO}_3$  [2] and in  $\text{La}_{0.85}\text{Sr}_{0.15}\text{MnO}_3$  [3] revealed the occurrence of a gap at  $q = 1/8$ , indicating a new periodicity of 4 lattice spacings within the ( $a,b$ ) planes (Fig. 1*a*). In connection with the low doping regime, we propose an interpretation in terms of reverse charge segregation. In this picture, *hole-poor*  $4 \times 4$  ferromagnetic clusters tend to form on manganese sites within the ( $a,b$ ) planes. Those clusters are weakly coupled across hole-rich boundaries located on oxygen sites (Fig. 2), leading to a superstructure of orthogonal stripes. This picture is quite well supported by spin-wave calculations [3] (Fig. 1*b*). This is, to our knowledge, the first observation of stripes in a ferromagnetic state.

[1] M. Hennion, F. Moussa *et al.*, Phys. Rev. Lett. **81**, 1957 (1998); *ibid.* **94**, 57006 (2005).

[2] M. Hennion, F. Moussa *et al.* Phys. Rev. B **73**, 104453 (2006).

[3] S. Petit, M. Hennion, F. Moussa *et al.*, Workshop on Self-organized Strongly Correlated Electron Systems, Seillac (France) May 29-31, 2006.

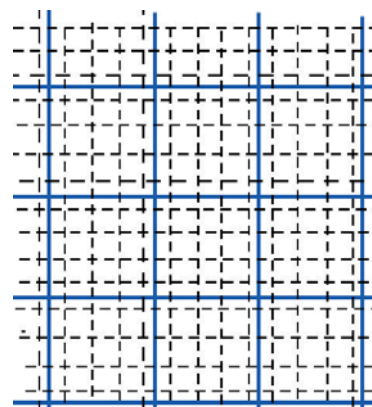
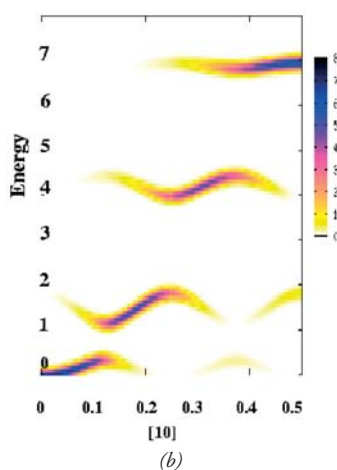
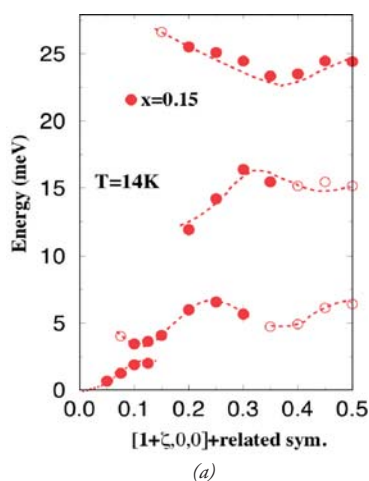


Figure 2

Figure 1

# H5. SPIN-WAVE DISPERSION IN ORBITALLY ORDERED $\text{La}_{0.5}\text{Sr}_{1.5}\text{MnO}_4$

D. SENFF<sup>1</sup>, F. KRÜGER<sup>2,3</sup>, S. SCHEIDL<sup>2</sup>, M. BENOMAR<sup>1</sup>, Y. SIDIS<sup>4</sup>, F. DEMMEL<sup>5</sup>, AND M. BRADEN<sup>1</sup>,

<sup>1</sup> II. Physikalisches Institut, Universität zu Köln, Zùlpicher Str. 77, D-50937 Köln, Germany

<sup>2</sup> Institut für Theoretische Physik, Universität zu Köln, Zùlpicher Str. 77, D-50937 Köln, Germany

<sup>3</sup> Instituut-Lorentz, Universiteit Leiden, P.O. Box 9506, 2300 RA Leiden, The Netherlands

<sup>4</sup> Laboratoire Léon Brillouin, CEA-CNRS, F-91191 Gif sur Yvette Cedex, France

<sup>5</sup> Institut Laue Langevin, BP 156, 38042 Grenoble Cedex 9, France

The colossal magneto-resistivity in manganites is only partially explained by the Zener double-exchange mechanism; the larger part of it appears to arise from the competition of two states: the metallic ferromagnetically ordered state on the one side and the insulating one with a cooperative ordering of charges, orbitals and spins (COS) on the other side [1, 2]. The insulator-to-metal transition consists in switching from a phase with long or short-range COS correlations into the metallic state where spins are aligned either by an external field or by spontaneous magnetic order. The combined COS ordering has first been studied in the pioneer work by Wollan and Koehler [3] and by Goodenough [4] proposing the so-called CE-type arrangement, which is illustrated in Fig. 1(a). For half doping, i.e. equal amounts of  $\text{Mn}^{3+}$  and  $\text{Mn}^{4+}$ , there is a checkerboard arrangement of different charges. In addition the  $e_g$  orbitals at the  $\text{Mn}^{3+}$  sites form zigzag chains. The CE-type charge and orbital arrangement will yield a ferromagnetic interaction in the zigzag chains and an [antiferromagnetic] interaction in-between. The magnetic excitations in the ferromagnetic metallic

manganites have been studied for many different compositions (for a recent summary see Ref. [5]). In view of the large amount of data on the ferromagnetic phases, it may be surprising that there is still no detailed study of magnetic excitations in the antiferromagnetic COS states. Besides the intrinsic complexity of the CE-type magnetic ordering, such a study is severely hampered by the twinning of the manganite crystals in the perovskite phases. We, therefore, have chosen the layered material  $\text{La}_{0.5}\text{Sr}_{1.5}\text{MnO}_4$  to study the magnon dispersion in the COS state (Fig. 1).

We were able to separate the magnon branches parallel and perpendicular to the zigzag-chains, as only one twin orientation contributes to a given quarter-indexed magnetic superstructure reflection. When going from the antiferromagnetic zone center  $(0.75, -0.75, 0)$  along the  $[1, 1, 0]$  direction one determines the spin-wave dispersion parallel to the zigzag chains (Fig. 2, right) and, when going along the  $[1-10]$  direction, one measures the dispersion perpendicular to the chains. This behavior is corroborated by the structure factor calculations presented in Fig. 2 as discussed below. The raw-data scans unambiguously demonstrate that

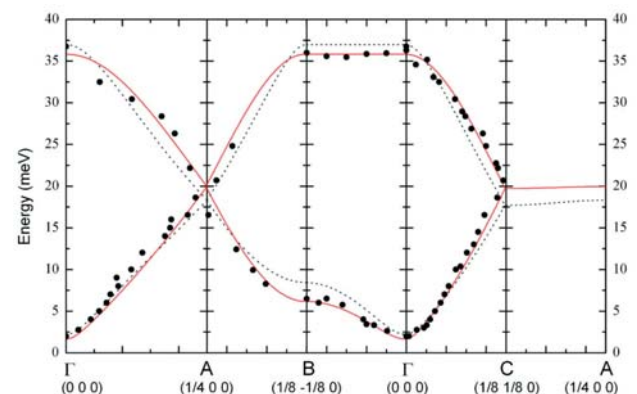
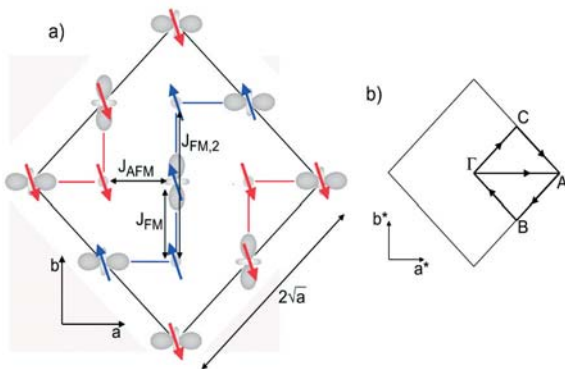


**Figure 1.** (a) Schematic representation of the CE-type ordering in the  $(a, b)$  plane of half-doped manganites with three magnetic interactions parameters. Notice that the FM zigzag chains run along the  $[110]$  direction. (b) Sketch of the magnetic Brillouin zone, displaying the high-symmetry points  $\Gamma = (0, 0, 0)$ ,  $A = (1/4, 0, 0)$ ,  $B = (1/8, -1/8, 0)$ ,  $C = (1/8, 1/8, 0)$  and the path of the calculated dispersion. (c) Dispersion of the magnetic excitations in  $\text{La}_{0.5}\text{Sr}_{1.5}\text{MnO}_4$  in a direction parallel to  $[100]$  ( $\Gamma$ -A), perpendicular to the chains ( $\Gamma$ -B) and parallel to the chains ( $\Gamma$ -C). The solid and broken lines give the spin-wave dispersion calculated with a two parameter set.

## SUPERCONDUCTIVITY AND MAGNETISM

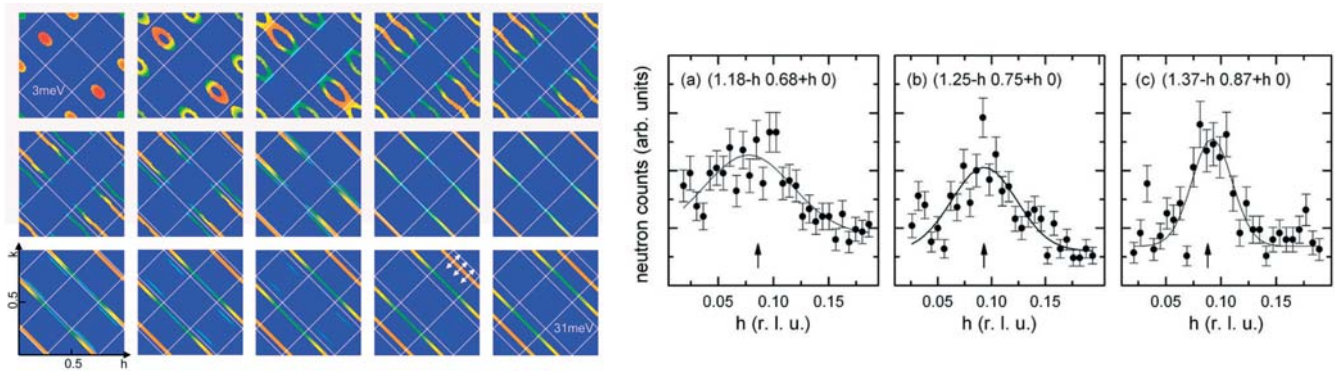


**Figure 2.** (left panel): Constant energy cuts through the calculated spin-wave structure factor with constant energy resolution of 2 meV within each plot, and with energy steps of 2 meV between adjacent plots, showing the dispersion and scattering distribution of the lowest magnon bands. (right panel): Constant energy scans along the direction indicated by arrows in the 29 meV cut (above) to experimentally verify the one-dimensional character of the high-energy magnetic scattering. The arrows indicate the expected positions of the magnon.

the dispersion along the zigzag chains is much steeper than perpendicular to them. The magnetic structure has to be considered as a weak antiferromagnetic coupling of strongly coupled ferromagnetic zigzag chains. The obtained magnon dispersion is presented in Fig. 1(c). The branch propagating along the chains ( $\Gamma$ - $C$  path), is much steeper than the branch propagating perpendicular to it, ( $\Gamma$ - $B$  path). At the magnetic zone boundaries  $C$  and  $B$  we find magnon energies of 19meV and 6.5 meV, respectively. At the  $C$  point where  $q$  is parallel to the chains, the end-point of the acoustic branch coincides with that of the lowest optic branch, whereas there is a large gap between these branches along the  $\Gamma$ - $B$  path. The magnon branch along the  $[100]$  direction ( $\Gamma$ - $A$  path, at  $45^\circ$  with respect to the chains), exhibits an intermediate dispersion.

The spin-wave dispersion has been calculated using the Holstein-Primakoff transformation with a simple spin-only Hamiltonian illustrated in Fig. 1(a). The  $\text{Mn}^{3+}$  and  $\text{Mn}^{4+}$  spins were fixed to the values  $S = 2$  and  $S = 1.5$ , respectively. Taking into account only the two nearest-neighbor  $\text{Mn}^{3+}$ - $\text{Mn}^{4+}$  spin interactions for pairs within and in-between the zigzag chains,  $J_{\text{FM}}$  and  $J_{\text{AFM}}$ , one obtains a good description of the measured dispersion denoted by broken lines in Fig. 1(c). However, there remain significant discrepancies: it is impossible to simultaneously describe the large initial slope of the spin-wave dispersion along the chains and the relatively lower zone-boundary frequencies. This behavior implies the relevance of an additional longer-distance interaction parameter acting along the ferromagnetic chains. Indeed, a fully satisfactory description is obtained by including a ferromagnetic interaction for  $\text{Mn}^{4+}$ - $\text{Mn}^{4+}$  spin pairs connected through a  $\text{Mn}^{3+}$  site within a zigzag chain. Fig. 2 (left) presents the calculated

magnon scattering intensities in the form of constant energy cuts. One can see how the anisotropic spin-wave cones develop around the magnetic Bragg peaks with finite structure factor. At intermediate energies those magnetic Brillouin zones in which there is no elastic scattering also contribute. Fig. 2 further illustrates that, well above the maximum of the acoustic magnon perpendicular to the zigzag chains, the system looks like a magnetically one-dimensional system as the magnons disperse only along the zigzag chains. The one-dimensional character was verified by special constant-energy scans (Fig. 2). The dominant ferromagnetic coupling is further seen in experiments upon heating across the charge and orbital ordering.

The strong ferromagnetic interaction in the zigzag chains not being restricted to the nearest neighbors indicates that electrons are not fully localized in the COS phase as well. The large and non-local ferro-magnetic interactions in the zigzag chains yield considerable resemblance between the COS and the metallic phases. This resemblance might be essential to understand the capability of manganites to switch between the metallic ferromagnetic and the insulating COS phases. These results have been published in reference [6].

- [1] Y. Tokura and N. Nagaosa, *Science* **288**, 462 (2000).
- [2] Y. Motome et al., *Phys. Rev. Lett.* **91**, 167204 (2003).
- [3] E.O.Wollan and W.C. Koehler, *Phys. Rev.* **100**, 545 (1955).
- [4] J.B. Goodenough, *Phys. Rev.* **100**, 564 (1955).
- [5] Y. Endoh et al., *Phys. Rev. Lett.* **94**, 017206 (2005).
- [6] D. Senff, F. Krüger, S. Scheidl, M. Benomar, Y. Sidis, F. Demmel and M. Braden, *Phys. Rev. Lett.* **96**, 257201 (2006).

# H6. COMPETING ORDER PARAMETERS IN LIGHT-RARE-EARTH HEXABORIDES

J.-M. MIGNOT<sup>1</sup>, G. ANDRÉ<sup>1</sup>, M. SERA<sup>2</sup>, AND F. IGA<sup>2</sup>

<sup>1</sup> Laboratoire Léon Brillouin (CEA-CNRS), CEA/Saclay, 91191 Gif sur Yvette Cedex

<sup>2</sup> ADSM, Hiroshima University, Higashi Hiroshima, 739-8530, Japan

Orbital phenomena associated with  $d$  electron states are known to be central to the physics of transition-metal oxides, and have been extensively studied. In the case of  $f$  electrons, which are subject to strong spin-orbit coupling, the proper description of orbital degrees of freedom is based on *multipoles*. Ordering phenomena involving higher-rank multipoles (quadrupoles, octu-poles, etc.) are currently attracting a great deal of interest, because they might account for several elusive phase transitions observed in rare-earth or actinide compounds ( $\text{Ce}_{1-x}\text{La}_x\text{B}_6$ ,  $\text{SmRu}_4\text{P}_{12}$ ,  $\text{NpO}_2$ , etc.). Multipole moments, being tensor quantities, can give rise to a variety of ordered states classified according to the symmetry of their order parameter. Interesting properties are expected to occur if a competition takes place between different types of order, involving multipole components of different symmetries. Such a situation may be realized in the cubic (CsCl-type) hexaboride compounds  $\text{Ce}_{1-x}\text{R}_x\text{B}_6$  ( $R$ : Pr, Nd), where the light rare-earth Ce, Pr, and Nd have different multiplet ground states ( $J = 5/2, 4$ , and  $9/2$ , respectively), and thus different multipole moments.

$\text{CeB}_6$  is considered the archetype of a pure antiferro-quadrupolar (AFQ) order, realized in the so-called “phase II” below  $T_Q = 3.2$  K, prior to the onset of a long-range magnetic order in “phase III” below  $T_N = 2.3$  K [1]. In the latter phase, the Ce magnetic moments form a noncollinear, planar,  $2k$ - $k'$  structure, described by the 4 propagation vectors  $\mathbf{k}_{1,2} = (1/4, \pm 1/4, 1/2)$  and  $\mathbf{k}'_{1,2} = (1/4, \pm 1/4, 0)$ . The preformed order of the  $O_{xy}$  ( $O_{yz}$ ,  $O_{zx}$ ) quadrupole moment components, with the wave vector  $\mathbf{k}_Q = (1/2, 1/2, 1/2)$ , produces a staggered anisotropy on the Ce sublattice, which is thought to be responsible for the unusual type of magnetic structure adopted by the system below  $T_N$ . Substitution of another rare earth ion (including La) strongly suppresses phase II, giving way to a rich pattern of ordered phases as a function of both concentration (Fig. 1) and applied magnetic field. Most of these phases have a clear magnetic signature, but quadrupole, and possibly higher multipole couplings are likely to play a role. The present study aims at understanding the microscopic mechanisms responsible for the stability of the different structures. Neutron diffraction measurements have been reported in Refs. [3,4] for  $\text{Ce}_{1-x}\text{Pr}_x\text{B}_6$  and  $\text{Ce}_{1-x}\text{Nd}_x\text{B}_6$ , respectively. Here we present our results for the latter system, together with a brief discussion of their implications as to a possible role of quadrupole interactions.

Powder and single-crystal experiments were performed on the multidetector diffractometer G4-1 and the lifting-counter diffractometer 6T2, using isotopic (<sup>11</sup>B: 98.6%) samples prepared in Hiroshima.

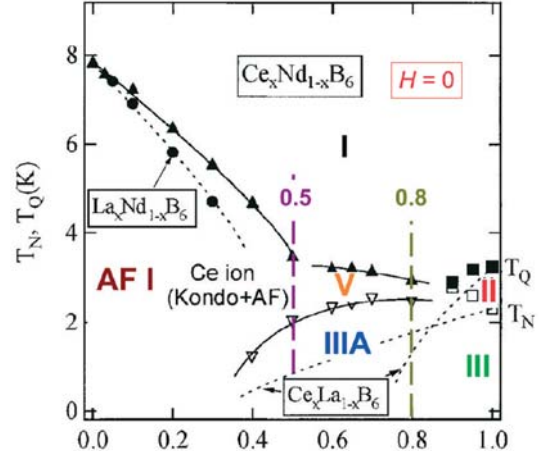


**Figure 1.** Phase diagram of  $\text{Ce}_{1-x}\text{Nd}_x\text{B}_6$  in zero applied magnetic field; the vertical dashed lines correspond to the concentrations studied experimentally;  $\text{Ce}_{1-x}\text{La}_x\text{B}_6$  data are plotted for comparison. (after Ref. [2])

The powder diffraction patterns (Fig. 2) reveal two clearly distinct regimes. For  $x = 0.5$ , the systems first orders below  $T_N$  in a simple AFI structure  $\mathbf{k}_{\text{AFI}} = (0, 0, 1/2)$ , similar to that found in pure  $\text{NdB}_6$ . Resistivity measurements suggest that, in this regime, the Ce ions are weakly coupled to the Nd magnetism and retain Kondo fluctuations inside the AFI ordered state. The fact that the  $0\ 0\ 1/2$  reflection is absent implies that the moment direction is parallel to the fourfold axis, pointing to an effect of ferroquadrupolar  $O_2^-$  type interactions between Nd moments as in pure  $\text{NdB}_6$  [5]. For  $x = 0.8$  (Fig. 2, upper frame), the structure forming below  $T_N$  is incommensurate with  $\mathbf{k}_{\text{inc}} = (0.237, 0.237, 1/2)$ . At lower temperature, a lock-in transition takes place to the commensurate (C) wave vector  $\mathbf{k}_{\text{com}} = (1/4, 1/4, 1/2)$ .

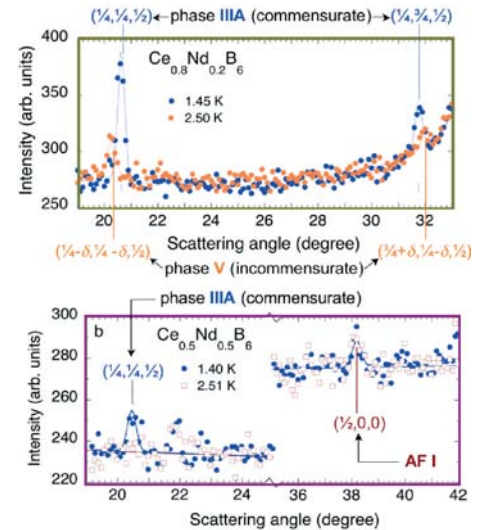


**Figure 2.** Powder diffraction patterns for  $\text{Ce}_{1-x}\text{Nd}_x\text{B}_6$  ( $x = 0.8$  and  $0.5$ ) measured in the ground state at  $T_{\text{min}} \oplus 1.4$  K and in the intermediate phase below  $T_N$ .

## SUPERCONDUCTIVITY AND MAGNETISM

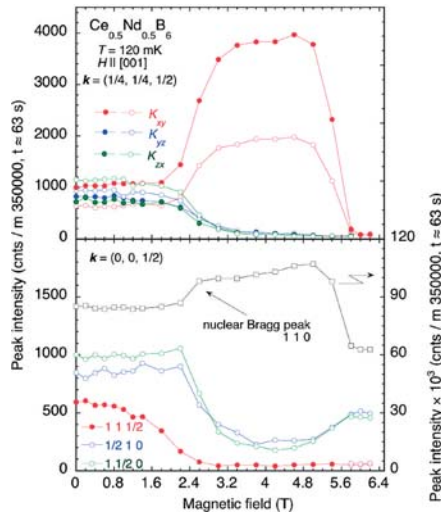


**Figure 3.** Field dependence of Bragg intensities for different C (upper frame) and AFI (lower frame) satellites at  $T = 120$  mK.

This situation in phase IIIA is reminiscent of the compound  $\text{PrB}_6$ , where the structure was analyzed as  $2-k$  and ascribed to an effect of quadrupole interactions between  $O_{xy}$ -type moments. The absence of  $k'$ -type peaks, in contrast to the  $\text{CeB}_6$  case, reflects the lack of long-range AFQ order associated with  $k_Q$ .

In the Nd-rich compound  $x = 0.5$ , the low-temperature transition again corresponds to the appearance of a commensurate component at  $k_{\text{com}}$  but, in this case, the high-temperature AFI reflections are not suppressed (Fig. 2, lower frame), suggesting that ordering behaviors associated with Ce and Nd moments somehow coexist.

This assumption is supported by the single-crystal results. At the lowest temperature of  $T = 120$  mK, the intensity of the AFI peak  $1 \ 1/2 \ 0$  is indeed comparable to that of the C satellite  $5/4 \ 1/2 \ 1/4$ . When an external field is applied along  $[001]$ , the intensities plotted in Fig. 3 indicate a repopulation of the C domains above  $H_1 \approx 2.4$  T (upper frame), consistent with the hypothesized  $2-k$  planar,  $\text{PrB}_6$ -like structure. More surprisingly, this change is accompanied by a steep suppression of the Bragg peaks associated with the AFI single- $k$  domains  $k_x$  and  $k_y$  (lower frame). Those associated with  $k_z$ , on the contrary, decrease smoothly to zero from  $H = 0$  to  $2.4$  T. This leads us to propose that the AFI ( $k_x$  and  $k_y$ ) and C ( $k'_{y2}$  and  $k'_{z2}$ ) components are actually coupled by pairs (e.g.  $k'_{y2}$  with  $k'_x$ ), and contribute to one and the same structure within a given domain. We further speculate that the two components may reflect, respectively, the Ce and Nd contributions, with Ce moments forming a structure similar to the planar  $2-k$  state mentioned above, and Nd moments an approximately AFI state along the normal to the planes. In this picture, the

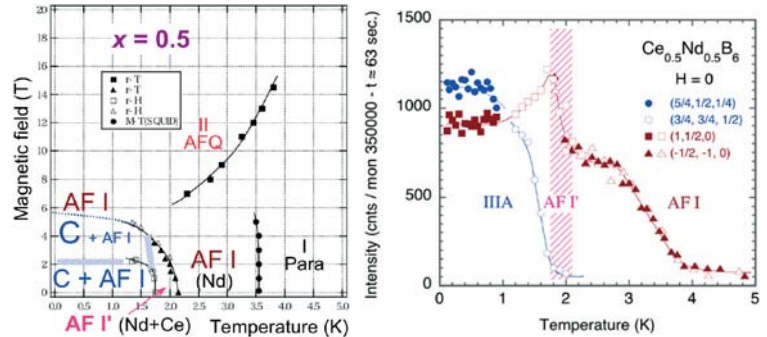


**Figure 4.** (left):  $(H, T)$  magnetic phase diagram of  $\text{Ce}_{0.5}\text{Nd}_{0.5}\text{B}_6$  (data for bulk measurements from Kawaguchi et al.). (right):  $T$  dependences of the intensities of C and AFI satellites at  $H = 0$ .

effect in low fields implies no true domain repopulation but a mere reorientation of the Nd moments within the  $k'_{xy} - k'_z$  domain.

Above a second transition field  $H_2 = 5.4$  T, the C structure is steeply suppressed, and AFI order is restored, with only the two domains  $k_y$  and  $k_z$  populated. This is consistent with moments oriented, within each domain, along the propagation vector. In high fields, no evidence was found for the AFQ transition line derived from bulk measurements. The results in applied fields are summarized by the phase diagram drawn in Fig. 4.

Finally, we want to point out the interesting observation of an intermediate region in the phase diagram, between 1.7 and 2.5 K in zero field, which is characterized by a steep increase in the AFI component just before the C order sets in. We believe that it denotes the ordering of Ce moments in the existing AFI structure of Nd, likely associated with the suppression of Kondo fluctuations.

In conclusion, the complex pattern of ordered phases found in the  $\text{Ce}_{1-x}\text{Nd}_x\text{B}_6$  solid solutions appears to reflect the rather unique competition of two different types of quadrupolar couplings, predominantly FQ between the Nd  $O^0_2$  moments, and AFQ between the Ce  $O_{xy}$ -type moments. Neutron diffraction under conditions of high magnetic fields and very low temperatures has proved invaluable in revealing the details of the magnetic phases. It should now be complemented by x-ray synchrotron measurements to probe directly the order of multipole moments.

- [1] J.M. Effantin, J. Rossat-Mignod, P. Burlet, et al., J. Magn. Magn. Mater. 47&48 (1985) 145.
- [2] S. Kobayashi, Y. Yoshino, S. Tsuji, M. Sera, F. Iga, J. Phys. Soc. Jpn. 72 (2003) 25.
- [3] J.M. Mignot, M. Sera, F. Iga, Physica B 383 (2006) 41.
- [4] J.M. Mignot, G. André, M. Sera, F. Iga, Physica B (in press).
- [5] S. Awaji, N. Kobayashi, S. Sakatsume, S. Kunii, M. Sera, J. Phys. Soc. Jpn. 68 (1999) 2518.

# H7. SPIN REDISTRIBUTION BY ENTANGLEMENT IN AN ORGANIC MAGNET

A. ZHELUDEV<sup>1</sup>, V. O. GARLEA<sup>1</sup>, S. NISHIHARA<sup>2</sup>, Y. HOSOKOSHI<sup>3</sup>, A. COUSSON<sup>4</sup>, A. GUKASOV<sup>4</sup>, K. INOUE<sup>5</sup>

<sup>1</sup>HFIR Center for Neutron Scattering, Oak Ridge National Laboratory, Oak Ridge, TN 37831-6393, USA.

<sup>2</sup>Department of Physical Science, Osaka Prefecture University, ,Osaka 599-8531, Japan.

<sup>3</sup>Department of Physical Science, Osaka Prefecture University, Osaka 599-8531, Japan; Institute for Nanofabrication Research, Osaka Prefecture University, Osaka 599-8531, Japan.

<sup>4</sup>Laboratoire Leon Brillouin, CEA-CNRS Saclay, France.

<sup>5</sup>Department of Chemistry, Hiroshima University, Hiroshima 739-8526, Japan.

A fundamental feature of quantum mechanics is entanglement, defined as a physical realization of linear superpositions of simple multi-particle states [1]. Entangled particles are physically interdependent even though they may be spatially separated. Entanglement of spin degrees of freedom in molecular magnets holds great promise for spintronics devices [2]. Rather complex entangled states are realized in applied magnetic fields. For each magnetic group of atoms the spin is quantized, and the magnetization can have only discrete values. Due to entanglement though, the spin density can be arbitrarily re-distributed, resulting in seemingly paradoxical fractional local magnetization. Recent experiments on the 5C1 and 6T2 [6] polarized neutron diffractometers at the ORPHEE reactor yielded a direct quantifiable experimental observation of this effect in a novel organic molecular magnet.

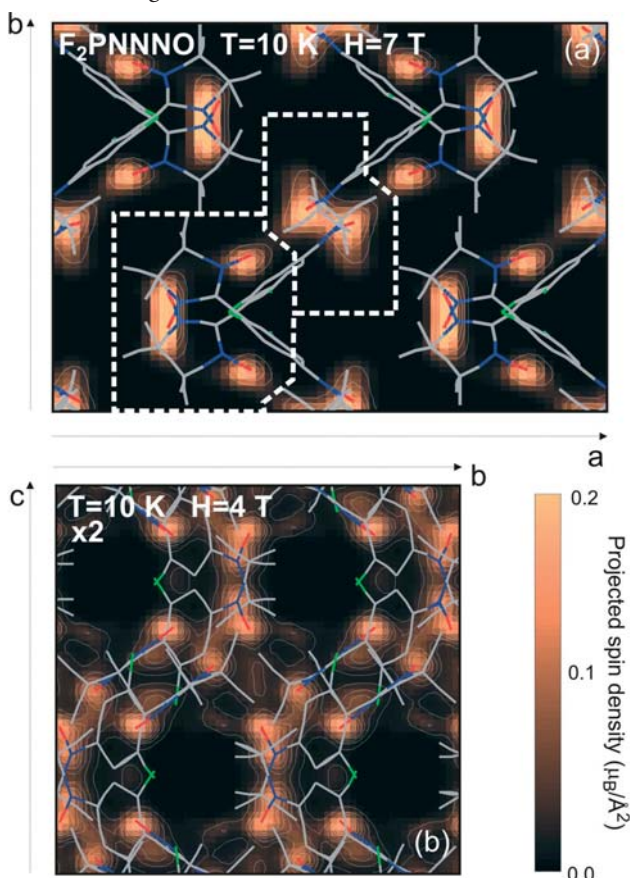


**Figure 1.** Experimental spin density distribution in a  $F_2PNNNO$  spin-tetramer at  $T = 10$  K, as reconstructed using the Maximum Entropy method. Areas outlined with thick dashed lines were used to estimate the spin populations on the nitronyl nitroxide and *tert*-butyl nitroxide.

Our model material, 2-[2,6-difluoro-4-(*N-tert*-butyl-*N*-oxyamino)phenyl]-4,4,5,5-tetramethyl-4,5-dihydro-1*H*-imidazol-1-oxyl-3-oxide,  $F_2PNNNO$  for short, is a prototypical spin tetramer system [3]. The magnetic properties are due to two unpaired electrons that reside in  $p^*$  antibonding molecular orbitals of the nitronyl nitroxide (NN) and the *tert*-butyl nitroxide (tBuNO) groups, respectively. These  $S = 1/2$  spins are coupled via a ferromagnetic intramolecular exchange constant  $J_F \sim 35$  meV.

When in crystalline form,  $F_2PNNNO$  molecules are arranged in pairs, so that their tBuNO groups are close enough for AF interactions of magnitude  $J^{AF} \sim 5.8$  meV. The result is a two-molecule unit containing four interacting spins. Its unique ground state is a non-magnetic singlet. In the presence of an external magnetic field applied along the  $z$  axis, the excited state with the lowest energy has a total spin  $S_{total} = 1$  and a spin projection  $S_z = +1$ . We shall denote this state as  $|1,+1\rangle$ . Its wave function is heavily entangled: by diagonalizing the Heisenberg Hamiltonian of the tetramer we find that it actually is a linear combination of four "pure" (non-entangled) spin wave functions:  $|1,+1\rangle = a|\underline{\quad}\rangle + b|\underline{\quad}\rangle - a|\underline{\quad}\rangle - b|\underline{\quad}\rangle$ , where  $a \sim 0.46$  and  $b \sim 0.54$ . The most striking consequence of this entanglement is an imbalanced spin density distribution  $S_z(\mathbf{r})$ : the local spin populations of the NN groups are equal, but different from those of the tBuNO groups. The ratio  $R$  of these spin populations is given by  $R = a^2/b^2 \sim 1.39$ . If entanglement was absent, and only pure spin-projection states were allowed, then, due to the weakness of the central antiferromagnetic bond, the lowest-energy excited state would have been  $|\underline{\quad}\rangle$ , with  $R_{pure} = 1$ . If quantum mechanics failed altogether, the spins would behave as classical moments. They would align themselves in the  $(x,y)$  plane and tilt slightly in the field direction. It is easy to show that the resulting imbalance in  $S_z(\mathbf{r})$  would be minuscule:  $R_{classical} = 1 + |J_{AF}|/4|J_F| = 1.04$ . Thus, a large imbalance of NN and tBuNO spin densities in  $F_2PNNNO$  can be considered a *signature of spin entanglement*.

To prepare the tetramer in its  $|1,+1\rangle$  excited state high magnetic fields of  $H = 7$  T or  $H = 4$  T were used to lower its energy as much as possible. The data were then taken at an elevated temperature of  $T = 10$  K that made this state partially populated. The main technical challenge of measuring the spin density distribution is the very small total magnetization, estimated at less than half a Bohr magneton for the 2-molecule unit comprising about 100 atoms. Polarized neutron in the crystal.

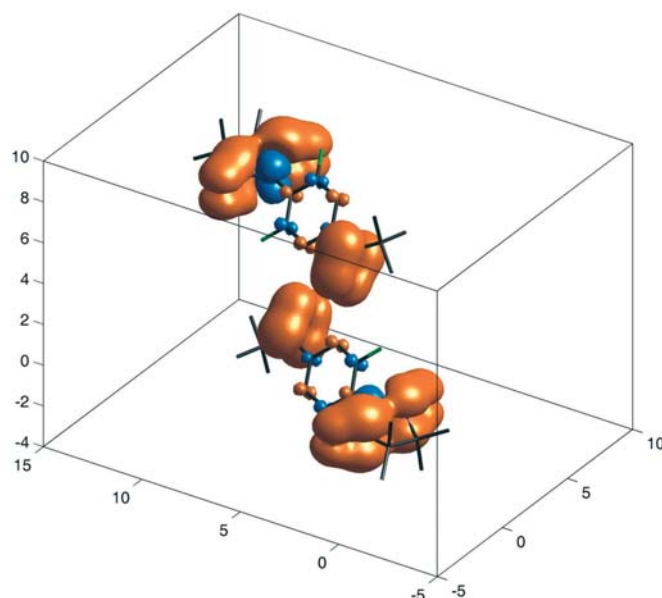


**Figure. 2** Experimental spin density distribution in a F<sub>2</sub>PNNNO spin-tetramer at T = 10 K at H = 7 T and T = 10 K, as reconstructed using atomic orbital expansion. The isosurfaces are drawn at  $1 \times 10^{-3} \mu_B/\text{\AA}^3$  (orange) and  $-1 \times 10^{-3} \mu_B/\text{\AA}^3$  (blue) levels. The axes show Cartesian coordinates in Angstroms.

In the experiments the so-called flipping ratios of 70 Bragg reflections were measured. Maximum entropy (Fig. 1) and atomic orbital expansion (AOE, Fig. 2) were used to reconstruct the real-space magnetization distribution.

A very good measure of the reliability of the AOE reconstruction is its result for the total tetramer magnetization:  $m = 0.48(2) \mu_B$  and  $m = 0.28(2) \mu_B$ , for  $H = 7$  T and  $H = 4$  T, respectively. These values are consistent with existing bulk susceptibility data, and are in excellent agreement with a thermodynamic quantum-mechanical calculation for a single tetramer:  $m = 0.59 \mu_B$  and  $m = 0.32 \mu_B$ , respectively. With this assurance of the validity of our approach, we obtain experimental estimates for the imbalance between the NN and tBuNO spin populations:  $R = 1.53(3)$  and  $R = 1.51(2)$ , for  $H = 7$  T and  $H = 4$  T. The quantitative agreement with theoretical predictions for entanglement-induced spin redistribution in F<sub>2</sub>PNNNO is remarkable.

Our polarized neutron diffraction results not only provide a direct evidence of spin entanglement, but also help understand the microscopic interactions that cause it. In Fig. 2, note the negative density in the vicinity of the apical carbon atom of the NN group. This large negative spin population [4] plays a key role in the ferromagnetic intra-molecular coupling  $J_F$ . It is a part of a sign-alternating spin density wave that propagates across the phenyl ring and connects the positively populated N sites of the NN and tBuNO fragments over a large distance. This density-wave mechanism is analogous to Ruderman-Kittel-Kasuya-Yosida interactions in metals.

AF interactions  $J_{AF}$  between tBuNO groups of the two molecules comprising each tetramer span a shorter distance, and are more conventional in nature. They are due to direct exchange and arise from molecular orbital overlap.

The simplicity and isotropic nature of delocalized magnetic *sp*-electrons in organic molecules make them useful as a testing ground for fundamental quantum mechanics. In the particular case of F<sub>2</sub>PNNNO we are able to detect and precisely quantify the redistribution of spin density caused by entanglement of four interacting quantum spins, and learn about the microscopic mechanisms of these entangling interactions.

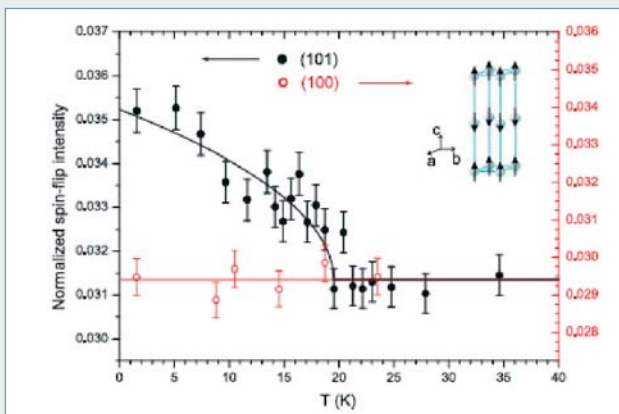
A full report on this study can be found in Ref. [5].

- [1] Mermin, N. D., *Physics Today* **38**, 38 (1985).
- [2] Leuenberger, M. N. and Loss, D., *Nature* **410**, 789 (2001).
- [3] Hosokoshi, Y., Nakazawa, Y. and Inoue, K., *Phys. Rev. B* **60**, 12924 (1999).
- [4] Davis, M. S., Morokuma, K. and Kreilick, R. W., *J. Am. Chem. Soc.* **94**, 5588 (1972).
- [5] A. Zheludev, V. O. Garlea, S. Nishihara, Y. Hosokoshi, A. Cousson, A. Gukasov and K. Inoue, cond-mat/0609299.
- [6] A. Gukasov, A. Goujon, J.-L. Meuriot, C. Person, G. Exil and G. Koskas, *Physica B, Proceedings of PNCMI-2006*, Berlin (see also in this report).

[C1. S. P. Bayrakci] **Magnetic Ordering and Spin Waves in  $\text{Na}_{0.82}\text{CoO}_2$**

$\text{Na}_x\text{CoO}_2$ , the parent compound of the recently synthesized superconductor  $\text{Na}_x\text{CoO}_2\cdot(\text{H}_2\text{O})_y$ , exhibits bulk antiferromagnetic order below  $\sim 20$  K for  $0.75 < x < 0.9$ ,  $y = 0$ . We have performed neutron scattering experiments on a  $\text{Na}_{0.82}\text{CoO}_2$  single crystal and observed for the first time Bragg reflections corresponding to A-type antiferromagnetic (AF) order (i.e. ferromagnetic *ab*-planes antiferromagnetically coupled along the *c* axis). The magnetic order is characterized by magnetic moments directed along *c*\* axis, causing the elastic neutron scattering cross section to vanish for purely magnetic Bragg reflections such as  $\mathbf{Q} = (0,0,1)$  (see figure). On other Bragg reflections, both nuclear and magnetic signals are superimposed, and polarized neutron scattering technique becomes essential to extract the weak magnetic signal. After calibrating the magnetic intensity measured for  $\mathbf{Q} = (1,0,1)$  against the intensity of the  $(1,0,0)$  nuclear peak, we could extract a value of the ordered magnetic moment equal to  $0.13 \pm 0.02$  mB per Co atom. The observation of transverse magnetic excitations along the *c*\* direction was comparatively straightforward and the results can be perfectly described by the standard spin-wave theory. However, both the weakness of the ordered magnetic moments and the damping of the spin-wave excitations suggest that  $\text{Na}_{0.82}\text{CoO}_2$  may correspond to an itinerant magnetic system.

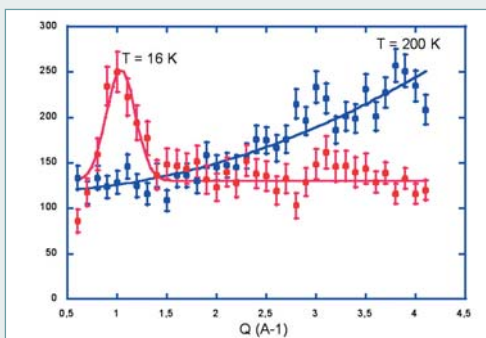
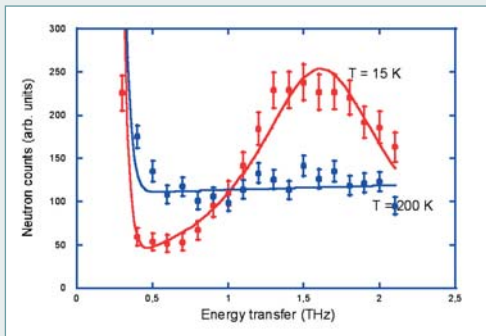
[Collaboration : S. P. Bayrakci, B. Keimer, D. P. Chen, C. T. Lin, MPI Stuttgart – I. Mirebeau, Ph. Bourges, Y. Sidis, LLB – M. Enderle, ILL – J. Mesot, PSI]



S. P. Bayrakci et al., Phys. Rev. Lett. **94**, 157205 (2005)

Normalized spin-flip intensity for  $\mathbf{Q} = (1,0,1)$  and  $(1,0,0)$  plotted as a function of temperature. The data were taken with the neutron polarization  $\mathbf{P} // \mathbf{Q}$ , at an incident neutron energy of  $E_i = 14.7$  meV. The lines are guides to the eye. Inset: A-type AF structure, represented with Co spins // *c*

[C2. O. Mentré] **Spin gap in the one-dimensional  $S = 1/2$  spin-ladder compound  $\text{Bi}_2\text{Cu}(\text{P}_{1-x}\text{V}_x)\text{O}_6$**



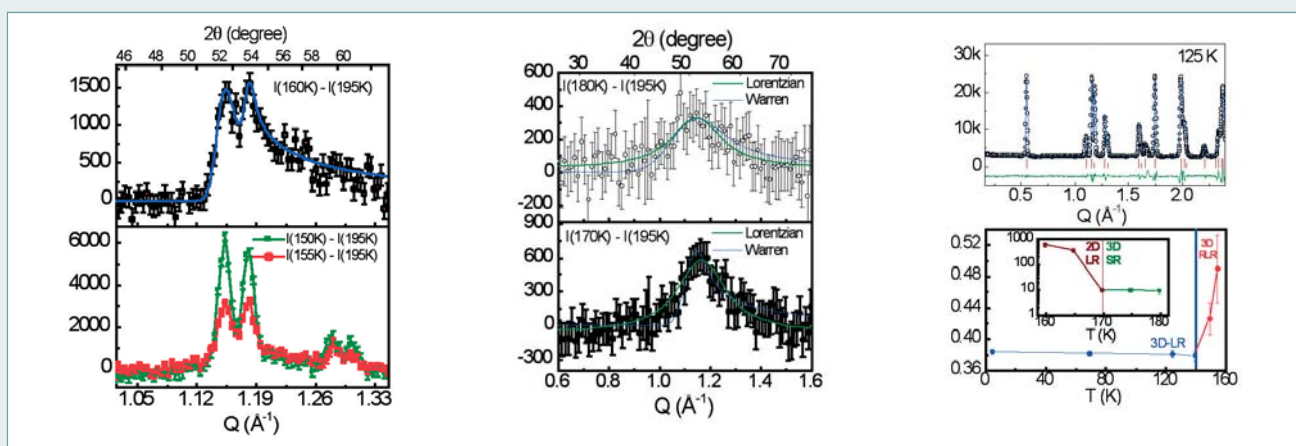
Spin ladders, spin-Peierls, or more generally dimer-chain systems have proven to be a very rich subject because of their essential quantum nature, at the crossroad between one and two dimensions.  $\text{Bi}_2\text{Cu}(\text{P}_{1-x}\text{V}_x)\text{O}_6$  belongs to this new interesting class of materials. The analysis of its crystallographic structure shows that the copper ions, carrying an  $S = 1/2$  spin, form zigzag two-legs ladders running along the *c* axis, with rungs parallel to the *b* direction. Two adjacent ladders are separated by nonmagnetic  $\text{Bi}$  ions and  $\text{PO}_4$  and  $\text{VO}_4$  groups, depending on the substitution level *x*. These  $\text{PO}_4$  and  $\text{VO}_4$  groups strongly affect the competition between magnetic couplings along the legs, along the rungs, and between adjacent ladders, leading in turn to different ground states. These structural properties are closely related to the spin dynamics. The evolution of the spin susceptibility as a function of temperature is typical of a spin-gap system for  $x < 0.7$ , while this spin-gap behaviour is lost for  $0.7 < x < 1$ . Inelastic neutron scattering measurements performed on powder samples with  $x = 0, 0.6, 0.9$ , and  $1$  enabled us to directly measure this spin gap for  $x = 0$  and  $0.6$ . The figures show typical  $\omega$  scans performed at fixed  $\mathbf{Q} = 1 \text{ \AA}^{-1}$  [above], and typical  $\omega$  scans performed at fixed energy transfer  $\omega = 1.5$  THz (6 meV) [under]. Cooling down to 15 K unambiguously shows the appearance of dynamical correlations peaked around  $\mathbf{Q} = 1 \text{ \AA}^{-1}$ , which corresponds to half the distance between copper spins. Further investigations on single crystals are planned to improve the description of the magnetic response.

[Collaboration : O. Mentré, F. Leclercq Hugueux (LPCS, ENSCL, Villeneuve d'Ascq) S. Petit, M. Hennion (LLB)]

## SUPERCONDUCTIVITY AND MAGNETISM

**[C3. S.M. Yusuf] Two- and three-dimensional magnetic ordering in the bilayer manganite  $\text{Ca}_{2.5}\text{Sr}_{0.5}\text{GaMn}_2\text{O}_8$** 

This neutron diffraction study on the bilayered manganite  $\text{Ca}_{2.5}\text{Sr}_{0.5}\text{GaMn}_2\text{O}_8$  has revealed a crossover phenomenon – from 3D short-range (SR) to 2D long-range (LR), then to restricted 3D LR (RLR), and finally to true 3D LR – in the antiferromagnetic correlations between the [010] oriented Mn spins in the  $a$ - $c$  plane (Figs. *a-c*). The effect takes place over a wide temperature range. Here  $3d$  magnetism and superexchange interactions are involved. The observation of a marked decrease in the resistivity on cooling and of a large negative magnetoresistance ( $\sim 50\%$ ) near the 3D LR Néel temperature suggest that the electronic and magnetic properties are strongly coupled and dimension-dependent. The present study is therefore highly relevant to the ongoing search for new 2D materials in the field of spintronics.



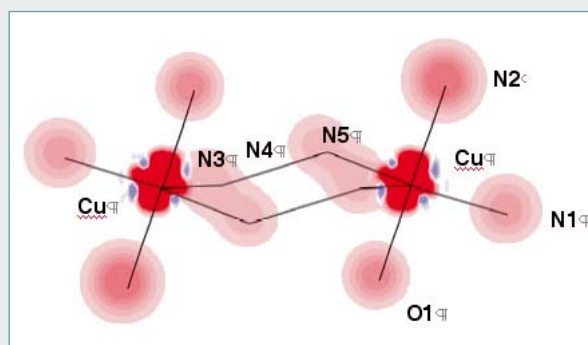
(a) Magnetic neutron diffraction patterns at 160, 155 and 150 K; nuclear background at 195 K has been subtracted out. The solid curve in the upper panel is a calculated profile using the 2D Warren function; in the bottom panel, lines are guides to the eye. (b) Magnetic diffraction patterns at 180 and 170 K; solid curves are calculated profiles using 2D Warren functions and 3D Lorentzian functions. (c) Top: Rietveld-refined neutron diffraction patterns at 125 K; bottom: half width at half maximum (HWHM), averaged for the 3D Bragg peaks (100) and (001). Inset: temperature dependence of the spin-spin correlation length  $\xi$ . [Collaboration: S.M. Yusuf, M. D. Mukadam, Bhabha Atomic Research Centre, India; J. M. De Teresa, P. A. Algarabel, C. Marquina, and M. R. Ibarra, Universidad de Zaragoza-CSIC, Spain; I. Mirebeau, J.-M. Mignot, LLB]

**[C4. C. Aronica] Ferromagnetic Interaction in an Asymmetric End-to-End Azido Double-Bridged Copper(II) Dinuclear Complex**

The nature of the intramolecular magnetic coupling in azido double-bridged copper(II) dinuclear complexes appears to be highly correlated to the coordination mode of the bridging azido ( $\text{N}_3$ ) groups. As a matter of fact, almost all the End-On complexes ( $\text{>N-N-N}$  bridging mode) present a triplet ground state ( $S = 1$ ) while the majority of End-to-End complexes ( $\text{-N-N-N-}$  bridging mode) either display a singlet ground state ( $S = 0$ ), or behave as two independent spins. A new End-to-End azido-bridged copper(II) complex  $[\text{Cu}_2\text{L}_2(\text{N}_3)_2]$ , with L : 1,1,1-trifluoro-7-(dimethylamino)-4-methyl-5-aza-3-hepten-2-onato, has been synthesized and characterized. Despite the rather long Cu–Cu distance ( $5.105(1)\text{\AA}$ ) measured from the x-ray diffraction crystal structure determination, the magnetic interaction is ferromagnetic with  $J = +16\text{ cm}^{-1}$  ( $H = -J S_1 S_2$ ). The experimental spin distribution from polarized neutron diffraction has been found to be localized mainly on the Cu(II) ions. Small delocalization has been observed on the ligand (L) and terminal azido nitrogen atoms, whilst it is strictly zero on the central nitrogen. Such a picture denotes a large contribution of the  $d_{x^2-y^2}$  orbital (in the  $\text{CuN}_2\text{N}_5$  plane) and a small population of the  $d_z$  orbital (along the Cu– $\text{N}_3$  direction), in agreement with our calculations.

[C. Aronica, E. Jeanneau, D. Luneau, H. El Moll, G. Pilet, Laboratoire des Multimatiériaux et Interfaces, Villeurbanne; M. A. Carvajal, V. Robert, Laboratoire de Chimie, ENS Lyon; B. Gillon, A. Goujon, A. Couson, LLB]

Experimental induced spin density in  $[\text{Cu}_2\text{L}_2(\text{N}_3)_2]$  at 2 K and  $H = 5\text{ T}$  projected along the  $b$  axis. Low levels only are represented: from  $0.02\text{ mB}/\text{\AA}^2$  to  $0.1\text{ mB}/\text{\AA}^2$  by steps of  $0.02\text{ mB}/\text{\AA}^2$ .



**[C5. J. Manson] Neutron diffraction study of a molecule-based 2-dimensional magnetic compound  $Mn(dca)_2(pym)(H_2O)$ : spin density and magnetic phase diagram.**

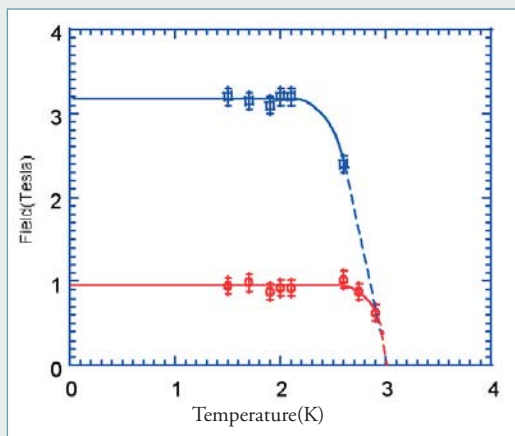


**Figure 1.** Magnetic phase diagram (H,T) of  $Mn(dca)_2(pym)(H_2O)$ .

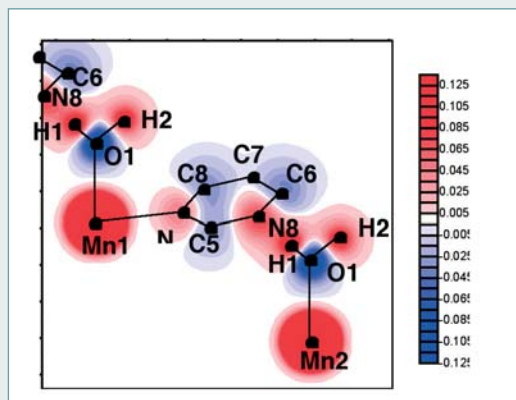


**Figure 2.** Induced spin density projection along the perpendicular to the O1H1N8 plane at 5 K under 4.5 T

The  $Mn^{II}(dca)_2(pym)(H_2O)$  compound (with  $dca = N(CN)_2$  and  $pym = N_2C_4H_4$ ) presents a 2-dimensional structure formed by layers in which the  $Mn^{2+}$  ions are alternately related by single or double (-NC-N-CN-) dicyanamide bridges. These layers, stacked along the  $c$ -axis, are connected by hydrogen bonds between the coordinated water molecules and N atoms of the pyrimidine rings and of the dicyanamide groups. The magnetic phase diagram established by single-crystal diffraction is reported in Fig. 1. In the AF1 structure, the antiferromagnetic ordered  $Mn^{2+}$  layers are AF-coupled to each other, while in the AF2 phase, above the spin flop transition, the layers are ferromagnetically coupled. In order to investigate the magnetic interaction pathways in this compound, particularly between the layers, the induced spin density has been determined by polarised neutron diffraction in the paramagnetic state at 5 K under a field of 4.5 T. The spin density map shown in Fig. 2 clearly evidences a positive spin density on the hydrogen atom of the N8..H1-O1 hydrogen bond, which overlaps with the positive density of the nitrogen atom N8 of the pyrimidine ring. This overlap favors AF coupling between the layers in zero field.

[Collaboration: J. Manson, Department of Chemistry and Biochemistry, Eastern Washington University, USA; B. Gillon, A. Gukasov, A. Cousson, LLB]

**[C.6. A. Goujon] Photoswitchable molecular compounds studied by neutron powder diffraction.**

Determining the magnetic structure of photoswitchable magnets is a main goal to understand the mechanism of photo-excitation. Neutron powder diffraction reveals the magnetic structure of compounds and provides an understanding of magnetic and structural correlations (nature, length scale). A dedicated sample holder has been designed to allow photoexcitation measurements to be performed *in situ* on the powder spectrometer G4-1. Ancillary equipments, such as a pulsed laser (Nd:YAG, *Minilite II*) or optical fibers, were also installed on G4-1. The design of the sample holder takes into account the need (i) to work with about 1 g of powder, and (ii) to illuminate homogeneously the majority of the powder in order to induce sizeable photo-conversion. Photoexcitation of a  $[Fe_{0.52}Zn_{0.48}(btr)_2(NCS)_2](H_2O)$  powder was carried out at 15 K using a pulsed laser light ( $\lambda = 532$  nm). At low temperature, the spin conversion is easily obtained by LIESST (light-induced excited spin state trapping) effect, and accompanied by huge structural changes. Fig. 1 shows a comparison between the low-spin (LS) state spectrum and the photoinduced state obtained after 20 hours. A mixing of the LS and photoinduced HS fractions was evidenced, indicating that 30% of the sample was converted to the HS state. The kinetics of the photoexcitation is shown in Fig. 2. The partial photoconversion is well explained by the strong absorption of the powder. This result is encouraging and further work is underway to increase the yield of photoexcitation.

[A. Goujon, B. Gillon, G. André, A. Gukasov, LLB]

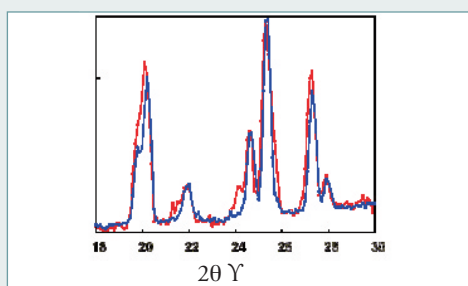


**Figure 1.** Diffraction pattern of Fe(btr) measured at 2 K (blue): LS state; (red): after 20 hours of photoexcitation.

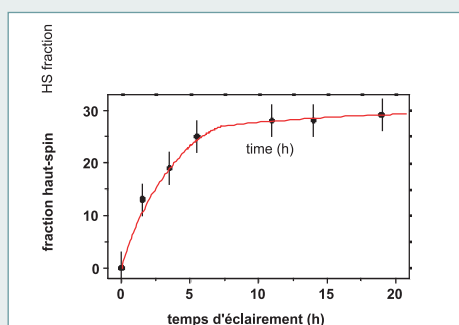


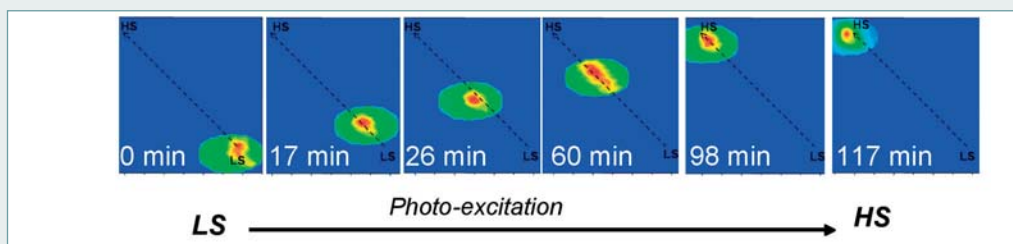
**Figure 2.** Kinetics of the photoexcitation in  $[Fe_{0.52}Zn_{0.48}(btr)_2(NCS)_2](H_2O)$  at  $T = 15$  K.

## SUPERCONDUCTIVITY AND MAGNETISM

**[C7. A. Goujon] Neutron Laue diffraction on the spin crossover crystal  $[\text{Fe}(\text{ptz})_6](\text{BF}_4)_2$  showing continuous photo-induced transformation**

Structural aspects of photoinduced phase transitions in spin-crossover compounds have been investigated by neutron Laue diffraction. A photocrystallographic experimental setup has been installed on the vertical-axis Laue diffractometer VIVALDI at the Institut Laue Langevin. The structures of the ground state and of the metastable LIESST (Light Induced Excited Spin State Trapping) state of the  $\text{Fe}^{\text{II}}$  spin-transition compound  $[\text{Fe}(\text{ptz})_6](\text{BF}_4)_2$  in the quenched state were determined at  $T = 2$  K. The results show that the local structure change upon photoinduced spin transformation is essentially an expansion of the  $\text{Fe}-\text{N}_6$  core without lowering of the  $O_h$  symmetry of the Fe environment. The  $\text{Fe}-\text{N}$  distance is increased by  $0.21 \text{ \AA}$  and the unit-cell volume by about 2%. It was found that the local structure of the photoinduced phase is very close to that of the high-temperature high-spin state. The evolution of the (0,-2, 8) Laue spot, as a function of the total irradiation time, is shown in the figure. For the first time, a progressive character of the photoinduced phase transformation was evidenced in spin-crossover compounds. The observed continuous shift clearly rules out the nucleation and growth of like-spin domains (LSDs) in the phase transformation. It also shows the basically homogeneous character of the photoexcitation process.

[A. Goujon, B. Gillon, A. Cousson, A. Gukasov, LLB; F. Varret, GEMAC, Versailles; G. McIntyre, ILL, Grenoble]



Absence of LSDs during photo-excitation of the spin-crossover crystal  $[\text{Fe}(\text{ptz})_6]\text{BF}_4$  rhombohedral phase (Goujon et al., Phys. Rev. B, 2006)

**[C8. A. Tamion] Magnetization depth profile of (Fe/Dy) multilayers**

The magnetization of  $[\text{Fe } 3\text{nm}/\text{Dy } 2\text{nm}]$  multilayers has been studied. The samples were thermally evaporated under ultra-high vacuum at different substrate temperatures varying from 320 K to 870 K. In order to get the magnetization depth profile of these Transition Metal/Rare Earth (TM/RE) multilayers, an investigation of the structural, chemical, and magnetic properties was carried out. The samples were studied by High Resolution Transmission Electron Microscopy (HRTEM), Three-Dimensional Atom Probe (3DAP) and Polarized Neutron Reflectivity (PNR). The multilayers have been found to be rather homogeneous, except for the first two bilayers deposited on the substrate: the mainly crystalline structure of the first Fe layers leads to an enhancement of the ordering temperature of amorphous Dy. Moreover, at low temperature, a negative exchange coupling between Fe and Dy layers has been evidenced. Magnetization profiles have also been calculated by Monte Carlo simulations to support the PNR fits.

[Collaboration : A. Tamion, P.-E. Berche, E. Talbot, C. Bordel and D. Blavette (Université de Rouen), F. Ott (LLB)]

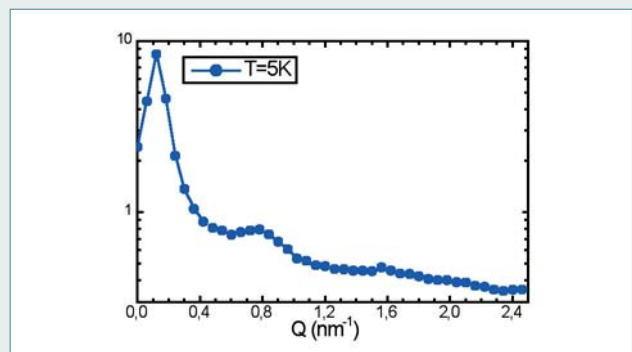
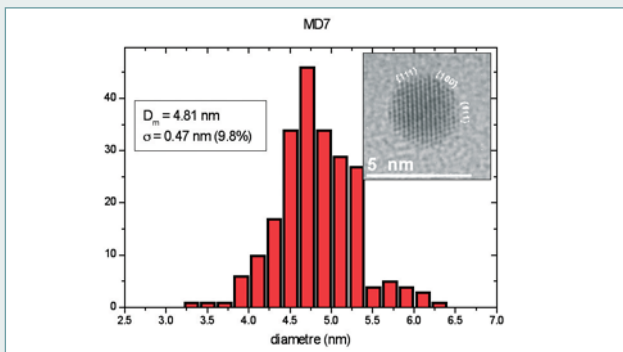


Samples deposited at a substrate temperature of 570 K. There is some interdiffusion between the Fe and the Dy layers. (left) at room temperature, no moment was found in the Fe layer because of its amorphous nature; (right) at 100 K, the Fe and Dy-Fe layers order antiferromagnetically. The layers in contact with the substrate behave very differently from the top layers.

### [C9. M. Delalande] Polarized SANS studies of FePt Magnetic Nanoparticles

Small angle neutron scattering with polarized neutrons (SANS POL) has been performed on films of FePt nanoparticles prepared by first diluting the powder in deuterated toluene (0.1% volume concentration) then drying it out. Magnetization measurements show a superparamagnetic behavior below 25 K. The saturated magnetization is  $290 \text{ emu/cm}^3$ , about 25% of the value for bulk FePt. The particle size distribution is centered around 4.8 nm (left frame) with a 10% dispersion. SANS POL data taken at  $T = 5 \text{ K}$  in an applied field of  $H = 2.1 \text{ T}$  (right frame) exhibit a peak at around  $0.8 \text{ nm}^{-1}$  indicative of an inter-particle distance of about 8 nm. This is in agreement with a picture of particles of diameter 5 nm linked by organic molecules of length 3 nm. As the temperature is increased a slight shortening of the inter-particles distance is observed.

[Collaboration: M. Delalande, A. Marty (DRFMC, CEA Grenoble); G. Chaboussant, S. Gautrot (LLB)]

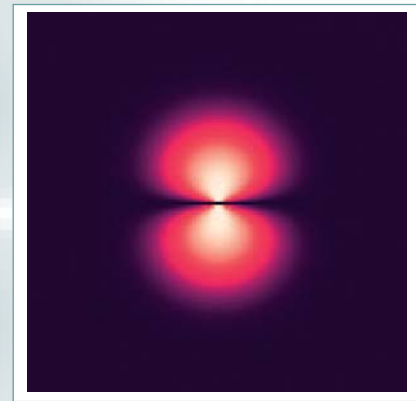
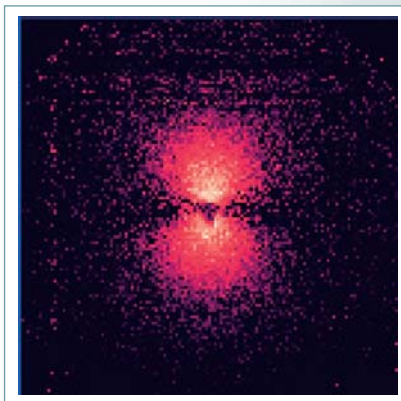


(left): Size distribution and TEM image of 5 nm FePt particles. (right): SANS POL data ( $\Delta I = I^+ - I^-$ ) of FePt particles at 5 K in a field of 2.1 T. The inset shows the 2D SANS signal; the ring structure reveals a magnetic contribution at  $Q \approx 0.8 \text{ nm}^{-1}$ .

### [C10. G. Viau] Small Angle polarised neutrons studies of dispersed magnetic Co-Ni nanowires

Small angle neutron scattering with neutron polarisation (SANS POL) has been performed on dispersed magnetic nanowires presenting a wide range of sizes and shapes. The length range from 40 to 500 nm and the diameter is usually comprised between 5 and 20 nm. The metallic nanowires are embedded in a polymer matrix (PMMA or polystyrene) with the objective of achieving isolated individual nanowires, which can be structurally oriented in an applied field during the polymerization process. The longer-term motivation is to study not only the static magnetic properties like the magnetization vector inside the wires, but also to investigate the dynamical properties of these quasi-1D systems. SANS POL experiments on two types of nanowires (long ones and bulky ones) have been performed at room temperature and under a magnetic field (0.5 T) strong enough to align the wire magnetization. A clear magnetic contribution, evidenced by a net difference between *up* and *down* polarisation signals (see figure) is observed. The results are in agreement with a uniform magnetization inside the wires.

[Collaboration: G. Viau, ITODYS Jussieu), T. Maurer, G. Chaboussant, F. Ott, S. Gautrot, LLB]



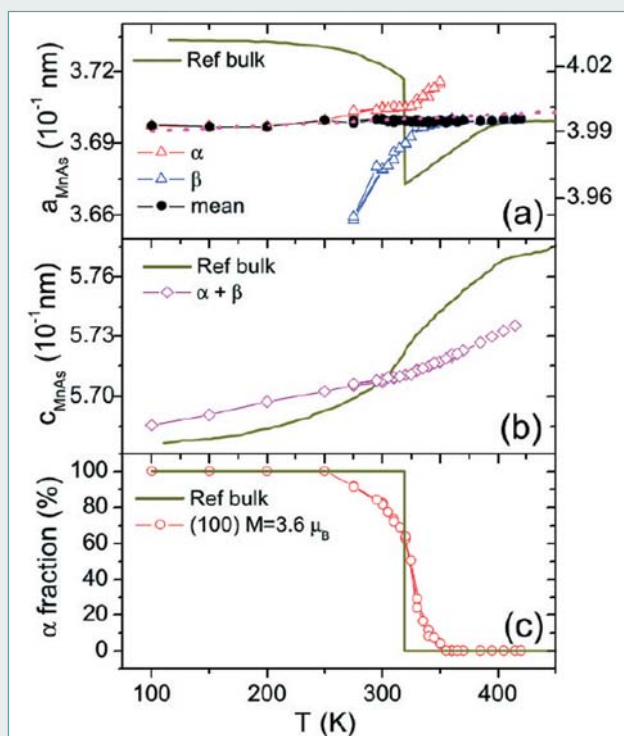
(left): Experimental SANS POL data ( $\Delta I = I^+ - I^-$ ) of "bulky" nanowires (12 nm diameter and 40 nm length).

(right): Simulation of the magnetic contribution using a uniform magnetic form factor.

[C11. V. Garcia] Magneto-structural phase transition in MnAs epilayers grown on GaAs(111)B substrates

MnAs thin films have recently attracted considerable interest due to their growth compatibility with GaAs, and potential applications in spintronics with semiconductors. Bulk MnAs is ferromagnetic in the hexagonal  $\alpha$ -phase from low temperature to 313 K where it displays a first-order phase transition to the orthorhombic  $\beta$ -phase. Thin films grown on GaAs(111)B substrates have good crystalline quality with a single epitaxy, atomically sharp MnAs/GaAs interfaces, and smooth surfaces. Also the magnetic phase transition is extended to higher temperature (335 K) in MnAs/GaAs(111)B systems, which is of great interest as the main limitation of MnAs for applications is its low Curie temperature. The evolution of the in-plane and out-of-plane parameters of MnAs epilayers was followed from 100 to 420 K using neutron diffraction (4F1 spectrometer, LLB) to understand the link between structural and magnetic properties in MnAs thin films. The main results from these experiments are summarized in the figure: (i) Contrary to bulk material, the mean in-plane parameter is almost constant from 100 to 420 K and follows that of GaAs due to epitaxial strain. (ii) This epitaxial strain induces an  $\alpha$ - $\beta$  phase coexistence in a wide temperature range (275–350 K). (iii) At low temperature, the  $\alpha$ -phase is subject to large in-plane compression but the magnetic moment is close to that of the bulk material ( $\approx 3.6 \mu_B$ ), the  $\beta$ -phase nucleation induces partial relaxation of the ferromagnetic phase up to 350 K, where it disappears. (iv) The unit-cell volume is almost constant before and after the phase coexistence, suggesting that the volume variation is not the leading parameter of the loss of magnetism. We think that the magnetic phase transition could be extended to higher temperature in MnAs epilayers grown on an appropriate substrate having a slightly different in-plane parameter or dilatation coefficient.

[Collaboration: V. Garcia, M. Marangolo, M. Eddrief, INSP, Paris – Y. Sidis, Ph. Bourges, F. Ott, LLB]



Temperature dependence of structural parameters of a 100 nm thin film of MnAs grown on GaAs(111)B substrate. (a), (b) temperature dependence of the in-plane and out-of-plane parameter for both phases deduced from neutron diffraction on MnAs(100) and MnAs(002), respectively. The in-plane and out-of-plane parameters of bulk MnAs are added. (c)  $\alpha$ -phase fraction deduced from integrated intensity of the spectra along MnAs(100) and considering a constant magnetization per Mn. The mean in-plane parameter calculated from this  $\alpha$ -phase fraction, is added in (a) together with the evolution of the GaAs parameter.









# MATERIALS SCIENCE & APPLICATIONS

# LABORATOIRE LÉON BRILLOUIN

# MATERIALS SCIENCE & APPLICATIONS

## Introduction

Materials Science activity at the LLB covers a variety of research fields including metals, alloys, polymers, geological materials, nanocomposites, organic materials, thin films... They are at the frontier of chemistry, physics and engineering sciences. The objectives of these studies are to understand and predict how parameters such as the chemical composition, the atomic structure and the microstructure determine the properties measured in materials at the macroscopic scale. Most of these studies have direct applications in technology and industry. This interdisciplinary activity addresses several of the main challenges of this beginning of century: advanced materials for energy storage and nuclear energy, new materials for information technology, aeronautics. A large number of the materials science research performed at the LLB is funded by companies and by research contracts.

Neutron scattering provides a wide range of tools to perform such studies:

- **Small Angle Neutron Scattering (SANS) and reflectometry** are key tools to study materials at the nanoscale: thin films, precipitates, pores, cavities, meso and nano porous structures...ranging in size between 1 and 100 nm.
- **Texture and strain scanning:** the strong penetration of the neutrons allows an analysis in volume, and thus to obtain information representative of the whole material.
- **Inelastic neutron scattering spectroscopy**, owing to the large incoherent neutron scattering cross-section of the  $^1\text{H}$  nucleus, is a unique tool, able to provide a global view of the dynamics of highly protonated systems (water,  $\text{H}_2$ ,  $\text{CH}_4$ , polymers) in bulk or under confinement.

## New technologies for Energy - Energy storage

The energy system in the foreseeable future will probably be a combination of multiple renewable and non-renewable energy sources as well as reversible and non-reversible energy conversion devices. Among these, **lithium batteries** and hydrogen-based storage such as **fuel cells** are prime candidates. During the last two years, a significant body of work has been devoted to these fields at the LLB. The studies have been conducted either as an in-house activity, or as collaborations or as external users performing experiments. This activity is in increasing evolution.

### FUEL CELL RESEARCH

---

Among all the emerging possibilities for storing energy, hydrogen is the ideal fuel and H-cells are one of the most attractive energy conversion device. In principle, hydrogen fuel-cell technology can be highly efficient and powerful in energy conversion, scalable and modular in engineering construction, clean, quiet, and safe in operation. However, formidable challenges exist in the present R&D stage. The major obstacles include the high cost in catalyst loading, corrosion, poisoning of electrodes and severe demands on the properties of electrolytes.

Since it drives the performances of the whole system, the management of water within the polymer electrolytes (Nafion) is another major issue. Inelastic Neutron Scattering spectroscopy has been used in combination with NMR relaxometry to track down the dynamical behavior of water within the porous structure of a Nafion membrane. [HI, J.-C. Perrin]. It has been shown that, when the membrane is sufficiently hydrated, there is no significant decrease of the water diffusion coefficient between the nanometric and the micrometric scales. Though, at lower hydration, the lamellar structure of the Nafion at the nanometric scale is responsible for a striking decrease of the water mobility.

The economic viability of fuel cells being mostly limited by the cost of the noble metal catalyst, a significant activity is devoted to rationalize its use, for example by a significant increase of the catalyst specific surface [CI, G. Carrot]. Grafting polymers from platinum nanoparticles permits : (i) to control the dispersion because polymer-grafted nanoparticles give very homogeneous Langmuir films where the distance between particles may be adjusted with the surface pressure. (ii) to improve both the compatibility of the particles with the membrane and the deposition onto gold electrodes.

Another approach consists in using solid electrolytes. Part of the LLB in house research has recently focused on a neutron-scattering study of the dynamics of protons in yttrium-doped barium cerate (BCY) [H2, N. Malikova]. BCY shows a high proton conductivity at  $\sim 800^\circ\text{C}$ , a temperature range acceptable for industrial power generation for onboard vehicle applications. This relatively high operation temperature facilitates the dissociation of hydrogen molecules at the anode-electrolyte interface and the suppression of peroxide intermediates at the cathode without using noble metal catalysts. The experimental approach capitalizes on the exceptional sensitivity of neutron to hydrogen for proton-diffusion study and the high contrasts among the elements in BCY for structural characterization of the electrolyte under different atmospheric and temperature conditions. So far, we have shown that the onset of proton mobility, and therefore conductivity, is closely related to a phase change within the BCY matrix. Work is underway for a global assessment of the detailed dynamics. This work is supported by the Outgoing Marie-Curie International Fellowship granted to Natalie Malikova. This is a joint research program between Argonne Nat. Lab/IPNS and LLB.

#### REVERSIBLE ENERGY SOURCES: LI BATTERIES RESEARCH

Besides fuel cell, a possible route to the industrial production of viable high specific energy/power energy sources for non-polluting vehicles and portable devices are batteries. The ionic conductivity performances of an electrolyte, *i.e.* the ionic macroscopic transport, are intimately linked to the dynamics and topological properties of the medium in which the ions migrate.

PEO (polyethylene oxide) complexed by Li salts is currently used in lithium solid polymer electrolyte batteries. The ionic conduction mechanism in bulk is now well understood: the polymer local segmental dynamics at short time (ps to the ns) drives the lithium transport properties. Ionic conduction preferentially takes place in the amorphous fraction of the polymer. Inducing polymer amorphisation by confinement makes it possible to increase the conduction performances. Porous alumina membranes, also referred as AAO (Anodic Aluminum oxide) are macroscopically highly ordered confining systems made of oriented parallel cylindrical channels. During the first year of her PhD, K. Lagrené (LLB) has focused on the synthesis, the customizing of the topology of AAO membrane and the confinement of PEO within the pore network [C2, K. Lagrene]. These steps have been highly successful and the work will now continue to characterize the PEO+Li conductivity under this highly anisotropic confinement.

The LLB is also involved in the LISSIL project, recently funded by the ANR (PNANO call 2006, Jean Le Bideau, CMOS/ Montpellier & IMN/Nantes). The studied system is Ionogel, a recently patented (CNRS) ionic liquid confined by sol-gel methods in a silica matrix. We will study and correlate the charges migration phenomena, the structuration and the dynamics of these highly confined ionic liquids. The strategy is to use complementary time and space multi-scales techniques (TOF, NSE, NMR relaxometry and confocal spectroscopy). Here again, the target application are lithium rechargeable batteries.

#### OIL INDUSTRY ORIENTED RESEARCH

During the first stages of the oil extraction process, instead of pure oil, the gross output of a derrick comes as a very stable water-oil macro-emulsion. While the focus is supposed to be set on oil itself, one has to deal with non negligible undesired amount of water. Understanding the stability mechanism of that macro-emulsion is therefore a key issue for the oil industry.

A collaboration between IFP (Institut Français du Pétrole) and LLB (see Highlight J. Jestin, in the Soft Matter chapter) has led to the development of an original method using SANS to characterize the structure and composition of interfacial films of asphaltenes (a system usually used as a model for "crude oil") in water/oil macro emulsions. The correlations made between the molecular organization at the local scale and the macroscopic properties of the emulsions offer new perspectives to investigate stability mechanisms during oil production.

This widening gap between demand and supply is leading several major oil companies to consider unconventional resources. Among these, "Tight Gas Reservoirs" (TGR), usually sandstone or carbonate rocks, are already discovered but are not in active production yet, due to technological inefficiency to produce at economical rates. The key issues for the TGR production enhancement are related to the control of the liquid / gas phase transitions under confinement.

This kind of TGR systems are also prime candidates for the underground storage of green house gas such as  $\text{CO}_2$ . LLB is part of the teams applying for a  $\text{CO}_2$ . In this framework, neutron scattering is a perfect tool offering:

(i) High penetrating power for working at high temperature (up to  $400^\circ\text{C}$ ) and high pressures (up to 5 kbar) corresponding to the actual TGR environment.

(ii) Isotopic substitution which can be used to unambiguously separate the contributions of the matrix, the liquid or the gaseous phase.

The following questions could be assessed: what is the structure of the porous material, what is the fluid inside the porous material, what is diffusivity of liquids inside such material...

## Materials for the nuclear energy – New composite materials

A significant share of the materials science activity at the LLB deals with the development of advanced materials for the nuclear industry (new fuels or new steels). The LLB has taken part for the last ten years in the research projects concerning the ageing of nuclear reactor materials. SANS brings a characterisation of the microstructure evolution of materials constitutive of the Pressure Water Reactor primary circuit, subjected to important requests (irradiation, thermal ageing, hydridation etc.). Thus, the precipitation of solute atoms or of defects induced by the neutron irradiation were highlighted in ferritic alloys (vessel, piping etc.), and Zr alloys (fuel cladding guide-tube materials). The clusters formation has direct effects on the mechanical properties. The prediction of these materials behaviour in-service conditions requires the knowledge of the mechanisms of precipitation. Also the research in new composite materials (metallic alloys and reinforced polymers) has been very active during the last two years.

### ADVANCED MATERIALS FOR THE NUCLEAR INDUSTRY

---

The last fifty years have shown how much the development of civil nuclear reactors (both prototype and industrial) required a considerable effort of R&D in the field of materials. The severe environment associated with nuclear reactors (high temperature and pressure, irradiation, corrosion, thermo-mechanical stresses, chemical compatibility) asks numerous questions in materials science.

New alloys are being developed in collaboration with the CEA/DEN (Direction de l'Energie Nucléaire), primarily with Service de Recherche de Métallurgie Appliquée SRMA (Y. de Carlan, JL Bechade, J. Henry, A. Alamo) and with the Service de Recherche de Métallurgie Physique SRMP (L. Chaffron, F. Legendre). Strong and fruitful collaborations exist with these two groups since 10 years.

In particular, the ODS (Oxide Dispersion Strengthened) martensitic or ferritic alloys [H3, M.H. Mathon] have been widely studied in order to understand the relationships between the fabrication process, the obtained microstructure and the mechanical behavior. SANS experiments have shown that the way to introduce the yttrium oxides for the mechanical alloying could be a key point to obtain a very fine distribution of nano-oxides after consolidation. The highest performances of some ODS steels are related to an oxides size of about 2 nm.

The effects of the milling conditions and the evolution of the oxides under annealing are under study. In the near future, we will focus on the behavior of these materials under external sollicitation such as irradiation, thermal ageing or friction stir welding. Furthermore, the 9CrW martensitic steels - candidates for the internal structure of future generation reactors or spallation sources – are always the object of various works such as helium bubbles precipitation under irradiation or the influence of the chemical composition on the nanometric carbide formation.

A major long run issue for nuclear based energy is the safe management of the nuclear waste. This issue has been addressed by collaboration between the LI2C group of Univ. Pierre et Marie Curie (Prof. P. Turq) and the LLB. In this framework, the ANDRA has funded the PhD thesis of Natalie Malikova [C3, N. Malikova]. Diffraction, time-of-flight (ToF), Neutron Spin-Echo (NSE) and Molecular Dynamics (MD) simulations have been combined to provide fine information, at a quantitative level, on the behavior of water and ions in clays (particularly Cs<sup>+</sup> a potential radionuclide).

### NEW COMPOSITE METAL ALLOYS

---

For industrial applications, metallic materials must, more and more often, show very good mechanical properties at high temperatures (250–400°C). A way of improving the mechanical performances of steels (Fe-5%Cr) at high temperatures consists in modifying the secondary precipitation by introducing alloying elements. In collaboration with D. Delagnes et al. [H4, D. Delagnes] of the Ecole des Mines d'Albi, a study of tool steels has been performed by SANS. This work shows a strong correlation between the secondary carbides precipitation, the mechanical resistance at high temperature and the Charpy impact energy.

In response to the need to reduce the energy consumption and the carbon dioxide emissions, the industry of transport, in particular aeronautics, seeks steels with very high mechanical characteristics. American research and industry have developed a

production process of new steels by designing a microstructure reinforced by a double precipitation of nanometric carbides and intermetallic phase. The principle of this double reinforcement opens the way to new families of materials. With the same aim, the AMARAGE project, funded by the ANR call “Matériaux et Procédés” undertakes this research on martensitic steels alloyed with C, Cr, Mo, Ni, Al, Co or V hardened by simultaneous precipitations of carbides of Mo and intermetallic Ni-Al. This project runs from 2006 to 2009. It is coordinated by Aubert&Duval and networks five research laboratories (CROMeP/Ecole des mines d’Albi, CEMES/Toulouse, LSG2M/École des Mines de Nancy, LLB, GPM/Rouen).

### NEW COMPOSITE POLYMER MATERIALS

The LLB is involved in an ANR (with J.P. Salvetat/ CRMD Orléans) dedicated to the study of the mechanical reinforcement of polymer matrix charged with carbon nanotubes (BIONANOCOMP, a “white project” of the 2005 ANR call, funded from 2005 to 2008). A potential application is the production of biocompatible artificial tendons. LLB neutron beams will be used to check the aggregation states of the nanotubes within the matrix. Inelastic neutron scattering experiments are also scheduled to check potential modifications of the polymer local dynamics as a function of the nanotubes loading.

### FUTURE TRENDS

A collaboration with DEN/LMPC (J. Lechelle) aims at reducing the heterogeneous character of the distribution of plutonium in microstructure MOX (reduction of the hot points). For that, sintering additives ( $\text{TiO}_2$ ,  $\text{Cr}_2\text{O}_3$ , S) can be added to the MOX. It allows a more important grain growth. When the introduced quantity is higher than the limit of solubility of chromium in the solid solution  $(\text{U,Pu})\text{O}_2$ , chromium can precipitate in the form of  $\text{PuCrO}_3$  and pin the grain boundaries. The size distribution of the pores is thus modified in the presence of Cr. SANS experiments should allow to characterize the porosity evolution during the sintering. Also, texture measurements will be performed to determine if the crystallographic texture can be modified during the grain growth in the presence or not of additives.

The studies relating to materials of nuclear interest carried out in collaboration with the DEN (SRMA B. Marini) should be extended to the stainless steels used for the internal structures of PWR reactors. These steels present an embrittlement under irradiation probably induced by the formation of defect clusters or of dislocation loops. The analysis by SANS would make it possible to define and quantify these objects. These materials being subject to very strong amounts of irradiation, an important lapse of time was necessary after irradiation so that the radioactivity allows the handling of the samples.

## Advanced materials for Information technology

### SPIN ELECTRONICS

A large amount of work is dedicated to the study of the magneto-electronic properties of multilayer systems of nanometric thickness. This field is now referred to as “*spin electronics*” and aims at using the magnetic properties of some materials to create a new generation of electronic devices.

In this field, a large part of the materials science research of the last 3 years has been devoted to the search of new materials in the form of thin film suitable for spin-electronic devices. A number of these materials have been characterized by polarized neutron reflectometry at the LLB. We can mention materials such as  $\text{Fe}_3\text{O}_4$  and  $\text{CoFe}_2\text{O}_4$  (DRECAM/SPCSI), MnAs (INS Paris), GaMnAs, Fe/Ge (Acad. Science Pologne), SiC:Fe (LPM, Univ. Poitiers [**C4**, **A. Declémy**]), ZnO:Co (UMR CNRS –Thalès). Polarized neutron reflectometry allows to characterize the magnetization depth profiles (thickness of the films, magnetization orientations in the different layers of spin-valve systems).

Another large field of research deals with magnetic oxides which offer a wealth of properties. Recently, a very active field topic has been the search for magneto-electric materials in which the magnetic behavior can be controlled by an electrical field. Materials such as  $\text{BiFeO}_3$  are presently being studied in collaboration with the UMR CNRS-Thalès.

## RECORDING MEDIA

---

Rewritable DVD disks use some complex tellurium based covalent alloys. These alloys display some optical properties that depend strongly on the atomic arrangement. Writing or erasing a bit is achieved by amorphizing or recrystallizing a small zone of a thin layer through a laser pulse. The recrystallization process is the time limiting step. In order to find some more efficient alloys, it is necessary to understand what drives both the optical contrast and the recrystallization kinetics. Different classes of Te-alloys have been investigated in the liquid state by neutron diffuse scattering on the 7C2 diffractometer. Some general features have been extracted from neutron scattering characterization of the liquid state : there is a relation between the structure of the liquid, the number of valence electrons per atom and the phase change ability [H5 J.P. Gaspard].

## FUTURE TRENDS

---

The growth of thin films structures and multilayers is now well mastered. Even though there is still a large number of material combinations to be studied, the interest is now shifting towards nano-particles and nano-patterns. The confinement of the magnetic properties does not anymore take place only in one direction (thickness of the film) but in 3 directions.

The fabrication of such nano-objets can be performed either by a top-down approach (use of electronic lithography or alumina membranes) or by a bottom-up approach in which the systems self-organize in nanostructures : formation of magnetic stripe domains in materials such as MnAs (INS Paris) or FePd (DSM/DRFMC, Grenoble), formation of nanoclusters of Co in an insulating matrix (SiO<sub>2</sub> or TiO<sub>2</sub>) during a sputtering process. Most of these materials exhibit strange or at least anomalous transport properties. The knowledge of the organization of these materials is thus of great interest since the detailed organization of the nanoparticles controls the electrical transport properties. A number of studies combining polarized neutron reflectometry and SANS have been undertaken in such systems.

In particular we are studying magnetic nanowires synthesized by a chemical route (ITODYS/G. Viau). This bottom-up approach allows to build very clean magnetic objects. It might be possible to implement them in electronic devices such as HF filters or antennas. This topic is the PhD Thesis subject of Thomas Maurer who has joined the LLB at the end of the year on a BDI contract.

# Metallurgy - Engineering

## RESIDUAL STRESSES – STRAIN SCANNING

---

Internal and residual stresses in materials have a considerable effect on material properties, including fatigue resistance, fracture toughness and strength. The weak absorption makes neutron diffraction a unique non-destructive tool to determine the complete tensors of the residual stresses in crystalline materials and to establish 3D cartographies. The principle of the technique, called Neutron Strain Scanning, is to use crystal lattice as an atomic strain gauge to measure strain distributions with a sub-millimeter spatial resolution. The stresses are thus calculated from the measured strains using elasticity laws.

Since 1989, the LLB has a diffractometer devoted to the characterization of the residual stresses. This instrument continuously evolved in order to meet the needs of the industrial partners (determination of three-dimensional cartographies of the stress field in massive parts weighing up to 500kg) as to those of the scientific community based on a finer analysis of deformation heterogeneities.

The engineering activity is currently funded by industrial partners and has been reinforced during the last years. Among the main industrial collaborations, we can mention the recent work carried out with CETIM (Centre Technique des Industries Mécaniques), which has consisted in the determination of residual strains in two cylinder heads of boat engines (weight of 150kg).

Very recently, an important collaboration was re-initiated with Dassault Aviation, following preliminary validation measurements carried out successfully in 2003. LLB is now involved in a large research program aiming at characterizing the residual stress fields in a part of a Mirage 2000 fighter wing at different steps of its conception, by coupling neutron diffraction measurements and finite elements calculations.

The development of a compact tensile machine [C5, V. Klosek] in collaboration with the LPMTM (Laboratoire des Propriétés

Mécaniques et Thermodynamiques des Matériaux) generates new fundamental studies. This machine adapted on the Euler's cradle of the G5.2 and 6T1 diffractometers gives the possibility of following "in situ" the evolution of the residual stresses and texture under uniaxial loading. The deformation mechanisms, the heterogeneities of deformation, the stress induced phase transformations or the local mechanical behaviours of heterogeneous materials are new research field opened to study.

In collaboration with V. Ji from the LIM (Laboratoire d'Ingénierie des Matériaux) at ENSAM Paris, measurements were performed on «duplex» steel (50% ferrite and 50% austenite) to analyze in situ, by neutron diffraction, the evolution of local macro-stresses in each phase as a function of the applied strain. Diffraction peaks for both phases could be recorded simultaneously. The method was validated and will be applied on other kind of materials.

### CRYSTALLOGRAPHIC TEXTURE

---

A large part of the activity was dedicated to the recrystallization phenomena study in copper alloys [C6, S. Jakani]. A detailed study of bronze and brass alloys is also in progress. Measurements of diffraction of the neutrons highlighted that the distribution and the values of the stored energy according to the crystallographic orientations vary with the added element. Moreover, the "in situ" recrystallization studies allow to evaluate the activation energy for each material. The activation energy decreases with the deformation rate but increases with the content of alloy element. This work will be coupled to a microstructural analysis.

The description and the prediction of the mechanical properties of materials require an analysis of the mechanical behaviour on the grain scale. The polycrystalline materials can be regarded as multiphase materials, each phase being associated with a crystallographic orientation and thus a mechanical behaviour. The "in situ" studies of elastic and plastic strain under uniaxial load will make it possible to quantify these heterogeneities of deformation. The first studies performed on a CuSn 9% alloy showed significant differences between the crystallographic orientations. This type of study will be carried out on various FCC materials such as copper alloys, steels...

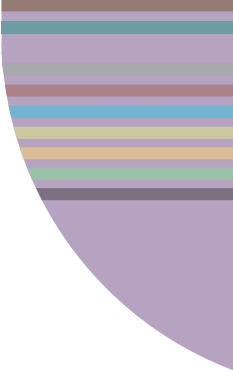
### FUTURE TRENDS IN METALLURGY STUDIES

---

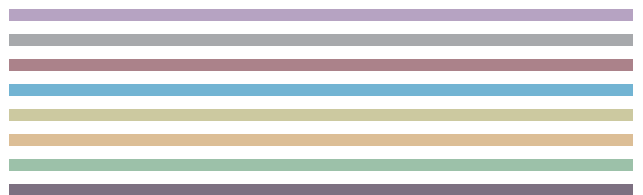
In the near future, two new scientific themes will be developed at the LLB in collaboration with ENSAM/Paris.

The first one is the study of memory-shape alloys (MFA). MFA alloys undergo a martensitic phase transformation which leads to a change in macroscopic form following a temperature variation. This phase transformation is characterized by a weak volume variation and an important shearing according to a crystalline plan and a well defined crystalline direction. Any manufacturing treatment can induce this transformation. It is of primary importance to control the impact of a deformed state on the phase transformations. Thus, this process will be applied to Cu-Al-Be and Cu-Zn-Al alloys for which one will endeavour to understand the evolution of the microstructural and mechanic state under mechanical sollicitation.

The second one is the study of the martensite transformation under load in steels. "In situ" neutron diffraction measurements under load will allow to obtain a description of the stress state as well as the phases in presence according to the loading. This work will be undertaken in collaboration with the DEN/SRMA.



# MATERIALS SCIENCE & APPLICATIONS



- H1.** QENS study of water dynamics in the Nafion membrane.  
J.-C. Perrin, S. Lyonnard, F. Volino, A. Guillermo
- H2.** Proton Conduction in yttrium doped barium cerate.  
N. Malikova, J.-M. Zanotti, C.K. Loong
- H3.** Small angle neutron scattering investigation of ODS martensitic steels.  
M.H. Mathon, Y. de Carlan, P. Olier, L. Chaffron, C. Cayron, S. Ukai, A. Alamo
- H4.** Influence of alloying elements on nanometric carbides precipitation in 5% chromium martensitic steels.  
P. Michaud, D. Delagnes, P. Lamesle, M.H. Mathon
- H5.** Rewritable DVD, RAM memories: between the electronic structure and the recording ability, neutron scattering shed some light.  
J.-P. Gaspard, V. Coulet, C. Bichara, C. Steimer, M. Wuttig, B. Beuneu
- [C1. **G. Carrot**] Self-assembling via Langmuir-Blodgett films and SANS characterisation of polymer-grafted platinum nanoparticles: a possible application in fuel cells.
- [C2. **K. Lagréné**] Dynamics of a polymer confined in macroscopically monodisperse oriented pores.
- [C3. **N. Malikova**] Dynamics of water and ions in clays: a concurrent TOF, NSE and MD study.
- [C4. **A. Declémy**] Ferromagnetic Fe-implanted SiC: New results towards a Diluted Magnetic Semiconductor.
- [C5. **V. Klosek**] A compact tensile machine for in situ neutron diffraction study of materials under external loading.
- [C6. **S. Jakani**] Deformation and recrystallization mechanisms of CuSn alloys (bronze).

# H1. QENS STUDY OF WATER DYNAMICS IN THE NAFION MEMBRANE

JEAN-CHRISTOPHE PERRIN, SANDRINE LYONNARD, FERDINAND VOLINO, ARMEL GUILLERMO

UMR SPram 5819 DRFMC/CEA Grenoble

Proton Exchange Membrane Fuel Cells are electrochemical devices developed for energy systems able to offer a competitive and clean alternative to standard oil based power suppliers. The key element of the cells is the ionomer membrane that must allow for proton transport from the anode to the cathode. The ionic conductivity insured by the acidic functionalities ( $\text{SO}_3^-$  groups) strongly depends on the hydration state of the membrane. Since the swelling state of the membrane can vary under operative conditions in a fuel cell, the hydration level appears as a crucial parameter for optimizing the performances. Moreover, proton conductivity and water dynamics are strongly coupled. In this work, we focused on the confinement effects on water mobility at the molecular level, as a function of the water loading in the Nafion. For this purpose, we have used QuasiElastic Neutron Scattering (QENS) to investigate the nano to picosecond molecular dynamical behaviour of the water adsorbed in the membrane.

**Experiments.** The QENS experiment were performed at 25°C on the time of flight (TOF) spectrometer Mibemol of the LLB with incident wavelengths  $\lambda_i = 5.2 \text{ \AA}$  and  $8 \text{ \AA}$  corresponding to an elastic resolution of  $\Delta E = 140 \text{ \mu eV}$  and  $40 \text{ \mu eV}$  FWHM respectively. The time scale has been extended to the nanosecond range by a complementary backscattering (BS) experiment performed on IN16 of ILL ( $\lambda_i = 6.27 \text{ \AA}$ ;  $\Delta E = 1 \text{ \mu eV}$ ).

**Sample preparation.** The membrane samples have been prepared from almost dry to fully hydrated. The combination of sorption measurements and SANS experiments allowed us to know with precision the quantity of water in each sample. We characterize this quantity by the parameter  $\lambda$ , which corresponds to the number of water molecules per ionic  $\text{SO}_3^-$  group.

**Data analysis.** In this work, local diffusion in confined geometry, long-range diffusion and atomic granularity are accounted for in a single model in the full  $Q$ -range ( $0.34 < Q < 2.25 \text{ \AA}^{-1}$ ). The raw data analysis shows that the spectra needs to be analysed in terms of the superposition of two kinds of dynamics in the water-swelled Nafion that necessarily corresponds to the existence of two types of protons that are not exchangeable within the longer time-scale of the experiments ( $\sim 600 \text{ ps}$ ). As a consequence, the experimental intermediate scattering function has been written as the sum of two components witch correspond respectively to “fast” (few ps) and “slow” ( $> 100 \text{ ps}$ ) motions<sup>(1)</sup>:

$$I_{\text{exp}}(Q, t) = \text{Amp} \times [N_{\text{fast}} \times I_{\text{fast}}(Q, t) +$$

$$N_{\text{slow}} \times I_{\text{slow}}(Q, t) + I_{\text{el}}(Q)] \times R(t) \quad (*)$$

$N_{\text{fast}}$  and  $N_{\text{slow}}$  correspond to the number of mobile protons involved in the corresponding dynamics,  $I_{\text{el}}(Q)$  is the elastic contribution of the polymer matrix,  $R(t)$  is the temporal resolution function and  $I_{\text{fast}}(Q, t)$  and  $I_{\text{slow}}(Q, t)$  are the intermediate scattering functions written as:

- $I_{\text{fast}}(Q, t) = I_{\text{loc}}(Q, t) \times I_{\text{lr}}(Q, t)$ , where

$$I_{\text{loc}}(Q, t) = \exp \left[ -Q^2 \sigma^2 \left( 1 - \exp \left[ \frac{-(D_l / \sigma^2) t}{(1 + 2D_l Q^2 \tau_{\text{mi}})} \right] \right) \right]$$

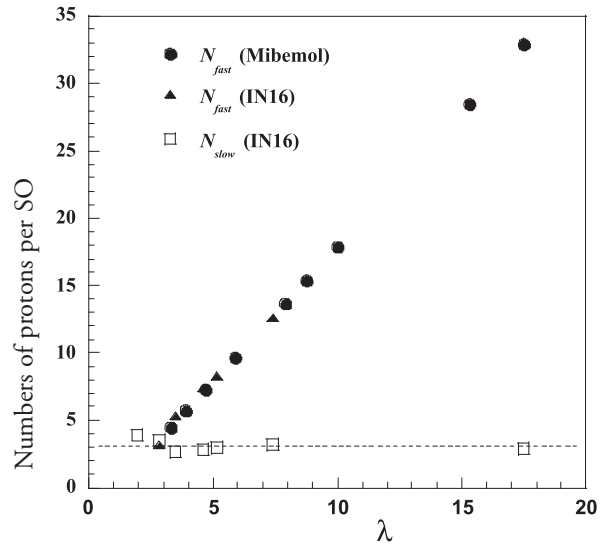
accounts for localized translational diffusion (with a diffusion coefficient  $D_l$  and a microscopic jump time  $\tau_{\text{mi}}$ ) inside a volume of typical size  $2\sigma$  and  $I_{\text{lr}}(Q, t) = \exp(-D_l Q^2 t)$  accounts for long range diffusion<sup>(2)</sup>.

- $I_{\text{slow}}(Q, t) = (1 - a(Q)) + a(Q) \times \exp(-t / \tau_{\text{slow}})$ ,

where  $a(Q) = \exp(-Q^2 \sigma_{\text{slow}}^2)$  is the EISF of the slow motion (characteristic time  $\tau_{\text{slow}}$  and characteristic distance  $2\sigma_{\text{slow}}$ ). The quasielastic spectra have been calculated by numerical Fourier transform calculations of expression (\*).

**Results.** The proton population of the “slow” motion is found to be constant over all the swelling range at the value  $N_{\text{slow}} \sim 3$  (Figure 1), whereas the “fast” population  $N_{\text{fast}}$  increases almost linearly with the total number of water molecules  $\lambda$ .

Figure 1



This result pleads in favour of the existence of the hydronium ion as a long life-time entity in the Nafion. This picture is supported by the evolutions of the residence times  $\tau_{mi}$  and  $\tau_{slow}$  (Figure 2) and the characteristic confinement domains ( $2\sigma$  and  $2\sigma_{slow}$ ) (Figure 3) which show that the 3 “slow” protons are diffusing  $\sim 50$  times slower than the “fast” protons, in a confinement domain of almost identical size.

Figure 2

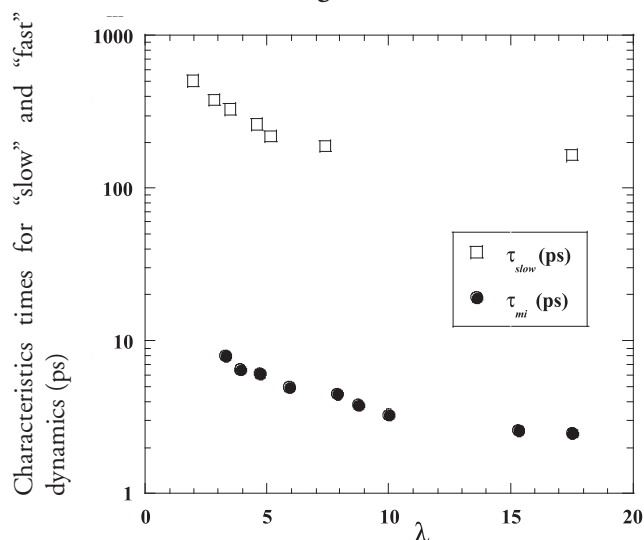
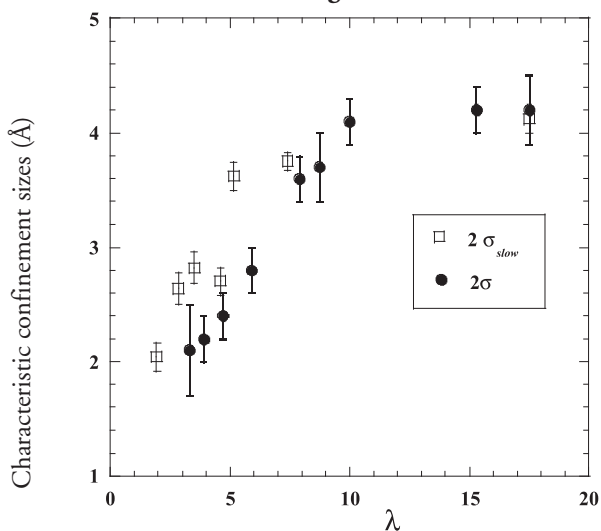
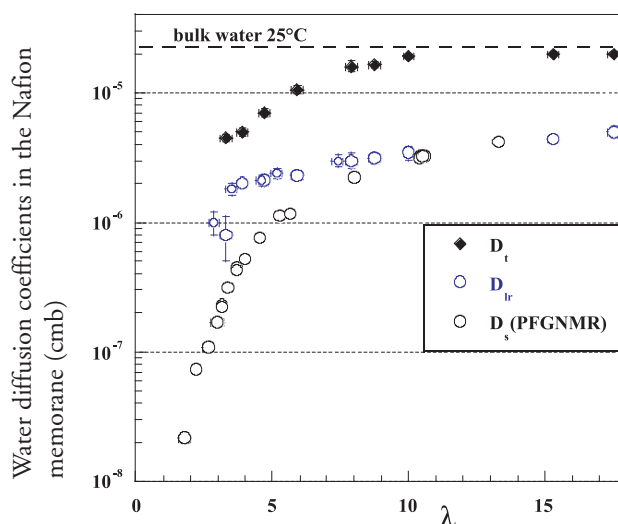


Figure 3



The evolution of these parameters, together with that of the local and the long-range diffusion coefficients (Figure 4) illustrates the progressive acceleration of the water dynamics when hydrating the membrane. For the highest hydration states, the local behaviour is very close the one observed in bulk water. Moreover, as soon as  $\lambda \sim 3$ , a long-range diffusion coefficient must be introduced in order to fit the quasielastic spectra in both experiments. The water can thus diffuse at larger distances than  $2\sigma$  for very small amount of water.

Figure 4



Above  $\lambda \sim 10$  the long-range diffusion coefficient is equal to the self-diffusion coefficient measured by pulsed field gradient NMR at the micrometer scale. This remarkable property of the membrane tells us that there is no slowing down of the diffusion between the nanometric and the micrometric scales when the membrane is sufficiently hydrated. At low hydration, the difference between the two diffusion coefficients can be attributed to the lamellar structure of the Nafion at the nanometric scale as revealed by NMR relaxometry experiments<sup>(3)</sup>.

(1) Perrin, J.-C.; Lyonnard, S.; Volino, F. *J. Phys. Chem B*, accepted for publication.

(2) Volino, F.; Perrin, J.-C.; Lyonnard, S. *J. Phys. Chem B* **2006**, *110*, 11217.

(3) Perrin, J.-C.; Lyonnard, S.; Guillermo, A.; Levitz, P. *J. Phys. Chem B* **2006**, *110*, 5439.

## H2. PROTON CONDUCTION IN YTTRIUM DOPED BARIUM CERATE

N. MALIKOVA<sup>1,2</sup>, J.-M. ZANOTTI<sup>1</sup> & C.K. LOONG<sup>2</sup>

<sup>1</sup>Laboratoire Léon Brillouin, CEA-Saclay, 91191 Gif-sur-Yvette

<sup>2</sup>Argonne National Lab., Intense Pulsed Neutron Source, Argonne, IL, USA

One of the major challenges in the development of hydrogen fuel cells remains the choice of electrolyte. Severe demands exist on a number of its properties including very high ionic and very low electronic conductivity, high thermal and chemical stability and durability. Yttrium doped barium cerate (BCY) meets many of the above requirements. It has been studied intensively since the first observation of its high proton conductivity at elevated temperatures ( $> 600^\circ\text{C}$ )<sup>[1]</sup>. Barium cerate has a perovskite-type structure, in which substitutions of  $\text{Ce}^{4+}$  by  $\text{Y}^{3+}$  cause the formation of oxygen vacancies. The doped material is hygroscopic, it absorbs water dissociatively resulting in the formation of hydroxyl groups (see Figure 1). At temperatures above  $400\text{--}500^\circ\text{C}$ , hydrogen atoms in the structure become mobile, leading to proton conductivity (20% yttrium doping necessary for optimal conductivity). While the ultimate interest is the macroscopic motion of H atoms under an applied electric field, the understating of the mechanism itself requires the knowledge of the local proton environment. It is studied here using a combination of inelastic and quasi-elastic neutron scattering, taking advantage of the complementary techniques available on pulsed (IPNS, ANL) and continuous (LLB, Saclay) neutron sources. The experimental data are to be complemented with microscopic simulation at a later stage.

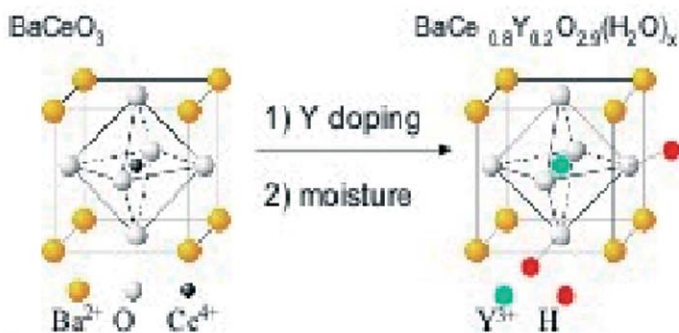


**Figure 1:** Idealised (cubic) structure of barium cerate and its yttrium-doped counterpart containing hydroxyl (OH) groups.

In recent neutron diffraction experiments, the structural phase transitions of the underlying perovskite network, as a function of temperature and water uptake, have been highlighted as a crucial factor determining the behaviour of H atoms<sup>[2]</sup>. A monoclinic ( $I2/m$ ) phase has been identified as a phase accommodating the H atoms in the structure at room temperature. Furthermore, our measurements on the QENS spectrometer at IPNS, providing concurrent structural and dynamic information, give evidence for a link between the disappearance of the monoclinic ( $I2/m$ ) phase at around  $400^\circ\text{C}$  and a change in the proton dynamics as indicated by the mean-squared displacement determined from the Debye-Waller factor (see Figure 2).

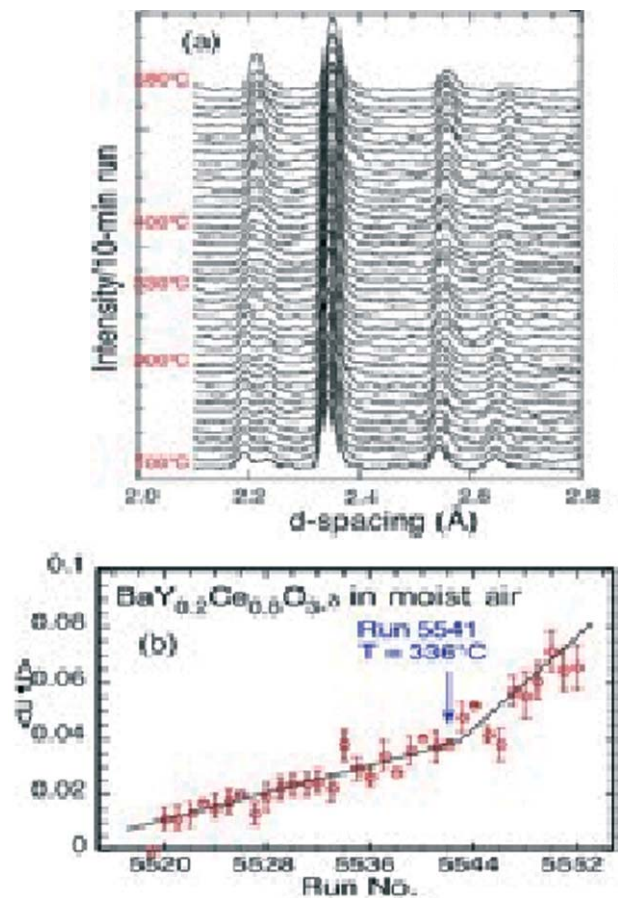


**Figure 2:** Concurrent data collection of the diffraction patterns of BCY and the hydrogen atom mean-square displacements (QENS spectrometer, IPNS).

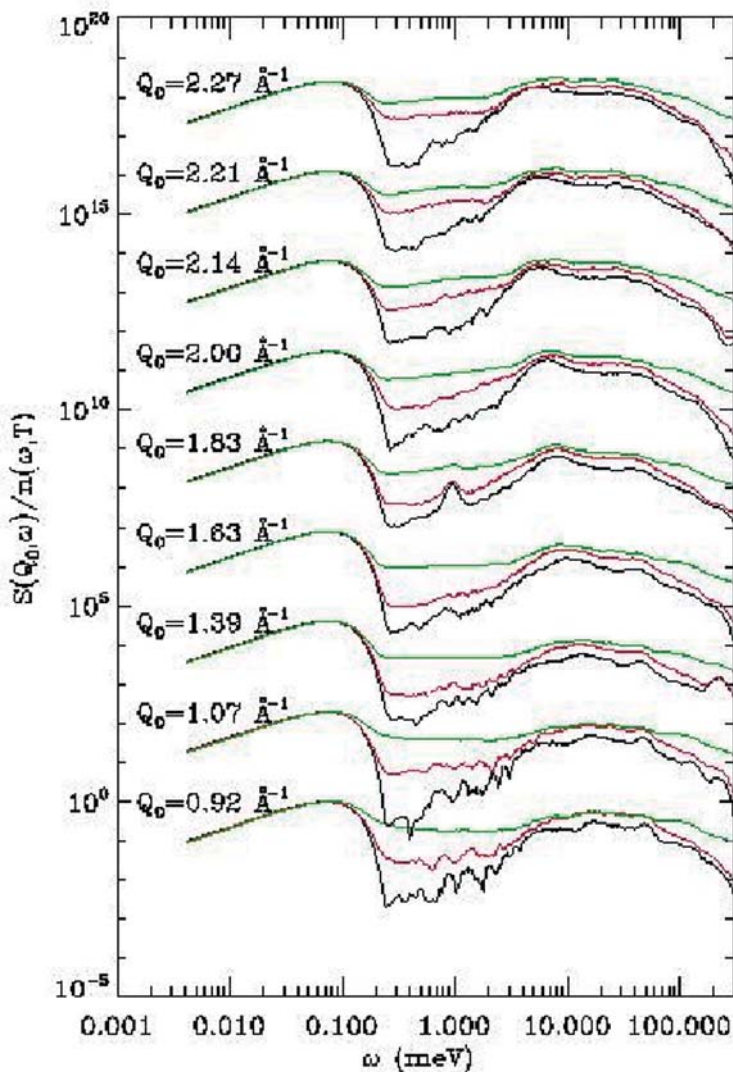


**Figure 3:** Susceptibility representation of low-resolution quasi-elastic data (650°C, MIBEMOL) on wet BCY (green), dry BCY (red), background (=quartz tube, black).

We are currently complementing the existing quasi-elastic neutron data with more detailed measurements, at varying resolutions, to elucidate the  $Q$ -dependence of the observed hydrogen motion.

Using a flow-cell set-up, allowing in-situ hydration and dehydration of the BCY system, we have collected both low- and high-resolution data, at the MIBEMOL spectrometer (LLB, resolution (FWHM) of 150  $\mu\text{eV}$ ) and IRIS spectrometer (ISIS, resolution (FWHM) of 18  $\mu\text{eV}$ ) respectively.

Susceptibility representation of the low-resolution data (Figure 3), indicates increased signal in the region 0.3-2 meV upon hydration of the BCY sample as well as around 100 meV. The observed quasi-elastic broadening is reproduced well using a trans-rotational model, giving rise to a narrow and broad component. In agreement with previous quasi-elastic neutron scattering studies, the  $Q$ -independent rotational broadening is of the order of 1-2 meV (HWHM). However, in the  $Q$  range studied (0.8 - 3.0  $\text{\AA}^{-1}$ ), the translational broadening shows rather a weak  $Q$  dependence. Data in a lower  $Q$  region are probably necessary in order to determine the corresponding diffusion coefficient.

Aside from quasi-elastic spectrometers, the pulse-source HRMECS spectrometer (IPNS, ANL) provides a very wide dynamic range (up to  $E=600$  meV in energy transfer over a large  $Q$ -range). High-energy transfers are essential to probe the phonon and local modes involving hydrogen and the surrounding heavier atoms. Experimental phonon density of states of BCY is to be used as a check in the choice of inter-atomic force fields, the key parts of any microscopic model of the system.

**Acknowledgements:** Argonne National Laboratory is operated by the University of Chicago for the U.S. Department of Energy. This research is funded by a European Community Marie-Curie Fellowship (N.M.).

[1] H. Iwahara *et al.*, Solid State Ionics 77 (1995) p.289.

[2] K. Takeuchi *et al.*, Solid State Ionics 138 (2000) p.63.

# H3. SMALL ANGLE NEUTRON SCATTERING INVESTIGATION OF ODS MARTENSITIC STEELS

M.H. MATHON<sup>1</sup>, Y. DE CARLAN<sup>2</sup>, P. OLIER<sup>3</sup>, L. CHAFFRON<sup>4</sup>, C. CAYRON<sup>5</sup>, S. UKAI<sup>6</sup>, A. ALAMO<sup>2</sup>

<sup>1</sup>LLB(CEA-CNRS), <sup>2</sup>DEN/SRMA, <sup>3</sup>DRT/S3ME, <sup>4</sup>DEN/SRMP, CEA/Saclay, 91191 Gif-sur-Yvette, France

<sup>5</sup>CEA/Grenoble, DTEN/SMP, 17 rue des Martyrs, 38054 Grenoble, France

<sup>6</sup>Nuclear Fuel Research Group, O-arai Engineering Center, JNC 4002, Narita, Ibaraki, 311-1393, Japan

The materials reinforced by oxide dispersion, usually called ODS (Oxide Dispersion Strengthened), have a vast applicability because of their excellent mechanical resistance at medium and high temperatures. In general, ODS alloys are manufactured by mechanical alloying from elementary powders and consolidated by hot extrusion or HIP (High Isostatic Pressure). Iron based ODS could be used for nuclear applications between 550°C and 900°C. Indeed, they present good dimensional stability and excellent resistance to swelling under irradiation due to their body centered cubic structure and also good creep resistance because of the dispersion of nanometric  $Y_2O_3$  oxide particles.

The main objective of this work is to study the evolution of the oxide dispersion during the different stages of the fabrication, that is, after mechanical alloying, consolidation process (extrusion or HIP) and after thermal treatments. For this purpose, Small Angle Neutron Scattering (SANS) experiments were used to characterize the nanometric  $Y_2O_3$  oxide distribution in the matrix. Also, the A ratio of the magnetic and nuclear SANS contrasts between matrix and particles gives information on the chemical composition of the

martensitic alloys presenting a lower chromium content (9%). The SANS experiments show the existence of nanometric (<10 nm) oxides in all materials but their volume fraction depends strongly of the alloy (see figure 1). The ferritic alloy 12YWT which presents exceptional creep-rupture properties, contains the most homogeneous and fine oxide distribution. For the MA957, the volume fraction of very small oxides (radius of 1 nm) is lower. Concerning the low Cr material, the size distribution is larger in relation with their worse creep properties.

In the aim to be able to reproduce and improve the 12YWT steel, different mechanical alloying conditions and thermal treatments were tested.

The volume fraction of small oxides observed after ball milling is higher if the yttrium oxides are introduced as a mixture of  $Fe_2O_3$  and  $Fe_2Y$  intermetallics than as  $Y_2O_3$  micro powder. Those small oxides could be the first step of a new precipitation of nano-phases or “the residues” of the mechanical alloying (MA). A heat treatment during 1 hour at 850°C and at 1100°C, induces the precipitation of new nano-oxides with a different chemical composition from the one observed in the MA powder. This result proves that the mechanical alloying produces a partial solid solution supersaturated in yttrium, titanium and oxygen and that a new precipitation occurs during the consolidation treatment. After 1h at 1100°C, the size distribution is quite similar to the Y12WT one...

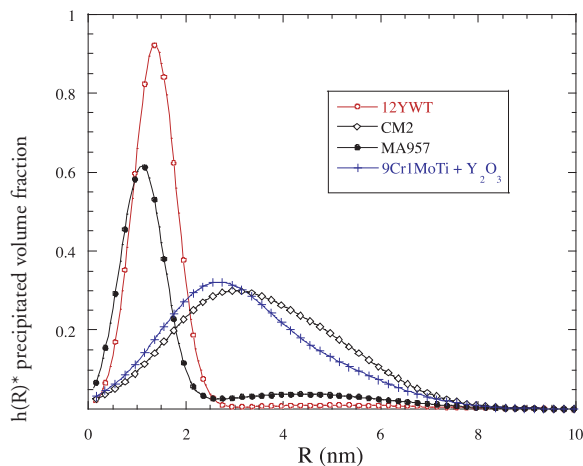


Figure 1 :  $Y_2O_3$  clusters size distribution in consolidated ODS alloys.

particles.

In the present study, several commercial or experimental ODS martensitic/ferritic materials have been investigated at consolidated state: MA957 manufactured by INCO metal and the Japanese steel 12YWT (12%Cr) produced by Kobe containing 12% of chromium, and two experimental

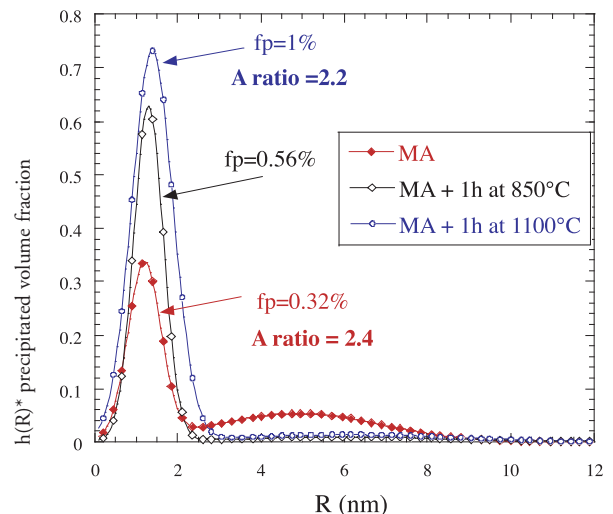


Figure 2 :  $Y_2O_3$  size distribution evolution under thermal treatment.

## H4. INFLUENCE OF ALLOYING ELEMENTS ON NANOMETRIC CARBIDES PRECIPITATION IN 5% CHROMIUM MARTENSITIC STEELS

P.MICHAUD <sup>1,2</sup>, D.DELAGNES <sup>1</sup>, P.LAMESLE <sup>1</sup>, M.H.MATHON <sup>3</sup>

<sup>1</sup> Ecole des Mines d'Albi-Carmaux, CROMeP, Campus Jarlard, route de Teillet 81013 Albi, France

<sup>2</sup> Aubert & Duval, 63770 Les Ancizes, France

<sup>3</sup> Laboratoire Léon Brillouin (CEA-CNRS), CEA Saclay, 91191 Gif-sur-Yvette, France

Tempered martensitic steels containing 5% chromium, mainly used for forging and high-pressure die casting tools show a limited lifetime due to the severe thermo-mechanical working conditions. The resistance to stress at high temperature of these steels is directly related to the stability of alloyed carbides which are formed above 450°C during tempering. In order to improve high temperature mechanical properties, the more relevant route is to modify the secondary precipitation by introducing alloying elements. Consequently, carbide forming elements (W, Mo, V, Nb) as well as elements influencing the precipitation kinetics (Co, Ni) were added to a low-silicon AISI H11 steel previously studied, the well known Aubert & Duval steel : ADC3 (reference) <sup>[1]</sup>. The characterization of carbides formed during the heat treatment was carried out using techniques such as X-ray diffraction and Transmission Electron Microscopy (TEM). However, these techniques were not efficient enough to evaluate parameters of the population of small carbides with an average size lower than 5 nm. Thus, in order to evaluate the size distribution and the volume fraction of the secondary precipitates of nanometric size, small angle neutron scattering (SANS) experiments were performed. Also, the A ratio of the magnetic and nuclear contrasts between matrix and particles gives information on the chemical composition of the particles.

In this study <sup>[2]</sup>, twelve grades of steel with different alloying additions were compared to the reference. Alloying additions corresponding to each grade is presented in table 1.

The neutron scattering experiments were performed at Léon Brillouin Laboratory on PAXE small angle instrument. Measurements were performed at room temperature, under a saturating magnetic field H=2 Teslas perpendicular to the incident neutron beam direction, in order to separate the magnetic and nuclear scattering cross-sections.

Reference	ADC3
Mo	Ref + 1.8%Mo
MoMo	Ref + 3%Mo
MoMoCo	Ref + 3%Mo + 3%Co
V V	Ref + 1%V
Ni	Ref + 1.5%Ni
NiNi	Ref + 3%Ni
Co	Ref + 3%Co
W	Ref + 1.6%W
Nb	Ref + 0.06%Nb
NiMo	Ref + 1.5%Ni + 1.8%Mo
NiV	Ref + 1.5%Ni + 0.7%V
NiW	Ref + 1.5%Ni + 1.2%W

**Table 1:** Alloying additions (in weight percent)

Volume fraction evaluated by SANS have shown that the number of small carbides ( $d < 5$  nm) are about 100 times higher than the number of carbides with an average radius of 15 nm. Actually, this population of small carbides ( $d \sim 3$  nm) will be more efficient in pinning dislocations and improving mechanical properties. The results have shown that a significant modification of the volume fraction and chemistry of nanometric precipitation are observed only for Mo, V and Ni additions (figure 1). The figure 1 shows green bars for the beneficial effect of Mo and V additions, whereas red bars represent detrimental effect of Ni addition on the volume fraction of small carbides.

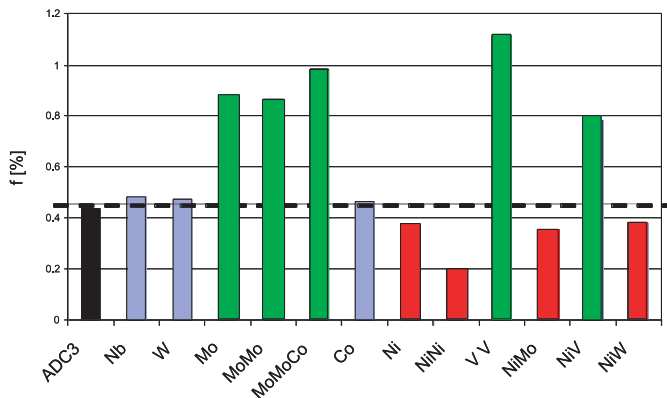
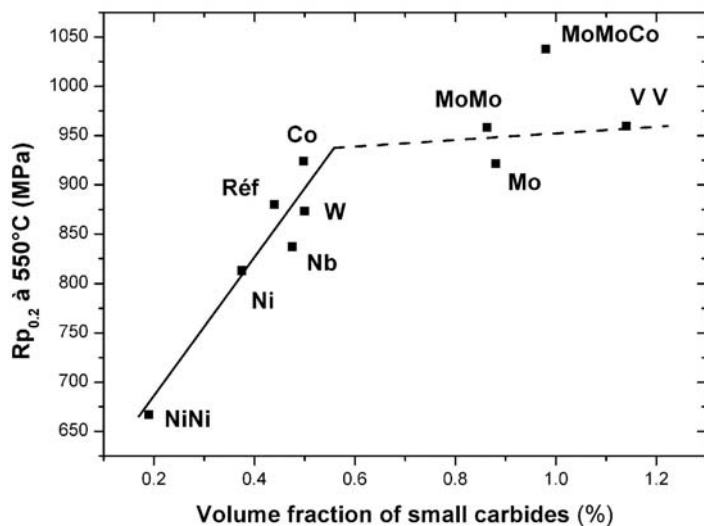


**Figure 1:** Influence of elements on the volume fraction of small carbides (d ~ 3 nm)

Moreover, results of mechanical properties showed that the volume fraction of small precipitates (VC in all grades and  $Fe_3Mo_3C$  in molybdenum grades) directly influences the



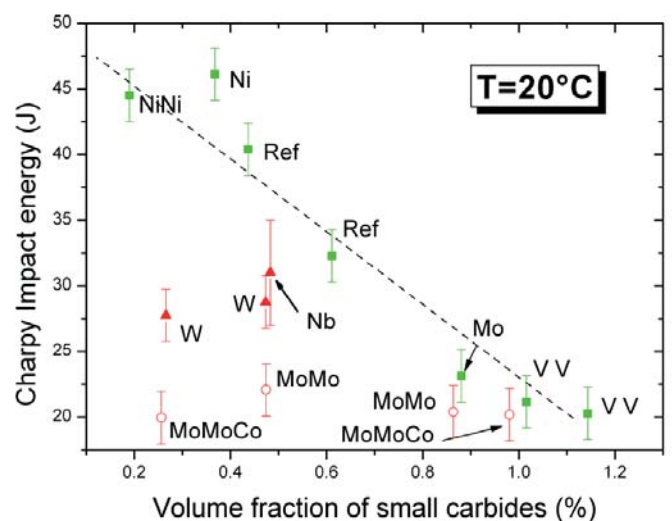
a)

**Figure 2:** relationship between volume fraction of small carbides and a) yield strength at 550°C. b) the Charpy impact energy.

mechanical resistance at high temperature (figure 2.a) but results in a detrimental effect on Charpy impact energy (figure 2.b). Red points on figure 2.b illustrate the influence of coarse carbides on Charpy impact energy.

In addition, above a volume fraction threshold (~ 0.6%), a saturation of the yield strength is observed. Two different mechanisms dealing with interaction modes between dislocations generated during the quench and precipitates are presented in [2] to explain the saturation.

The first hypothesis considers that increasing number of carbides in addition to the heterogeneity of precipitation can induce formation of Orowan Islands [3]. In that case, increasing the volume fraction of precipitates only increases the heterogeneity of the distribution, the “mean free path” of dislocations between Orowan Islands remaining constant [2]. The second hypothesis assumes a modification in main carbides crossing mechanism of precipitates by dislocations when volume fraction is above 0.6% (figure 2.a), changing from Orowan mechanism with formation of dislocation loops to shearing mechanism [2].



b)

[1] D.Delagnes, P.Lamesle, M.H.Mathon, N.Mebarki, and C.Levallant, Mater. Sci. Eng., Vol A394, pp 435-444 (2005).

[2] P.Michaud, PhD thesis, Ecole des Mines de Paris, 2006.

[3] V.Mohles, B.Fruhstorfer, Acta. Mat., V50, pp 2503-2516 (2002).

## H5. REWRITABLE DVD, RAM MEMORIES: BETWEEN THE ELECTRONIC STRUCTURE AND THE RECORDING ABILITY, NEUTRON SCATTERING SHED SOME LIGHT.

JEAN-PIERRE GASPARD<sup>1</sup>, JEAN-YVES RATY<sup>1</sup>, MARIE-VANESSA COULET<sup>2</sup>, CHRISTOPHE BICHARA<sup>3</sup>, CHRISTOPHE STEIMER<sup>4</sup> ET MATTHIAS WUTTIG<sup>4</sup>, BRIGITTE BEUNEU<sup>5</sup>

<sup>1</sup>Inst. Phys., Université de Liège (Belgique), <sup>2</sup>Laboratoire TECSEN, UMR6122, CNRS- Université Paul Cézanne, Marseille, <sup>3</sup>CNRS/CRMN/UPR7251, Marseille, <sup>4</sup>RWTH, Inst. Phys., Aachen (Allemagne), <sup>5</sup>LLB

Data storage and memory devices utilizing the optical and electrical properties of phase-change (PC) materials are important for multimedia applications<sup>1</sup>. The pseudo-binary chalcogenide compound  $(\text{GeTe})_2\text{-Sb}_2\text{Te}_3$  ( $\text{Ge}_2\text{Sb}_2\text{Te}_3$ ) is one of the reference materials for commercial DVD-RAM (digital versatile disc-random access memory) because it presents good optical and electrical contrast.

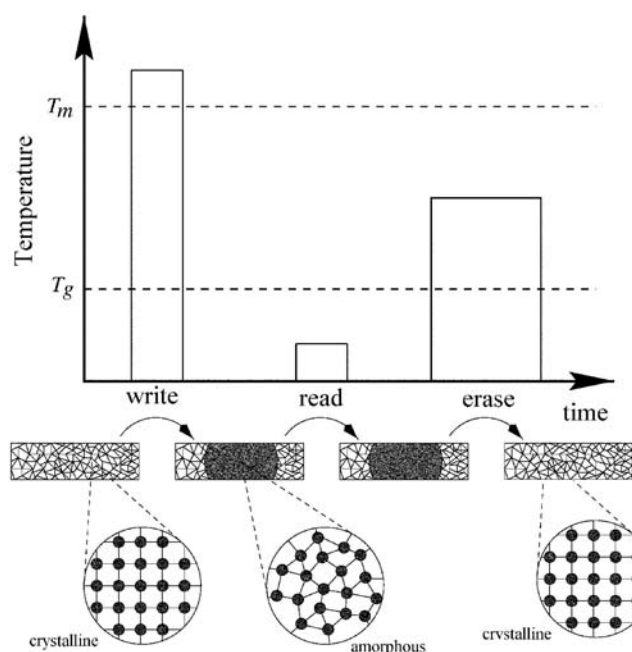


**Figure 1:** Write, read and erase sequence.  $T_g$  is the glass transition temperature and  $T_m$  is the melting temperature.

More precisely, the GeSbTe phases have the ability to easily crystallise and amorphise under the action of a laser pulse, basic process of commercial phase-change optical disks. During this reversible process, the crystal is locally melted to obtain an amorphous spot (crystal-liquid-amorphous transitions): this corresponds to the recording process. In a second time, this spot can be recrystallised (amorphous-crystal transition) by using a less intense laser beam, this is the

erasing process (Fig. 1). The recrystallisation of the material is the slower process. In order to develop faster phase-change materials, it is necessary to understand the transformation mechanism and the structural origins of the phase change from amorphous to crystal.

A number of new materials for optical and electronic non-volatile pc-storage have been identified by trial and error [1]. Recently, microscopic models of the amorphous and crystalline states have been suggested to explain the working mechanisms of PC-materials [1], [3]. However, much less is known however about the liquid state of these materials despite its prominent role for both amorphization and re-crystallization. Indeed, amorphization is achieved by quenching the liquid, while the fast re-crystallization of amorphous regions takes place above the glass-transition temperature, suggesting that it might proceed through the under-cooled liquid state. Therefore an in-depth knowledge of the structure of the liquid state improves our understanding of both the amorphization and the re-crystallization mechanisms.

Many-ternary Te-based alloys were studied in the liquid state by neutron scattering on the 7C2 diffractometer. The structure of the liquid was shown to depend primarily on the average number of electron per atom.

Using the ratio between the heights of the first two peaks of the total scattering function  $S(q)$ , two classes of liquids were defined (Figure 2).

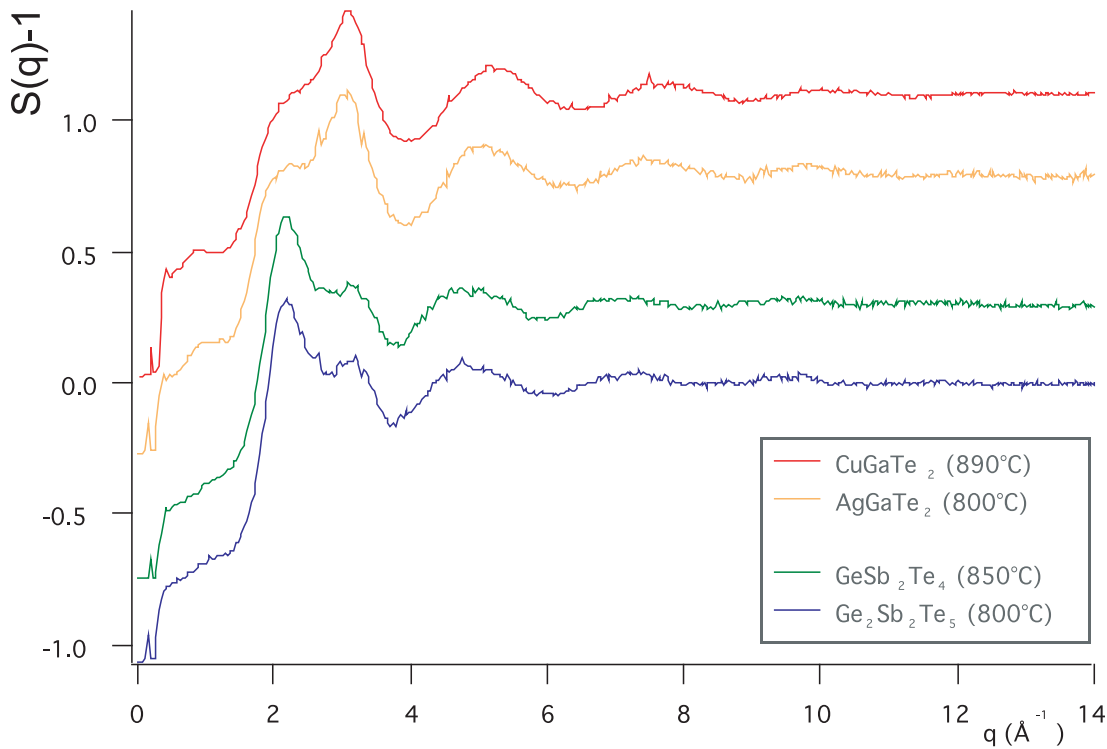


**Figure 2:** Structure factor of alloys with  $e/a > 4.5$  (upper part) and  $e/a < 4.5$  (lower part).

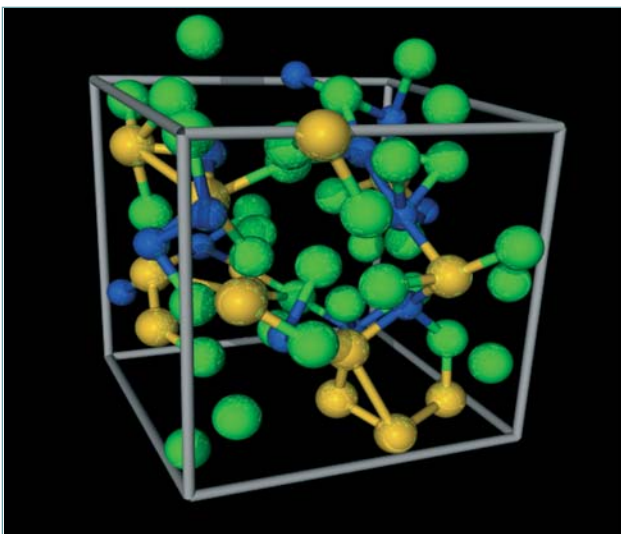


**Figure 3:** A snapshot of the liquid  $\text{Ge}_2\text{Sb}_2\text{Te}_5$  liquid alloy

In the first class with a low number of electrons per atoms ( $N_{e/a} < 4.5$ ), the structure of the liquid is tetrahedral-like similarly to the solid and the contrast in electrical/optical properties is not sufficient to qualify the material for PC availability. On the contrary, the second class of materials with a higher number of electrons per atoms ( $N_{e/a} > 4.5$ ) has an octahedral-like local structure and possesses a PC capability.

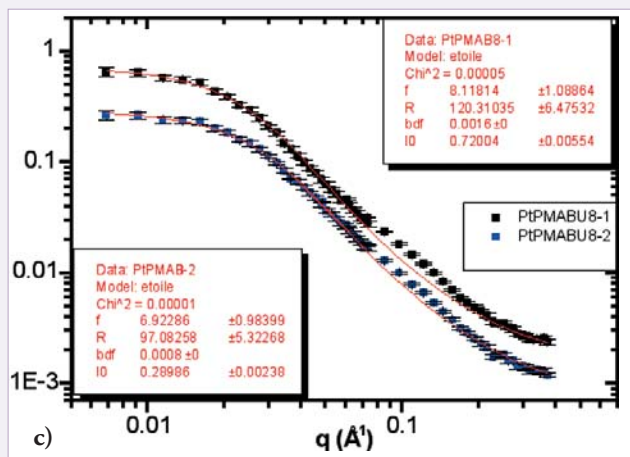
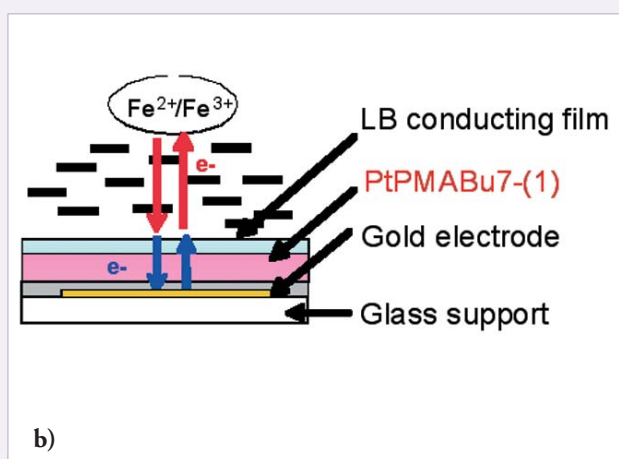
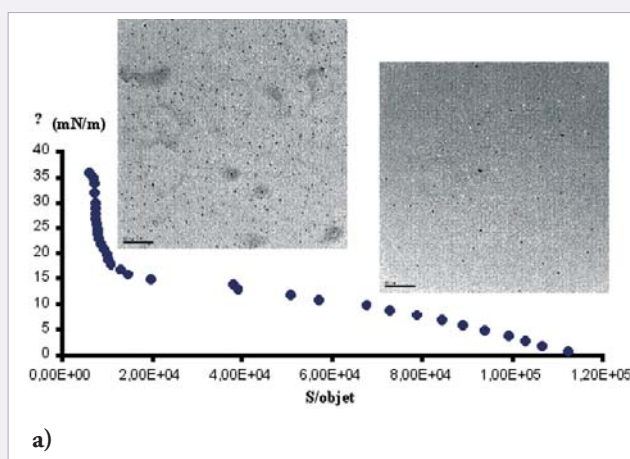
The local structure of these complex amorphous or liquid materials is largely under discussion ([2], [3], [4]). It cannot be directly extracted from the neutron data only, and other investigations are needed. In parallel to the experimental analyses, computer simulations of the liquid structure are been performed (ab initio molecular dynamics). From these *ab initio* MD experiments, that compare well to the experimental data in the case of  $\text{Ge}_2\text{Sb}_2\text{Te}_5$ , a detailed analysis of the local order will be made (Figure 3).

It is clear that finding generic features that qualify suitable PC-materials requires a fundamental understanding of the parameters that drive the transition between tetrahedral and octahedral environments. The transition region (around 4.5 electron/atom) will be more closely investigated, as well as the effect of the atomic radii for a given electron/atom ratio.

[1] G.-F. Zhou, *Mat. Sci. and Eng. A* 304-306, 3 (2001).  
 [2] A. Kolobov, P. Fons, A. Frenkel, A. Ankudinov, J. Tominaga, and T. Uruga, *Nature Materials* 3, 703 (2004).  
 [3] W. Welnic, A. Pamungkas, R. Detemple, C. Steimer, S. Blügel, and M. Wuttig, *Nature Materials* 5, 56 (2006).  
 [4] A.V. Kolobov, J. Haines, A. Pradel, M. Ribes, P. Fons, J. Tominaga, Y. Katayama, T. Hammouda and T. Uruga, *PRL* 97, 035701 (2006)

[C1. G. Carrot] Self-assembling via Langmuir-Blodgett films and SANS characterisation of polymer-grafted platinum nanoparticles : a possible application in fuel cells.

We synthesized platinum nanoparticles possessing electrocatalytic properties which are used as catalyst in the reduction of oxygen in fuel cells. The study of their electrical and electrochemical properties is performed after deposition on gold electrodes via Langmuir-Blodgett (LB) films. To improve the dispersion of the particles in the LB film as well as the deposition step, we grafted polymer chains onto the platinum



nanoparticles. Well-dispersed LB films can be obtained directly from the polymer-grafted-particles solution and the distance between particles may be adjusted depending on the degree of compression (Figure 1a). We are currently conducting electrical and electrochemical measurements onto these materials and the transfer onto gold electrodes can be done without the presence of fatty acid (Figure 1b). SANS spectra of two polymer-grafted nanoparticles with different molecular weights but the same grafting density are shown in Figure 1c (particle matching). First they show a plateau at small  $q$  which attests that the objects are individual and well-dispersed. We used a model of polymer star (chains connected together to a very small core) to fit the form factor. This model permitted us to determine both the number of chains (between 5 and 8, depending on the polymerisation batch), the radius of gyration of the polymer corona and the chain molecular weight.

[Collaboration : G. Carrot, LLB, H. Perez, SPAM, CEA-Saclay]

**Figure 1:** (a) Compression isotherm from polymer-grafted platinum nanoparticles and corresponding TEM images at different degrees of compression (surface pressure,  $P=2$  mN/m (left image);  $P=26$  mN/m (right image)) (b) Configuration scheme for electrochemical measurements (c) Neutron scattering spectra obtained from the grafted polymer chains at two different polymerisation time (particle matching): fit with a polymer star mode (particle matching).

[C2. K. Lagréné] Dynamics of a polymer confined in macroscopically monodisperse oriented pores.

Thanks to numerous theoretical developments spanned over few decades, it is now possible to draw a close relationship between polymer rheology in the bulk and polymer dynamics at the molecular level. Nevertheless, numerous technical applications are a step forward of the theoretical developments and already take advantage of the peculiar properties of polymers in interfacial situations or deep confinement. In the scope of my thesis work, we focus on the influence of confinement on hydrogenated polyethylene oxide (<sup>h</sup>PEO) with high molecular mass 100 000 g/mol (the critical entanglement mass ( $M_C = 3600$ )). As confining material, we use Anodic Aluminium Oxide (AAO) membranes. AAO are a class of materials showing an extremely well defined and anisotropic porous structure made of macroscopically aligned micrometers long cylinders with nanometre size diameter (Fig. 1). The isotropic "average out" of the dynamical information occurring in non-oriented systems can then be overcome by proper orientation of the AAO pores axe relative to the beam. The topology is described by the pore

diameter,  $D_p$ , the inter-pores distance,  $D_{int}$ , and channels length,  $L_c$ . We have shown that the topology can be tailored so as to obtain fairly mono-disperse pores with diameter in the range 11 to 45 nm. The Small Angle Neutron Scattering (SANS) contrast matching technique is used to evidence that PEO can be fully and uniformly confined within the AAO porous network. We probe the properties of the confined polymer by differential scanning calorimetry and incoherent quasi-elastic neutron scattering. The ratio  $R_G / D_p$  sharply drives the properties of the confined polymer. Upon confinement, for  $D_p / R_G > 2$ , a strong depression of the melting point temperature is observed but above the bulk melting point the PEO dynamics is not affected. For  $D_p / R_G < 2$  no melting transition is detected and the PEO protons mean-square displacement is significantly reduced compared to the bulk behaviour.

[K. Lagrené and J.-M. Zanotti, *Proceedings of the QENS 2006 conference, MRS Symp. Proc.*, accepted.]

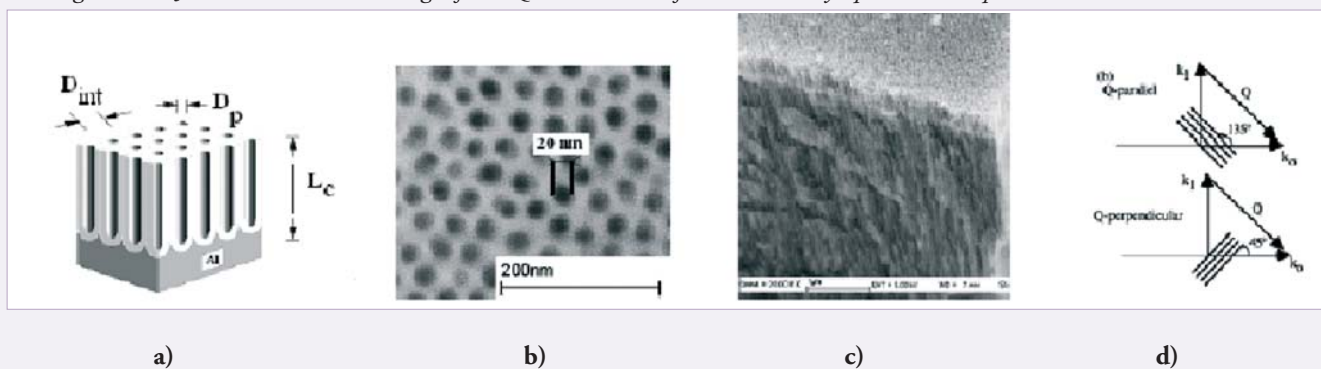


**Figure 1.** a) Schematic drawing of a porous alumina membrane. b) Scanning Electron Microscope (SEM) image of a LLB made AAO membrane. Here, the pore diameter is 20 nm. c) 3D SEM view of an actual LLB made AAO membrane showing the macroscopic alignment of the cylindrical pores in the bulk of the membrane (scale is 1  $\mu\text{m}$ ). d) Schematic illustration of how relative orientation of AAO samples to the incident beam ( $k_0$ ) and measurement of the intensity scattered in a detector at  $2\theta = 90^\circ$  (i.e. along  $k_1$ ), can provide information (sensed along  $Q$ ) on confined PEO dynamics parallel (top) and perpendicular (bottom) to the AAO cylinders axes.

### [C3. N. Malikova] Dynamics of water and ions in clays: a concurrent TOF, NSE and MD study

The potential application of clays as components of barriers around underground storage sites of radio-active waste has recently intensified the study of mobility of water and ions (both natural, e.g.  $\text{Na}^+$ , and potential radionuclides, e.g.  $\text{Cs}^+$ ) in these systems. At a more fundamental level, these investigations shed light onto dynamics of liquids in confined charged media and phenomena at a solid/liquid interface. The dynamics of water in a montmorillonite clay has been investigated here on the picosecond timescale by quasi-elastic neutron scattering (time-of-flight (TOF) and neutron spin echo (NSE) techniques) and classical molecular dynamics (MD) simulations.

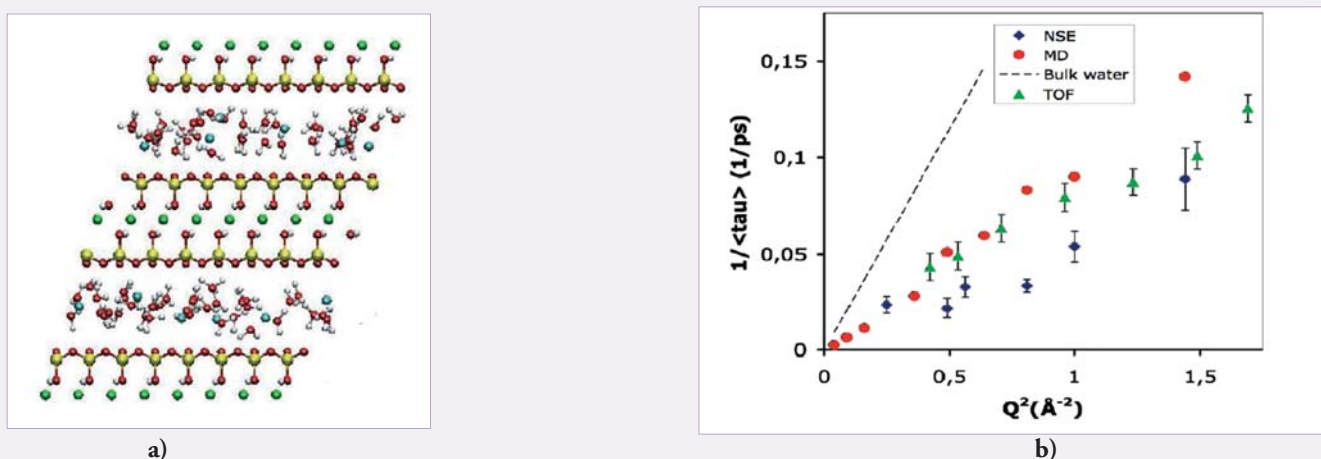


**Figure 1.** a) Atomic structure of a hydrated clay used in MD. Mobile species: water molecules (white and red),  $\text{Na}^+ / \text{Cs}^+$  ions (blue). b) Inverse relaxation times versus the wave-vector for two-layer hydrate of Na-montmorillonite.

MD shows that while  $\text{Na}^+$  ions have no specific adsorption sites on the clay surface,  $\text{Cs}^+$  ions exhibit a jump diffusion between sites allowing coordination to six oxygen atoms of the adjacent clay layers. In the bulk, on the picosecond-nanosecond timescale, water molecules diffuse by a combination of translational and rotational motion. In the case of clays, this behaviour is necessarily modified by the narrow confinement between two parallel clay layers. Never-the-less, while the water diffusion coefficient in case of a single confined water layer is an order of magnitude lower than in bulk water ( $1-2 \times 10^{-10} \text{ m}^2/\text{s}$ ), in the two-layer clay hydrate the diffusion coefficient is already almost half of the bulk value ( $1 \times 10^{-9} \text{ m}^2/\text{s}$ ,  $D_{\text{bulk}}=2.3 \times 10^{-9} \text{ m}^2/\text{s}$ ). This is seen both in experiment and simulation.

*PhD thesis of N. Malikova (LI2C/ANDRA), [Collaboration LI2C (Université P&M Curie, Paris VI, CNRS) and LLB ] Malikova, Cadène, Marry, Dubois & Turq, J. Phys. Chem. B 110, pp.3206-3214, 2006.*

#### [C4. A. Declémy] Ferromagnetic Fe-implanted SiC: New results towards a Diluted Magnetic Semiconductor

SiC is a good candidate for diluted magnetic semiconductors which could be used in spin-electronic devices. It has a wide band-gap (3.1 eV), low spin-orbit coupling, excellent transport properties and has reached a mature state of industrial development. In order to create magnetic SiC, substrates have been implanted with Fe ions at the LMP Univ. Poitiers (at doses of the order of  $5 \cdot 10^{16}/\text{cm}^3$ ). After annealing (700-900°C), a ferromagnetic behavior has been observed with a high Curie temperature (up to 700°C). Polarized neutron reflectivity has allowed to probe the magnetization of the SiC:Fe films as a function of the depth. From the PNR reflectivity (Fig. 1), it is possible to reconstruct the magnetization profile (Fig. 2). The complicated shape of the fitted magnetization profile through the depth of the sample is connected to the multi-implantation process. The measured profile corresponds quite well with the implantation profile which can be simulated with SRIM. The fact that we are dealing with a magnetic semi-conductor needs to be confirmed. Until now, EXAFS shows that there are no Fe atoms in the very near Fe environment which excludes the presence of Fe clusters. The possibility of secondary phases such as  $\text{Fe}_3\text{Si}$  needs to be checked.

*[Collaboration: A. Declémy, M. Drouet, C. Dupeyrat, D. Babonneau, J. Mimault, T. Girardeau, D. Eyidi, M.F. Beaufort, J.P. Eymery, Université de Poitiers, F. Ott, M. Viret, LLB/SPEC Saclay.]*

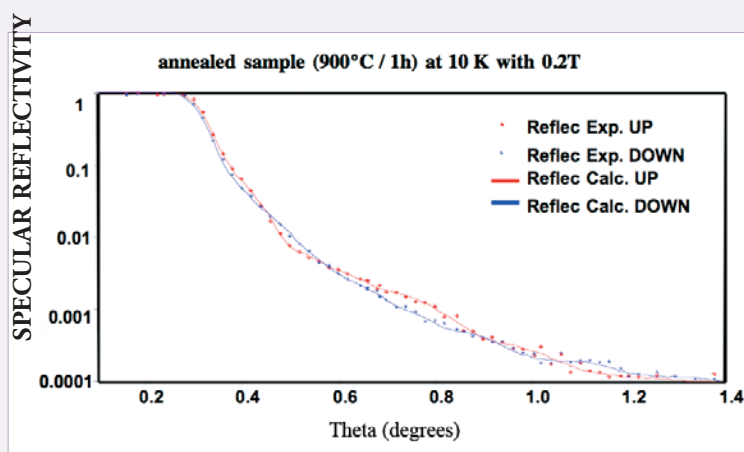


**Figure 1:** polarized neutron reflectivity of an SiC:Fe sample measured at 10K (fits in solid lines)

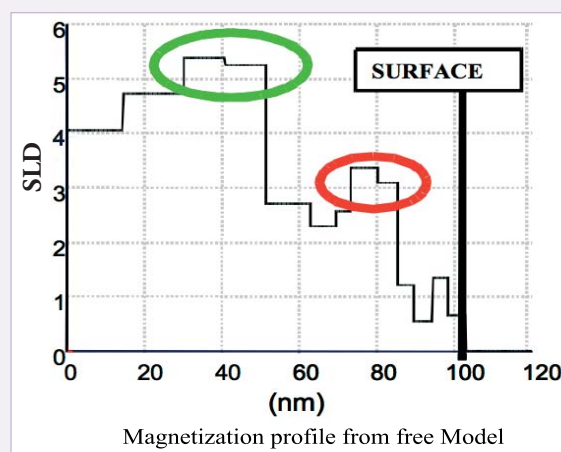


**Figure 2:** Reconstruction of the Fe implantation profile from the PNR. The fit is very close to the calculated implantation profile

#### [C5. V. Klošek] A compact tensile machine for in situ neutron diffraction study of materials under external loading

In order to characterize the behaviour of materials under mechanical loading, a very compact tensile machine was recently developed at LPM TM. This machine is designed to be mounted on the Eulerian cradles of G5.2 and 6T1 diffractometers: to allow a huge variety of sample orientations, its frame consists in two side columns on which are fixed the plates supporting the tensile heads (Fig. 1). It thus now becomes possible to analyse elastic and plastic behaviours of materials during a tensile test by in situ neutron diffraction. This machine is an incomparable tool to study deformation mechanisms under external loading of materials: macro- and micro-strains, texture or stored energy can now be measured as a function of applied load (up to 30 kN). First tests were performed on a brass (Cu-Zn) alloy sample. Figure 2 shows the (111) diffracted peaks recorded on G5.2 at three different loadings, with their corresponding FWHM ( $\lambda = 3.03 \text{ \AA}$ ). At low strain, the peak is essentially shifted toward lower angles (elastic deformation mainly). At higher strain, the peak broadens, traducing the plastic deformation of the material.

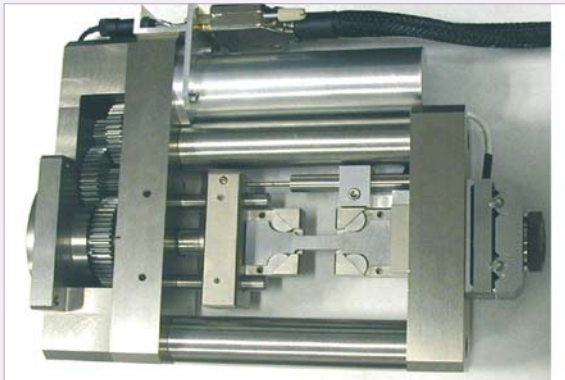


Figure 1: the tensile machine, equipped with a sample

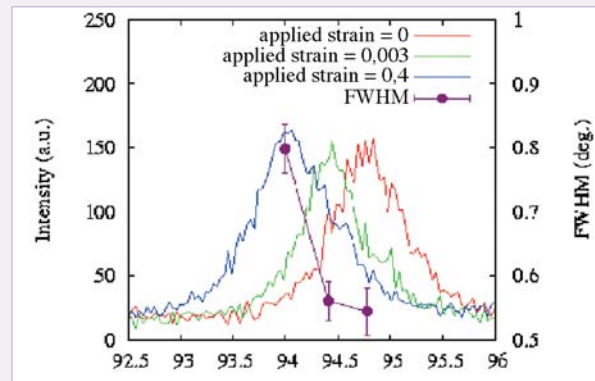


Figure 2: (111) peaks and FWHM recorded on G5.2 for several loadings

[Collaboration: V. Klosek, M.H. Mathon, LLB; V. Ji, LIM-ENSAM, Paris; R. Chiron, LPMTM, Villetaneuse]

#### [C6. S. Jakani] Deformation and recrystallization mechanisms of CuSn alloys (bronze)

The optimization of the macroscopic properties requires the comprehension of the deformation and recrystallization mechanisms. In the case of the copper and of its alloys, the deformation step conditions mainly the mechanisms of recrystallization. Neutron diffraction, performed on 6T1, was used to characterize the deformation texture, stored energy after various rates of rolling (between 0 and 90% of deformation) and the activation energy of recrystallization with “in situ” measurements. The addition of tin (4 to 9%) in pure copper lowers the stacking fault energy. Thus, it is not astonishing to observe a texture of deformation primarily consisted of the a fibre (with the Brass and Goss components). During cold rolling, stored energy increases with the deformation rate but contrary to the case of pure copper and brasses, its distribution is homogeneous between the various crystallographic orientations. A light increase of energy is observable with the tin content. Measurements of kinetics of recrystallization reveal that the energy of activation of the recrystallization process decrease with the deformation rate but remains much more important than in pure copper. The recrystallization is accompanied by the development of the orientations C {112} <11-1> and G {110} <001>. These results show that recrystallization is not only interpretable by stored energy but that the kinetic aspect via the grain boundaries mobility is a prevalent factor in the presence of tin. The presence of an element of addition can then reinforce the energy stored by decreasing the mobility of dislocations and thus act on the dynamic phase of restoration. By the same mechanism, the recrystallization is slowed down. The copper alloys thus present distinct behaviours, a priori depend on the nature of the element of addition which acts differently on the mechanisms of deformation and the mobility of dislocations and the grain boundaries.

[Collaboration: S. Jakani, S. Melusson, M.H. Mathon, LLB]

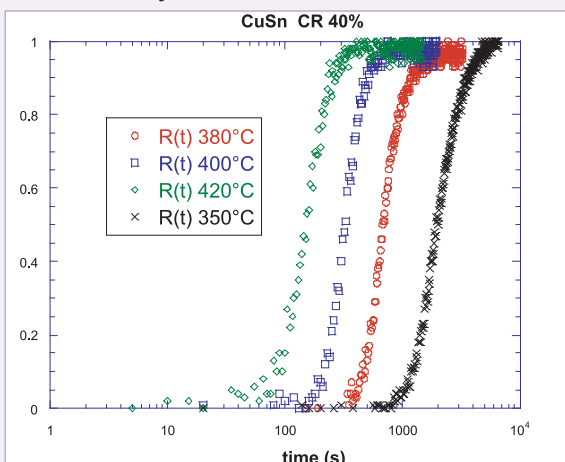


Figure 1: Recrystallization kinetic on the CuSn4% cold rolled up 40%

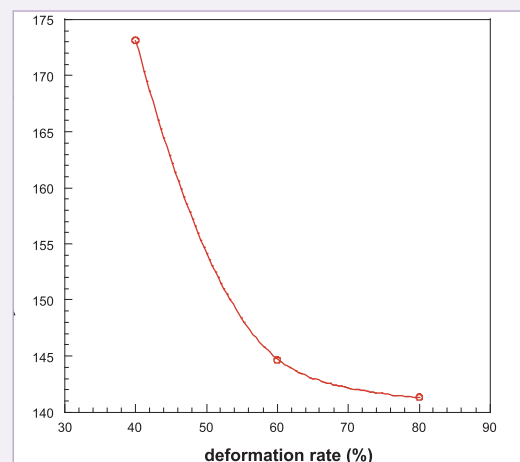


Figure 2: Recrystallization activation energy (kJ/mol) versus the deformation rate.







## SOFT MATTER

LABORATOIRE LÉON BRILLOUIN

# SOFT MATTER

## A- Introduction

Future axes of research in soft matter will develop, by mutual enrichment, in external teams, mixed collaborations and in-house research; finding new routes is a commitment for the LLB team.

The contribution below covers different trends, taking the opportunity to put into perspective related recent work, by ourselves and/or others, including highlights and clips. These trends include **New synthesized polymers**, a field of obvious interest, to **Systems under external constraints**, currently raising much interest, and **Confinement and surface effects**, a recent trend gathering several LLB projects, to finish with **Ternary mixed systems**, the largest set of various situations involving many teams. Our knowledge based on polymers, has evolved towards **mixed systems involving polymers**. Among the different specific advantages of neutron radiation, **deuterium labelling** is the one which should benefit this kind of system, as well as other subjects, in the different techniques: SANS, reflectivity, as well as quasielastic scattering.

## B- New synthesized polymers

New synthesis routes for polymers are constantly being developed by chemists; LLB has the right experience to analyse the chain conformation and arrangement. **Deuteration**, which implies additional synthesis (that of the deuterated monomer), is a very powerful tool and is particularly worth achieving.

Let us refer to recent studies such as **polyelectrolytes with a conjugated backbone**, which enables us tuning the right correct the good water solubility theoretical ingredients of a “wormlike chain to globule” conformational transition, addressing in particular the question of annealed versus frozen charge distribution along the chain [*CI*, P. Vallat] (thesis) - Rawiso).

Other research for new polymers has been conducted and will be developed, for instance on conjugated conducting polymers (G. Hadziioannou, Strasbourg)

Another theme, which is currently rising, is polymers resulting from **supramolecular associations**: systems come from J. M. Lehn team (E. Buhler), and other laboratories. These systems exploit the potential of deuteration of a key chemical group (P. Mésini), or solvent trapped inside the molecular thread (L. Bouteiller). Other associations give birth to polymer-like objects: for example, in polyrotaxanes, between a POE chain and cyclodextrins. This subject was studied by LLB associate team (L. Auvray - P. Guégan, Evry), and recently revisited (Hadziioannou-Lapp).

## C - Systems under external constraints

A more widespread group of projects corresponds to polymers which are often well known at rest, but not understood when subjected to the various environments and constraints of real life. For that purpose, in addition to the aforementioned strength of the technique, rather thick and complex sample environment devices can be used owing to **high penetration power of neutron**.

### 1 - PRIMARY MIXTURES UNDER MECHANICAL CONSTRAINTS

---

Primary mixtures are made of object which are all identical, except for a fraction of them which is deuterated, permitting unique studies of the individual objects and of their interaction. We focus first on pure polymer systems, for which mechanical deformation behaviour is of interest and sometimes of prime importance to industrial applications. Studies of conformation and arrangement of chains under shear or stretching deformation, now achieved only on simple linear polymers, will yield important information on other architectures. Beyond the behaviour of liquid crystalline polymers in shear induced phases which is studied in detail, (L. Noirez), and the fundamental questions on entanglement effects in stretched rings compared to linear chains (M. Rawiso, J. Combet), there is much to be done on architectures found frequently in real life high performance polymers. Starting with such a common polymer as polyethylene, which contains **branched chains** of different branching rates, we have studied how branched objects arrange and deform in monodisperse blends as well as in mixtures with less branched chains (modelled here by linear chains), in collaboration with the Laboratoire des Polymères Organiques de Bordeaux [*C2*, S. Desvergne] (thesis) - Brûlet). This kind of system should be studied more, in link with expert laboratories.

## 2 - ELECTRIC OR MAGNETIC FIELDS

As the materials need to be more and more multifunctional, a variety of external constraints should be explored in the near future, among which are the electric and magnetic fields. The experiments can be **static or oscillatory**, using cyclic measurements or time of flight focalisation as developed in Munich and Berlin (A. Wiedenman J. Gahler).

The behaviour of **ferrofluids** in several magnetic configurations has been initiated and performed at LLB. This includes studies on mixed systems. Previously, SANS has used visual techniques, to show accurately that magnetic nanoparticles can be included in the membrane of a polymer vesicle (“polymersome”), and SANS remains an easy direct way to show in situ that a **field deforms the membrane of the vesicle** [C3, O. Sandre].

The organization of **magnetic nanoparticles** along the field in a **polymer matrix** has been studied in a ferrolatex, derived from mixing polymer latex and ferrofluid colloidal suspensions. Application of a constant magnetic field during water casting induces anisotropy in the filler network [C4, F. Cousin].

## 3 - BINARY POLYMER-PARTICLE SYSTEMS: MECHANICAL CONSTRAINTS AND REINFORCEMENT.

Constraint effects have been extended to **binary mixed systems**, in particularly soft polymers associated with hard nanoparticles at LLB. Various strategies of chemical synthesis of **grafted particles** are developed by G. Carrot at LLB and in collaboration with the CROPS laboratory of University of Marseille 1 (D. Bertin), in the thesis of J. Vinas [C5, J. Vinas] and with the SPAM (H. Perez), with the aim of applications in fuel cells (see Section Materials). Similar work has been performed by external teams (L. Billon, J. Peyrelasse, Pau) using other grafting routes also avoiding aggregation. The LLB project of relation, for a **nanocomposite** material, between **mechanical reinforcement** and the dispersion of grafted nanoparticles at rest, its evolution under deformation, and the deformation of labelled chains [C6, J. Jestin] is just now being developed in the thesis work of C. Chevigny.

Also, a study of **natural latex** mixed with natural (and dried) **clay** is currently running in collaboration with Campinas University (T. Doi, post-doc, L. T. Lee). The stretching of the sample has shown the importance of other entities, such as calcium aggregates, present in these systems.

**Combinations of mechanical and magnetic field** deformation have been recently explored. The competing effects of mechanical rotation and applied field at constant orientation results in orientation of the ferrofluids structure at an intermediate direction which is  $q$  dependent, in agreement with calculations (E. Dubois, R. Perzynski, E. Cebers, Univ. Paris 6). The response to a mechanical **deformation** of the **field oriented ferrolatex** described above [C4, F. Cousin] shows a clear orientation dependent modulus, which should allow better understanding of reinforcement. Studies of ferro - polymersomes [C3, O. Sandre] under shear are being attempted.

Association of hard particles with the liquid crystalline systems formerly studied in Montpellier are also planned (J. Oberdisse).

## D - Confinement and surface effects

With the rapid development of nanotechnology, the problem of confinement is met in a large variety of situations where degrees of freedom are reduced close to a surface. Polymer chains are thus particularly sensitive to such effects.

Here again, neutron scattering is a powerful tool: the spatial profiles can be studied by **reflectivity**, and the **chain conformation** by SANS. A first simple situation of confinement is that of a chain in a **thin film** of nanometric thickness lower than the “natural” global size of the chain in bulk. This is well suited to a “primary mixture” study by labelling some of the chains in order to measure their conformation. We showed formerly (A. Brûlet- J.P. Cotton) that this conformation remains Gaussian at intermediate sizes, while apparent stretching appeared at large  $q$  (small distances), linked to the presence of surface, either acting on some chains, or giving additional scattering, as proposed by other authors (Russel et al). Extension of these studies can make use of **Quasi-Elastic Neutron Scattering** (QENS), combined with deuteration, as proposed by A. Brûlet. Indeed, low thickness also induces some apparent changes of  $T_g$ , as explored by many authors in macroscopic experiments. The corresponding change in the dynamics of dynamics has scarcely been studied (Frick, ILL).

Using deuteration again, one can observe how confinement affects deformation, modulus and  $T_g$  shift in **small nanolatex beads** immersed in an elastic latex matrix [H1, Y. Rharbi].

**Other confined systems** involve polymer © particle binary systems. The study of polymer conformation in nano-cylindrical

mesopores has been started in external collaboration (C. Stilling - L. Noirez). An LLB thesis is ion-conducting polymer inside non-porous aluminium films, with application to fuel cells (J.M. Zanotti, K. Grenet) is detailed in Section *Nanomaterials*. See also the effect of confinement on liquid crystal transitions (D. Morineau) in the Section *Phase transition*.

A very rich new class of binary **polymer particle** systems related to confinement is nanoparticles inside the polymer matrix. Beyond the “filler network” effect due to connectivity of particles aggregates, it has long been suspected that the solid particles give birth to a kind of “**less mobile**” **polymer layer** near their surface, which also plays a role in reinforcement. Such aspect of chain dynamics in a confined geometry is now revisited by many groups. **Quasi-Elastic Neutron Scattering** (QENS), combined with deuteration, in a bulk sample is planned in the thesis of N. Jouault (codir. S. Said, Y. Grohens, Lorient).

Finally, beyond confinement, novel experimental observations carried out by controlling the boundary conditions between various polymer and their substrates give new perspective on their nature. Indeed, it has been shown [H2, H. Mendil], PhD, that the molten state of these polymers, far from any transition, reveal hitherto unknown long range correlations.

## E - Ternary mixed systems

Probably the widest part of future activity at LLB in terms of systems and users is **mixed systems**, which associate polymers, surfactants and particles. Their technological future spans many applications: food and agricultural products, pharmaceuticals, biotechnology, even biology. Neutrons are useful because of the possibility of **contrast variation**.

### 1 - BULK

---

A good example of system allowing many ways of using contrast is water, **polyelectrolyte and proteins**: here one can use mixtures of water and heavy water which match the protein, the polymer or the deuterated version of the same polymer. This enables us to “see” the different species separately, and even some deuterated chains among other non deuterated ones, or labelled counterions [H3, J. Gummel]. Such detailed insight helps understand similar protein-polymer complexes studied by external users (M. Axelos, Nantes), for which deuteration is not available, or where it has been achieved (C. Tribet, ESPCI, P. Dubin, Amherst-US). One group is currently studying an **acacia gum** component macromolecule associating polysaccharide and protein moieties [C49, C. Sanchez]. Complexes can also involve cationic polymers (L. Auvray, M. Zeghal, Evry) or surfactants (D. Langevin) complexed with flexible or more rigid (**DNA**) polyelectrolytes; this is related to cell targeting for pharmaceuticals or **gene therapy** (cancer treatment, for example). Adding polymer can also modify the rheology of well-known surfactant structures like giant micelles (C. Ligoure - L. Ramos, Montpellier).

Studies also deal with polymer plus nanoparticles colloids in a solvent. For example, PNIPAM polymer adsorbs on silica, which creates a composite gel, with thermosensitive rheology properties induced by PNIPAM collapse above a threshold of the order of 40 °DC (D. Hourdet - L. Petit (thesis), ESPCI). Polymer can also stabilize quantum dot nanoparticles in a solvent, for which the final colour of the dispersion depends on the sizes involved (N. Lequeux, A. Fragola, ESPCI - C.Chassenieux, Le Mans). Systems of polymer plus mineral particles, in solution, are also present when studying (**bio**)**mineralisation** as currently performed [C10, C. Gérardin], or planned for the case of diatomea silica backbone (J. Bibette - A. El Harrak).

Indeed the number of expected new systems is very large. In **pharmacology**, drug release is associated with trapping molecules in complexes, or networks; other biotechnological networks can be studied, benefiting from former basic studies on networks in LLB-ICS teams. To conclude, let us cite a bit more far-fetched systems, such as these gathered from the Autoassemblages de Biomolécules Végétales research group, which associates physico-chemistry with food and agronomy. As an already advanced study, let us mention the work on derivatives of cutin and suberin, some biopolymers of the “plant skin”, which can form membranes, but also original hollow microtubes (J.P. Douliez, INRA, L. Navailles, F. Nallet, CRPP). Meanwhile, **ABV** interest is growing in various types of associations: proteins with polyphenols in fruit juices or wines (as modelled already by catechine - $\beta$ -casein association), starch with proteins, triglycerides with phospholipids), combined growth of amylose with amylopectine inside starch grains...

Achievement for these systems would be complete if a dream became reality: a technological jump in **deuteration of natural products**.

### 2 - PLANAR SURFACES: REFLECTIVITY

---

In parallel with SANS, surface reflectivity studies of the same kinds of mixed systems **use and will use the same possibilities of contrast variation**. In some cases, the third component is only the substrate. In a study of pH-responsive interfaces grafted with polyelectrolyte or polyampholyte, what is important is a good contrast with respect to substrate and solvent, here D<sub>2</sub>O, together with the accuracy of the analysis [H4, Y. Tran].

The swelling dynamics of the ultra-thin polyacrylamide (PAM) spin-coated films in saturated vapor of water were studied by measuring the profile of D<sub>2</sub>O or H<sub>2</sub>O fraction in the film (725 Å) at different exposure times. Interestingly, the chain diffusion coefficient was found to be an order of magnitude higher in D<sub>2</sub>O, due to the stronger D<sub>2</sub>O-PAM interaction [C12, J. Daillant]. Real ternary systems in contact with surface are a field where the reflectivity team is expert. Accompanying such studies is now

a trend for links with other properties. First example, the structural properties of adsorbed poly(N-isopropylacrylamide), PNIPAM, and mixed PNIPAM-SDS layers are correlated to **gas permeation behaviour of thin foam films** [C7, L. T. Lee]. Second example, depositing **nanoparticles on a solid substrate** can be done by dragging the nanoparticles by the dewetting of particle-surfactant-polymer solutions, followed by capillary attractions between particles; minimal nanoparticle-substrate attraction is required, hence it is important to know the correlation particles to substrate. A hydrophobic surface is modelled by the air-water surface, and the contrast of silica can be varied in the ternary system, allowing a definite conclusion on the existence of depletion layer [C8, L. T. Lee]. A project of L. T. Lee is to study the typical distances involved for nanoparticles deposited on a surface, both along the perpendicular direction and along the surface plane. An **easily reversibly tuning** of these distances will be provided by the use of a three-component system : particles plus solvent plus thermosensitive polymer. In the case of optosensitive particles (quantum dots) these distances will control optics of the coating. Finally, going towards more bio-inspired systems, organisation of **cellulose with xyloglucan** at the surface of the primary cell wall has been mimicked by multilayers of cellulose whiskers and polyelectrolytes of the opposite sign and is studied by reflectivity [C11, B. Jean].

### 3 - SURFACE IN VOLUME, AND FROM VOLUME TO SURFACE.

Other systems enable us to study surfaces, from a volumic sample. Beyond previous work on **foams**, recently refocused on single films (J. Etrillard, E. Terriac, Rennes), are **emulsions** promising systems: here, even if the sizes of the droplets are microns, much larger than the accessible range, a large enough quantity of interface is dispersed inside the sample volume. It can be shown that its structure involves nm scale in asphaltene-based emulsions created during the production stage, since drilling brings water together with oil [H5, J. Jestin], while other asphaltene emulsions can be studied for transportation application (F. Argylier, IFP-D. Langevin, Orsay).

Particles also play a surfactant role for some so-called “**Pickering**” emulsions; some of these particles are studied in bulk (P. Perrin, A. Roudot, ESPCI). Emulsion associating particles and PNIPAM for temperature tuning are also part of L. T. Lee’s project.

It has also been possible to observe silica particles **both dispersed in volume** (using SANS) and **on a silicon wafer** in contact with the dispersion, using **grazing incidence small angle scattering**; one observes a characteristic length in both situations on the spectrometer PAPHYRUS [C13, G. Chaboussant]. Though flux is low, neutrons provide some advantages (contrast, penetration) for such a combined study.

We have also proposed to study the relation **between volume and surface** situations by observing what happens to bulk complexes when transferred from the bulk dispersion to the surface. The surface can be an air-water one; presently in progress are studies of protein-based objects (aggregates, protein-polymer or surfactant complexes) in volume and surface, to end with studies of the same systems in foams - which can be seen as a reflectivity study (M. Axelos, B. Novales, INRA Nantes).

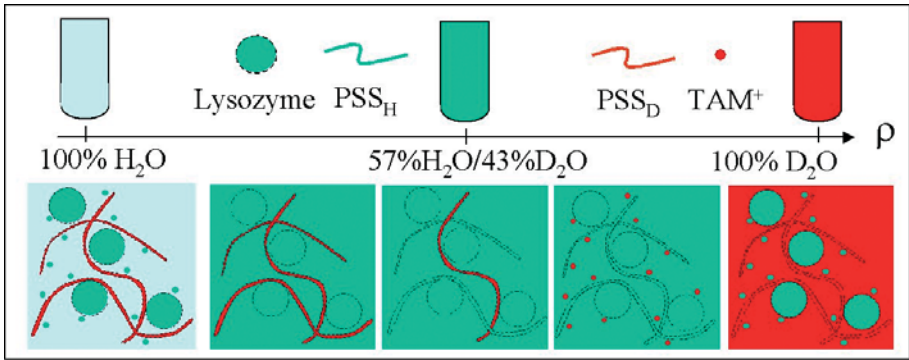
The surface can also be a hard substrate: by creating a polyelectrolyte layers or multilayer, **lysozyme surface traps** can be created by similarity with polyelectrolyte-lysozyme complexes in volume with enzymatic activity control (project of F. Cousin). This is very similar to former studies of biochips. Such systems can also be created at the surface of particles.

## F - New instrumentation and new systems

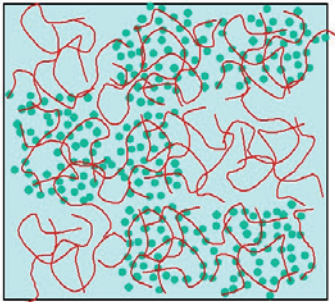
A *fourth* class of systems is only just emerging, as it is **linked with instrumentation** progress in the Small Angle techniques, namely **VSANS** (“**TPA**”, see *Instrumentation* section). Access to lower values of  $q$  ( $5 \cdot 10^{-4} \text{ \AA}^{-1}$ ), will enable the study of larger objects, when contrast variation is useful, or when **light scattering is impossible or difficult** (e.g. dark or very turbid inhomogeneous systems). To start with, we will study compact objects since their scattering cross-section is higher for the same size. Thus systems involving larger particles or larger aggregates are good candidates. This is obviously consistent with some of the projects discussed above in mixed systems; like confined systems, soft-hard composites, and complexes between polymers and surfactant or proteins.

Last, but not least, a large new instrument now exits one mile from the LLB site, namely the **SOLEIL** synchrotron. For example, **X + N combined studies** of the same system, which can be seen as a contrast variation, are very interesting. These have been done successfully in polyelectrolyte systems by M. Rawiso and J. Combet. We have to develop the complementarities between neutron and X rays radiations both for the projects of our users as well as our own.

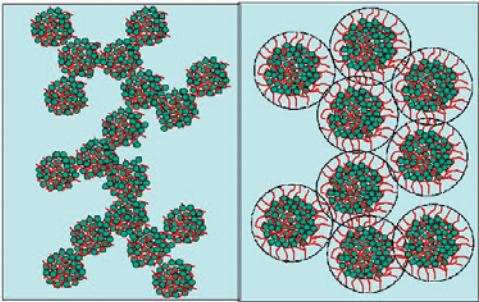
# SOFT MATTER



(a)



(b)



(c)



- H1. Nanomechanics and glass transition of confined polymers within spherical nanosized particles  
Y. Rharbi, N. Bassou, F. Boué
- H2. Novel frontier between liquid and solid states in polymers: identification of a macroscopic solid-like mode in the molten state.  
H. Mendil, P. Baroni, L. Noirez
- H3. Chain form factor and counterions release in polyelectrolytes-proteins complexes : beyond the usual contrast matching method  
J. Gummel, F. Cousin, F. Boué
- H4. pH-responsive interfaces grafted with polyelectrolyte or polyampholyte  
Y. Tran, S. Sanjuan, N. Pantoustier, P. Perrin
- H5. A SANS study of the adsorbed asphaltene layer in water-in-hydrocarbon emulsions  
J. Jestin, S. Simon, T. Palermo, L. Barré

[C1. P. Vallat]

Molecular structure of conjugated polyelectrolytes

[C2. S. Desvergne]

Two polymers made of the same segments which do not mix because of their different architecture

[C3. O. Sandre]

Smart hybrid magnetic polymersomes

[C4. F. Cousin]

Anisotropic reinforcement of latex films by magnetic nanoparticles

[C5. J. Vinas]

Stimuli-sensitive hybrid nano-objects: polymerisation from silica nanoparticles synthesized in aqueous medium.

[C6. J. Jestin]

Dispersions of polymer grafted nanoparticles in a same polymer matrix: the effect of deformation

[C7 et C8 L.T. Lee]

Interfacial and thin-film properties of complex systems

[C9. C. Sanchez]

Conformation of arabinogalactane-peptide from Acacia gum: a new model based on SANS and ab initio calculations

[C10. C. Gerardin]

Hybrid polyion complex micelles precursors for Highly stable metal [C. hydroxide colloids]

[C11. B. Jean]

Cellulose whiskers-based multilayers

[C12. J. Daillant]

Effect of solvent-polymer interaction in swelling dynamics of ultra-thin polyacrylamide films: A neutron and x-ray reflectivity study

[C13. G. Chaboussant]

Study of adsorbed nanoparticles at a solid-liquid interface by neutron surface scattering

# H1. NANOMECHANICS AND GLASS TRANSITION OF CONFINED POLYMERS WITHIN SPHERICAL NANOSIZED PARTICLES

Y. RHARBI<sup>1\*</sup>, N. BASSOU<sup>1</sup>, F. BOUE<sup>2</sup>

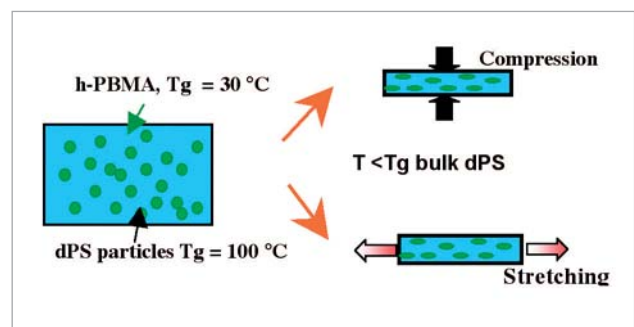
<sup>1</sup>Laboratoire de Rhéologie, UMR 5520, BP 53 Domaine universitaire 38041 Grenoble

<sup>2</sup>LLB CEA-CNRS, bat 563, CEA-Saclay, 91991 Gif-sur-Yvette

\*Rharbi@ujf-grenoble.fr

It is most likely that a polymer's environment affects its dynamics, rheological properties and more particularly its glass transition temperature ( $T_g$ ). This idea is backed up by "Brillouin Light Scattering", and ellipsometry results from Forrest and al.<sup>1,3</sup>, and Keddie and al.<sup>2</sup> on both supported and free standing ultrathin films. They suggest that the  $T_g$  of polystyrene is reduced below the bulk values with a decrease in film thickness ( $h$ ) for  $h < 50$  nm. For free standing film, where thickness  $h \sim 20$  nm, the  $T_g$  is reduced by about  $60^\circ\text{C}$  below the bulk value. Other experiments suggest that the  $T_g$  of supported polymethyl methacrylate (PMMA) on certain solid surfaces, increases with decreasing film thickness.<sup>4</sup> However, the situation of a polymer confined within another polymer has not been thoroughly investigated. This situation is particularly crucial for a good number of applications; polymer blends, copolymers, composites... In this work we propose to study the influence of the proximity of two polymers on their glass transition and their dynamics.

We developed a method which combines Nanomechanics with Small Angle Neutron Scattering (SANS) to study the deformation modes of polymers confined within nanosized domains (20 to 200 nm). The work consists of analyzing the deformation modes of deuterated nanosized polymer particles, dispersed individually within matrices of another polymer using SANS (Schema 1). The project involves two major stages: 1) we prepare films containing deuterated polystyrene d-PS nanoparticles, dispersed in a perfectly individual manner within polybutyl methacrylate (PBMA) matrices. 2) Thereafter we apply mechanical stress to the films (compression), and we study the variations of the nanoparticles' form factor. Film preparation was carried out in two steps: 1) Synthesis, via emulsion polymerization, of deuterated d-PS nanoparticles ( $T_g^{\text{bulk}} = 100^\circ\text{C}$ , diameter ranging from 20 to 200 nm) and hydrogenated h-PBMA particles ( $T_g^{\text{bulk}} = 28^\circ\text{C}$ , diameter 50 nm). 2) Preparation of films via evaporation of a mixture of h-PBMA and dPS dispersions. PBMA particles were cross-linked during emulsion polymerization with 0, 1, 5 and 10% ethylene glycol dimethacrylate (EGDA). Small angle neutron scattering (SANS) experiments were carried out on the spectrometer PAXY (Saclay).



Schema 1. Experimental procedure

We optimized the experimental conditions for sample preparation in order to achieve perfect dispersion of the dPS particles within h-PBMA matrices. We obtained SANS spectra describing all the characteristics of the form factor of individual particles (Figure 1). The films were compressed at different temperatures in a home-made compression device.

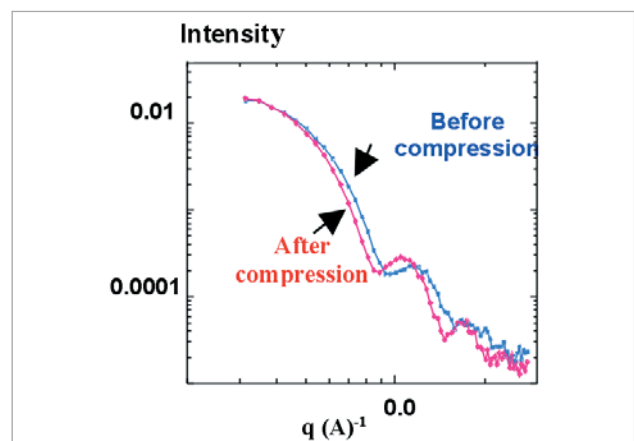
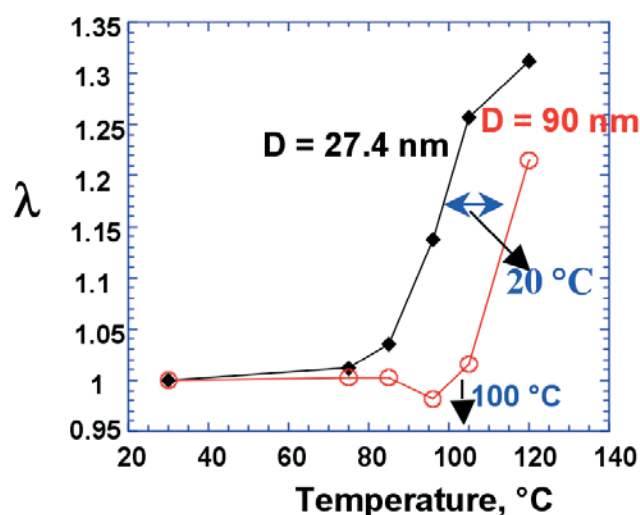


Figure 1. SANS spectra of dPS particles (90 nm, 2%) in crosslinked PBMA matrix (10 % crosslinker), before and after compression at  $120^\circ\text{C}$ .

In figure 1, we show the spectra of a film containing 90 nm dPS particles within a cross-linked PBMA matrix, before and after deformation. The form factor of the dPS particles changes upon compression which infers that the dPS nanoparticles undergo deformation within the PBMA matrix.

## SOFT MATTER

We developed a model for analyzing the SANS spectra of compressed nanoparticles and for calculating the deformation rate  $\lambda$ . In figure 2, we show the nanomechanical spectra,  $\lambda$  vs. temperature for 90 nm and 27.4 nm dPS nanoparticles within cross-linked PBMA matrices (10% crosslink). The 90 nm sized d-PS particles undergo deformation, under compression, for temperatures  $T > T_g$  of the bulk polystyrene (100 °C). Whereas the 27 nm sized dPS particles begin to deform at about 20°C below the bulk  $T_g$  (Figure 2). These results suggest that the nanomechanical properties and particularly the  $T_g$  of 90 nm sized d-PS particles are similar to those of the bulk polystyrene. On the other hand, the nanomechanical properties of 27 nm particles are influenced



**Figure 2.** Nanomechanical spectra: deformation rate  $\lambda$  vs. temperature for 90 nm and 27.4 nm dPS nanoparticles in cross-linked PBMA matrices (10% cross-link).

by their environments and their  $T_g$  is about 20° C lower than that of bulk polystyrene (Figure 2). The onset temperature for the dPS deformation depends on the  $T_g$  of the confined polymer ( $T_g^{\text{conf}}$ ) and is most likely similar to it. In Figure 3, we show the  $T_g^{\text{conf}}$  values vs. the dPS particle diameter. One can clearly see two behaviors: when the dPS particles are larger than 50 nm,  $T_g^{\text{conf}}$  is constant and similar to the bulk value. When the dPS particles are smaller than 50 nm,  $T_g^{\text{conf}}$  decreases continuously as the particle size decreases. This result is similar to that reported on ultra-thin polystyrene films<sup>1-3</sup> and is one of the first experiments that clearly show the similarity between confinement in thin polymer film and in blends.

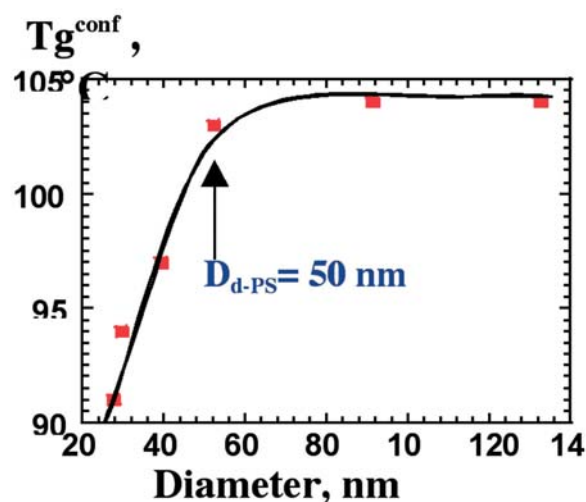


**Figure 3.** The onset temperature for the dPS nanoparticle deformation, calculated from figure 2, as a function of particle diameter. The PBMA matrices were crosslinked with 10 % cross-linker.

- [1] J.A. Forrest, K Dalnoki-Veress, J.R. Stevens and J.R. Dutcher, Phys. rev. Lett. 77, 2002-2005 (1996); 77, 4108 (1996).
- [2] Joseph L Keddie, Richard A.L. Jones and Rachel A. Cory, Europhys. Lett. 27,59, (1994)
- [3] J.A. Forrest, K Dalnoki-Veress, Advances in Colloids and interface Science, 94, 167, 2001
- [4] Joseph L Keddie, Richard A.L. Jones and Rachel A. Cory, Faraday Discuss.98, 219-230, (1994)

## H2. NOVEL FRONTIER BETWEEN LIQUID AND SOLID STATES IN POLYMERS: IDENTIFICATION OF A MACROSCOPIC SOLID-LIKE MODE IN THE MOLTEN STATE.

HAKIMA MENDIL, PATRICK BARONI, LAURENCE NOIREZ

Laboratoire Léon Brillouin (CEA-CNRS), CEA-Saclay, 91191 Gif-sur-Yvette

Polymers are produced and daily used but their dynamic properties far from being understood, fascinate by their puzzling properties. Indeed, polymers present unexplained large time scale relaxations; reinforced polymers display incredibly high moduli; the polymer dynamic at nanometric [1] and at filmic states [2] reveal solid-like characters incompatible with the conventional macroscopic viscoelastic properties [3]. Various flow behaviours display inexplicable instabilities. One of the most spectacular ones, is the shear induced phase transition observed in the liquid state of liquid-crystal polymer melts [see photograph below and reference 4].

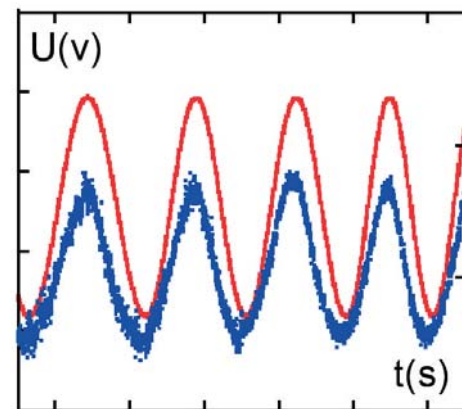
Novel experimental observations carried out at the LLB by controlling the boundary conditions between the polymer and its substrate, give a fresh perspective on their true nature. Indeed, the common and fundamental denominator in flow experiments is the no-slippage interacting condition between the fluid and the substrate(s). The several tens' years of apparent agreement between macroscopic rheological experiments and theoretical models, promoted the no-slippage condition as a postulate, reinforcing the idea that the no-slippage liquid-solid boundary is usually fulfilled.



Above a critical shear rate, the isotropic liquid of liquid crystal polymers (left photo) transforms in a strongly birefringent oriented phase (right photo). Photos are obtained between crossed polarisers in the (velocity, neutral axis) plane.

However, the emergence of new disciplines as microfluidics together with the observation of unexpected macroscopic instabilities as exposed above, shows that the fluid properties are actually strongly dependent on the scale of the observation and also on the nature of the surface interactions, driving numerous studies to reconsider now the static and the dynamic friction states between the fluid and the substrate. Combining the tribology to dynamic relaxation measurements (CEA patent), we propose a new type of dynamic experiment where the interaction of the polymer to the substrate is controlled. Under optimal conditions, we show that the molten state of polymers, far

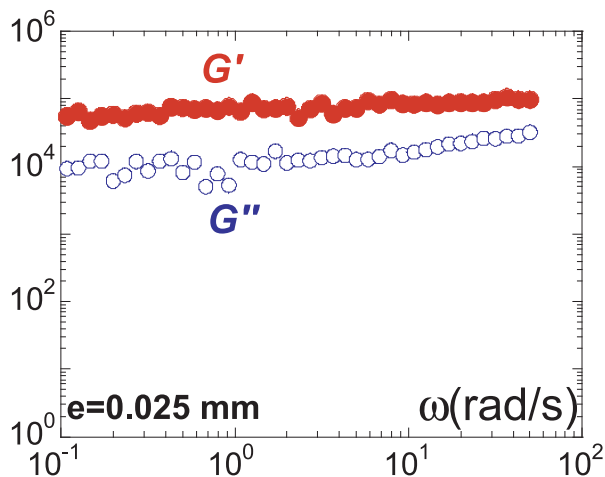
away from any transition, reveals so far unknown long range correlations [5]. The signature of an unpredicted elastic mode, is identified by the invariance of the dynamic response versus frequency and by the in-phase input strain and resulting output stress waves (see figure below).



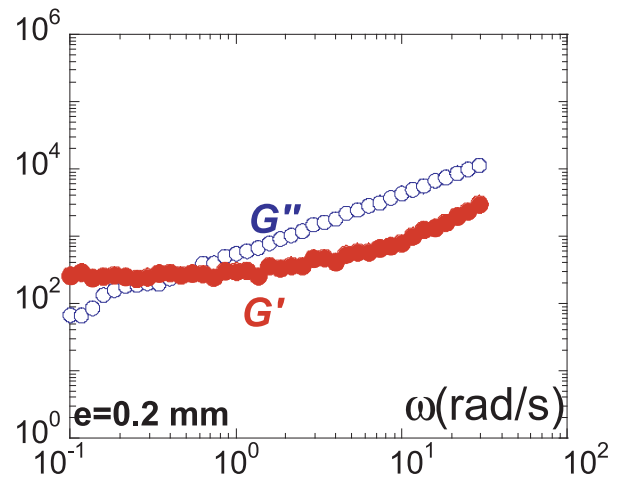
In phase entrance strain wave (red points) and resulting output wave (resulting torque - blue points) plotted versus time, evidencing a solid-like response for an ordinary polybutylacrylate at 100°C above the glass transition temperature ( $M_w = 40000$ ,  $I = 1.1$ ,  $\omega = 0.1 \text{rd/s}$ ).

This elastic property is a dimensional parameter; it progressively vanishes by increasing the sample thickness, as shown in the following figures (from a to c). The solid-like response observed at low thickness (here 0.025mm) is no more measurable at large thickness (typically 1mm) and is progressively dominated by the conventional polymer viscoelastic response (figure c). The sample is an ordinary polymer measured about 100°C far away from the glass transition temperature.

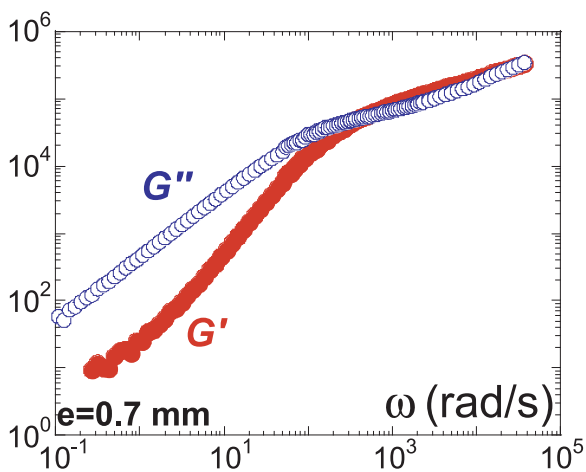
The identification of this size-dependent elasticity is of fundamental importance. It implies that the system contains unexpected giant time & length correlations at scales much larger than those described of the usual viscoelastic description (Rouse, reptation). Indeed, the low thickness solid-like response (typically measured at 0.020-0.040mm) corresponds to a gigantic scale with respect to the individual molecular scale (which is about 50-100Å). The definition of the conventional elementary polymer relaxation time described as the intercept of the  $\omega$  and  $\omega^2$  scaling of the viscous and the elastic responses respectively, should be revisited since it does not reflect a terminal relaxation time.



a)



b)



c)

This experimental observation, carried out on various polymer types (LC-polymers, Polybutadiene, Polymethacrylates, Polybutylacrylates...) should shed light on various disagreements between experimental observations, theoretical developments and applications and open new routes for the understanding of polymer science and complex fluid dynamics, including the up to date active debate on the discontinuous dynamic behaviour from nanometric to macroscopic scale dynamics.

Dynamic relaxation spectra showing the linear response of the viscous ( $G''$ ) (●) and the elastic ( $G'$ ) (●) moduli versus frequency, at different sheared thicknesses ( $e=0.025\text{mm}$ ,  $0.2\text{mm}$ ,  $0.7\text{mm}$ ). The sample is a monodisperse polybutylacrylate ( $M_w=47000$ ) measured at  $T=T_g + 90^\circ\text{C}$ .

1. H.Wu, S. Granic, *Science* **258** (1992) 1339.
2. P.A. O'Connell, G.B. McKenna, *Science* **307** (2005) 1760.
3. "Viscoelastic Properties of Polymers", J.D. Ferry, . Wiley & Sons Editor (1980).
4. C. Pujolle-Robic, L. Noirez, *Nature* **409** (2001) 167
5. H. Mendil, P. Baroni, L. Noirez, *Eur. Phys. J. E (Focus Point)* **19** (2006) 77-113, *ibidem*, *Eur. Phys. E* **19** (2006) 20, H. Mendil, I. Grillo, P. Baroni, L. Noirez, *Phys. Rev. Lett.* **96** (2006) 077801.

# H3. CHAIN FORM FACTOR AND COUNTERIONS RELEASE IN POLYELECTROLYTES-PROTEINS COMPLEXES : BEYOND THE USUAL CONTRAST MATCHING METHOD

J. GUMMEL, F. COUSIN, F. BOUÉ

Laboratoire Léon Brillouin, CEA-CNRS UMR12, CE Saclay, 91191 Gif sur Yvette Cedex, France

Understanding the mechanisms driving the formation of complexes of polyelectrolytes and proteins of opposite charges is of a fundamental importance as such complexes are often encountered in biological or industrial situations [1]. A large variety of macroscopic structures can be formed depending on the kind and strength of the interactions involved in the system. We show here how the combination of SANS with contrast matching permits the full determination of the structures formed by a model system. This system, made of lysozyme (positively charged protein) and PSSNa (negatively charged polyelectrolyte), is both model from the physico-chemical point of view and from a neutron contrast point of view because PSS can be easily deuterated and  $\rho_{\text{PSSH}} = \rho_{\text{lyso}}$ .

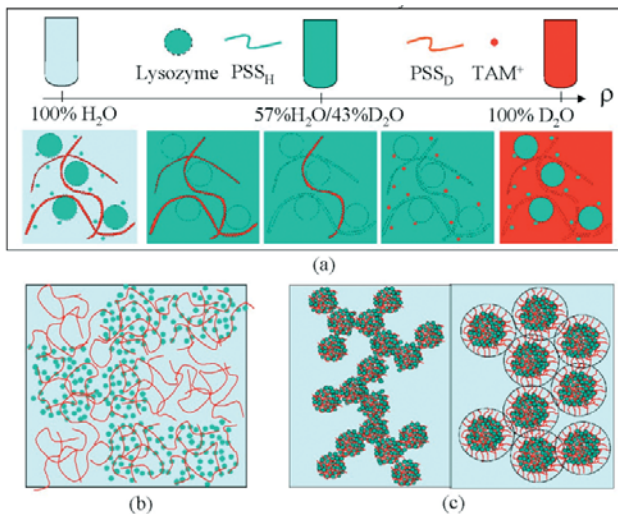


**Figure 1.** (a) Neutron density length  $\rho$  in the system (b) Gel structure (c) Globular structure.

Firstly, we have used PSSD to watch separately the protein and the polyelectrolyte inside the complexes. Three main structures can be formed in the system when changing the ratio of negative to positive charges  $[-]/[+]_{\text{intro}}$  and the length of the PSS chains [2] for a given pH and a given ionic strength (50mM) : (i) For  $[-]/[+]_{\text{intro}} < 5$  and for long PSS chains, the structure is a network formed by PSS chains cross-linked by lysozyme (Fig 1.b). Macroscopically, samples are gels. (ii) For  $[-]/[+]_{\text{intro}} < 5$  and for short PSS chains, lysozyme and PSS chains are embedded in dense 3-D aggregates that arrange in a fractal network at a larger scale (Fig 1.c). Macroscopically, samples are liquid. (iii) For  $[-]/[+]_{\text{intro}} > 5$  and whatever the chain length, the internal structure of the lysozyme changes. After an initial strong electrostatic

binding, lysozyme is progressively unfolded thanks to an hydrophobic contact with PSS. The two chainlike objects are finally organized in a homogeneous costructure (not shown here). We focus then on the role of  $[-]/[+]_{\text{intro}}$  structure on the dense 3-D aggregates formed by small chains [3]. The primary complexes are always formed with radii around 10 nm and organize at a higher scale in aggregates of fractal dimension 2.1. The systematic use of the contrast matching of PSS<sub>D</sub> in SANS have allowed the determination of the species composition and the water content, yielding the compactness and the inner charge ratio  $[-]/[+]_{\text{inner}}$ . The primary complexes have : (i) an inner charge ratio  $[-]/[+]_{\text{inner}}$  close to 1 whatever  $[-]/[+]_{\text{intro}}$ , (ii) a high total volume fraction (0.25 to 0.4), (iii) an increase of the radius with an increase of  $[-]/[+]_{\text{intro}}$  (from 75 Å up to 150 Å) and a (iv) a shell of PSS chains when  $[-]/[+]_{\text{intro}} > 1$ . There are free proteins if  $[-]/[+]_{\text{intro}} < 1$  and free PSS chains if  $[-]/[+]_{\text{intro}} \gg 1$ . This inner charge stoichiometry is recovered for different charge density of components (tuned by pH for lysozyme and by sulfonation rate for PSS) and proves the dominant role of direct electrostatic interactions in complexation. The primary complexes aggregate at a higher scale with a fractal dimension of 2.1 characteristic of Reaction Limited Colloidal Aggregation often found in charged systems. The size of primary complexes is limited by the total ionic strength of solution.

We present now to experiments with specific labelling tricks that takes benefit from  $\rho_{\text{PSSH}} = \rho_{\text{lyso}}$  to go further in the understanding of the complexation process.

## Conformation of a PSS chain within complexes [4]:

The pictures of the two types complexes that can be formed when  $[-]/[+]_{\text{intro}} < 5$  (gel or dense globules) suggest that the transition between the two regimes correspond to the overlapping concentration of the chains  $c^*$  : when the chains are in semi-dilute regime, the network pre-formed by PSS chains is cross-linked by proteins but when they are in dilute regime, chains collapse with proteins to form globules. In order to check this assumption, the persistence length  $l_p$  of the chain within the gel has to be measured to get  $c^*$ .  $c^*$  is indeed proportional to  $1/N^{1/2} l_p^{3/2}$  where N is the number of repetitions units per chain. Experimentally, the system shifts from one regime to another for an N lying between 350 and 600 for  $[\text{PSS}] = 0.1 \text{ mol/L}$  with  $[\text{lyso}] = 40 \text{ g/l}$  and  $I = 50 \text{ mM}$ . But if one calculate  $c^*$  with  $l_p = 50 \text{ Å}$  (value taken from literature for pure PSS solutions), the system must stay in semi-dilute regime for  $N > 30$ . The chains should thus be largely shrunk when interacting with proteins.

In order to measure  $l_p$ , we have made several mixtures of PSS<sub>H</sub>, PSS<sub>D</sub> and lysozyme in a solvent that matches both PSS<sub>H</sub> and lysozyme with  $[PSS_H+PSS_D] = 0.1$  mol/L and  $[lyso] = 40$ g/l. The only remaining terms in the scattered intensity are due to the correlations between deuterated PSS monomers  $S_{DD}(q)$  that write :

$$S_{DD}(q) = \Phi_D S_{1D}(q) + \Phi_D^2 S_{2DD}(q)$$

where  $\Phi_D$  is the volume fraction of PSS<sub>D</sub> chains,  $S_{1D}$  the intra-chains signal and  $S_{2DD}$  the structure factor between monomers from distinct chains. As shown in insert of figure 2.a and 2.c, the interpolation at  $\Phi_D = 0$  enable a direct measurement of  $S_1(q)$  :

$$S_{DD}(q)/\Phi_D = S_{1D}(q) + \Phi_D S_{2DD}(q)$$

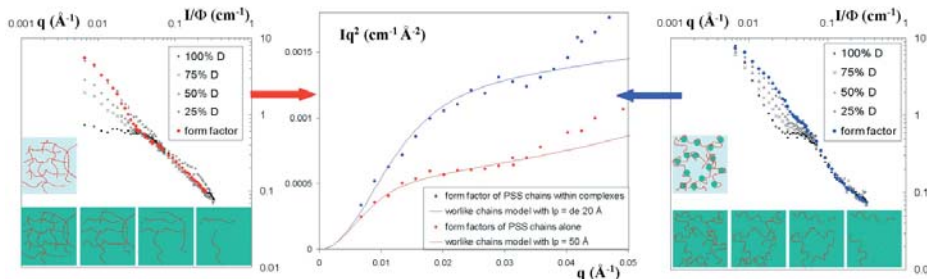


**Figure 2.** Measurement of form factor within complexes : (a) and (c) experimental value of  $I(q)/\Phi_D = f(\Phi_D)$  and interpolation to  $\Phi_D = 0$  without proteins (a) or with proteins (c). Insert show the principle of experiment. (b) Comparison of form factor in Kratky plot and scattering modelization with model of wormlike chains.

The measurement made with or without lysozyme are presented in figure 2.a and 2.c. The comparison of the form factor in Kratky plot show a large shrinking of the chains with lysozyme. A fit of the form factor by a wormlike model show that the  $l_p$  value of 50Å is recovered without proteins but the  $l_p$  is reduced to 20Å when interacting with proteins. Finally, a calculation of  $c^*$  with  $[PSS] = 0.1$  mol/L and  $l_p = 20$ Å show that the transition from dilute to semi-dilute regime should occur for  $N \sim 500$  that perfectly matches the value obtained experimentally.

### Experimental proof of the counter-ions release during complexation [5].

The counter-ions release is commonly considered as one of the main driving process of the complexation due to the entropic gain associated with the release. Though this is confirmed by simulations, there is not yet an experimental direct proof of such release. We have tested this hypothesis with a 'black or white' experiment by performing SANS measurement on samples that should scatter or not when all species except counterions are matched. This is based on the hairy shell of PSS chains that surrounds the globular complexes in diluted regime as soon as the introduced charge ratio  $[-]/[+]_{intro}$  is higher than 1. In case of release,

counterions must be all expelled from the core of the hairy globules but not completely from the shell as there should remain Manning condensation on the free PSS chains. The only samples that should provide a scattering are the ones for which  $[-]/[+]_{intro} > 1$  because the counterions decorate the shell (see figure 3). The matching is experimentally performed by replacing the usual  $Na^+$  counterions of hydrogenated PSS chains by deuterated TAM<sup>+</sup> counterions. Such counterions have a large contrast with a 57% $H_2O$ /43% $D_2O$  solvent that matches both lysozyme and PSS<sub>H</sub> chains. Results are presented in figure 3 and unambiguously prove the counterions release : 'naked' samples do not scatter though hairy samples scatter. The counterions scattering is proportional to the one of the chains (obtained with PSS<sub>D</sub> chains and hydrogenated TAM<sup>+</sup>, not shown here). This confirms that the counterions decorate the shell

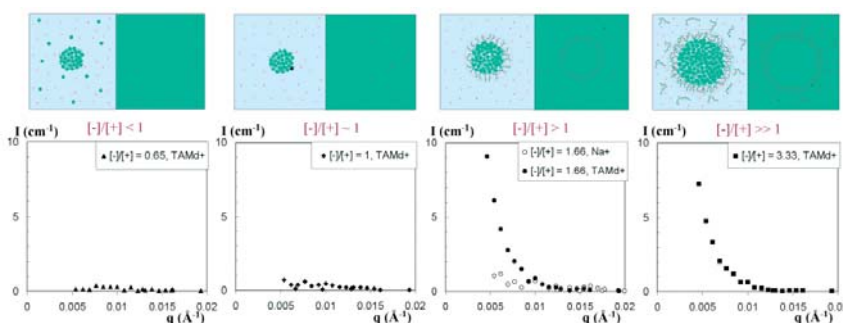


**Figure 3.** Upper part : Contrast of globular complexes made with lysozyme and hydrogenated PSS chains with deuterated TAM<sup>+</sup> counter-ions in either a 100% $D_2O$  solvent or in a 57% $H_2O$ /43% $D_2O$  solvent. Lower part : low  $q$  SANS scattering in a 57% $H_2O$ /43% $D_2O$  solvent. From left to right : increase of the  $[-]/[+]_{intro}$ .

- [1] C.L. Cooper, P.L. Dubin, A.B. Kayitmazer, S. Turksen, *Curr. Opin. Coll. Interface Sci.*, (2005), **10**, 52-78.
- [2] F. Cousin, J. Gummel, D. Ung, F. Boué, *Langmuir*, (2005), **21**, 9675-9688 .
- [3] J. Gummel, F. Boué, B. Demé, F. Cousin, *J. Phys. Chem. B* (2006) accepted.
- [4] J. Gummel, F. Cousin, F. Boué, in preparation.
- [5] J. Gummel, F. Cousin, F. Boué, in preparation.

## H4. PH-RESPONSIVE INTERFACES GRAFTED WITH POLYELECTROLYTE OR POLYAMPHOLYTE

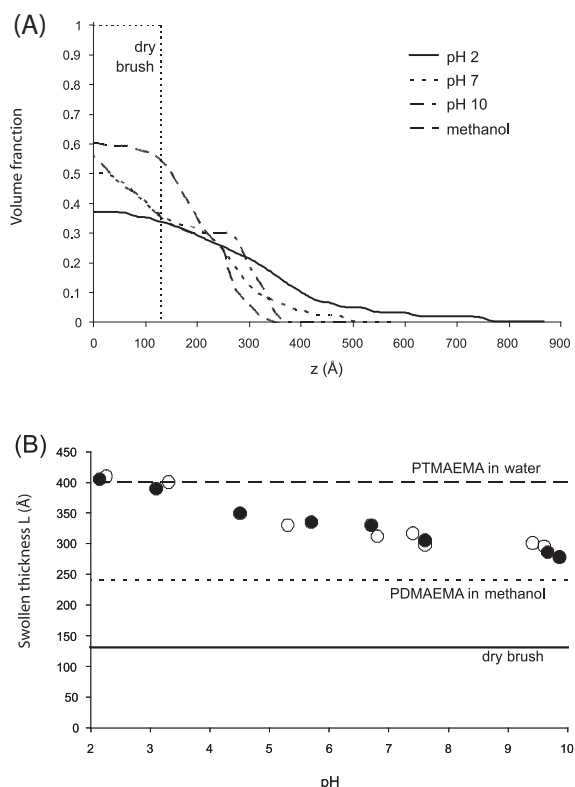
Y. TRAN, S. SANJUAN, N. PANTOUSTIER, P. PERRIN

Laboratoire de Physico-chimie des Polymères et des Milieux Dispersés.ESPCI, 10 rue Vauquelin, 75005 Paris

Interfaces grafted with polyelectrolytes are of great interest in a wide field of industrial and biological applications as well as in academic research. They are extensively used for the improvement of adhesion, lubrication, tribology, wetting properties or colloidal stabilization. More recently, some strategies are developed for the functionalization of surfaces with polymer brushes to realize smart surfaces with switchable-adaptative-responsive properties and to generate micro-patterned polymer monolayers.<sup>1-2</sup> Responsive polymer brushes are attractive owing to the change of the conformation of attached chains according to external conditions. As example, neutral polymer chains are sensitive to a good or a bad solvent. For polyelectrolyte chains, the influence of environment on their charge is decisive for the stretching. An important distinction has to be made regarding “strong” polyelectrolyte for which charges are fixed and “weak” polyelectrolyte which are pH-dependent. Polyampholytes bear both positive and negative charges along the chain. With an excess of charge, polyampholyte chains are as stretched as polyelectrolyte chains. With an equal ratio of positive and negative charges, the chains are collapsed due to the attraction between oppositely charged monomers and the expulsion of counterions.<sup>3</sup> Stimuli-responsive interfaces investigated here are grafted with polyelectrolyte and polyampholyte. In particular, we are interested in the deformation amplitude of brushes with the variation of pH.

The synthesis was performed by the “grafting from” method using surface-initiated controlled polymerization to obtain dense polymer brushes with well-defined molecular mass and low polydispersity. First, the halogenated group-functionalized initiator was anchored to the silica surface in self-assembled monolayers. Then, chains were grown from the surface by atom transfer radical polymerization (ATRP). Finally, neutral polymer brushes were converted into polyelectrolyte or polyampholyte brushes by *in situ* chemical reactions.

The swelling of poly(2-dimethylaminoethyl methacrylate) (PDMAEMA) polybase brush was investigated as a function of pH and compared to the stretching of poly(2-trimethylaminoethyl methacrylate) (PTMAEMA) quenched brush. PMAA-*st*-PDMAEMA random copolymer of 1:1 molar ratio was investigated as polyampholyte brush. Neutron reflectometry allowed the determination of the monomer volume fraction profile perpendicular to the surface. The swollen thickness was deduced and compared to the values measured by ellipsometry.



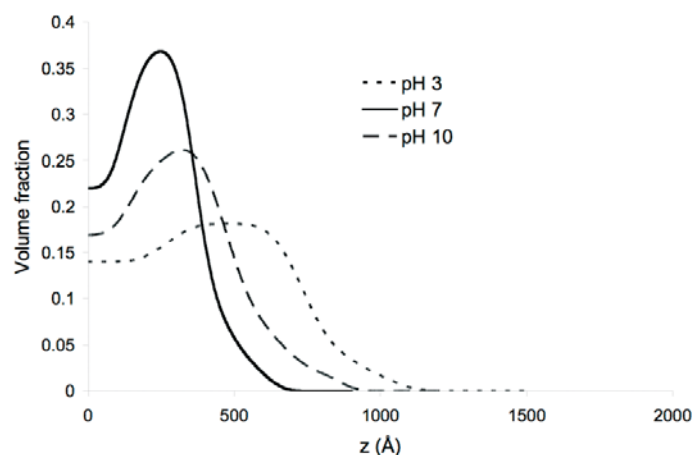
**Figure 1.** (A) Monomer volume fraction profile of PDMAEMA brush at various pH and in methanol. (B) Swollen thickness of PDMAEMA brush as a function of pH, measured by ellipsometry (○) and neutron reflectivity (●).

Figure 1A shows the monomer volume fraction profile of PDMAEMA brush at pH 2, pH 7 and pH 10 and in methanol. The profile of the dry brush was also given for comparison. The brush was less extended in methanol than in water and was more stretched as pH decreased. The shape of the profiles was analyzed in more detail by fitting the profiles with a parabolic function (predicted for a neutral brush in good solvent) or a Gaussian function (predicted for a polyelectrolyte brush in osmotic regime). The profile of PDMAEMA brush in methanol (respectively at pH 2) could be well adjusted by a parabolic function (respectively a Gaussian shape) as expected. In contrast, the profile at pH 10 was quite far from a Gaussian profile and is closer to a stepwise distribution as predicted for weakly charged polymer brushes.

The swollen thickness can be deduced by computing the normalized first moment of the density profile. These data obtained from neutron reflectivity technique were similar to the values measured by ellipsometry (Figure 1B). There was no hysteresis effect with the pH proving that the brush swelling was completely reversible. The swelling behavior of the pH-responsive brush was between the behavior of a neutral polymer in good solvent and a strong polyelectrolyte brush in osmotic regime, as expected.

We expected the polyampholyte brush to behave as a polyelectrolyte brush at very low and very high pH owing to an excess of charge. It should collapse in the pH range of zero net charge owing to the attraction between oppositely charged units of equal proportion.

The volume fraction profiles of PDMAEMA-*st*-PMAA brush at various pH are shown in Figure 7. The brush was rather stretched at pH 3. It was significantly contracted at pH 7 and the situation was intermediate at pH 10. The chains were not collapsed onto the surface as for a dry brush. The density profile shows a non-monotonic decrease with the distance from the surface. A higher density zone likely due to the attraction between oppositely charged units was observed. This barrier-like zone could hinder the ionization of monomer units close to the surface. It could prevent a collective ionization and reduce the collapse of the polyampholyte brush. In addition, it was found that the amplitude of deformation was higher in the pH range of zero net charge for less dense brushes.



**Figure 2.** Volume fraction profile of PDMAEMA-*st*-PMAA polyampholyte brush at various pH.

An application of ionic polymer brushes in microfluidic devices is developed. We build microchannels with one-wall covered by the polymer brush. We investigate the electro-osmotic properties by determining the velocity of the flow under an electric field while varying the ionization of the polymer with pH.

We are also interested in the exchange of ions. Scanning Electro Chemical Microscopy (SECM) is used to follow the release of specific ions from the polymer brush. Using selective and sensible microelectrodes, we aim at the detection of protons of the polymer brush.

Neutron reflectivity experiments were performed on EROS with the help of Fabrice Cousin and Alain Menelle.

1 Advincula R. C., Brittain W. J., Caster K. C., Ruhe J. "Polymer brushes", Wiley-VCH, Weinheim, **2004**.

2 Ruhe J., Ballauff M., Biesalski M., Dziezok P., Grohn F., Johannsmann D., Houbenou N., Hugenberg N., Konradi R., Minko S., Motornov M., Netz R.R., Schmidt M., Seidel C., Stamm M., Stephan T., Usov D., Zhang H. *Adv. Polym. Sci.* **2004**, *165*, 79-150.

3 Dobrynin A. V., Colby A. H., Rubinstein M. *J. Polym. Sci. Part B, Polym. Phys.* **2004**, *42*, 3513-3538.

# H5. A SANS STUDY OF THE ADSORBED ASPHALTENE LAYER IN WATER-IN-HYDROCARBON EMULSIONS

J. JESTIN<sup>1</sup>, S. SIMON<sup>2</sup>, T. PALERMO<sup>2</sup>, L. BARRÉ<sup>2</sup>

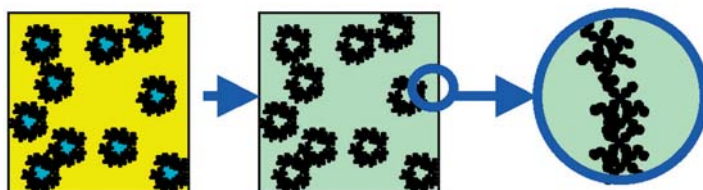
<sup>1</sup> Laboratoire Léon Brillouin (CEA-CNRS), CEA- Saclay, 91191 Gif sur Yvette Cedex, France.

<sup>2</sup> Institut Français du Pétrole (IFP), 1-4 avenue de Bois-Préau 92000 Rueil-Malmaison, France.

During oil production, crude oils are typically produced as water in crude oil (w/o) emulsions, which are often very stable. Among the indigenous natural surfactants contained in the crude oils, asphaltenes and resins are known to play an important role in the formation and stability of w/o emulsions [1]. Until now, the stability of the oil/water interface, and particularly the contribution of asphaltene, has been studied mainly from a rheological point of view [2]. Correlations between stability and mechanical properties of the interfaces have been highlighted. Nevertheless, less is the knowledge about the structural organisation of the molecules at the interface and the link between the structure at the local scale and the stabilization mechanisms [3].

We present a new and original method to visualize the interfacial film in liquid-liquid petroleum emulsion by SANS measurements. Though the droplet size is micronic, one structure in the system is a few nanometer, which the water-oil interface, and also some 10 nm asphaltene large fractal-like aggregate present in the oil [4] can be linked to this interface. Neutron scattering is here used at its best, owing to contrast matching of the two liquid phases: by adjusting the scattering length density of the aqueous to the one of the organic phase, we measure the residual scattering contribution of the interface only. Emulsions are water in oil (xylene) mixtures stabilized by asphaltenes, which are the higher molecular mass, the denser, the more polar and aromatic components of crude oils. We showed the possibility to reach to the local structure of the interface (size, composition) and to the linkage of asphaltene aggregate structures between bulk and interface.

To make SANS measurements accurate and meaningful, a specific protocol is used. Asphaltene is dissolved into xylene, and the solution is mixed with water; after the emulsification process (strong stirring), two liquids phases appear, a packed droplet water phase and a supernatant, which separates by decantation. A specific attention was made to know precisely (by weighing) the volumic fractions of oil and water in each phases. It allowed us to measure independently the scattering from the initial asphaltene solution, from the supernatant and from the packed droplet water phase. The oil phase is a mixture of normal and deuterated xylene, the water phase is a mixture of normal and deuterated water. Depending on the deuterated species fractions, we can separate the scattering contribution of the different components of the system. Special care (figure 1) was made in the banks measurements (incoherent scattering and residual asphaltene bulk scattering) to background subtraction to be sure to get the interface scattering.



**Scheme 1.** The use of neutrons: inner and outer scattering densities are matched, and one look at the scale of the interface.

By matching the asphaltene signal, we can see the water droplets scattering contribution and have an access to the quantity of interface. Systematic experiments were performed by varying the amount of resins (which is related to the size of asphaltenes aggregates), the pH of the aqueous phase, which change the asphaltenes-asphaltenes interactions and the ageing times of the emulsions, to study slowing down effects.

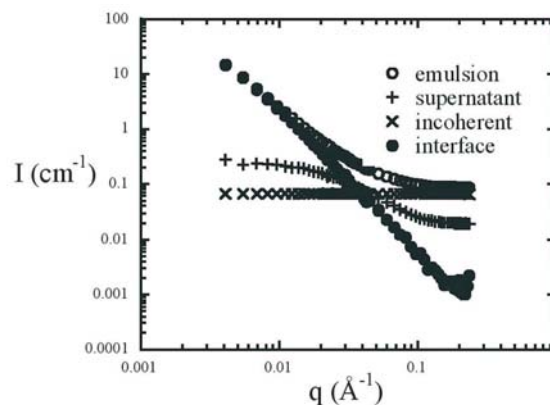


**Figure 1.** Specific treatment of emulsion measurements in the two liquid phase matching contrast condition to extracted the interface scattering signal after subtraction of the contributions of both incoherent scattering and asphaltene bulk scattering.

From bulk SANS measurements in initial solutions and supernatant, we can deduce radius of gyrations and molecular mass of asphaltene aggregates using the Zimm approximation. We observe a systematic decrease of these quantities after the emulsification process (table 1). This suggested a preferential localisation of the large aggregates in the interface.

Asphaltenes Aggregates	$R_g$ (Å)/ $M_w$ (g.mol <sup>-1</sup> ) before emulsification (initial solution)	$R_g$ (Å)/ $M_w$ (g.mol <sup>-1</sup> ) after emulsification (supernatant)
Small	66 / 9.76.10 <sup>4</sup>	61 / 9.79.10 <sup>4</sup>
Medium	84 / 1.81.10 <sup>5</sup>	74 / 1.45.10 <sup>5</sup>
Large	106 / 3.02.10 <sup>5</sup>	90 / 2.37.10 <sup>5</sup>

**Table 1.** Variation of the size and of the mass of the asphaltene aggregates before and after emulsification.

The interface scattering signal obtained after subtraction of background shows a decrease of the intensity as  $q^{-2}$  which is the sign of the scattering of two dimensional objects (figure 2).

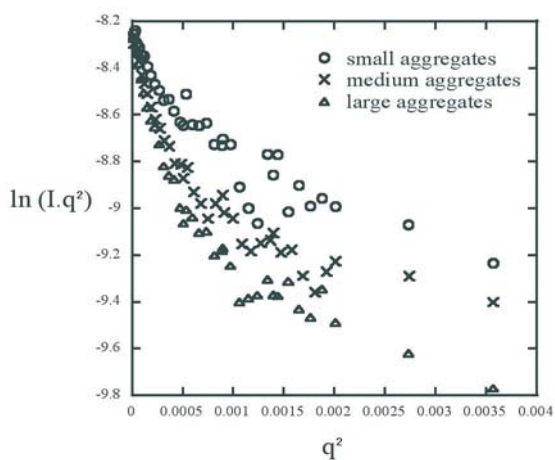


**Figure 2.** The interface scattering, in a  $\log(q^2 I(q))$  versus  $q^2$  plot: the thickness of the interface is given by the slope of the curves assuming a flat disk model.

The signal could be analysed using a simple flat disk model from which we could extract the thickness of the interface. The most important result is that the thickness of the interface is directly correlated to the asphaltene aggregate sizes in bulk: The larger the aggregates in bulk, the thicker the interface. Measurements in asphaltene matching conditions displays a Porod law, as expected, with a specific surface yielding the water droplets radius, in situ. Coupling these values with independent asphaltene adsorb amount in grams per grams of water droplets, using classical adsorption measurement methods, permit to calculate the quantity of molecules in grams per surface unit. The obtained adsorption values are consistent with a structural organization of aggregates as a mono layer at the interface. The stability of the emulsion could be analysed with a simple criterion: the quantity of water resolved after centrifugation and discussed as function of the structural parameter of the interface [5]. The main conclusions could be summarizing as follows: the interface is stabilized by the larger asphaltene aggregates, organized as a monolayer. The thickness of the interface is directly correlated to the asphaltene size in bulk and the larger is the layer the more stable is the emulsion; the lower is the quantity of resolved water after centrifugation. Increasing the pH of the aqueous phase (from neutral to basic values) seems to contribute to the ionization of the polar fraction of the aggregates. This changes the interaction between aggregates inside the layer, which becomes more repulsive, and induced a decreasing of the number of objects per surface unit and in fact, of the emulsion stability. To conclude, we have demonstrated the capacity of SANS measurement to characterize the structure of liquid-liquid interface in the case of petroleum emulsion and the links between this organization at the local scale and the stability of the emulsions. From a larger point of view, this demonstrates the ability of SANS to study macro emulsions and would be applied to a large panel of experimental systems.

- [1] Sjöblom J., Aske N., Aufler I.H., Brandal O., Havre T.E., Saether O., Westvik A., Johnsen E.E., Kallevik H. *Advances in Colloid and Interface Science* **2003**, 100-102, pp. 399-473
- [2] Bourriat P., Kerri El N., Gracia A., Lachaise J. *Langmuir* **2004**, 20, pp 7459-7464
- [3] Czarnecki J., Moran K. *Energy & Fuel* **2005**, 19, pp 2074-2079
- [4] Fenistein D., Barré L., Broseta D., Espinat D., Livet A., Roux J.-N., Scarcella M. *Langmuir* **1998**, 14, pp 1013-1020
- [5] Jestin J., Simon S., Barré L., in prepar. for *Langmuir*

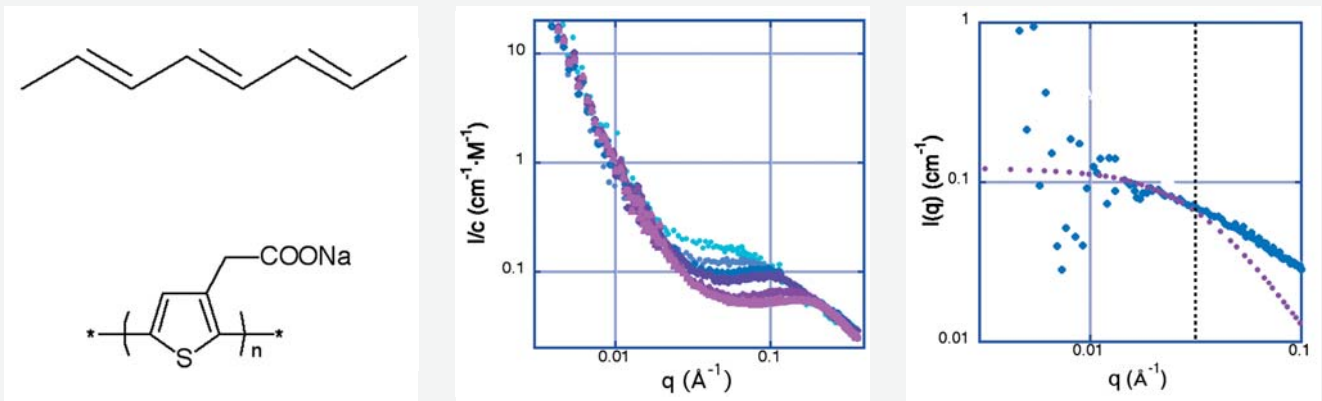
**[C1. P. Vallat] Molecular structure of conjugated polyelectrolytes**

Conjugated polyelectrolytes are a new class of polyelectrolytes. Their backbone consists of an alternation of simple and double (and/or triple) bonds. Thanks to this conjugation,  $\pi$ -electrons are delocalized along the backbone. Therefore, the polarizability of these chains is strongly enhanced and can even modify the structure of the solutions.

We study aqueous solutions of a specific conjugated polyelectrolyte: poly(3-thiophene acetic acid)(P3TAA). This macroion is prepared at different degrees of ionization. In a first step, our aim is to study the behavior of these chains in solution when they are completely ionized (with sodium as a counter-ion: P3TNaA) and compare it to the case of saturated polyelectrolytes. While the polyelectrolyte character of the chains can not always overcome the strong polarizability of rigid conjugated polyelectrolytes, the flexible chains of P3TNaA are soluble on a molecular level. It also appears that the behavior of this polyelectrolyte is that of a hydrophilic flexible saturated polyelectrolyte apart from a stronger tendency to self-aggregate (stronger upturns at low  $q$  values). However, the heterogeneities are in small quantities and the scaling laws predicted for flexible polyelectrolytes also apply here.

When salt (monovalent cation) is added to the solutions, upturns remain unchanged. Moreover, when the signal of the heterogeneities is subtracted, it appears at high enough ionic strength that the chains behave as neutral polymers with a correlation length  $\xi_c$  of 40Å (i.e.  $I(q)=1/(1+q^2\xi_c^2)$ ). This highlights two important facts. **First**, the fact they do not vanish shows heterogeneities are not a polyelectrolyte effect: they differ from what observed for polyions at low ionic strength, or with divalent cations. They exist prior to the polyelectrolyte state, i.e. in the neutral state (degree of ionization zero). **Second**, the fact that they do not increase shows an absence of macroscopic aggregation, even without electrostatic repulsion and in spite of the strong polarizability linked to conjugation. We believe this is due, in this particular example, to the flexibility of the backbone.

[Collaboration : P. Vallat, J.-M. Catala, F. Schosseler, M. Rawiso, Institut Charles Sadron, Strasbourg and LLB]



Left: general scheme of conjugated polymer (top) and molecular structure of P3TNaA (bottom)

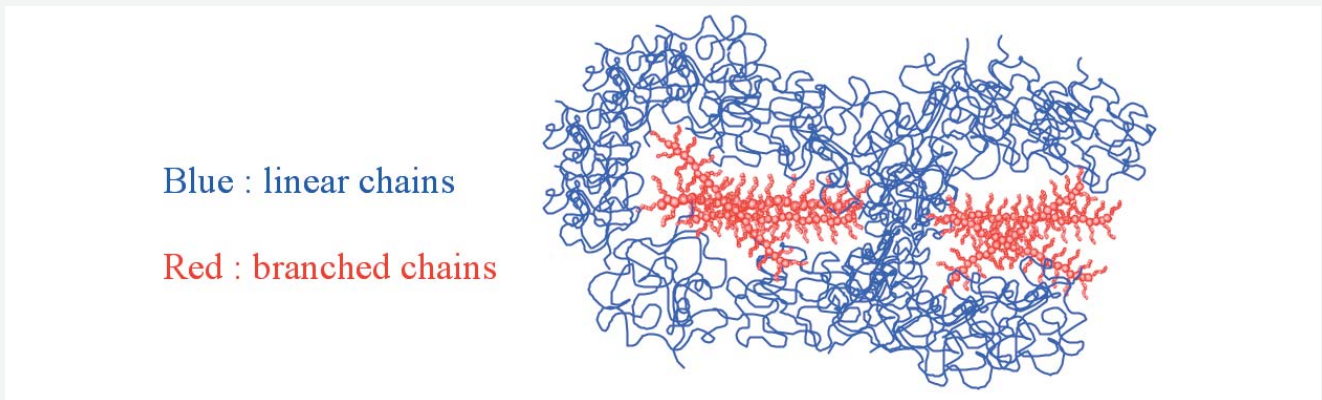
Middle: effect of concentration  $c$  of salt-free aqueous solutions of P3TNaA;  $c=0.08$  (top) to  $1 \text{ mol}\cdot\text{L}^{-1}$  (down)

Right: effect of addition of salt on solutions of P3TNaA solutions – upturn subtracted (full diamonds). Comparison with Lorentzian fit (empty diamonds).

**[C2. S. Desvergne] Two polymers made of the same segments which do not mix because of their different architecture**

We have mixed deuterated polystyrene linear chains with branched polystyrene chains (“polymacromonomers”), allowing the localisation of the two species by SANS. Deuterated and non deuterated segments can be considered as equivalent here. In spite of this, SANS shows that the linear chains interpenetrate weakly with the branched ones. For the most compact branched architectures, the mixture remains very inhomogeneous at the 10 nm scale, as the result of a kind of depletion, and also in agreement with mean field theory (H. Fredrickson). Our observation can be related with the coexistence of chains of different branching rate in real.

[Collaboration : S. Desvergne (thesis), F. Boué, J. P. Cotton, A. Brûlet, LL; Y. Gnanou, V. Herroqueuz, LCPO Bordeaux]



### [C3. O. Sandre] Smart hybrid magnetic polymersomes

Novel magnetic nano-composites are obtained by the self-assembly in water of polypeptide-based diblock copolymers polybutadiene-*b*-poly(glutamic acid) combined with either hydrophilic or hydrophobic  $\gamma$ -Fe<sub>2</sub>O<sub>3</sub> nanoparticles. These hybrid supramolecular objects are either filled micelles (3-d) or hollow vesicles with a magnetic membrane (2-d). At first, we have used isotropic SANS (PACE spectrometer) to explore the different types of objects formed and prove the formation of closed magnetic membranes (before their visualization by AFM and TEM); the membrane thickness has been calculated using Kratky-Porod plots. [1] Then, the deformation of such polymersomes with a magnetic membrane has been studied as a function of an applied magnetic field intensity by anisotropic SANS on the PAXY spectrometer. Here again, the use of SANS was of great importance to determine the anisotropic deformation of the membrane quantitatively. [2] These magnetic colloids are also able to respond to stimuli such as pH and ionic strength due to the presence of the polypeptide block, forming thus “multi-responsive” nanocapsules. These superparamagnetic hybrid self-assemblies offer attractive potentialities in biomedicine of staying for some time in the blood, due to their dimensions (100-500 nm), of manipulation by an external magnetic field, of local heating by a radio-frequency field for cancer radio-therapy, and of contrast enhancement in Magnetic Resonance Imaging. *Collaboration* : . O. Sandre - R. Perzynski, LI2C Paris 6, F. Chécot- S. Lecommandoux LCPO Bordeaux.

[1]- (a) Lecommandoux, S., Sandre, O., Checot, F., Perzynski, R. *Progress in Solid State Chemistry* 34, 2006, p 171. (b) Lecommandoux, S., Sandre, O., Checot, F., Rodriguez-Hernandez, J., Perzynski, R. *Journal of Magnetism and Magnetic Materials* 300, 2006, p 71.

[2]- Lecommandoux, S., Sandre, O., Checot, F., Rodriguez-Hernandez, J., Perzynski, R. *Advanced Materials* 17, 2005, p 712.

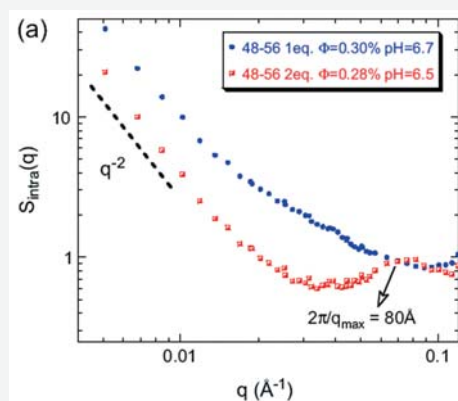
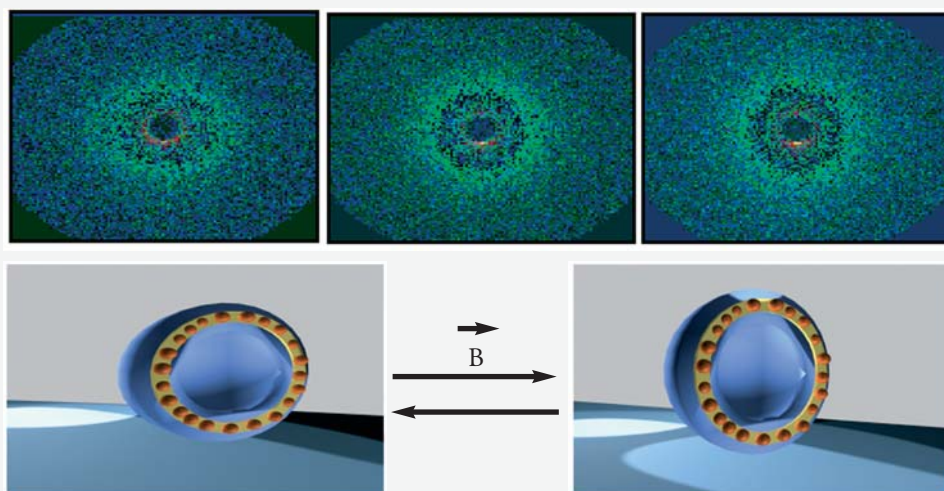


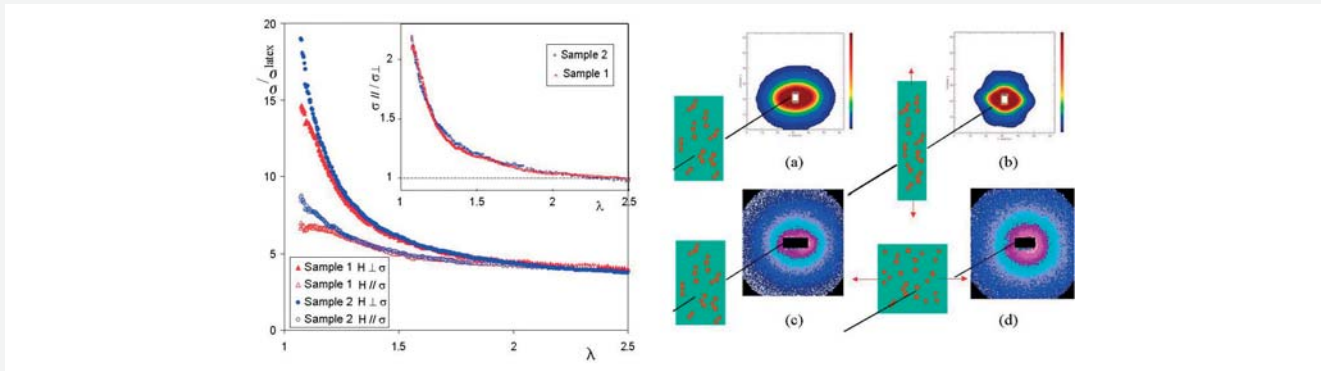
**Figure 1** (a) Intra-aggregates' structure factor  $S_{\text{intra}}(q)$  for hydrophobic nanoparticles associated to PB<sub>48</sub>-*b*-PGA<sub>56</sub>, as measured by SANS. (b) Deformation of hollow magnetic shells of the same polymersomes proven by the anisotropy of the 2D SANS patterns under a magnetic field (oriented horizontally) of variable intensity, and its schematic representation.



**[C4. F. Cousin] Anisotropic reinforcement of latex films by magnetic nanoparticles**

The mechanical properties of polymeric films can be strongly enhanced by the addition of mineral charges within the polymeric matrix. Recent work from LLB made on films obtained by mixing aqueous solutions of nanoparticles have shown that the mechanical reinforcement is controlled by the size and morphology of aggregates of silica nanoparticles after drying. The morphology of aggregates can be precisely tuned by the pH as it controls the surface charge of nanoparticles and thus electrostatic interactions between nanoparticles during drying. In order to get an additional degree of control on the morphology of the aggregates, we have replaced here the silica nanoparticles by magnetic nanoparticles ( $\gamma\text{-Fe}_2\text{O}_3$ ) of the same diameter ( $\sim 10$  nm). The maghemite nanoparticles have firstly be coated by a thin silica layer to get exactly the same surface properties as the silica nanoparticles. We have then obtained homogeneous films latex reinforced by maghemite nanoparticles. When the film is dried without external magnetic field, dipolar magnetic interactions are negligible and the properties of the film are very similar to the one made with silica nanoparticles. When the films are dried under a magnetic field, nanoparticles form chainlike aggregates in the direction of the films. This has a dramatic effect on the mechanical properties of the film : the reinforcement is much higher in the direction parallel to the film than in the direction perpendicular to the film. The reinforcement anisotropy can reach a value of 2 at small deformation ! This is linked to the local structure of chainlike aggregates within the films determined by SANS. When the deformation is parallel to the applied field, aggregates organized themselves though they are broken when the deformation is perpendicular to the film.

[Collaboration : C. Ménager, V. Cabuil, LI2C, Université Paris VI, I. Dubois, J. Jestin, F. Boué, F. Cousin, LLB]



**Left:** reinforcement as a function of deformation (insert anisotropy of deformation)

**Right:** SANS experiments : (a) and (c) spectra before deformation, (b) deformation parallel to the field (d) deformation perpendicular to the field

**[C5. J. Vinas] Stimuli-sensitive hybrid nano-objects: polymerisation from silica nanoparticles synthesized in aqueous medium.**

We are developing new methods in the synthesis of hybrid nano-objects polymer/inorganic particles in aqueous media. We are synthesizing monodispersed nanometric silica particles which are then functionalized through reaction with alkoxy silanes containing an initiator moiety. This new method allowed us to gain in the control of the colloidal stability and to improve the polymerization conditions through a higher amount of initiating sites. Moreover, the polymerisation of thermo- or pH-sensitive monomers will give us an additional degree of liberty in the control of the shape of our objects. These model objects may lead to potential applications as bio-markers, drug delivery systems or diagnostic tools. We use SANS to characterise in details the synthesized particles and the evolution in size of the particles with the change of some reaction parameters and by checking the colloidal stability through the different reaction steps (fonctionnalization, polymerization). Also, by using contrast matching, we can follow the evolution of the polymer layer with polymerization time. The next experiences will also focus on the characterization of the solution properties of our objects by varying the pH or the temperature.

[Collaboration : J. Vinas, D. Gigmes, D. Bertin CROPS, Université de Marseille I, G. Carrot, F. Boué, LLB]

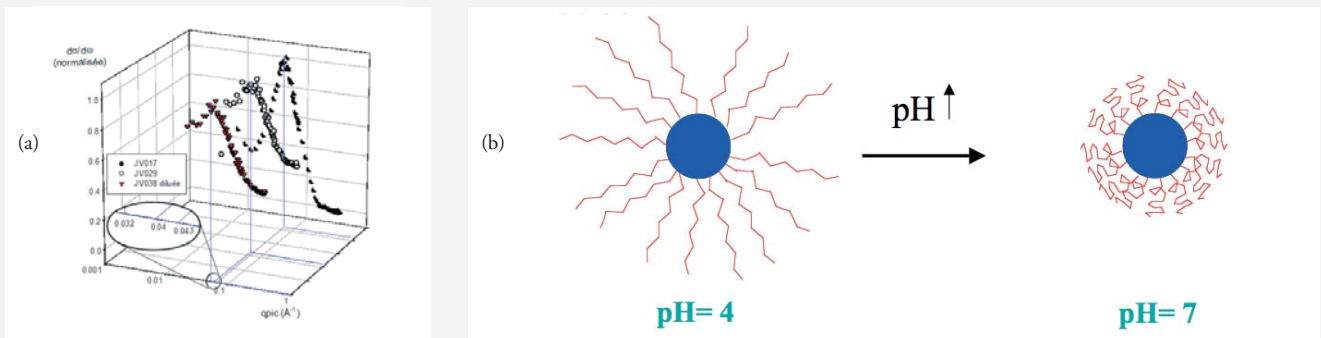
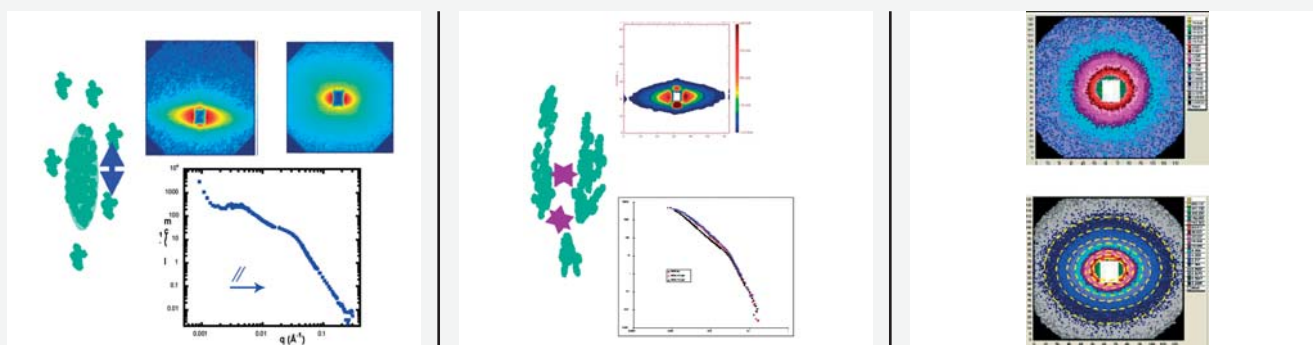


**Figure 1.** (a) SANS measurements of different particle sols. (b) Reversible changes in chains conformation depending on pH (stimuli-responsive polymers)

**[C6. J. Jestin] Dispersions of polymer grafted nanoparticles in a same polymer matrix : the effect of deformation**

Recently nanoparticles with grafted chains were synthesized owing to grafting from controlled radical polymerization in polar organic solvent. After purification, we obtain a stable sol, with silica cores of the same size as in the original sol, and characterize the polymer layer around the silica core using contrast matching [1]. We then disperse these particles in a polymer matrix of the same polymer as the grafted one. We observe that they **re-aggregate**, in different ways depending on the synthesis. Observation under deformation permits to refine the differences between two cases: left, coexistence of large deformable compact aggregates (responsible for a elongated scattering pattern) with small aggregates responsible for a correlation peak in  $I(q)$  along the parallel ( $//$ ) direction; middle: large deformable fractal-like aggregates (elongated scattering pattern,  $I(q)$  curves shifted along  $q$ ). We can also observe the polymer corona among matrix chains of different labelling. We conclude from the patterns anisotropy (silica core, right above, corona, below) that the corona is interpenetrated with the matrix chains, and deformed with a similar ratio.

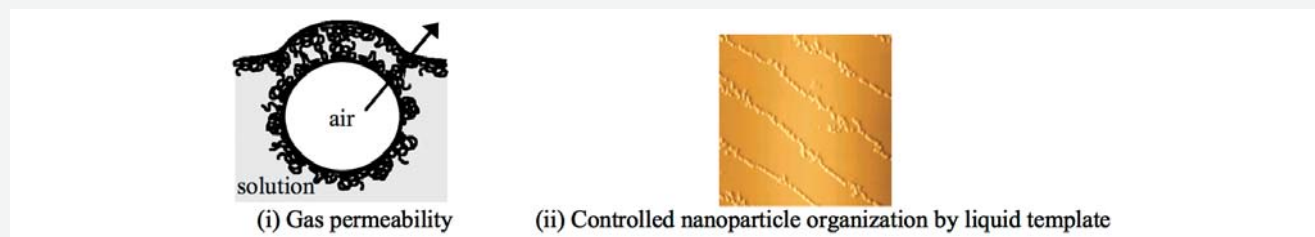
[Collaboration : A. El Harrak, S. Lorrain, G. Carrot, J. Oberdisse, J. Jestin, F. Boué, LLB]



[1] G. Carrot, A. El Harrak, J. Oberdisse, J. Jestin, F. Boué, *Soft Matter*, in press

**[C7 & C8 L.T. Lee] Interfacial and thin-film properties of complex systems**

This project aims to correlate interfacial structures of complex systems (polymer-surfactant-nanoparticle) with their thin film properties that are of relevance in potential applications. Neutron reflectivity used in conjunction with isotopic substitution provides a unique route to obtain structural and compositional information of surface layers in multicomponent systems. Here, we show two examples where structural and compositional information of adsorbed mixed layers are correlated with: (i) soap film stability and gas permeability, and (ii) thin-film dewetting as liquid template for nanoparticle organization on solid substrates.

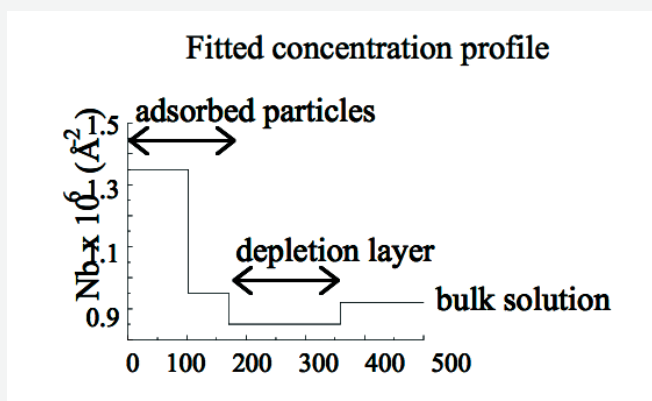
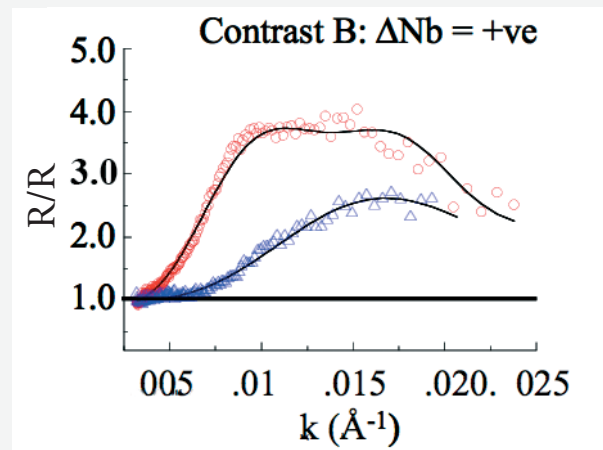
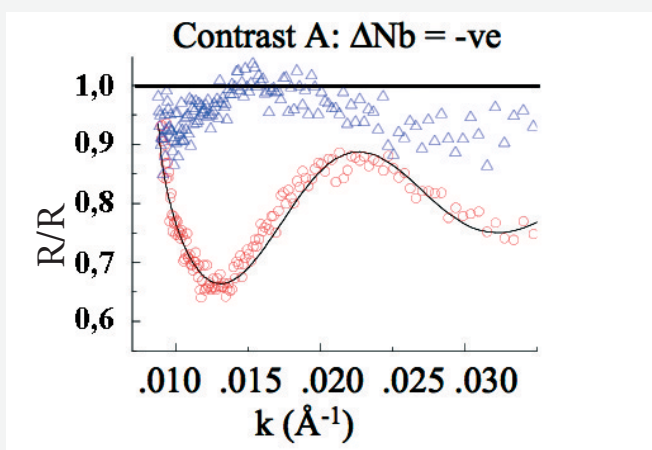


(i) Gas permeability of polymer-surfactant layers The structural properties of adsorbed poly(N-isopropylacrylamide) (PNIPAM) and mixed PNIPAM-SDS layers are correlated to gas permeation behavior of thin foam films. The gas permeability coefficient ( $K$ ) of the liquid film is evaluated from the rate of diminishing size of microbubbles ( $d \sim 250$  nm) formed on the surface of the solution. Irrespective of film thickness and physical appearance, the gas permeability of a film stabilized by PNIPAM alone is low ( $K \approx 0.045$  cm/s) compared to that stabilized by SDS alone ( $K \approx 0.10$  cm/s). This is explained by the characteristic concentration profile of the adsorbed polymer layer: a monomer-rich proximal zone ( $\phi_p \sim 1$ ) and a solvent-rich central zone. The closed-packed structure of monomers in the proximal zone thus acts as an efficient barrier to gas permeation - an explanation supported by the non-dependence of the proximal zone and of  $K$  on polymer chain length. For polymer-surfactant mixtures,  $K$  increases with surfactant/polymer ratio in the adsorbed layer up to  $K \approx 0.14$  cm/s. Mixed layers therefore show reduced efficiency as gas barrier, a result attributed to mutual decrease in the structural order of the adsorbed species.

[Collaboration: L.T. Lee, LLB; G. Andreatta, J.-J. Benattar, SPEC-CEA, Saclay]

(ii) Thin-film liquid template for controlled nanoparticle organization Thin films of charged polymer solutions dewet a solid substrate to form complex patterns that depend on solution and drying conditions. The dewet morphologies offer a potential method for templating nanoparticles into 2-dimensional complex patterns. Here, we focus on forming nanoparticle chains. The method involves dragging the nanoparticles by the dewetting liquid followed by capillary attractions between particles; minimal nanoparticle-substrate attraction is thus required. For aqueous dispersions of charged polymers and nanoparticles deposited on hydrophilic substrate, 2-dimensional arrays of nanoparticle chains extending over several hundred microns can be formed (image above – cyclodextrin-grafted Au on mica,  $d \sim 5$  nm). On hydrophobic substrate, this liquid-template system fails. Neutron reflectivity results show that while nanoparticle (silica and gold colloids) adsorption to hydrophilic substrate (water-silica) is undetectable, adsorption at a hydrophobic surface (water-air) is significant and is mediated by the adsorbed polymer (PNIPAM). Addition of SDS reduces adsorption of the nanoparticles; interestingly, the concentration profile shows a depletion layer, indicating a progressive transformation from a hydrophobic to hydrophilic surface. This effect should enhance dewetting and nanoparticle organization.

[Collaborations: L.T. Lee, LLB; C. Rezende, F. Galembeck, University of Campinas, Brazil; F. Cousin, LLB]



Normalized reflectivity for silica nanoparticle ( $d \sim 15$  nm) adsorption at water-air interface in two contrast schemes.

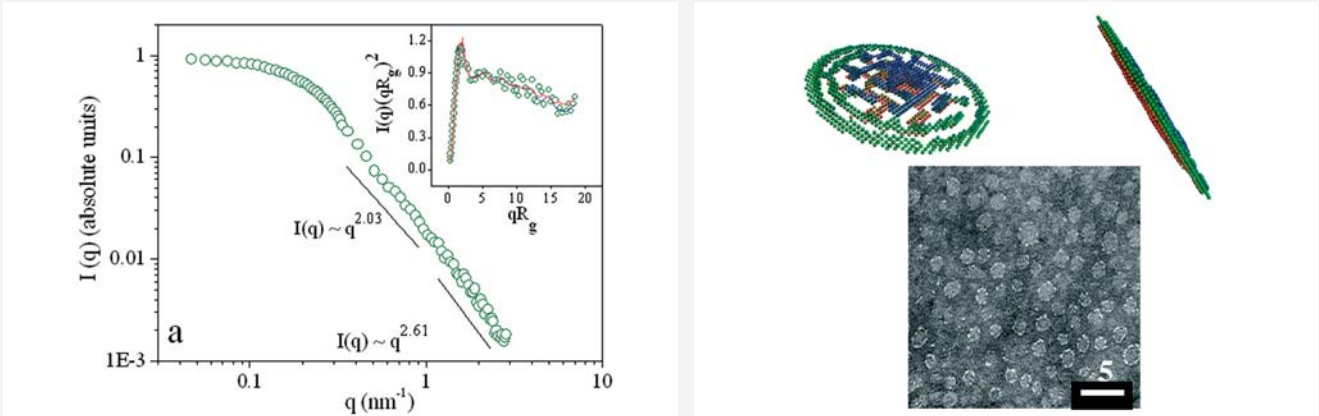
In this representation, all deviations from  $R/R_F = 1$  are due only to the adsorbed layer.  $\Delta N_b$  = difference in scattering length density between nanoparticle and solvent. Polymer solution (circle), polymer+surfactant solution (triangle).

Perspectives: Current studies concentrate on modulating the concentration profiles of nanoparticles at interfaces with special interests in stabilization of soft interfaces, and in optical properties. Emphasis is placed on the thermosensitive nature of PNIPAM-based polymers to produce reversible stimulus-responsive systems.

[C9. C. Sanchez] **Conformation of arabinogalactane-peptide from Acacia gum: a new model based on SANS and *ab initio* calculations.**

Biopolymers of the arabinogalactane-protein (AGP) type are everywhere in vegetal world, with many biological functions. Those extracted from Acacia gum are largely used in industry (stabilisation, emulsion, dispersion or adhesion). Conformation of the major molecular fraction, F1, an arabinogalactane-peptide ( $M_w : 2.86 \cdot 10^5$  g.mol<sup>-1</sup>), is highly hypothetical. SANS (Fig.1) is used here, together with *ab initio* calculations and microscopy (MET, cryo-MET, AFM), to propose a first model: a flat oblate ellipsoid of diameter  $\sim 20$  nm, thickness  $\sim 1.5$ - $1.9$  nm et and radius of gyration  $\sim 6.5$  nm. The central part resembles a fractal-like network of branches and aggregates,  $d_{\text{fractal}} = 2.6$ , a seen directly on the scattering.

[Collaboration : C. Sanchez ENSAIA-INPL, Nancy, A. Lapp, LLB, C. Schmitt & E. Kolodziejczyk, Nestlé, Lausanne, C Gaillard & D Renard, INRA-Nantes].



Form factor (SANS) of F1 at 25°C in D2O 50 mM NaCl, ab initio model and cryoTEM picture

[C10. C. Gerardin] Hybrid polyion complex micelles precursors for Highly stable metal [C. hydroxide colloids].

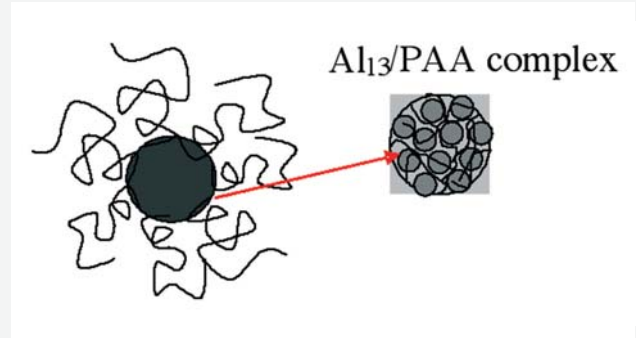
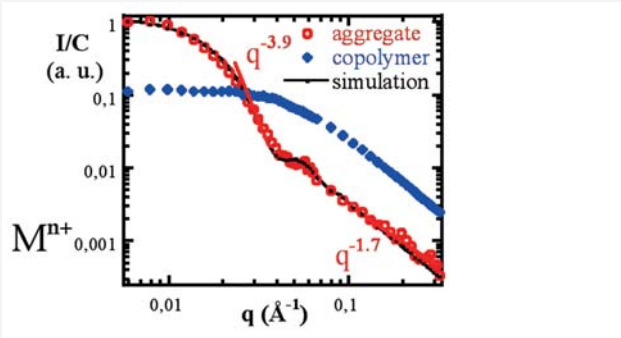
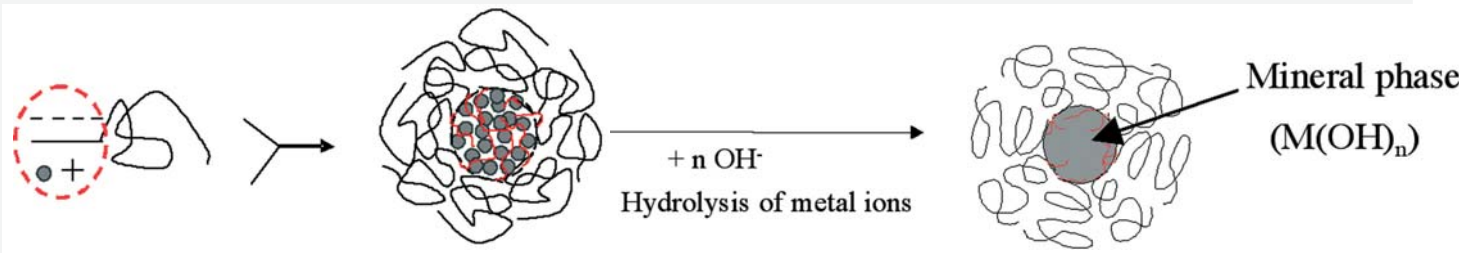
Anionic-neutral double hydrophilic block copolymers are used to control the growth and morphology of inorganic particles and directly prepare sterically stabilized suspensions of metal hydroxides. Metal hydroxides are obtained by hydrolysis of metal cations in the presence of the copolymers. The metal-complexing polyelectrolyte block ensures a *controlled growth of the inorganic phase* since the complexing functions act as poisons of the inorganic polycondensation reactions, whereas the neutral block ensures steric stabilization of the colloids.

The first synthesis step is the *induced assembly* of the copolymers in the presence of the oppositely charged multivalent inorganic species. The formation of the hybrid polymeric-inorganic nanoaggregates is induced by complexation of the inorganic ions. The micellar aggregates present a core-corona architecture characterized by scattering techniques (SANS and DLS).

The micelles are then used as *adjustable supramolecular precursors* for the formation of metal hydroxide particles. Hydrolysis of metal ions in the micellar core leads to *mineralization* of the colloids. The size of the stabilized particles can be tuned by adjusting the copolymer-to-metal ratio, the metal prehydrolysis ratio and the polymer block lengths. Finally, the morphologies of the hairy particles vary with the nature of the metal and with some synthesis parameters.

Gérardin et al *Angew. Chem. Int. Ed.*, **2003**, 42, 31, 3681. Sanson et al. *Phys. Chem. Chem. Phys.*, **2004**, 6, 1463.

[Collaboration : C. Gerardin, N. Sanson, M. In, L. Auwray, UMR5618 ENSCM UM1 CNRS Montpellier]



Comparison of SANS curves : Polymer alone (blue) and aggregate (red) of  $Al_{13}$  + PAA 1900 -b- PHEA 8200, at the same polymer concentration.



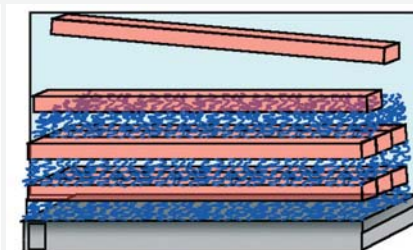
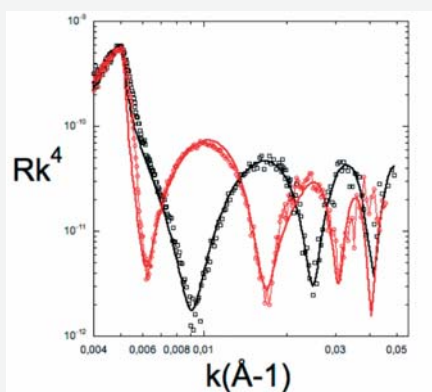
**[C11. B. Jean] Cellulose whiskers-based multilayers**

Layer-by-layer assembly is used here to prepare multilayer films composed of colloidal cellulose whiskers (negatively charged rod-like nanocrystals with cross dimensions between 2 and 25 nm, depending on the biological origin, and lengths between 0,3 and several mm) and a polycation, Poly-allylamine hydrochloride (PAH). They provide tools for understanding biopolymers interactions in primary cell walls and designing biocompatible materials.

Neutron Reflectivity experiments and AFM imaging allowed us to characterize the multilayers and results show that cellulose layers with a high packing density and low roughness can be obtained. A linear growth of the film with the number of layers was observed and oriented layers were prepared using ordered cellulose nanocrystals suspensions. Moreover, the possible replacement of PAH interlayers by positively charged nanoparticles such as chitin nanocrystals (rods) or mineral platelets (discs) was also evidenced.

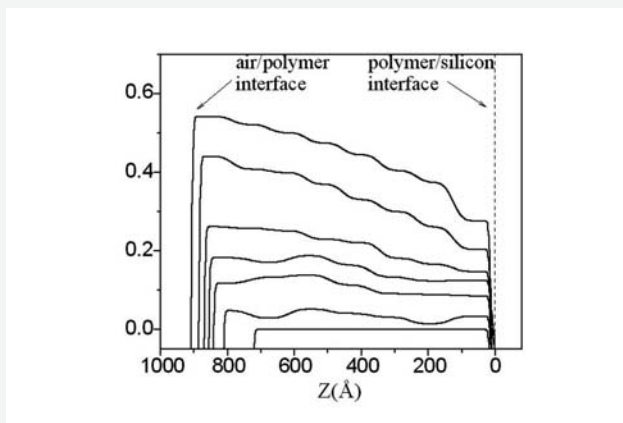
[Collaboration : B. Jean CERMAV-Grenoble and F. Cousin LLB]

**Figure 1.** Neutron reflectivity curves of a polyelectrolyte (blue in the drawing below) -cellulose whiskers (red) multi-layer *before* (black squares) and *after* (red circles) adsorption. Continuous lines are fits to a multilayer model.



**[C12. J. Daillant] Effect of solvent-polymer interaction in swelling dynamics of ultra-thin polyacrylamide films : A neutron and x-ray reflectivity study**

The swelling dynamics of the ultra-thin polyacrylamide (PAM) spin-coated films in saturated vapour of D<sub>2</sub>O and H<sub>2</sub>O were studied using neutron and x-ray reflectivity. A uniform scattering length density (SLD) profile represents the dry PAM films, whereas the SLD profiles corresponding to the swelled films were characterized with a decreasing solvent concentration along the film thickness from top surface to the film/substrate interface. The profile of D<sub>2</sub>O fraction in the film (725 Å) at different exposure times is shown in the figure below. The diffusion mechanism of D<sub>2</sub>O into the films was found to be a non-Fickian process, as the D<sub>2</sub>O diffusion coefficient was observed to be decreasing as a function of film thickness. The thickness dependent structural changes in the dry polymer films were suggested from the increased density of thinner films. The diffusion coefficient of polymer chains in the solvent on the contrary was independent of film thickness. A different nature of D<sub>2</sub>O-PAM interaction (stronger) as compared to H<sub>2</sub>O-PAM interaction was found to play a crucial role on the diffusion of polymer, where the diffusion coefficient of the chains was an order of magnitude higher in D<sub>2</sub>O as compared to that in the H<sub>2</sub>O. A lower value of the excluded-volume parameter in case of D<sub>2</sub>O also indicates stronger monomer-solvent interaction [1].



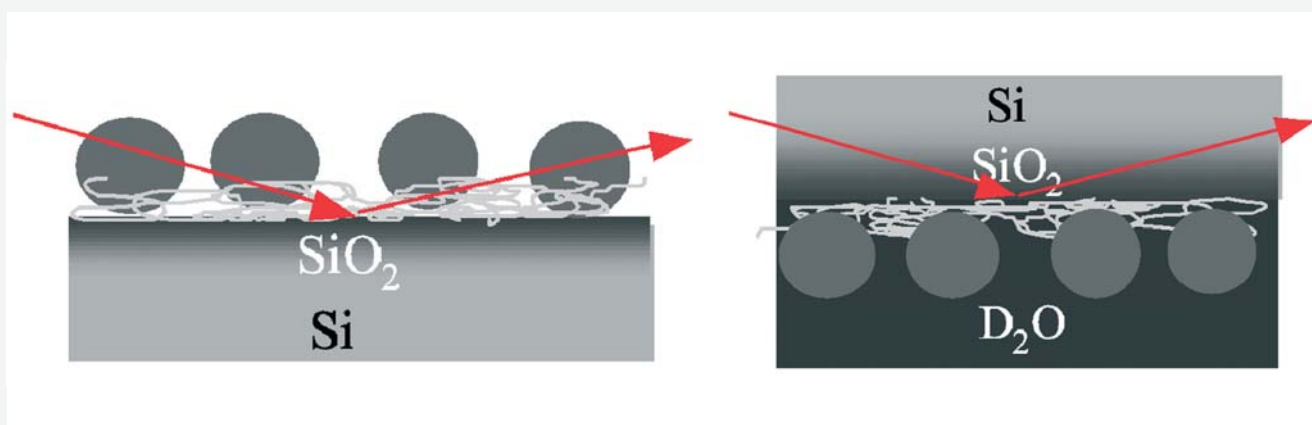
[1] submitted to Macromolecules (2006)

[Collaboration : M. Mukherjee, A. Singh, Saha Institute of Nuclear Physics, India, J. Daillant, LIONS, CEA-Saclay, A. Menelle, F. Cousin; LLB]

[C13. G. Chaboussant] **Study of adsorbed nanoparticles at a solid-liquid interface by neutron surface scattering.**

Using neutron surface scattering techniques like grazing incidence neutron small angle neutron scattering (GISANS) and Specular Neutron Reflectivity (SNR) we have characterised the adsorption process of  $\text{SiO}_2$  nanospheres (of radius 8-13 nm) at a silicon-water interface for different preparation process and chemical conditions. The silica nanospheres are dispersed in aqueous media and two different size of spheres have been tested. Prior to adsorption on the surface the spheres have been characterized in bulk solution by classical SANS and a classical extinctions of the form factor of spherical particles is observed. It reveals a very narrow size dispersion. In particular, it is possible to measure the lateral correlation length of a single layer of grafted beads and to derive information on the configuration of the grafted beads at the solid surface. GISANS measurements provide a clear cut answer through the measurement of the structure surface factor which is found to be reminiscent of a repulsive liquid, with correlation peaks coherent with the surface fraction obtain from SNR. The repulsion process between the spheres occurs during grafting. This is linked to the electrostatic process of adsorption on the negative spheres on the positively charged silicon wafer. Once a sphere has adsorbed on the surface, it locally inverses the charge surface and prevents adsorption of others spheres in its vicinity through electrostatic repulsions with a repulsion range dependent on the salinity but not on spheres radius. In effect, the surface electrical charges on the spheres prevent them from forming a dense adsorbed layer at the solid surface. The typical distance of the adsorbed beads is 50% larger than the diameter of the beads.

[Collaboration: F. Cousin, J. Jestin, G. Chaboussant, S. Gautrot, F. Ott (LLB)]



Left: Large spheres adsorbed at the surface (air-solid interface). Right: Small spheres adsorbed at the surface (solid-liquid interface). The greyscale corresponds to the scattering length density (SLD) of the species.



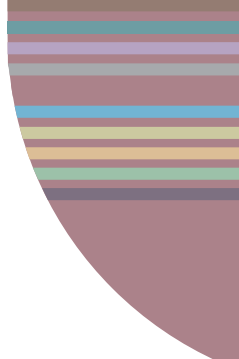






**LIFE SCIENCES**

**LABORATOIRE LÉON BRILLOUIN**



## A - Introduction

Neutron scattering in Life Sciences research emerged 15 years ago and is now playing an important role at the interface between biology, chemistry and physics. With a strong physical chemistry background obtained from studies on confined water, polymer solution and colloids, LLB was ready to tackle biological problems, especially the relationship between the structure and the dynamics of biological macromolecules in relation to the hydration water.

Protein is one of the basic components of food and makes all life possible. Amino acids are the building blocks of proteins. The structure and the specific behaviour of the thousands of proteins acting in living species is one of the major challenges of life science, and understanding of their role is of prime importance for medicine and pharmacology. All of the antibodies, enzymes and many of the hormones in the body are proteins. They are responsible for the transport of nutrients, oxygen and waste throughout the body. They also provide for the structure and contracting capability of muscles, and they provide collagen to connective tissues of the body and to skin, hair and nail tissues. Obviously, living species need proteins which are components of food and make all life possible.

Although X-ray with synchrotron radiation is a very powerful tool for structure determination of proteins, neutron scattering from crystallised proteins brings specific information mainly if a part of the protein is deuterated. A deuteration laboratory has been installed at ILL Grenoble and neutron protein crystallography measurements are mainly performed at ILL.

Research in Life Sciences at LLB focuses on two important aspects of the behaviour of proteins: their conformation in native and denatured states and their dynamics.

One of the challenges facing molecular biology is determining the rules that govern the acquisition by a nascent polypeptide chain of its three-dimensional and functional structure. Rapid progress in genome sequencing has made it all the more urgent to solve this problem. However, although protein folding is an extremely active field of research combining aspects of biology, chemistry, biochemistry, computer science, and physics, the detailed mechanisms of folding are not entirely clear.

All proteins fold in a defined and more or less compact conformation in times shorter than 100 seconds. If proteins randomly sought their lower energy conformation, the folding times would be larger than the universe lifetime. This is the Levinthal paradox. To solve this folding problem, various energy landscapes have been proposed. Studying protein unfolding and refolding is a good way to test all these hypotheses.

A complete understanding of protein folding requires the physical characterization of both native and denatured states and evaluation of the thermodynamic parameters of the system. This involves obtaining information concerning the structure and dynamics of proteins denatured under various conditions (temperature, pressure, chemical denaturant such as guanidinium chloride, pH).

Pressure has been used as a physicochemical perturbation to establish experimental conditions under which a different mechanism of aggregation might occur. The isolation of folding intermediates is crucial to understanding the protein misfolding and protein aggregation that are involved in many diseases (Alzheimer's and Parkinson's diseases, bovine spongiform encephalopathy). Moreover, transition between denatured states occurring under high pressure presents a great interest for the understanding of mechanisms involved into the amyloid diseases (due to beta-sheet formation).

Thus, characterisation of the denatured states of proteins is important for a complete understanding of the factors stabilising their folded conformation. Small-angle scattering, of either neutrons or X-rays, is a very powerful tool giving structural information at low and medium resolution. Incoherent Quasielastic Neutron Scattering (IQENS) directly probes the internal dynamics of biomolecules on the picosecond time scale, providing information on diffusive motions and the geometry of the motions observed. These two components change significantly during denaturation. IQENS is a dynamic technique complementary to NMR and molecular dynamics simulation.

Beyond the native proteins, we also study the role of hydration water on protein dynamics, the influence of temperature and the effect of different constraints such as the confinement or the pressure, or stimuli (light) or environment (crowding) on either conformations or dynamics of proteins.

Protein denaturation and dynamics are studied by the LLB team, at the Orph\_e reactor, by small angle and quasielastic neutron scattering, on the IN13 CRG instrument for which LLB contributes and also at ILL, Berlin, Julich and IPNS. The LLB is equipped with a confocal microscope and with the differential scanning calorimetry. Complementary information from UV visible absorbance spectroscopy, circular dichroism and fluorescence techniques is used.

## B- Some studies performed at LLB

### 1 - HYDRATION WATER AND BULK WATER

- *Liquid-liquid transition in interfacial water and role of water in protein dynamics*

Hydration water plays a major role in the stability, dynamics and function of biological macromolecules. Water confined in various systems from model systems (porous hydrophilic Vycor glass) to proteins (lysozyme, C-phycocyanin (CPC)) has been studied. Nanosecond-time-scale measurements of dynamics of interfacial, non-crystalline water from hydrated Vycor have been done from 77 to 280 K. The experimental dynamic results show that after exhibiting a glass transition at 165 K, interfacial water experiences a first order liquid-liquid transition at 240 K from a low density to a high density liquid. This is the first direct evidence of the existence of a liquid-liquid transition involving water. Moreover, we demonstrate that in hydrated lysozymes water dynamics is the driving force governing the slow, long range, protein internal motions that are relevant for protein-function. [C1, J.M. Zanotti].

- *Influence of solvent ( $H_2O$  and  $D_2O$ ) on dynamics of a hydrated C-phycocyanin protein*

The influence of the solvent ( $H_2O$  and  $D_2O$ ) on the dynamics of a hydrated C-phycocyanin protein has been investigated. The evolution of the mean-square displacements as a function of temperature is different in  $H_2O$  and  $D_2O$  which means that the protein dynamic behaviour is different in  $H_2O$  and  $D_2O$ . Different dynamic transition temperatures are obtained for  $H_2O$  and  $D_2O$  which was confirmed by results of differential scanning calorimetry [C2, S. Combet].

- *A direct determination of H-bond life time in bulk water*

Moreover, the high-Q performances of the spin-echo spectrometer MUSES, that measures the intermediate scattering function  $I(Q,t)$ , offered the opportunity to study hydrogen-bond dynamics in bulk water by following the dynamics at a Q value where deuterium-deuterium pairs (D-D pairs) contribute significantly. This original procedure allowed a direct determination of H-bond life-time, the temperature dependence of which follows a classical Arrhenius law, while all the transport properties of water exhibit a non-Arrhenius temperature dependence [H1, J. Teixeira].

### 2 - GLOBULAR PROTEINS IN NATIVE STATE

Several globular proteins have been studied so far by IQNS as  $D_2O$ -hydrated powders, including C-phycocyanin and parvalbumin. When describing protein dynamics, as biologists do, one has to consider a protein as a system designed for a specific biological function. The specificity of different parts of the protein has to be taken into account. This approach has been developed in the case of parvalbumin. Combined NMR and neutron scattering results suggested that peripheral water-protein interactions influence the protein dynamics in a global manner. We have determined that in the picosecond time range, the essential contribution comes from charged and polar side-chains residues at the protein surface. The formalism developed in the case of parvalbumin in hydrated powders, was subsequently extended to the case of small globular proteins (lysozyme, myoglobin, bovine pancreatic trypsin inhibitor (BPTI), calmodulin) in solution as well as to more complex systems as an enzyme, the aspartate transcarbamylase (ATCase) (J.-M. Zanotti et al, BBA, 2006).

- *Nanosecond dynamics of b-lactoglobulin (BLG) in a  $H_2O$ -protonated powder*

It must be noted that the neutron spin echo technique has been successfully used to probe the dynamics of protein. Our purpose was to learn about of the nanosecond dynamics of  $\beta$ -lactoglobulin (BLG) in a  $H_2O$ -protonated powder. The performances of the neutron spin-echo spectrometer MUSES allows one to get incoherent intermediate scattering functions (ISF) of hydrated BLG between 275 and 293 K for a Fourier time extending up to 1 nanosecond. From ISF, contributions from hydrogen atoms of surface water and of protein have been obtained. On one hand, the dynamics of the surface water follows a stretched expo-

ponential function (the exponent is  $\sim 0.5$ ), on the other hand, that of protein follows a single exponential function. This is in agreement with results from a photosynthetic C-phycocyanin (CPC) protein [C3, K. Yoshida] .

### 3 - UNFOLDED AND FOLDED STATES OF PROTEIN

---

#### 3A - THERMAL DENATURATION, PRESSURE DENATURATION

Several studies have been carried out on thermal (between 20° C and 95° C) and/or pressure (between 1 bar and 7000 bar) denaturation of protein. The thermal and pressure denaturated states have been characterized on the basis of polymer theory.

- *Effects of temperature and pressure on bovine pancreatic trypsin inhibitor (BPTI) protein*

The structural investigation by small angle neutron scattering allowed us to observe an increase of the radius of gyration of the protein in solution at 95° C and a reduction of this radius under 6000 bar. Quasielastic neutron scattering allowed us to observe an opposite effect of temperature and pressure on translational diffusion coefficient and internal relaxation time of BPTI in solution. Increasing temperature induces a faster dynamics of these global and internal motions whereas increasing pressure induces a slowing down of these motions [H2, M.-S. Appavou, PhD thesis, 2005].

- *Effect of temperature on apo-calmodulin protein*

The conformations of apo-calmodulin protein have been studied as a function of temperature by SANS experiments. It appears that apo-calmodulin loses progressively its structure between 40° C and 80° C. At high temperature, apo-calmodulin adopts a “polymer-like” conformation (SANS spectrum follows a Debye law for  $QRg < 3$ ), with a radius of gyration of 32 Å. However, the high-Q exponent of 2.3 suggests the existence of residual secondary structures, also seen by circular dichroism. Indeed the 2.3 value is between polymer chain values (1.7 or 2) and the compact chain value. The effect of temperature on protein dynamics is under investigation as well as the effect of pressure on both protein forms (apo- and holo-calmodulin) [C4, G. Gibrat, PhD thesis].

- *Milk  $\beta$ -lactoglobulin aggregation under high pressure*

The SANS measurements show that at a pressure value around 150 MPa  $\beta$ -lactoglobulin is characterized by a swollen state. At pressure around 300 MPa the protein begins to form irreversible aggregates. This aggregation occurs between swollen dimeric units of the protein, which is very different from heat-induced aggregation where the resulting gel is formed between unfolded monomeric units. [H3, C. Loupiac].

#### 3B - TRANSLOCATION

- *Protein refolding*

An original approach has been recently developed to studying protein refolding. It consists to performing *in vitro* translocation of an unfolded protein through nanochannel in lipid bilayer, synthetic nanoporous membranes, nanoporous track-etched PVDF membranes and aligned carbon nanotubes. Measurements of translocation events on single nanopore using fluorescence techniques usually associated with confocal microscopy (FRET or FCS) are now conceivable [H4, D. Lairez].

### 4 - CROWDED ENVIRONMENT

---

- *Influence of crowding on protein unfolding and stability*

The interior of cells is often filled with a very wide variety of “objects” with respect to the size and shape. Proteins are present *in vivo* in a very crowded environment. It is interesting to measure the influence of crowding on protein unfolding and stability. This study is related to recent theoretical predictions of measurable influence of macromolecular crowding on unfolded protein state, with a consequence of stabilization of the folded state. Model systems where the crowding is performed by Ficoll (F70) and the unfolded protein by PEG are under investigation. Contrary to what is generally assumed, chemical interactions between cosolutes (Ficoll) cannot be neglected [C5, S. Longeville].

- *Phase transition of metastatic extracellular matrix*

An important topic is the understanding of the processes of the tumour dissemination and cell invasion that liquefy the extracellular matrix gel and lead to its degradation. Experimental and theoretical developments have been made with a model system and lead to the conclusion that the gel degradation kinetics is diffusion-limited [C6, D. Lairez].

## 5 - PHOTO EXCITATION

- *Dynamics of a photoexcited C-phycoyanin*

In order to get a better understanding of the relationship between the dynamics and function of proteins, we have chosen to study the dynamics of a photoexcited C-phycoyanin, a light-harvesting protein, by synchronising a laser beam with a neutron beam. The aim of this study is to investigate whether dissipation of excitation energy in PC leads to modifications of the protein internal dynamics on longer timescales and larger amplitudes than that of localized vibrations of the protein pigments. The MIBEMOL data acquisition system has been successfully modified to synchronize the laser excitation flashes with the neutron pulses at the position of the sample and get “double beam” relative measurements (“light” and “dark”). This “double beam” procedure is extremely novel and eliminates spurious effects that could occur in the sample during the experiment [C7, S. Combet].

## 6 - FOOD INDUSTRY

- *Model systems of cryoconcentrated sucrose solutions*

Our collaboration with the food industry has been very productive (ENSBANA, Dijon and LLB). The objective of ENSBANA is to enhance the taste, texture or appearance of the food, to produce a product with a longer shelf-life or a healthier image, or to improve manufacturing. In the case of foods colloids, it is especially important to understand how the interfacial and aggregation behaviour of constituents (polysaccharides, proteins, pectins...) are affected by processing conditions or by molecular interactions with other constituents. The first results concern glass transitions of model systems of cryoconcentrated sucrose solutions and combine neutron scattering techniques and calorimetry measurements that are in full agreement: the first transition at  $-48^{\circ}\text{C}$  is to be correlated to a dynamic change of the sucrose molecule, whereas the other one seems to be linked to a change of water dynamic. The sharp evolution of  $\langle u_{\perp} \rangle$  seen at higher temperature (around  $-10^{\circ}\text{C}$ ) is due to ice melting, which acts like the dilution of the liquid phase [C8, D. Champion].

## C - Prospects

Our projects concern the continuation of activities about interfacial water, the extension of studies on thermal and pressure denaturation to other proteins, the continuation of studies of protein translocation through different nanoporous media, the continuation of studies on crowded environment (entire cells, extracellular metastatic matrix) and the influence of confinement on protein denatured states, the observation of photo-induced dynamics in protein. The conformation of membrane protein such as water channel in lipid bilayers is now ready to be investigated because of the significant progress in sample preparation. Other objectives deal, on one hand, with the conformation of big biological assemblies, and, on the other hand, with the crystallographic structure of protein using neutron crystallography, which in both cases needs some specific deuteration.

- *Interfacial water dynamics*

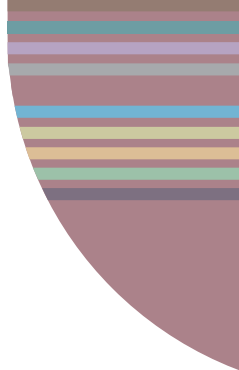
As far as interfacial water dynamics is concerned we now need to pursue the two following routes: observing the individual dynamics at times longer than few nanoseconds (low resolution solid NMR experiment, SCM) and accessing the collective dynamic behaviour. In this respect, inelastic X-ray scattering (ESRF) is a promising technique.

- *Photo-induced dynamics in protein*

The studies of the photo-induced dynamics in protein will be extended to other proteins (rhodopsin) as well as to photosynthetic proteins (allophycocyanin, phycoerythrin).

- *The study of conformation and dynamics of membrane proteins*

Membrane proteins are very difficult to purify in large amounts while it is necessary to get concentrated samples for neutron scattering. The AQP1 water channel (membrane protein) has already been purified from human red blood cells in the laboratory, and preliminary experiments are in progress to insert the protein in supported lipid bilayers for neutron reflectivity measurements. New perspectives have now been opened up by the possibility of obtaining recombinant water channels (AQPZ and GlpF) from bacteria *E. coli* in the laboratory, which has just been equipped for bacteria culture (S. Combet).



- *Focussing on conformations of big biological assemblies and accessing protein crystallographic structure by neutron crystallography*

In the post genomic area, one is aware that proteomics will be central to the functional genomics efforts. In the field of proteomics, neutrons can be decisive to solving conformations of big biological assemblies. For this purpose, efforts must be devoted to obtaining fully and specifically deuterated biological samples. We have already started activities in neutron protein crystallography. For this purpose, fully deuterated C-phycoyanin protein samples have been obtained in big amounts from cultures of cyanobacteria in D<sub>2</sub>O (Stage of DESS of A. Ould-Ouali, in collaboration with A. Boussac and D. Kourilovsky, SBE, DSV, Saclay). Location of protons and water molecules in a deuterated crystal of C-phycoyanin is now possible (collaboration with N. Adir, Israel; F. Meilleur, ILL) as well as studies of internal slow collective motions in big protein samples using spin-echo techniques.

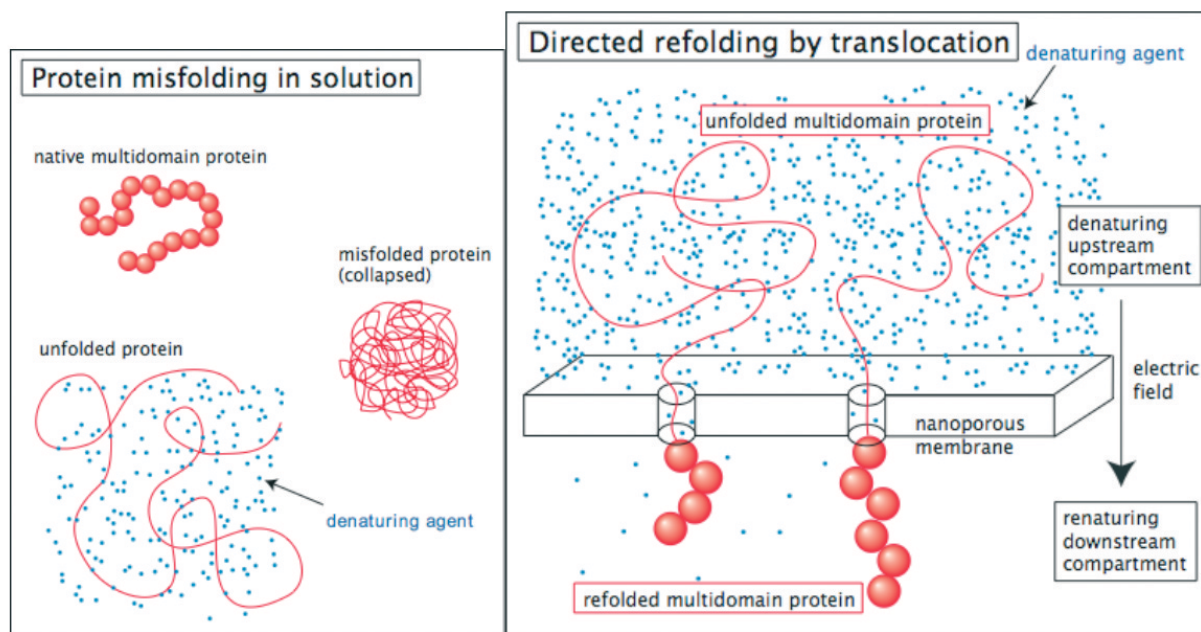
## D - Collaborations

A new contract for the CRG IN13 (collaboration LLB, IBS (Grenoble) and INFM (Italy)) has been signed. The CRG IN13 resumed on January 2005.

On January 2003, the Department of Life Sciences of CNRS has been renewed (for four years) the GDR-1862 entitled "Fonction et Dynamique des Macromolécules Biologiques" (Director: M.-C. Bellissent-Funel, Co-Director: J. Parello). In the frame of the GDR successful research activities have been undertaken. The most recent one concerns a School devoted to water in biological media (" l'Eau dans les milieux biologiques ", Roscoff, 25-29 October 2006).

One has to note the fruitful collaborations in Life Sciences, at the French and European level, with the following organisms: SBE (Service de Bio-Energétique), SPEC, CEA, Saclay, IBS and ILL, Grenoble; INRA, Nantes; University of Cergy-Pontoise; University of Porto, Portugal; Technical University of Munich; HMI at Berlin; Institut Curie (Orsay); Inserm, (Kremlin-Bicêtre hospital). At the level of CEA, a new group at the interface between chemistry, physics and biology has just been created. Collaborations involve also SPEC, LSI, University of Evry. A new collaboration in the field of food industry has become operative during the last two years with ENSBANA, Dijon. The long-time collaboration M. Desmadril (IBBMC, Orsay) is still active.

# LIFE SCIENCES



- H1.** Hydrogen-bond dynamics in bulk water  
S. Longeville, J. Teixeira
- H2.** Influence of temperature and pressure on structure and dynamics of a model protein belonging to the regulation of the enzymatic catalysis : the bovine pancreatic trypsin inhibitor : a neutron scattering study  
M.-S. Appavou
- H3.** Milk proteins aggregation under high pressure studied by small angle neutron scattering  
C. Loupiac, M. Bonetti, S. Pin, P. Calmettes
- H4** Protein refolding and translocation: biology meets nanoscience  
D. Lairez, J. Pelta, L. Auvray, O. Cuscito, M.-C. Clochard, M. Mayne-L'Hermite, G. Zalczer

[C1. J.M. Zanotti] Evidence that interfacial water is the driving force behind protein dynamics

[C2. S. Combet] Influence of hydration solvent on the dynamic transition of phycocyanin

[C3. K. Yoshida] Hydration water in dynamics of a hydrated beta-lactoglobulin

[C4. G. Gibrat] Thermal denaturation of apo-calmodulin.

[C5. S. Longeville] Influence of macromolecular crowding on protein folding and stability: a model for unfolded chain

[C6. D. Lairez] Phase transition of metastatic extracellular matrix: theory and experiment.

[C7. S. Combet] Dynamics of a photo-excited antenna protein

[C8. D. Champion] Glass transitions in cryoconcentrated sucrose solutions.

# H1. HYDROGEN-BOND DYNAMICS IN BULK WATER

STÉPHANE LONGEVILLE, JOSÉ TEIXEIRA

Laboratoire Léon Brillouin, CEA-Saclay, 91191 Gif-sur-Yvette, France

Water is a simple molecule made up of three atoms in a V configuration displaying an electronic distribution almost perfectly spherical. However, the properties of the liquid are very complex and not totally understood despite a huge number of experimental and simulation studies. In a very general way, one may say that the so-called "anomalous" behaviour of water derives from hydrogen bonds (HB) which generate an anisotropic potential and strong although fragile inter-molecular forces.

Historically, many experiments tried to catch and understand the topological and dynamic properties of HB and the way they may be related to the thermodynamic and transport properties of the liquid. Alternatively, the remarkable development of simulations of molecular dynamics made very popular "efficient potentials" to describing complex liquids such as water. For most of such potentials, the anisotropy of the potential is indirectly taken into account by the assumption of a molecular anisotropy fixed ad hoc in order to reconstitute, at the best and within classical concepts, the room temperature properties of liquid water. As a consequence, HB are poorly described because they are nothing more than a consequence of Coulombic forces between point charge molecules.

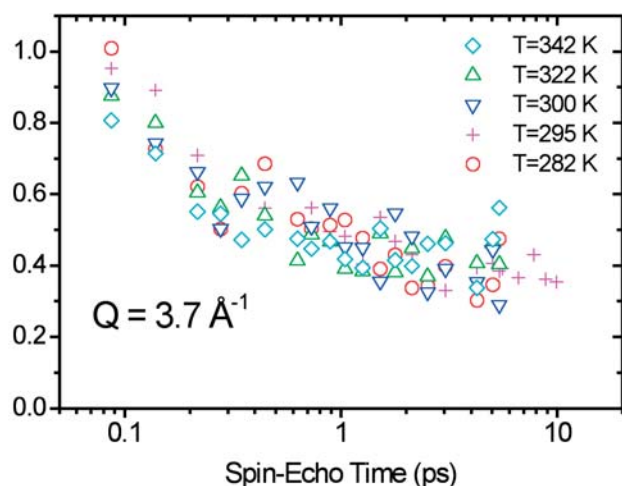
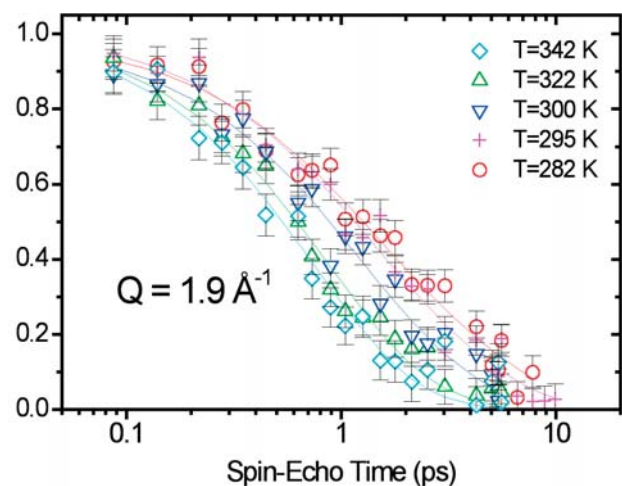
We have been among the experimentalists who, in the past, tried to identify the important role of hydrogen bonds, particularly studying the dynamics of supercooled water, i.e. at temperatures where they represent the determining factor. It is relatively difficult to isolate the dynamics of HB in a way that is, as much as possible, model independent. The performances of the spin-echo spectrometer MUSES, that measures the intermediate function  $I(Q,t)$ , gave us the opportunity of using an original way to studying HB dynamics in a way that is almost independent of other contributions to the scattered intensity.

We took profit of the good knowledge of the partial structure factors of heavy water ( $D_2O$ ). Looking into detail to the  $Q$  dependence of the three factors, one realizes that, by accident, at  $Q = 3.7 \text{ \AA}^{-1}$ ,  $S_{DD}(Q)$  is the only partial that contributes significantly to the scattered intensity. Consequently, the measurement of  $I(Q,t)$  at this value of the momentum transfer, yields a specific information about the dynamics of deuterium atoms directly implied in HB, and without any important contribution of the diffusion movements of the molecular centres of mass. In order to establish a convincing comparison, we measured as well  $I(Q,t)$  at  $Q = 1.9 \text{ \AA}^{-1}$ , i.e. at the vicinity of the structural peak in  $S(Q)$ , where the scattered intensity is maximum and all the motions contribute to the signal.

The two main results are depicted on the figure. The two time dependences take place in very different time domains. As expected, the dynamics of the DD pairs is naturally faster than the molecular motions. But, the more

important evidence concerns the temperature dependences, which are dramatically different. While at  $Q = 1.9 \text{ \AA}^{-1}$  we retrieve the well known non-Arrhenius temperature dependence of all the transport properties of water, at  $Q = 3.7 \text{ \AA}^{-1}$  the temperature dependence is much weaker and follows a classical Arrhenius law, demonstrating that, at the level of HB, there is no anomalous temperature dependence. This rather direct experimental determination of HB dynamics in liquid water reminds how important are all studies of bonds in water that can relate the two observed dynamics without calling for analytical, sometimes exotic models.

At this point, one may admit that the glass transition temperature of water (130 K) corresponds to the "freezing" of the motion of hydrogen atoms which remain extremely mobile even under 228 K, a virtual temperature that corresponds to numerical extrapolations of transport properties and that, actually, can be associated to the temperature of homogeneous nucleation of ice. In our view, this experimental result is a strong argument to say that temperatures obtained by extrapolations or from simulations reflect simply the increase of the number of HB with decreasing temperature and the formation of embryos



## H2. INFLUENCE OF TEMPERATURE AND PRESSURE ON STRUCTURE AND DYNAMICS OF A MODEL PROTEIN BELONGING TO THE REGULATION OF THE ENZYMATIC CATALYSIS : THE BOVINE PANCREATIC TRYPSIN INHIBITOR : A NEUTRON SCATTERING STUDY

M.-S. APPAVOU

Laboratoire Léon Brillouin, UMR 12 CEA-CNRS, CEA Saclay, 91191 Gif-sur-Yvette. France.

Motions in proteins occur at different time scale from millisecond for enzymatic reaction to femtosecond for electronic transitions. Quasielastic Neutron scattering allows to probe picosecond to nanosecond time scale internal motions [1]. Bovine Pancreatic Trypsin Inhibitor is a small protein belonging to the enzymatic catalysis. This protein is a model system because of its small amount of residues (58 amino acid residues) and low molecular weight value (6500 Da), these characteristics allowed molecular dynamic simulation studies [2]. It was also studied by several other techniques : BPTI has a very high stability since it cannot be denatured at temperature below 95°C as it have been shown by Raman spectroscopy [3] or at pressure below 14 kbar as shown by Fourier Transform Infrared spectroscopy [4,5]. This stability is due to the presence of three disulphide bridges and three salt bridges. We have studied the structure and the dynamics of native state and thermal [6] and pressure [7] denatured states of BPTI by neutron scattering technique. For our high pressure study, we used a hydrostatic pressure cell developed at the Laboratoire Léon Brillouin [8].

The structural investigation by small angle neutron scattering allowed us to observe an increase of the radius of gyration of the protein in solution at 95°C and a reduction of this radius under 6000 bar. (Figure 1)

The ellipsoidal shape of the molecule in the native state do not change between 22°C et 95°C but we have observed an increase of the volume of BPTI. Indeed, the shape of BPTI is modified from an ellipsoidal one to a spherical one at 3000 bar, while it is well represented by a micelle when applied pressure values reach 5000 and 6000 bar. (Figure 2)

Further experiments by infrared spectroscopy and by UV-visible spectroscopy as a function of temperature and pressure allowed us to confirm our results [6].

Quasielastic neutron scattering allowed us to observe an opposite effect of temperature and pressure on translational diffusion coefficient and internal relaxation time of BPTI in solution (Figure 3). Increasing temperature induces a faster dynamics of these global and internal motions whereas increasing pressure induces a slowing down of these motions.

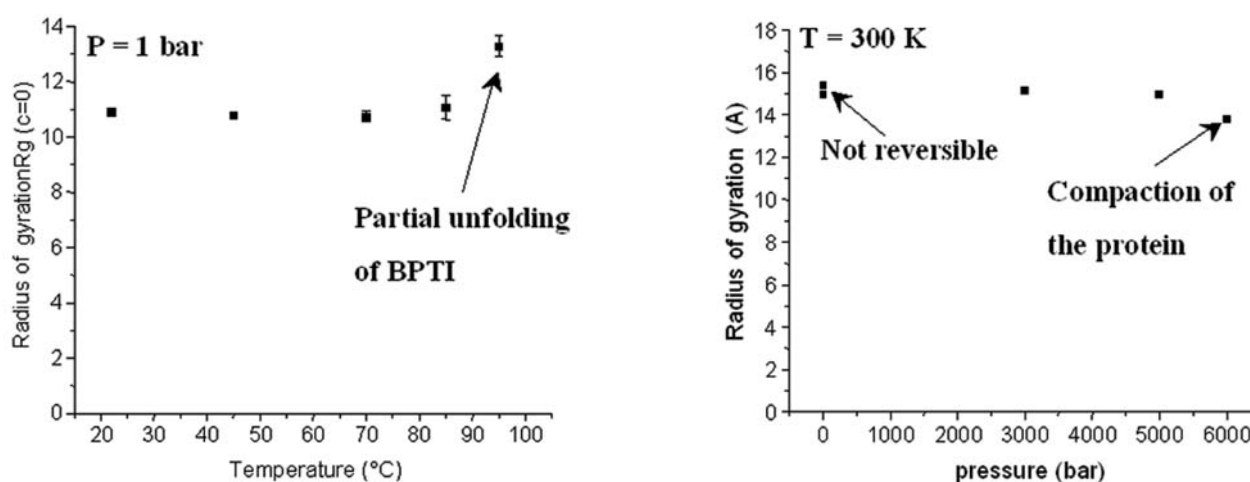


Figure 1 : Evolution of the radius of gyration of BPTI as a function of pressure (left) and as a function of temperature (right).

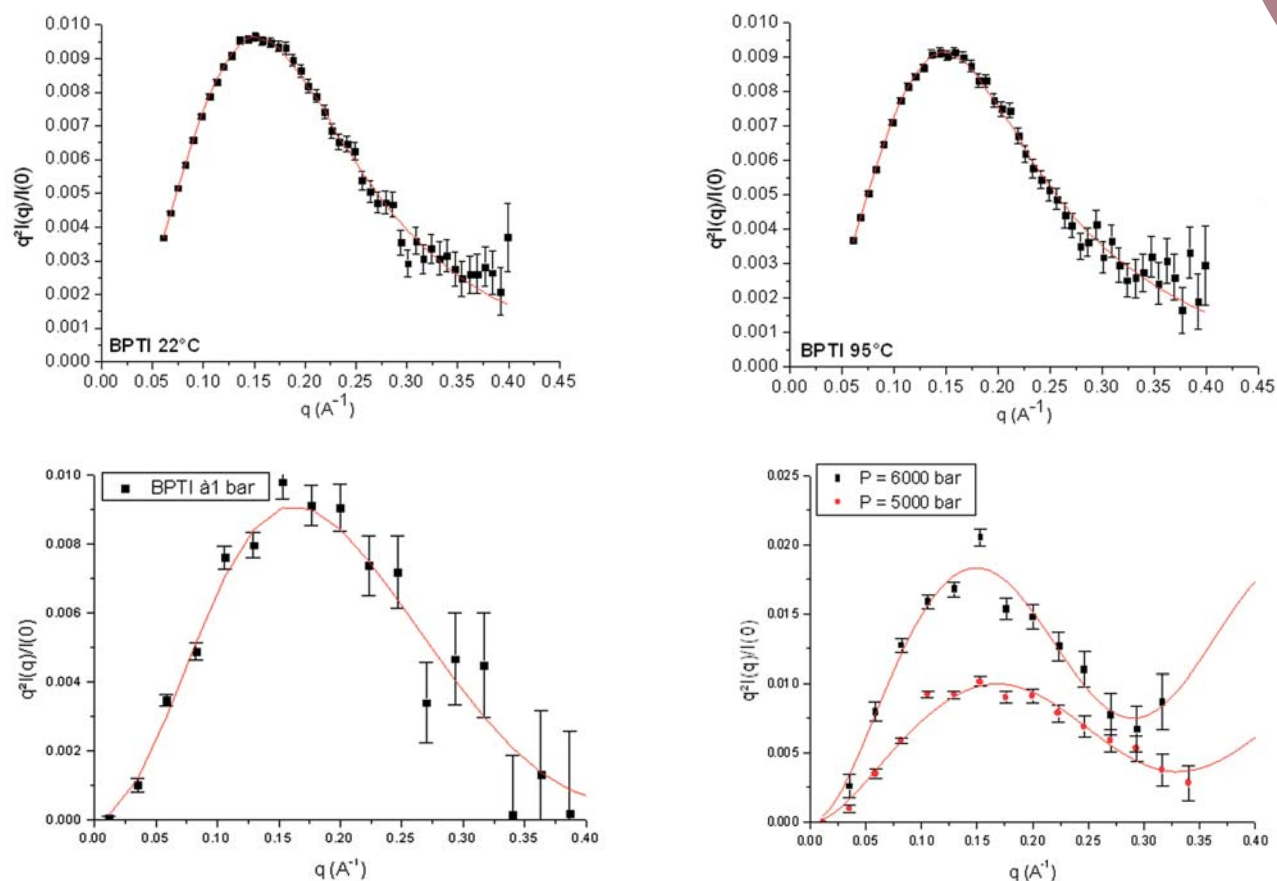


Figure 2 : Kratky plot of SANS spectrum for BPTI at ambient and high temperature (top) and at atmospheric pressure and high pressure (bottom).

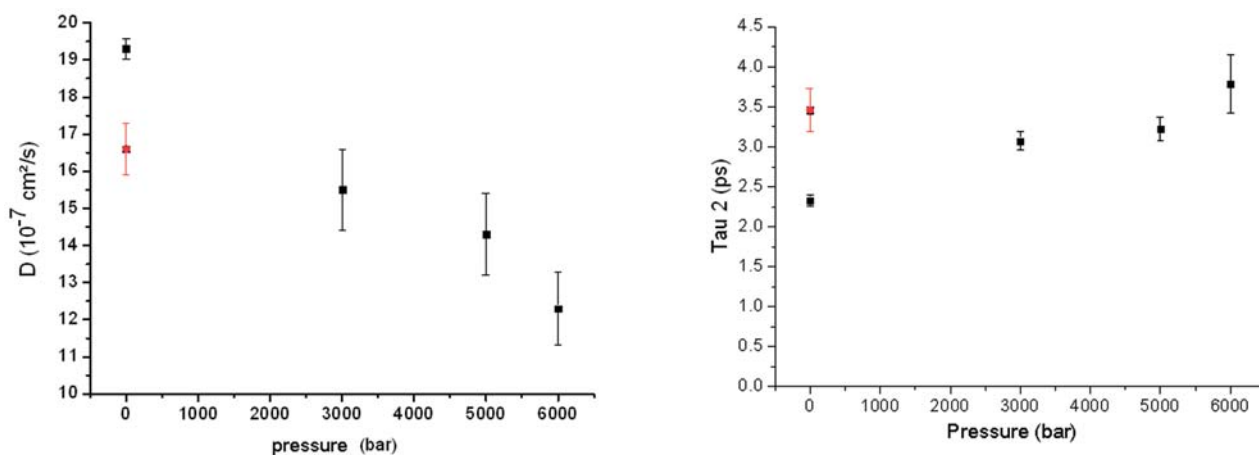


Figure 3 : Effect of pressure on global (left) and internal motions (right)

- [1] McCammon J. A. & Harvey S. C., *Dynamics of proteins and nucleic acids*, Cambridge, University Press, 1987.
- [2] Hayward JA., Finney JL., Daniel R.M., et Smith JC., *Biophys. J.*, **85**, 2003, pp 679-685.
- [3] Carmona P, Molina M, Rodriguez-Casado A, *Eur Biophys J*, **32**, 2003, pp137 –143
- [4] Goosens K, Smeller L, Frank J, Heremans K, *Eur. J. Biochem.*, **236**, 1996 , pp 254-262,
- [5] Takeda N, Nakano K, Kato M, Taniguchi Y, *Biospectroscopy*, **4**, 1998, pp 209-216
- [6] Appavou M.-S., Gibrat G., Bellissent-Funel M.-C., *BBA*, in preparation
- [7] Appavou M.-S., Gibrat G., Bellissent-Funel M.-C., *BBA*, **1764**(3), 2006, pp 414-423
- [8] Appavou M.-S., Gibrat G., Bellissent-Funel M.-C., Plazanet M, Pieper J, Buchsteiner A, and Annighöfer B, *J. Phys.: Condens. Matter* **17**, 2005, S3093-S3099.

### H3. MILK PROTEINS AGGREGATION UNDER HIGH PRESSURE STUDIED BY SMALL ANGLE NEUTRON SCATTERING

C. LOUPIAC<sup>1</sup>, M. BONETTI<sup>2</sup>, S. PIN<sup>3</sup>, P. CALMETTES<sup>4</sup>

<sup>1</sup>-Equipe d'Ingénierie Moléculaire et Sensorielle des Aliments et des Produits de Santé, ENSBANA, Dijon

<sup>2</sup>- Service de Physique de l'Etat Condensé, CEA, Saclay

<sup>3</sup>- Service de Chimie Moléculaire, URA 331 CNRS, CEA, Saclay

<sup>4</sup>- Laboratoire Léon Brillouin, UMR 12 CNRS, CEA, Saclay

The food scientist is commonly confronted with the challenge of modifying the formulation of a food product. The objective may be to enhance the taste, texture or appearance of the food, to obtain a product with longer shelf-life or healthier image, or to improve manufacturing efficiency by incorporating cheaper ingredient or adopting a new processing technology. The speed with which these objectives can be accomplished depends on the level of fundamental understanding that exists on the key physico-chemical factors affecting products properties. In the case of foods colloids, it is especially important to understand how the interfacial and aggregation behaviour of polymer constituents (polysaccharides, proteins, pectins...) are affected by processing conditions (heat, drying, freezing, shear forces), or by molecular interactions with other constituents (fat, hydrocolloids, aroma, water...). One of our goal is to improve insights into such factors by taking advantage of polymer science concepts and neutron scattering technique applications to such systems, to the systematic study of model food systems [1].

In foodstuffs, proteins are very often used for their functional properties. Most of the time their abilities to act as emulsifiant, gelation or foaming agents, are related to their structure. Processing foods under high pressure often results at the molecular level in structural changes of the protein [2]. Experimental and theoretical approaches indicate that one of the underlying mechanism of pressure unfolding is the penetration of water into the protein, several intermediate states of the protein have been shown to exist, with their properties depending on the experimental conditions [3]. The isolation of folding intermediates is crucial to understand protein misfolding and protein aggregation.  $\beta$ -lactoglobulin (BLG) is the main protein constituent of the milk whey from ruminant. This protein is an important functional protein in foods, as it is the major component of many dairy gel and emulsions. A basic challenge of this study was to better understand the mechanism of pressure unfolding, dissociation and aggregation of BLG. We used

pressure as a physicochemical perturbation to establish experimental conditions under which a different mechanism of aggregation might occur. From the small-angle neutron scattering (SANS) measurements the overall conformation of the  $\beta$ -lactoglobulin was studied at pH 7 on the dimeric form of the protein in a pressure range going from 50 to 300 MPa. These measurements were done "on-line" by gradually increasing the pressure. We can determine whether the dissociation of the dimeric units occurs and if the aggregation mechanism involves the monomeric form of the protein. To determine the pressure effects on the protein interactions and the variation of the value of the actual radius of gyration, the SANS measurements were performed at different protein concentrations.

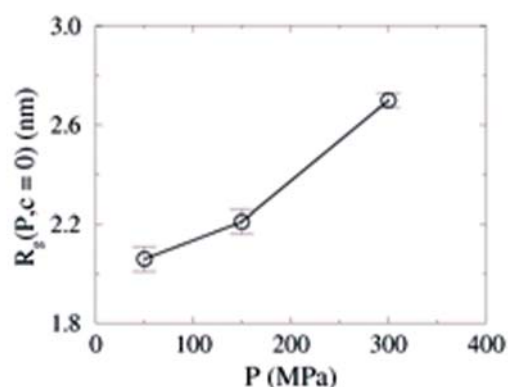


**Figure 1.** Value of the actual radius of gyration,  $R_g(c = 0)$  as function of pressure,  $P$ . Measurements as been made on PACE spectrometer. The range of the wave-number was between 0.07 and 0.74  $\text{nm}^{-1}$ . A sapphire-anvil cell specially designed to perform SANS measurements has been used (M. Bonetti, SPEC, CEA, Saclay)

One of the questions addressed in this work was to know whether or not the aggregation process induced by applying pressure involves the dimeric unit or monomeric unit of the protein. This has been answered by the analysis of the evolution of the radius of gyration as a function of applied pressure (Figure 1). Our analysis shows that no dissociation of the dimer occurs in the 50-150 MPa pressure range as our measured radius of gyration ( $R_g = 2.20$  nm) is far away from the monomeric form ( $R_g = 2.06$  nm). Increasing pressure up to 150 MPa leads to a swollen state of the protein that gives rise to an increase of the radius of gyration by about 7 %.

The measurements show an aggregation process occurring above 150 MPa, irreversible aggregates are formed at pressure around 300 MPa. This aggregation occurs between swollen dimeric units of the protein, which is very different that for heat-induced gel that occurs between unfolded monomeric units. Different parameters could lead to this swollen state of the protein after applying pressure: hindrance of water inside the protein matrix and/or change

in the hydrogen bonds network and/or breaking down the electrostatic bonds and some of the protein hydrophobic interactions. Within this pressure range, the observation of the second virial coefficient ( $A_2$ ) indicates that the interaction between macromolecules weakens although it remains repulsive (Figure 2).

It can be stated that a pressure value around 150 MPa leads to a swollen state of  $\beta$ -lactoglobulin and that at pressure around 300 MPa the protein begins to form irreversible aggregates. In the future it will be interesting to see the repercussion of this aggregation between dimeric units on the gels properties (rheological and neutron scattering studies).

*Biochimica and Biophysica Acta, 1764, 2006, p211-216*

- [1] Gimel J.-C., Durand D., Nicolai T., *Macromolecules*, 1994, **27**, 583-589.
- [2] Silva J.L., Foguel D., Royer C.A., *Trends Biochem. Sci.*, 2001, **26** (10), 612-618
- [3] Loupiac C., Bonetti M., Pin S., Calmettes P., *Eur. J. Biochem.*, 2002, **269**, 4731-4737

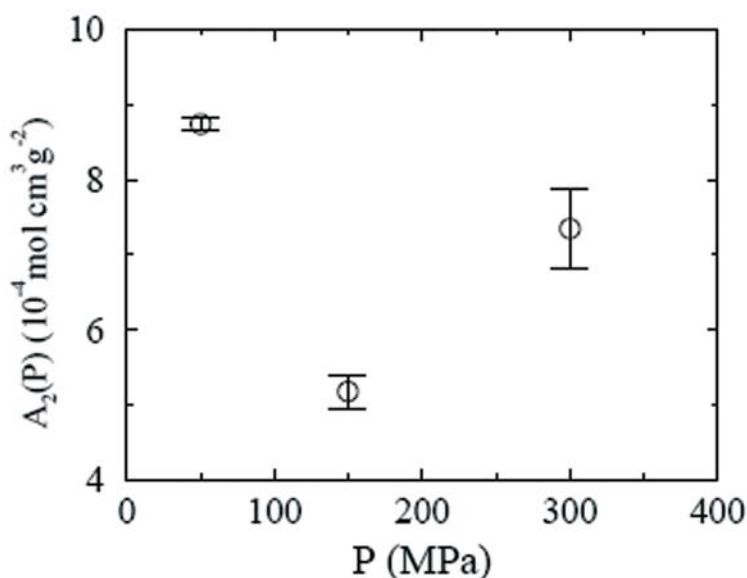


**Figure 2.** Second virial coefficient as function of pressure

## H4. PROTEIN REFOLDING AND TRANSLOCATION: BIOLOGY MEETS NANOSCIENCE

D. LAIREZ<sup>1</sup>, J. PELTA<sup>2</sup>, L. AUVRAY<sup>3</sup>, O. CUSCITO<sup>4</sup>, M.-C. CLOCHARD<sup>4</sup>, M. MAYNE-L'HERMITE<sup>5</sup>, G. ZALCZER<sup>6</sup>

<sup>1</sup> Laboratoire Léon Brillouin, CEA-CNRS UMR-12, CEA-Saclay, 91191 Gif-sur-Yvette cedex

<sup>2</sup> Groupe microenvironnements et comportements cellulaires, Université de Cergy-Pontoise, 95302 Cergy-Pontoise

<sup>3</sup> Laboratoire Matériaux Polymères aux Interfaces, CNRS-UMR 7581, Université d'Evry, 91025 Evry

<sup>4</sup> LSI, Ecole Polytechnique, CEA-DSM, CNRS, 91128 Palaiseau cedex

<sup>5</sup> Laboratoire Francis Perrin, URA-2453, DSM/DRECAM/SPAM, CEA-Saclay, 91191 Gif-sur-Yvette cedex

<sup>6</sup> Service de Physique de l'Etat Condensé, CEA-Saclay, 91191 Gif-sur-Yvette cedex

The understanding of protein folding is a central problem in present post-genomic biology. On one hand, protein misfolding is involved in many diseases: Alzheimer's and Parkinson's diseases, bovine spongiform encephalopathy... On the other hand, in many cases recombinant protein synthesis comes up against the formation of inclusion bodies. These inclusion bodies are solubilized using a denaturing agent such as urea or guanidinium chloride. Then *in vitro* refolding difficulties are often encountered, more particularly for high molecular weight and multidomain proteins. Current view of protein folding involves a minimum of free energy pathway through the conformational energy landscape. To progress in the understanding of protein folding, this paradigm needs to be overcome. Actually *in vivo*, the nascent protein folding mechanism, as well as unfolding-translocation-refolding cycles observed in many cases, suggests that sequential refolding is a key feature. Sequential refolding means that one extremity of the peptide chain begins to refold without the knowledge of the remaining peptide chain sequence. This is the key point we try to mimic *in vitro*.

Our approach consists in studying protein refolding by performing *in vitro* translocation (see Fig. 1), developing techniques to measure and control translocation time and developing nanoporous media adapted to this application. To this end, different strategies are investigated.

Protein translocation through single protein nanochannel in lipid bilayer is studied. Here, nanochannel is  $\alpha$ -Hemolysin from *Staphylococcus Aureus* that has been already used for DNA translocation. This single molecule experiment allows patch-clamp technique to be used for measurement of translocation events (frequency of events, duration of a single event, see Fig. 1).

Ref. 1 reports the first experiment concerned with *in vitro* translocation of an unfolded protein, Maltose Binding Protein, that has the ability to be unfolded at low concentration of denaturing agent ( $[Gdm-HCl] \sim 1 M$ ) leaving intact the proteic nanochannel. This result demonstrates translocation feasibility in the case of unfolded protein and opens up to new means of investigation for unfolding-refolding mechanism.

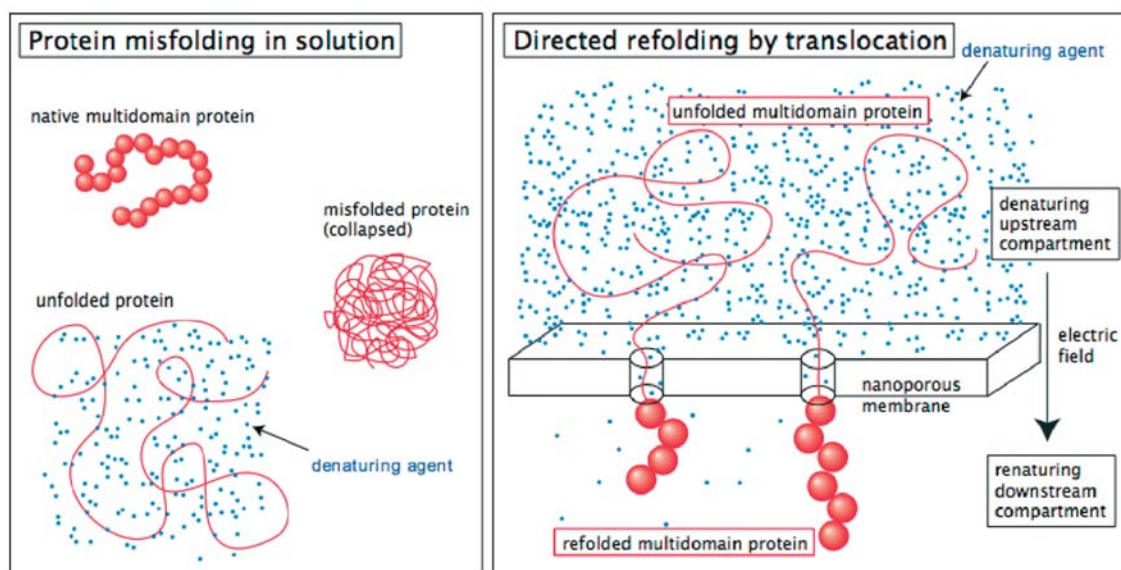


**Figure 1.** Protein refolding directed by *in vitro* translocation. An adequate translocation velocity should favour a correct refolding of multidomain proteins.

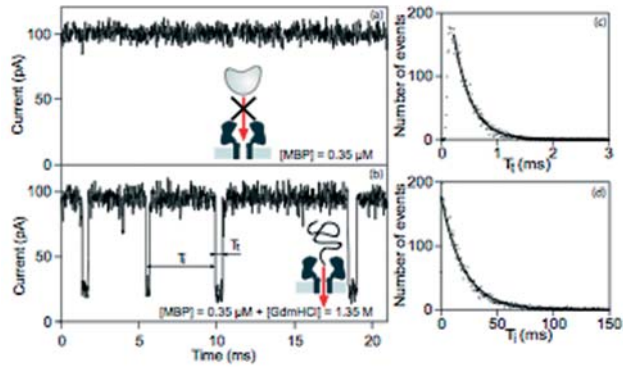


**Figure 2** (from Ref.1). Current traces through a-Hemolysin (at 100mV) in presence of Maltose Binding Protein (MBP) at  $0.35\mu\text{M}$ . Left: a) with denaturing agent, native protein cannot pass through the nanochannel. Measured current is constant (100 pA). b) with denaturing agent ([Gdm-HCl]=1.35M), MBP is unfolded the current trace decreases down to 20 pA when a molecule is in the pore. Right: c) Distribution of translocation times. d) Distribution of time intervals between two events.

Protein nanochannels technique knows limitations: fragility to osmotic gradient that should be necessary to direct the refolding of translocated proteins; low frequency of translocation events (single pore) leading to production of small quantities... For these reasons, synthetic nanoporous membranes have to be preferred and specially designed for this application. Two ways are currently investigated.

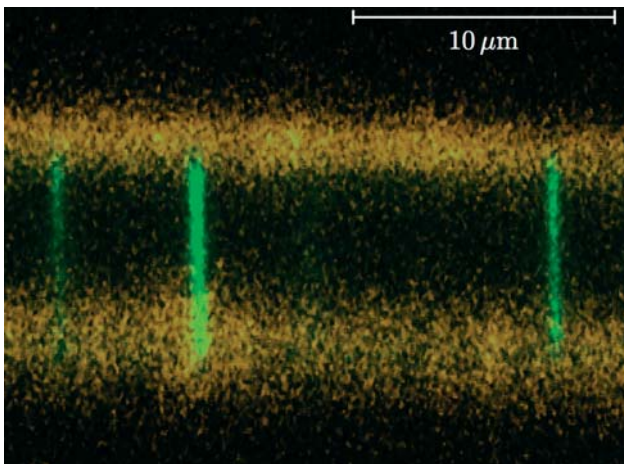


**Figure 3** (from Ref.2). PVDF membrane obtained by heavy ion irradiation and ion-track etching. Radicals that persist in nanopores after etching allows us a selective radiografting of poly(acrylic acid). Then a selective pore labelling with fluorophore is possible. The image the  $xz$ -plan cross-section of the membrane obtained by confocal laser scanning microscopy.

Nanoporous track-etched PVDF membranes are obtained by heavy ion irradiation of  $9\mu\text{m}$  thick PVDF films and track-etching. Nanopores have a nice straight cylindrical shape that has been evidenced by Small Angle Neutron Scattering. Recently, radiografting of poly(acrylic-acid) has been selectively driven at the surface of pore-walls. This chemical modification allows membrane pores to be selectively labelled with fluorescence molecules and then to be imaged by confocal laser scanning microscopy (see Fig. 3 and ref. 2). With so prepared membranes, measurement of translocation events on single nanopore using fluorescence

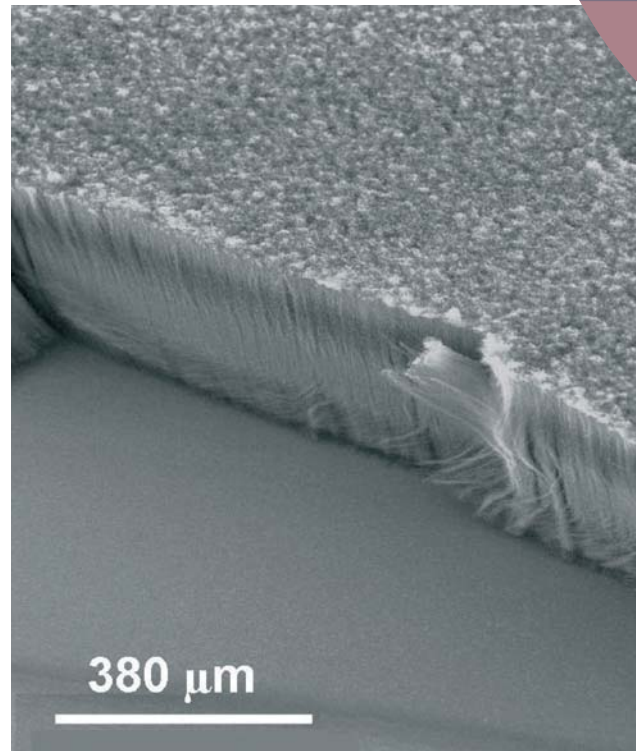


**Figure 4** (from Ref.3). Scanning Electron Microscopy image of aligned carbon nanotubes (a-CNT) synthesized on silicon substrates by aerosol-assisted catalytic chemical vapour deposition from toluene/ferrocene aerosol. The a-CNT obtained are multiwalled (J M. Pinault *et al.*, Nano Lett., 5, 12, 2394-2398 (2005).

techniques usually associated with confocal microscopy (such as Fluorescence Resonance Energy Transfer, or Fluorescence Correlation Spectroscopy) are now conceivable.

Aligned carbon nanotubes (nanotubes carpet see Fig. 4) are suitable to elaborate polymer-based composites in which the nanotube fillers exhibit a unidirectional orientation. After impregnation with polystyrene or epoxy-resin, a thinning procedure with a polishing device is performed to adjust the thickness of the composite and to open nanotube ends. Nanoporous membranes of  $100\text{-}200\mu\text{m}$  thickness are so elaborated with the hollow central channels of nanotubes as nanopores (Ref. 3). With respect to our application, the permeation characteristics of these membranes are very interesting with a monodisperse internal diameter of the order of  $7\text{ nm}$  (that can be adjusted) and an optimal pores density of the order of  $10^{10}\text{ tubes/cm}^2$ .

- [1] G. Oukhaled, J. Mathé, A.-L. Biance, L. Bacri, J.-M. Betton, D. Lairéz, J. Pelta, L. Auvray. "Unfolding of proteins and long transient conformations detected by single nanopore recording". Submitted in Phys. Rev. Lett.
- [2] O. Cuscito, M.-C. Clochard, S. Esnouf, N. Betz, D. Lairéz. "Nanoporous PVDF membranes with selectively functionalized pores". Submitted for publication in Nuclear Instr. Meth. Phys. Res. B
- [3] S. Barrau, M. Mayne-l'Hermite, D. Lairéz, C. Reynaud. "Control of aligned carbon nanotubes synthesis parameters for elaboration of nanoporous membranes". Submitted for publication in Chem. Phys. Lett.

### [C1. J.M. Zanotti] Evidence that interfacial water is the driving force behind protein dynamics

The atomic scale behaviour of water as a monolayer on a porous silica glass is the result of a subtle coupling of local rotational and long range translational dynamics. We have been able to discriminate between these two contributions to show that interfacial water experiences a glass transition at 165 K and a liquid-liquid transition at 240 K from a low-density to a high density-liquid. This unusual behaviour, compared to the bulk, is due to a strong weakening of the hydrogen-bond strength when water molecules lay in a 2D situation.

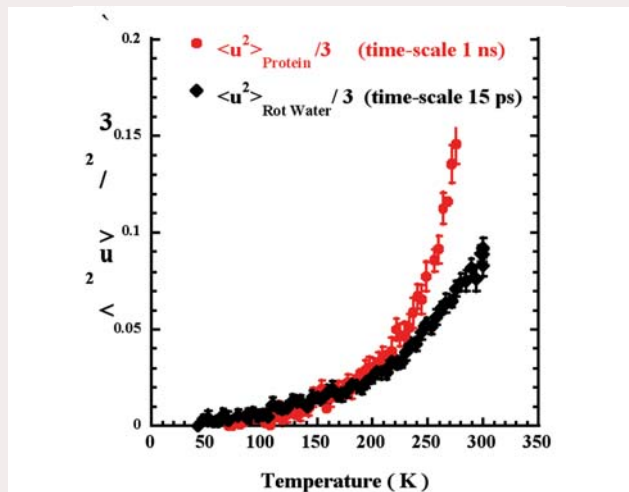


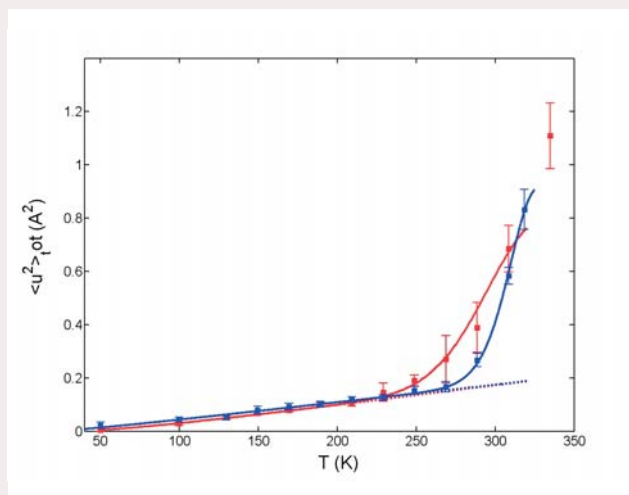
**Figure 1.** The atomic scale behaviour of water is the result of a subtle coupling of local rotational and long range translational dynamics. Here we show the temperature dependence of (i)  $\langle u^2 \rangle_{\text{Rot Water}}$  the short time scale (15 ps, i.e. 80  $\mu\text{eV}$ ) rotational mean-square displacements of interfacial water and (ii)  $\langle u^2 \rangle_{\text{Protein}}$  the hydrogen atom mean-square displacement of lysozyme hydrated with a monolayer of  $\text{D}_2\text{O}$ . We observe a strong correlation between the local reorientational transition in interfacial water at 220K and the onset of the long time (1 ns i.e. 1  $\mu\text{eV}$ ) large amplitude over-damped motions responsible for the  $\langle u^2 \rangle_{\text{Protein}}$  to increase above 220K. The observed correlation suggests that water dynamics is the driving force governing the protein-function-relevant slow, long range, protein internal motion.

The well-known protein dynamical transition is clearly visible at about 220 K (Fig.1) and is strongly correlated, to the onset of short time-scale reorientational fluctuations that initiate structural rearrangements within the transient H-bond network of interfacial water surrounding the protein. This result seems to be the first experimental evidence supporting a possible mechanism controlling protein dynamics. Within the framework of this model, the protein external side-chain short time motions, induced by fast water reorientational motion ( $\langle u^2 \rangle_{\text{Rot water}}$  Fig.1), propagate in a hierarchical way, along the protein structure from the residue side chains down to the protein core to induce the longer timescale protein backbone motion necessary for its function.

[Collaboration : J.M. Zanotti, M.C. Bellissent-Funel (LLB), Chen (MIT) and Kolesnikov (ANL/IPNS), *J. Phys.: Condens. Matter* 18 S2299–S2304 (2006)].

### [C2. S. Combet] Influence of hydration solvent on the dynamic transition of phycocyanin

Phycocyanin (PC) is a light-harvesting protein present in the antenna of cyanobacteria, where it is involved in the first steps of photosynthesis. This protein, which can be fully deuteriated, has been used as a model to study hydration water dynamics at



Mean square displacements of PC hydrated with 0.4 g  $\text{H}_2\text{O}/\text{g}$  PC (red) and PC hydrated with 0.46 g  $\text{D}_2\text{O}/\text{g}$  PC (blue).

protein surface by neutron scattering. The aim of the present study was to compare the influence of hydration solvent ( $\text{H}_2\text{O}$  and  $\text{D}_2\text{O}$ ) on the dynamics of PC by elastic neutron scattering. Samples of hydrogenated PC powder have been hydrated in  $\text{H}_2\text{O}$  (0.4 g/g PC) or  $\text{D}_2\text{O}$  (0.46 g/g PC) to obtain one similar monolayer of water molecules at the protein surface. Neutron elastic scattering spectra have been analysed by the double well-model. Evolution of the mean square displacements, as well as of associated thermodynamics values, was significantly different along the entire temperature range (20-320 K) between PC hydrated in  $\text{H}_2\text{O}$  and PC hydrated in  $\text{D}_2\text{O}$ . Dynamic transition temperatures between harmonic and anharmonic modes were, respectively,  $220 \pm 10$  K and  $270 \pm 20$  K for PC in  $\text{H}_2\text{O}$  and PC in  $\text{D}_2\text{O}$ . Differential microcalorimetry measurements confirmed these data with different slopes and vitreous transition temperatures between PC hydrated in  $\text{H}_2\text{O}$  (220 K) and PC hydrated in  $\text{D}_2\text{O}$  (235 K).

[Collaboration: S. Combet, G. Gibrat, M.-C. Bellissent-Funel, LLB; M. Tehei, ILL].

[C3. K. Yoshida] Hydration water in dynamics of a hydrated beta-lactoglobulin

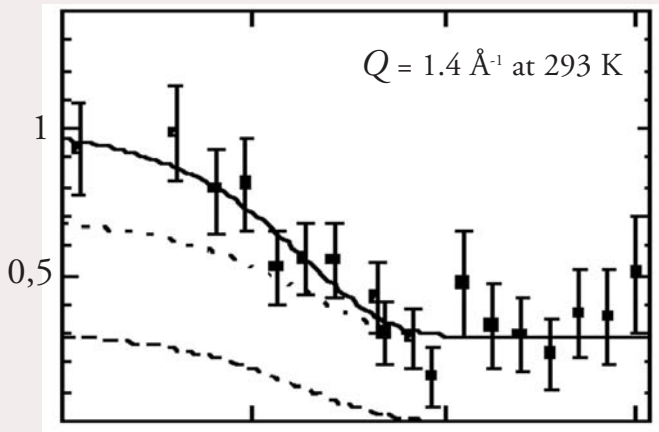


Figure 1. Typical intermediate scattering functions  $I(Q, t) / I(Q, 0)$  at  $Q = 1.4 \text{ \AA}^{-1}$  at 293 K. The solid line indicates the fitting results by the KWW equation. The upper and lower dashed lines are contributions from the protein and the surface water, respectively

It is well-known that water plays an important role in protein folding and function of proteins. Although computer simulation is a powerful tool to investigate the dynamics of protein and hydrated water, its result depends on the interatomic potential used in the calculation. Therefore, it is important to verify simulation results by comparing the calculated intermediate scattering function  $I(Q, t)$  with that obtained from experiment. In the present study, incoherent spin echo signals of a hydrated  $\beta$ -lactoglobulin protein were measured at 275 and 293 K. In the measured protein, ~69 % of water exists on the surface of the protein and the rest remains as the bulk. The intermediate scattering functions were divided into two contributions from surface water and protein, respectively, as shown in Figure 1. On one hand, the dynamics of the surface water follows a Kohlrausch-Williams-Watt (KWW) stretched exponential function (the exponent is ~0.5), on the other hand, that of the protein follows a single exponential. The behavior of elastic incoherent structure factor (EISF) as a function of  $Q$  shows the feature of the confined diffusion.

The present results are consistent with our previous results of hydrated C-phycoerythrin combining elastic and quasielastic neutron scattering and by molecular dynamics simulation. Moreover, the behavior of surface water is similar to that of water confined in hydrophilic porous materials. We can stress that water confined in hydrophilic porous materials is an adequate model to investigate water in biomolecules.

[Collaboration : K. Yoshida, T. Yamaguchi, Fukuoka Univ. , Japan; M.-C. Bellissent-Funel, S. Longeville, LLB]

[C4. G. Gibrat] Thermal denaturation of apo-calmodulin

Calmodulin is a small (16.7 kDa) calci-protein (a protein that can fix calcium ions) that is well adapted to neutron scattering experiments. Indeed, it allows reaching concentrations of about 100 g/L in physiological-like conditions (pH 7.5 and [KCl] ~ 100mM) without any aggregation. Moreover calmodulin is made of two N- and C-terminal domains, with a 70% sequence homology, linked by a central  $\alpha$ -helix. Despite the high sequence homology, these two domains show significantly different stabilities (about 10°C difference in thermal denaturation temperatures). It is so an interesting system to study the sequence-folding relationship.

From fluorescence, circular dichroism and UV absorption spectroscopy experiments, it is quite clear that for apo-calmodulin (calmodulin without calcium) thermal denaturation occurs at least in two steps, corresponding to the successive unfolding of the two N- and C-terminal domains (respectively  $T_m=63^\circ\text{C}$  and  $T_m=51^\circ\text{C}$ ). Holo-calmodulin (calmodulin with calcium) is stable up to 100°C. From SANS measurements, it appears that apo-calmodulin loses progressively its structure between 40°C and 80°C. At high temperature, apo-calmodulin adopts a “polymer-like” conformation (SANS spectrum follows a Debye law for  $QR_g < 3$ ), with a radius of gyration of 32Å. However, the high  $Q$  exponent of 2.3 suggests the existence of residual secondary structures, also seen by circular dichroism. Indeed the 2.3 value is between polymer chain values (1.7 or 2) and the compact chain value (4).

[Collaboration : G. Gibrat, LLB; G. Hui Bon Hoa, Inserm U473; Y. Blouquit, Inserm U759/Institut Curie-Orsay; C. Craescu, Inserm U759/Institut Curie-Orsay; M.-C. Bellissent-Funel, LLB]

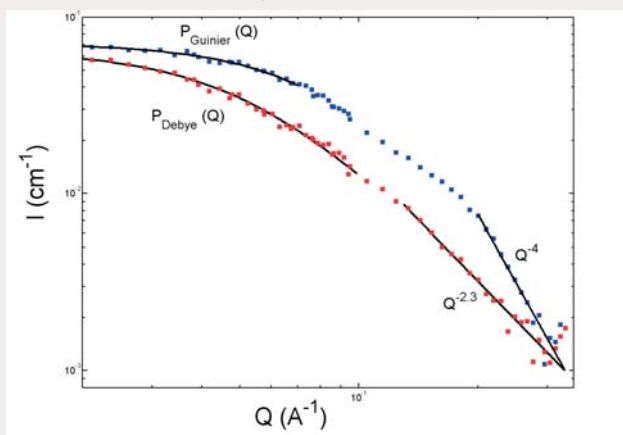


Figure 1. SANS spectra of native apo-calmodulin (in blue) and of calmodulin at 80°C (in red)

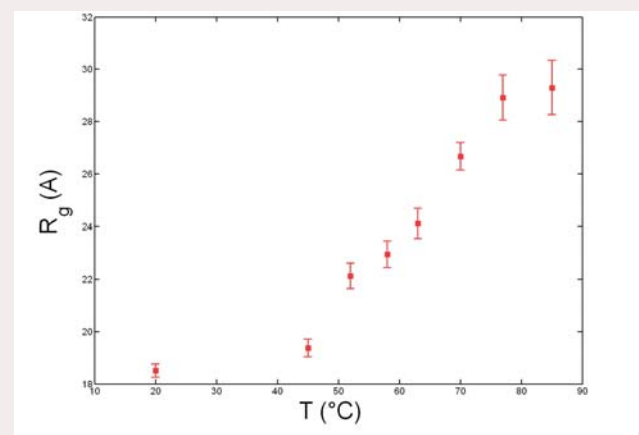


Figure 2. Radius of gyration of apo-calmodulin at 5g/L as a function of temperature

### [C5. S. Longeville] Influence of macromolecular crowding on protein folding and stability: a model for unfolded chain

The cytoplasm, the interior of cells, is filled with a very high quantity of objects with respect to shape and size. In most of the cases, each species is present at rather low concentration but the overall occupied volume fraction can reach  $\Phi \sim 0.3-0.4$ . The term "crowding" is generally used to describe this environment rather than high concentration which appears less appropriate in this context.

Under crowding environment protein-protein interactions play a fundamental role because the distances between molecules are of the order of few tens of Å. The crowding environment can affect some physical, chemical or biological properties of biological macromolecules [1][2]. The structure and the reactivity can be very strongly modified as a function of inert crowding agents. A particularly interesting aspect concerns the effect of crowding on protein folding and stability. Usually protein folding is studied *in-vitro* at very low concentration. Under such conditions small globular single chain proteins can unfold and refold quite rapidly depending mainly on the nature of the solvent.

The aim of our project is to search for the possible differences between the process of protein folding/unfolding studied *in-vitro* where the protein are very diluted and surrounded by solvent only and the mechanism *in-vivo* where proteins are in very crowded environment.

Theoretically the problem was studied by the introduction of the concept of excluded volume [3]. In a recent paper [4], Minton uses a statistical thermodynamic model to address the question. He predicted that inert cosolutes stabilize the native state of proteins against unfolding mainly by destabilizing the unfolded state and that the dimension of the unfolded state decreases with increasing the concentration of solute in a measurable way.

In a first series of experiment we have measured by SANS the effect of a classically used inert co-solute F70 on the conformation of a deuterated polymer (PEG). We choose a solvent mixture of  $D_2O$  and  $H_2O$  at the matching point of the F70 in order to observe only the polymer in good solvent, assumed to be a model for an unfolded chain [5].

On the contrary to what is generally assumed chemical interactions can not be neglected leading to partial segregation of the two components but we show that the polymer density is increase when adding F70.

[Collaboration: S. Longeville, LLB, B. Demé ILL]

[1] R. J. Ellis, Trends in Biochem. sciences **26** (2001) 597-604. [2] A. P. Minton, The J. of Biol. Chem. **276** (2001) 10577-10580. [3] Zhou Y. and C. K. Hall, Biopolymers **38** (1996) 273-284. [4] A. P. Minton, Biophysical J. **78** (2000) 101-109. [5] P. Calmettes et al, Biophysical Chemistry **53** (1994) 105-114

### [C6. D. Lairez] Phase transition of metastasic extracellular matrix: theory and experiment

The extracellular matrix is a gel made of various macromolecules that isolates organs. In tumour dissemination, invasive cells liquefy the extracellular matrix gel by producing proteolytic enzymes. We study the physical aspects of their actual role in cell invasion: proteinases by hydrolyzing peptide bonds between gel crosslinks, catalyze a phase transition from a gel and solid state to a liquid [1]. A key feature has to be considered: *in vivo*, the enzyme concentration range is so small that enzymes must diffuse within the gel to significantly damage it. Enzyme diffusion introduces space correlations and then controls the gel degradation mechanism [2] and its universality class [3].

Recently [4], a model system consisting in gelatin (denatured collagen) and thermolysin as proteinase was studied at different gel volume fraction,  $\phi_{gel}$  and enzyme concentration,  $[E]$ , and varying the solvent viscosity  $\eta_r$ . The degradation time  $t_c$  varies as:

$$t_c \propto \mu \eta_r \times \phi_{gel}^{2.50 \pm 0.05} \times [E]^{-1.46 \pm 0.07}$$

This result provides clear evidence, which was missing until now, that the gel degradation kinetics is diffusion-limited. We propose a scaling argument and reduced variables for anomalous enzyme diffusion that fully account for experiments. Plotting  $[E]\xi_0^3$  as a function of  $t_c/\tau_0$  with  $\xi_0$  the mesh size of the gel network and  $\tau_0$  the diffusion time of enzyme over this length, allows us to obtain a single master curve independent of  $\phi_{gel}$ . This scaling argument is consistent with self-attracting memory effect on enzyme random walk, i.e. enzyme has some facilities for going back in previously visited area (already damaged gel) rather than for exploring new area (intact gel).

This self-attracting random walk leads to a "Swiss Cheese" model for gel degradation that belongs to the continuum percolation class.

[Collaboration: D. Lairez, LLB, G. Zalczner and J.-P. Carton SPEC/DRECAM/DSM, J. Pelta, Université de Cergy-Pontoise]

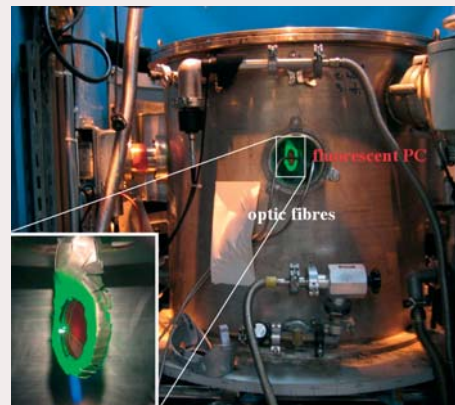
[1] H. Berry, J. Pelta, D. Lairez, and V. Larreta-Garde. Biochem. Biophys. Arch., 1524:110-117, 2000. [2] G. C. Fadda, D. Lairez, B. Arrio, J. P. Carton, and V. Larreta-Garde. Biophys. J., 85:2808-2817, 2003. [3] T. Abete, A. de Candia, D. Lairez, and A. Coniglio. Phys. Rev. Lett., 93:228301, 2004. [4] D. Lairez, J. P. Carton, G. Zalczner, and J. Pelta submitted for publication in Phys. Rev. Lett., 2006.

### [C7. S. Combet] Dynamics of a photo-excited antenna protein

Phycocyanin (PC), a blue protein present in the light-harvesting system of cyanobacteria, plays a key role in the first steps of photosynthesis. For the isolated PC, one part of captured light energy is dissipated *via* emission of fluorescence and the other part is dissipated by fast and localized dynamics of the pigment-protein complex. The aim of this project is to investigate whether dissipation of excitation energy in PC leads to modifications of the protein internal dynamics on longer timescales and larger amplitudes than that of localized vibrations of the pigments.

We measured photo-induced dynamics of PC on MIBEMOL time-of-flight spectrometer (LLB) with a pulsed Nd:YAG laser ( $\lambda = 532$  nm, 5 ns pulses) at different energy and frequency values (20 mJ and 14 Hz max.) to illuminate *via* optic fibres both sides of the sample (130 g/L of hydrogenated PC solubilized in 20 mM  $\text{Na}_2\text{DPO}_4$ ). MIBEMOL data acquisition system has been successfully modified to synchronize the laser excitation flashes with the neutron pulses at sample position and get “double beam” relative measurements (“light” and “dark”). This “double beam” procedure is extremely novel and eliminates spurious effects that could occur in the sample during the experiment. We used an aluminium sample holder surrounding sapphire glasses, which exhibit a much lower neutron scattering than quartz glasses. In a preliminary experiment, a difference of 3% between PC illuminated and PC in the dark has been observed in the maximum of elastic scattering peak, with the “low energy” mode of the laser (pulses  $\sim 110$   $\mu\text{s}$  similar to the duration of the neutron pulses  $\sim 87$   $\mu\text{s}$ ). Further experiments will take place very soon to improve this device (laser wavelength closer to the maximum absorption (620 nm) of PC, integrating sphere to illuminate the sample inside uniformly) and also to get reasonable statistics.

[Collaboration: S. Combet, J.-M. Zanotti, M.-C. Bellissent-Funel, LLB; J. Pieper, TU-Berlin].



Side view of the sample environment on MIBEMOL time-of-flight spectrometer during illumination experiments on PC. Insert: fluorescence of the PC (red color) in the sample holder with the green laser beam reflected on the cadmium mask.

### [C8. D. Champion] Glass transitions in cryoconcentrated sucrose solutions.

Since it drives the rate of diffusion limited bio-chemical reactions, the glass transition temperature is a key parameter for frozen food conservation. DSC signal of a maximally cryo-concentrated sucrose solution (50% sucrose mass fraction), considered here as a model system, shows a two steps baseline shift (Figure 1a).

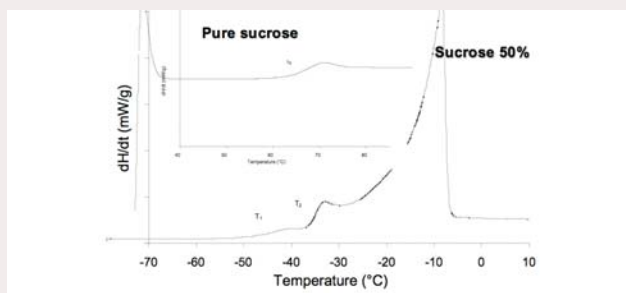
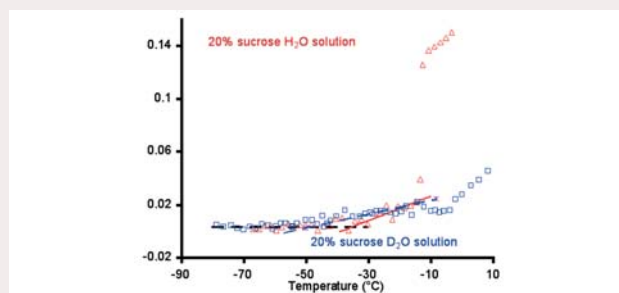


Figure 1 a): Comparison of the DSC results between a pure glassy sucrose and the cryoconcentrated sucrose solution.



b): Temperature dependence of the mean square displacements for 20% sucrose solution in  $\text{H}_2\text{O}$  and  $\text{D}_2\text{O}$ .

To identify the onset temperature of water mobility in a 20% sucrose solution, H/D isotopic labelling has been used to directly probe molecular motions of water ( $\text{H}_2\text{O}$ +sucrose) then sucrose ( $\text{D}_2\text{O}$ +sucrose). The mean square displacement ( $\langle u^2 \rangle$ ) as measured on Mibémol shows a small slope change at  $-37^\circ\text{C}$  and  $-48^\circ\text{C}$  in 20% sucrose/ $\text{H}_2\text{O}$  and sucrose / $\text{D}_2\text{O}$  mixtures respectively. These results are in fully agreement with DSC observations: the first transition at  $-48^\circ\text{C}$  is to be correlated to a dynamic change of the sucrose molecule whereas the other one seems to be linked to a change of water dynamic. The sharp evolution of  $\langle u^2 \rangle$  seen at higher temperature (around  $-10^\circ\text{C}$ ) is due to ice melting, which acts like the dilution of the liquid phase. In order to study if the water dynamical change around  $-35^\circ\text{C}$  affects the ice structure during its formation, diffraction studies were also carried out with MIBEMOL. The Bragg peak intensity were analysed as a function temperature during cooling. The crystallization of heavy water started at temperatures around  $-7^\circ\text{C}$ . This temperature is around the same as the temperature of  $\langle u^2 \rangle$  evolution variation (Figure 1b). The intensity of both  $Q=1.61 \text{ \AA}^{-1}$  and  $Q=1.71 \text{ \AA}^{-1}$  peaks were followed during temperature sweep. The observed change in the evolution of the  $Q=1.71 \text{ \AA}^{-1}$  peak intensity at the temperature around  $T_2$  on DSC (Figure 1a) may be the consequence of cubic ice formation. Indeed, confined water beyond the interfacial region created by the high cryo-concentration of sucrose may crystallize into a distorted form of cubic ice in contrast to bulk water which crystallizes into ordinary hexagonal ice.

[Collaboration : Champion D., Loupiac C., Simatos D., ENSBANA, Dijon and Zanotti JM (LLB)]







# INSTRUMENTATION

# INSTRUMENTATION

## Introduction

In 2004 and 2005, funding for the LLB was limited. Though investments were reduced the CAP2010 instrumentation program was continued. Mid 2005, the signature of the new contract for the LLB between the CEA and the CNRS opened up a bright future. The CAP2010 program is now moving ahead at full speed and nearly half of the spectrometers of the laboratory take advantage of our efforts.

## 2005-2006 achievements

### DIFFRACTION

Much effort has been made on the diffraction spectrometers. Most of the work has been devoted to the improving the detection efficiency of the spectrometers. This will enable us to reach two targets; to be able to perform experiments with smaller sample quantities; and to be able to perform experiments faster which will make it possible to measure more points of the temperature, magnetic field, pressures and/or concentration diagrams.

- The new High Resolution Powder Diffractometer **3T2** [CI, F. Damay] built with the support of “**Région Aquitaine**” was installed at the end of 2005. Compared to the previous version, it has higher number of larger detectors, and the efficiency is multiplied by 5. New protections will be installed end of 2006 to obtain a decrease of the background.

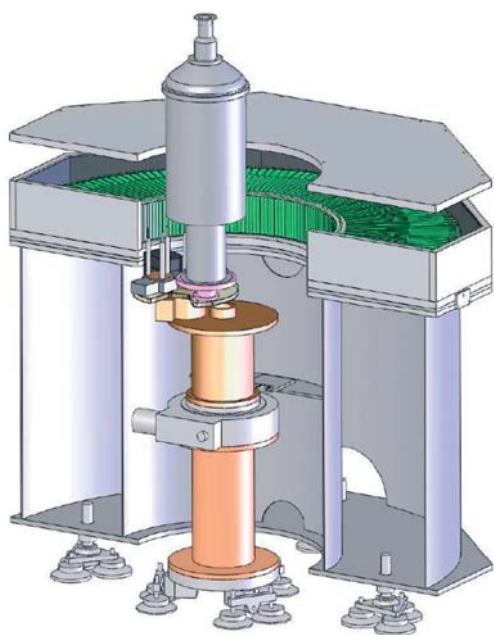


Figure 2. Modernized Very High Resolution Powder Diffractometer G4-2



Figure 1. VIP final design with multitubes detectors on 5C1

- The single crystal diffractometer **6T2** [HI, A. Gukassov] is now equipped with a XY multidetector of a surface of 26x26cm<sup>2</sup> from INEL branch with the help of the “**Rennes métropole**”. Development of software is now underway to enable more efficient use of a greatly increased collection of data.
- The design of the new detector of the **G6-1** powder diffractometer devoted to micro samples measurements is now completed [H2, I. Goncharenko]. It will use a set of 16 tube detectors. Tests with 8 tubes have confirmed an expected gain of intensity close to 30 compared to the current configuration. A new guide with supermirror coating was installed for this spectrometer in summer 2005.
- A new multitubes detector has been designed for the polarized neutron **5C1** crystal diffractometer (fig. 1). Its electronics, detectors and radial collimators have been ordered. It will take advantage as 6T2 did before of a large detection surface to improve the overall detection efficiency by a factor of more than 50. It will be installed in 2008.

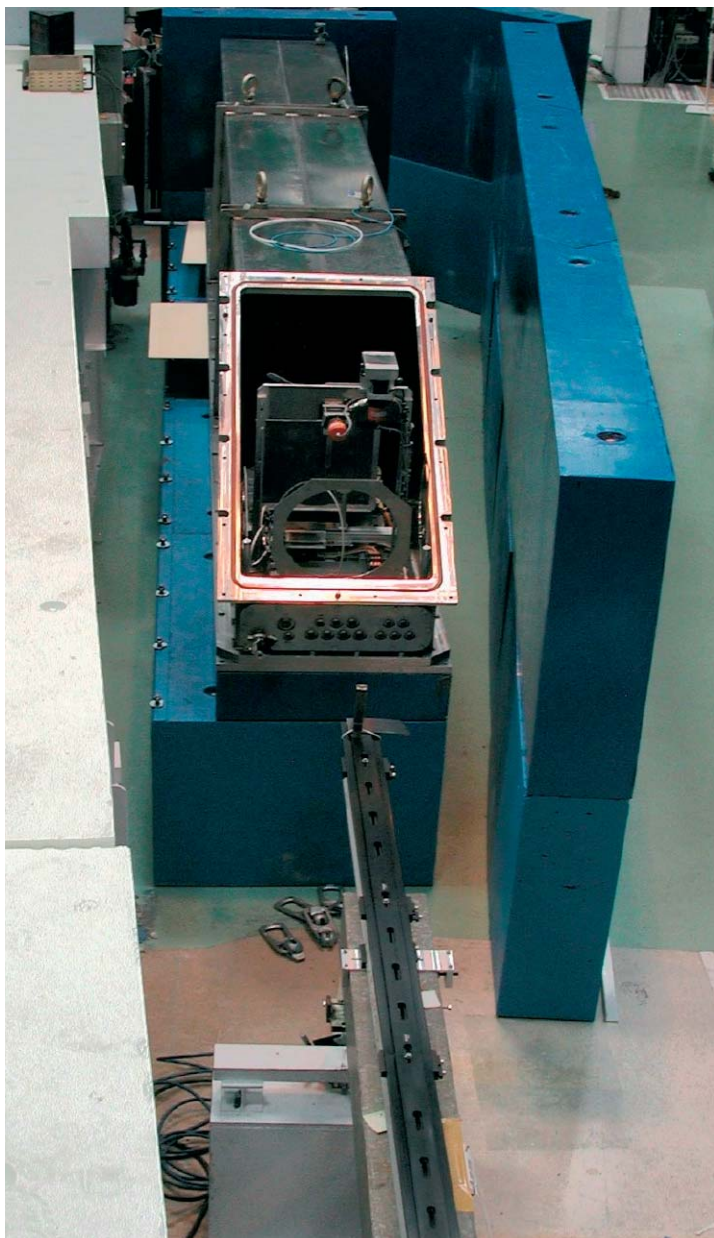


Figure 3. TPA spectrometer at October 2006

Our second important operation of CAP2010 in this area is the optimization of the Eros reflectometer for higher flux on the detector to measure thinner layers. This is a four-phase project. Phase 1, consisting of the change of the chopper, has already been done, and has provided a doubling in flux. Phase 2 consists of the shortening of the collimator. The design study has been done (fig. 4), and the collimator has been ordered. It should be delivered and installed in spring 2007 and should provide a flux gain of a factor of 5. Phase 3 consists of an optimization of the sample to detector space ; and phase 4, in a transfer of the spectrometer to a better end guide position.

In the field of innovative instrumentation for reflectivity, we have performed the first tests of the TilToF concept [C5, F. Ott]. It makes it possible to perform reflectivity experiments with white beams and opens the way to potential gains of intensity of an order of magnitude compared to usual monochromatic or time of flight reflectometers.

Two other important features must also be noticed. A new traction machine for small samples is now available on 6T1 and Diane. Installed on a three circles goniometer, it enables measurements on single grain in large grain alloys and will be mainly used for understanding energy and stress distribution in these alloys, which are more and more frequently used in industry. After a long shutdown due to technical problems, G4-2, the very high resolution powder diffractometer from Gatchina is under reconstruction. A new setup has been designed and will be installed at the beginning of 2007 (fig. 2).

#### LARGE SCALE STRUCTURES

In the field of the study of structure at large distances, the CAP2010 program comprises two main projects. The most important one is the construction of a new spectrometer for measurements at very small angles. Called TPA from the French "Très Petits Angles", it is a standard pinhole type small angle scattering spectrometer which has been designed to measure diffraction at  $Q$  values as low as  $10^{-5} \text{ \AA}^{-1}$  instead of  $10^{-4} \text{ \AA}^{-1}$  for our current small angle scattering spectrometer PAXY. It will enable the measurements of structures up to a  $1 \mu\text{m}$  in size, and will fill the gap between neutron and light scattering. Basic concepts of this new spectrometer were tested in 2004. It is equipped with a double multilayer monochromator [C2, S. Desert] and a multibeam collimator [C3, S. Desert] built with the help of our participation in the Joint Research Activities (JRA) "Neutron Optics" of the Integrated Infrastructure Initiative for Neutron Scattering and Muon Spectroscopy (NMI3) European program. The detailed design and fabrication of the main components started in 2005. Delivery and installation occurred in 2006 (fig. 3). All parts are now ready to be tested and are awaiting the restarting of the reactor.

An innovative detector with a CCD camera was developed for specific structural measurements at an intermediate scale, and soon provided very promising results [C4, P. Baroni].

## INELASTIC SCATTERING

Two main achievements have been realized in this field. The first one is a direct improvement of the flux available on the samples of the cold triple axis 4F1 and 4F2 [H3, B. Hennion]. Taking the opportunity of the preparation of the thimble change of 4F (fig. 5), we have installed new collimators equipped with  $m=3$  supermirrors within the 4F beam plugs. The flux gain at the sample place has been estimated at up to 80% under certain conditions, at the price of a (small) 15% loss in resolution. On the same instruments, we continue our efforts to improve the efficiency of polarized neutron experiments with polarization analysis, and a new polarized guide has also been purchased from the PNPI Gatchina. Installed in front of the graphite analyzer, it will provide a better flux and better polarization than the Eusler currently used. The second achievement is the definition and purchase of a new 10T superconducting coil for triple axis measurements. It should be delivered at the end of 2007.

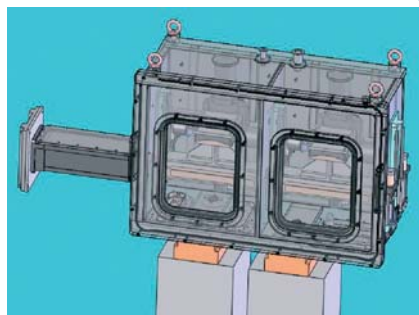


Figure 4. Eros short collimator

## EUROPEAN NMI3 PROGRAM

In October 2006 we reached the mid-term of our participation in the NMI3 of the 6<sup>th</sup> framework European program. This program includes two different aspects. The main part is the Access program and is used to support the access to our spectrometers to new non French European users. The second part of the program is the technical networks called JRA. We participate in three of them:

“Neutron optics “

With the aim of setting up intense micro-beams, we have performed fabrication and tests of magnetic neutron waveguides [C6, S.V. Kozhevnikov]. We have already reported the development of the multibeam for TPA done within this JRA.

”Detectors”

We have succeeded in setting up a detection module with its electronics of 50x50 mm<sup>2</sup>. We are now working on a project of tiling the space with many of these detection modules.

“Polarization Neutron Techniques”

We are working on setting up bent resonant coils for spin echo. This will allow the use of banana detectors to increase the counting efficiency of this type of spectrometers. With the collaborations obtained through this network, we have been able to install the longitudinal polarization analysis on our thermal single crystal diffraction spectrometer 6T2.



Figure 5. 4 steps of the works on beam tube 4. From left to right; 3T2, 4F1 and 4F2 in operation in June 2006, empty space beginning of July, thimble testing mid-July and 4F1-4F2 monochromator protection back in place in September.

## Projects

### MID TERM PROJECTS

Our modernization started with the CAP2010, projects will continue long after the end of this program. Our efforts will be put where neutrons will remain essential within the coming years: quasi-elastic scattering and small angle scattering.

In quasi-elastic scattering two projects are already underway.

While preparing Fa#, our future quasielastic spectrometer, improvements of Mibemol continue. 100 detectors have been added in the small angle positions between 5° and 15°. A 64x64 cm<sup>2</sup> XY multidetector is ready to be installed near the direct beam to simultaneously provide structural and dynamical information in the 10 Å range. When Fa# becomes available, all the detectors will be transferred to the new instrument. Fa# will benefit of all the Mibemol improvements. A new guide will be completely optimized for it and will use the latest neutron optics development to provide this future instrument with the best possible optimization of the flux/resolution function.

## INSTRUMENTATION

For the study of even lower energy transfer, our resonant spin echo Muses will be improved. We are currently engaged in an NMI3 JRA network to design and test a banana-type coil that will enable measurements simultaneously at 10 different angles. This is expected to be in use in 2008.

Our small angles scattering spectrometers have provided good performances to numerous users for many years. Up to now, improvements have essentially been made in sample environments. We must now improve the instrument itself. Two actions have been undertaken. New velocity selectors are being purchased. They will provide a gain of intensity estimated at 30%, a more reliable operation, and the possibility of doing experiments with lower wavelength. Also long term studies have been started for the replacement of our current detectors by larger ones with better efficiency. Another 40% increase of intensity is expected in this direction. Studies are also being made in the evaluation of the ability of the time of flight technique in providing an easy way to do measurement on large Q range with a single measurement.

7<sup>TH</sup> EUROPEAN FRAMEWORK PROGRAM

Having in mind the 7<sup>th</sup> European framework program that will start in 2008, projects of collaboration are currently being set up with our partners of the NMI3 program. Efforts will be focused on collaborative programs that will end with a delivery that can be used immediately by our users. We have proposed to work in five directions :

- Software : Instrument simulation, data extraction, visualization and analysis
- Optic : Multi-beams and lenses focusing, neutron guide ageing
- Detector : Multi-tile detectors and integrated electronics
- Polarization : resonant spin echo with banana type detector, he versatile station for users
- Sample environment : pressure, shear, laser

## LONG TERM PROJECTS

Other scientific areas will not be forgotten. A new innovative design for Diane, our strain scanner, is under preparation. The basic concept of the project is to provide an easy alignment of the sample by decoupling the sample stage from the systems of definition of the incident and scattered beams.

On longer time scale, we think that we are now at the maximum of flux delivery on the sample that can be performed on our triple axis with our source. Further improvement of our spectrometers to reduce the counting time or enable the measurements on smaller samples requires going towards multidetector systems. We are now undertaking the evaluation of **flat cone geometries** to find out if real improvements in efficiency can be provided by this technique. Conclusive arguments will be provided by simulation programs.

We intend also to evaluate **new cold sources design**. New codes have developed in neutronics laboratories which make it possible to obtain a realistic simulation of the neutron distribution and thermalization close to the core. They are fast enough to perform parametric studies, and as a consequence enable a better optimization of the shape and materials of the cold sources. In order to provide a good overall flux within a small size, our current cold sources suffer from under-moderation. The flux at large wavelength could certainly be increased by the use of new shape or new materials. These studies have to be started now, since if calculations show that an important gain can be reached, the requested modifications of the sources close to the core of the reactor will require long safety studies.

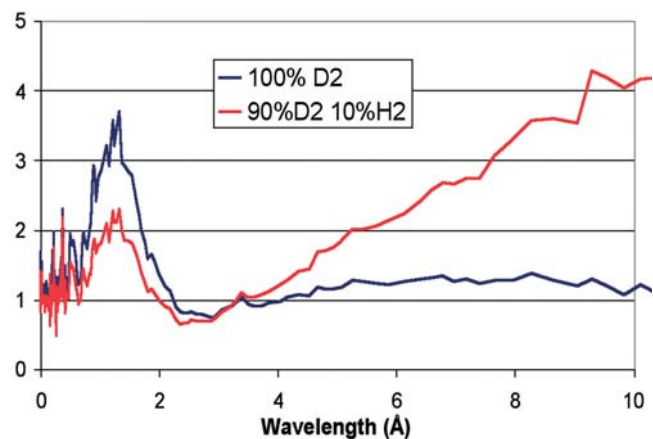
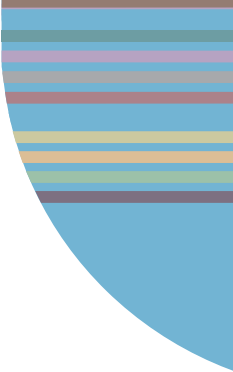
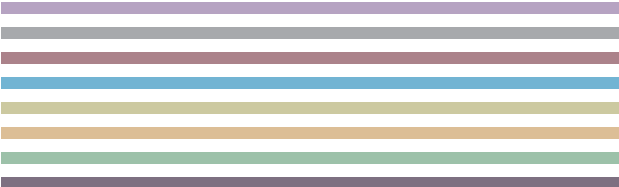
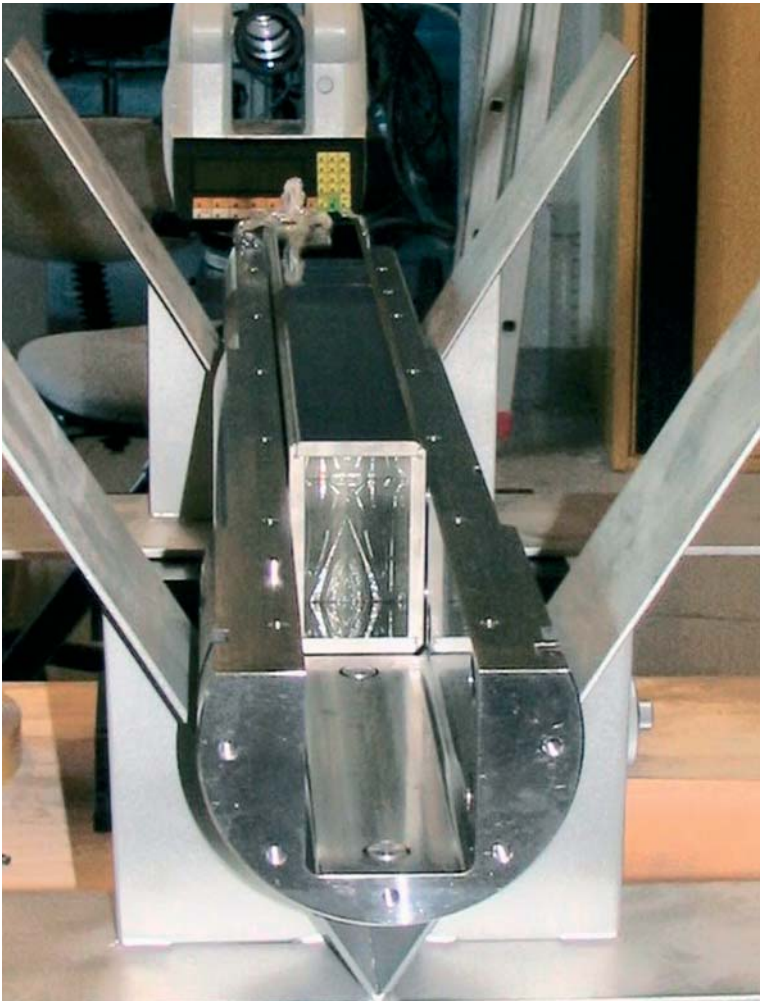


**Figure 6.** Evaluation of potential gain and losses in intensity compared to our current cold sources. Curves shown have been calculated with cold sources full of a mixture of liquid H<sub>2</sub> and D<sub>2</sub>.



# INSTRUMENTATION



**H1.** Super-6T2, a new position sensitive detector polarized neutron diffractometer

A. Gukasov, A. Goujon, J.-L. Meuriot, C. Person, G. Exil and G. Koskas

**H2.** G6-1 “Micro”, a powder diffractometer for micro samples measurements

I. Goncharenko, X. Guillou

**H3.** New Supermirror collimators for the in pile cold triple axis

B. Hennion, P. Boutrouille

**[C1. F. Damay]** Upgrade of the 3T2 High Resolution Powder Diffractometer

**[C2. S. Desert]** A double super-mirror monochromator for the new Very Small Angle Neutron Scattering spectrometer (TPA, Très Petits Angles)

**[C3. S. Desert]** Multi beam collimator prototype for the new Very Small Angle Neutron Scattering spectrometer (TPA, Très Petits Angles)

**[C4. P. Baroni]** New developments for 2D High Resolution Neutron Scattering Experiments. Application case and experimental evidences from crystals to polymer science.

**[C5. F. Ott]** TilTof a high intensity space-time reflectometer

**[C6. S.V. Kozhevnikov]** Magnetic neutron waveguides

# H1. SUPER-6T2, A NEW POSITION SENSITIVE DETECTOR POLARIZED NEUTRON DIFFRACTOMETER

A. GUKASOV, A. GOUJON, J.-L. MEURIOT, C. PERSON, G. EXIL AND G. KOSKAS

Leon Brillouin Laboratory,CEA-CNRS, CE Saclay, 91191 Gif sur Yvette, France.

Polarised neutron diffraction (PND) is an important technique to investigate interatomic or intermolecular magnetic interactions. PND takes full advantage of the neutron magnetic moment and gives a direct access to the spin density distribution in the unit cell. In contrast to electron density, usually determined from high precision X-ray diffraction techniques, the spin density distribution is directly related to the unpaired electrons. Thus, by comparing spin and electron densities, one can get insights into magnetic interactions. The PND has been extensively used at LLB using the 5C1 diffractometer. Recently it has been successively applied to the studies of anomalous spin densities in ruthenates [1], of the origin of the field-induced ferro-metallic state in bilayer manganites [2], of staggered field effects in the one-dimensional antiferromagnet [3], of photoinduced molecular switching compound [4].

PND is also traditionally of particular interest for the community of chemists working in the field of molecular magnetism. Thus spin density studies in molecule-based magnetic compounds have permitted to obtain a very important information about the magnetic interactions in : ferromagnetically coupled copper(II) dimers [5]; ferromagnetic superexchange through the non-magnetic Ti(IV) ion in a Ti(IV)-(semiquinone)<sub>2</sub> biradical [6] and the nature of the interaction in a Mn(II)-Ni(II) ferromagnetic chain compound [7]. Running a PND experiment is quite time consuming thus an improvement of PND diffractometers, which would boost the data acquisition rate, and as a consequence the precision of the information on spin densities is highly desirable.

Hence a new polarized neutron diffractometer has been commissioned at the ORPHEE reactor in Saclay. The instrument is installed on the thermal beam tube 6T2 at the ORPHEE reactor. Vertically focusing pyrolytic graphite is used to select the neutron of wavelength  $\lambda=1.4$  Å. The incident monochromatic beam is polarized with supermirror bender installed inside the monochromator protection. The bender has been designed and constructed in PNPI, Gatchina. It consists of 19 channels, each of 0.85 mm width, 50 mm height and 780 mm length. The supermirrors are deposited on 0.3 mm thickness glass and mounted with spacers of 0.85 mm thickness. An additional nonpolarizing supermirror focusing condenser can be inserted in the RF adiabatic flipper, when small samples are used. An adiabatic radiofrequency flipper [8] is installed between the polarizer and superconducting magnet of 7.5 Tesla, see Fig.1. The magnet is equipped by: <sup>3</sup>He insert, CuBe pressure cell, very high pressure (sapphire) cell, kappa-geometry and photo-excitation inserts.

To reduce the scattering from the sample environment a radial collimator is installed in the detector protection (Eurocollimators Ltd ) and covers 30° in vertical and horizontal directions. We found that the radial collimator reduces the scattering from the sample environment by a factor 10-20, which is of great importance for the performance of the diffractometer, working essentially in extreme sample conditions.

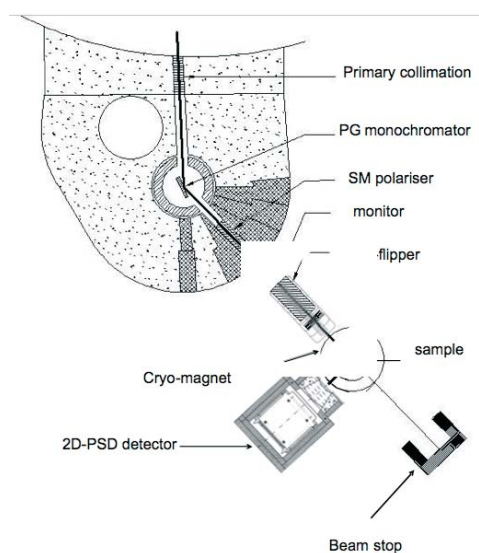


Figure 1. Schematic illustration of the Super-6T2 diffractometer.

The polarization of the incident beam was tested using CoFe single crystal and was found to be  $P_0=97\%$  (Flipping Ratio  $\sim 70$ ). Measurements on bench mark single crystals of CoFe and Ni using single counter, have shown the intensity gain of a factor of 15 compared to the intensity of existing polarized neutron diffractometer 5C1 at LLB. This gain factor will be increased even more with the use of the PSD. In this setup, the diffracted beam is collected by position sensitive multiwire gas detector BIDIM26 developed in ILL [9], fabricated by INEL and bought with the financial support of "Rennes Metropole". It is an individual readout square Multi-Wire Proportional Chamber (MWPC) with a single gas volume. The number of readout channels is (128X \* 128Y), with resolution 2\*2 mm. The vertical and horizontal acceptance angles of the PSD detector are 25°x25°, (0.19 steradian).

## INSTRUMENTATION

Spinning of sample and collecting of 2D images at only four consecutive detector positions will provide both integrated intensities and flipping ratios up to  $\sin(J/l) \sim 0.6 \text{ \AA}^{-1}$  in the horizontal plane and  $\sin(J/l) \sim 0.2 \text{ \AA}^{-1}$  in the vertical one. Then for the frames having low statistical accuracy flipping ratios will be re-measured with a longer exposition time to reach the required accuracy. Once the data collection is finished, the vertical axis of the crystal can be driven into the horizontal plane by using kappa-goniometer inserted in the magnet and the missing reflection intensities along the originally vertical crystal axis can be measured.

Data acquisition is realized by means of a EuroPsd microprocessor module designed at the LLB. The module assures connection between the driving computer and the ILL PSD interface via the IEEE 488 bus. It is able to sustain very high acquisition rates (up to 5 Mhz) and to run in different modes, like polarized neutrons, Time Of Flight (TOF) and time resolved modes. The module is equipped by an onboard (16 bit) memory adapted for detector sizes up to 512x512 channels. This makes the acquisition being totally independent from the performance and capacities of the driving computer.

Data are collected using a VISUAL BASIC (VB) software developed in LLB. We chose an industrial standard XML (Extended Markup Language) to store the data collected from the PSD. This standard describes in an easy and intuitive way how the information is stored. It has an advantage as well that it comes with ready made parsers and standard XML editors. The XML file created by the LLB acquisition software contains compressed data collected from the PSD and all current parameters of the diffractometer; date, time, angles, monitor, temperature etc. Visualization program, see Fig. 2, written in JAVA gives quasi-instantaneous visualization and access to any selected frame due to the XML standard, providing tabulation files. The same program assures: reading of frame content, binning and summation of frames and creation of dynamic mask of strongest pixels. Program for indexing, integration and flipping ratio calculations is written in Fortran 90 and MATFOR 4.

For the crystals having small lattice parameters the gain from using the PSD will be very small. In this case we consider a possibility to use several single crystal of different orientation simultaneously. In particular if crystals are mounted at different height, the Friedel pairs can be used to define the zero offsets in the horizontal plane and to separate reflections belonging to different crystals.

Quite large detector aperture (0.19 steradian) allows to measure polarized neutron diffraction from powder samples with a high efficiency. We note that its acceptance angle is nearly four times larger than that of the existing powder diffractometers G4.1 and G6.1 at LLB.

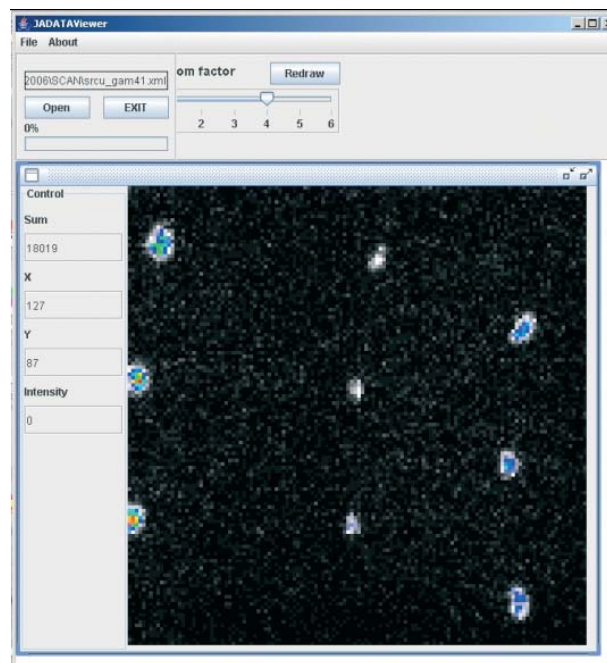


Figure 2. Visualization program window.

Using a long polarizing bender in combination with PSD on 6T2 improve the efficiency of the instrument by approximately a factor of 20-30 compared to the 5C1 diffractometer currently existing at the LLB. This will provide unmatched speed of data collection from very small samples with relatively large unit-cells.

- [1] A. Gukasov, M. Braden, R.J. Papoular, S. Nakatsuji and Y. Maeno. Phys Rev Lett. 80, 087202-1, 2002.
- [2] F. Wang, A. Gukasov, F. Moussa, M. Hennion, M. Apostu, R. Suryanarayanan and A. Revcolevschi. Phys Rev Lett, 91, 047204, 2003
- [3] Iwasa K, Kohgi M, Gukasov A, J. M. Mignot et al.. Phys Rev B Brief Reports 65 (5), 052408, 2002.
- [4] A. Goujon, B. Gillon, A. Gukasov, J. Jetic, Q. Nau, E. Codjovi, F. Varret. Phys. Rev. B., Rapid Comm. 67 (2003) 220401
- [5] M. Aebbersold, B. Gillon, O. Plantevin, L. Pardi, O. Kahn, P. Bergerat, I. von Seggern, F. Tuzek, L. Öhrström, A. Grand, E. Lelièvre-Berna. J. Am. Chem. Soc. 120(1998)5238-5245
- [6] Y. Pontillon, A. Bencini, A. Caneschi, A. Dei, D. Gatteschi, B. Gillon, C. Sangregorio, J. Stride, F. Totti. Angew. Chem. Int. Eng. Ed. 39 (2000) 1786-1788
- [7] B. Gillon, C. Mathonière, E. Ruiz, S. Alvarez, A. Cousson, T. Rajendiran, O. Kahn. J. Am. Chem. Soc. 124 (2002) 14433
- [8] A.F. Schebetov, N.K. Pleshanov, V.M. Pusenkov, B.G. Peskov, G.E. Shmelev, W.H. Kraan, P.T. Por, M.Th. Rekveldt, V.E. Mikhailova: Nucl. Instr..Meth. B94 (1994) 575.
- [9] N.K. Pleshanov, Nucl. Instr.. Meth. A 524 (2004) 273-286.

## H2. G6-1 “MICRO”, A POWDER DIFFRACTOMETER FOR MICRO SAMPLES MEASUREMENTS

I. GONCHARENKO, X. GUILLOU

Leon Brillouin Laboratory,CEA-CNRS, CE Saclay, 91191 Gif sur Yvette, France.

Pressures of about 30-50 GPa (about one tenths of pressure in the center of our planet) can be generated only in a small volume  $<0.1 \text{ mm}^3$  using anvil pressure cells. Study of such small sample is a challenge for neutron techniques. For more than a decade, the G6-1 diffractometer in the LLB was actively used in high-pressure studies. The focusing system, installed in 1996-1998, increased flux at the sample place by order of magnitude, making the G6.1 one of the most powerful “cold” diffractometers in the world. Since 1998, the LLB holds world record in maximal pressure for neutron studies (50 GPa), and the capabilities of our neutron instrumentation and pressure techniques have been demonstrated in various studies of magnetically frustrated systems [1], or magnetic properties of high-pressure oxygen [2].



**Figure 1.** The “hybrid” cell; the latest generation of high pressure cell compatible with X-rays and neutrons.

At the present, the G6.1 undergoes a major reconstruction, which should make it fully optimized for high-pressure studies and keep it competitive with instrumentations installed on the next generation neutron sources. The main features of the upgraded version of the G6.1 (“MICRO”) are:

- 1) supermirror guide before the monochromator;
- 2) monochromator allowing to vary wavelength from 2.3 to 5 Å ;
- 3) focusing system between the monochromator and the sample place
- 4) multidetector covering the optimal solid angle  $\sim 1$  steradian

### NEUTRON GUIDE ENHANCEMENT.

The G6-1 is located in the guide hall of the Orphée reactor. Far from the reactor the fast neutrons and gamma rays background is very low. Measurements at high pressures do not require high resolution. As a consequence, gain in intensity can be obtained using a lower resolution, that is to say a larger divergence of the incident beam. Neutron guide with  $m=2$  supermirror coating provide a double divergence in the horizontal and vertical directions compared to the previous G6  $^{60}\text{Ni}$  guide, and hence a nearly proportional increase of intensity. Monte Carlo simulations have been used to calculate the intensity distribution on the G6-1 monochromator (see fig. 2). They show that a gain of 2.9 in intensity on the monochromator can be achieved.

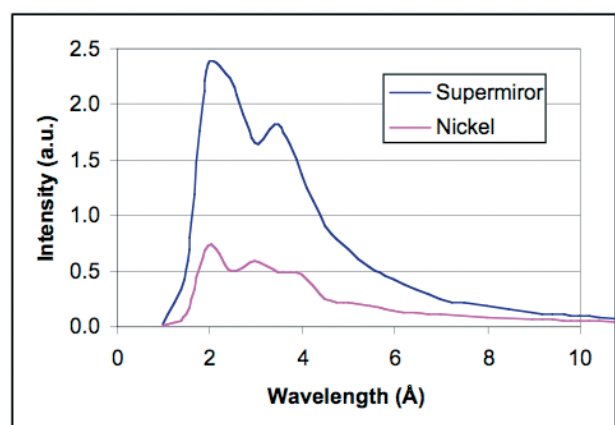


**Figure 2.** Intensity distribution calculated at the G6-1 monochromator for the two guide coatings :  $^{60}\text{Ni}$  (red) and  $m=2$  supermirror (blue).

The replacement of the G6 guide by elements with  $m=2$  supermirror coating has been done by the CILAS company in three steps, and is now completed.

2003: first 2.3 m within the beam plug, starting at 1.45 m from the cold source.

2001: elements between the beam plug and the reactor containment (a length of 9.8 m).

2005: last 23.7 m to the G6-1 monochromator.

All guide elements have been made in BORKRON glass except the last 21 m which have been made of borofloat glass. This provided additional 60% of intensity at the sample place (fig. 3). To take full advantage of the divergence given by the new guide, the G6-1 monochromator has now to be optimized.

## INSTRUMENTATION

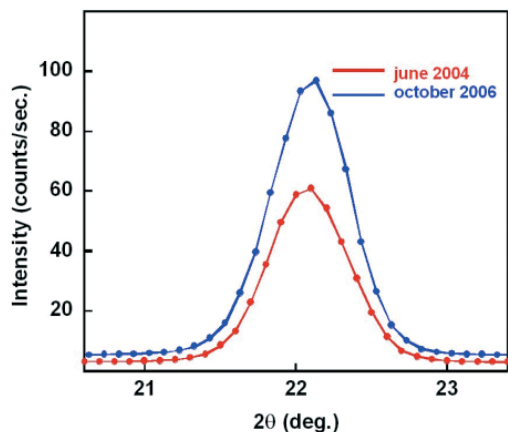


Figure 3. Bragg reflection from zeolite sample before and after the replacement of the guide

## MONOCHROMATOR OPTIMIZATION

The current monochromator used on G6-1 is made of 5 focusing blades of pyrolytic graphite of a mosaic of  $40'$ . Each blade has a height of 3 cm. Made 25 years ago, the maintenance of the focusing system is now difficult. In addition, a 1.6 gain in intensity can be obtained by using 9 smaller blades with a higher mosaic of  $60'$ . This new monochromator will also allow varying wavelength in the wider range  $2.3 < \lambda < 5 \text{ \AA}$  (compare to the present  $4 < \lambda < 5 \text{ \AA}$ ). It had been fabricated in June 2006, will be tested by the end of 2006.

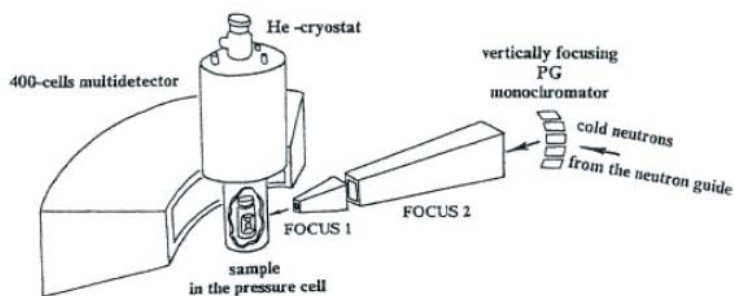


Figure 4. Full setup of the G6-1 instrument

## IMPROVEMENT OF THE FOCUSING SYSTEM

Between the monochromator and the sample a double stage converging guide enables to obtain a maximum density of

neutrons on the sample (see Fig. 4). Made with  $m=2$  and  $m=3$  supermirror coatings, it was optimized for the divergence delivered by the  $^{60}\text{Ni}$  coating of the guide. With a guide made with  $m=2$  supermirror coatings, the mirrors of the converging guide have to be replaced by higher  $m$  coatings in order to make full use of the highest intensity available.

## DETECTOR REPLACEMENT

The solid angle of the current multidetector of the G6.1



Figure 5. Test assembly of 8 linear-sensitive detectors.

(400 cell  $\text{BF}_3$  "banana-type" counter) is only 0.1 steradian. Development of new multidetector, having solid angle by order of magnitude larger than the actual one, is the most crucial part of the "MICRO" project. After taking into account requirements for spatial resolution, efficiency and stability for the new detector, an assembly of 16 linear-sensitive detectors stacked horizontally had been chosen. The detectors ( $2.54 \times 102.4 \text{ cm}$ ) had been fabricated by Reuter Stokes. In October 2005 a prototype assembly of 8 tubes (fig. 5) had been tested at the G6.1 in the real conditions of neutron. Result is presented on fig. 6.

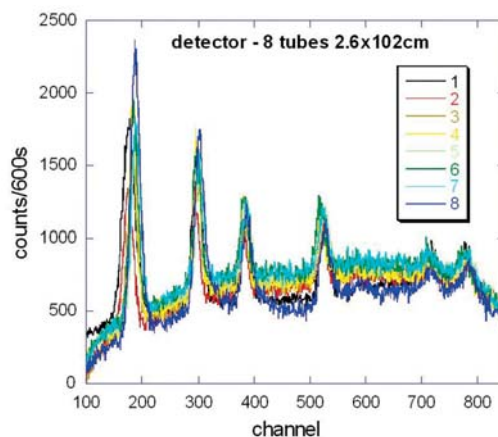
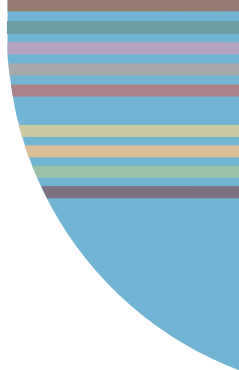


Figure 6. Neutron diffraction patterns collected by every tube of the test assembly at the G6.1.



Every single tube provided 70-90% of intensity of the banana detector, which results in gain in intensity of factor  $\sim 6$  for the 8-tubes assembly, and expected factor of 12 for the final 16-tubes assembly. After the positive results of the test, the work is focused on design and construction of the new supporting table and protection. The detectors will be installed on a translation stage within their protection as reported on fig. 7.

Two different configurations will be available. At 40 cm of the sample, they will provide a high flux, low resolution configuration covering an horizontal angle of  $100^\circ$  and vertical angle of  $\pm 25^\circ$ . Efforts are currently done in setting up of the electronics (fabricated by Mesytec) and developments of appropriate software for collection and treatment of 2-dimensional spectra. First experiments with the final 16-tube detector are expected in 2007.

[1] I. Mirebeau, I. Goncharenko, P. Cadavez-Perez, S.T. Bramwell, M. Gingras, J.S. Garner, *Nature* 420 (2002) 54.

[2] I. Goncharenko, O.L. Makarova, L. Ulivi, *Phys. Rev. Lett.* 93 (2004) 5, 2004 and I. Goncharenko, *Phys. Rev. Lett.* 94 (2005) 20

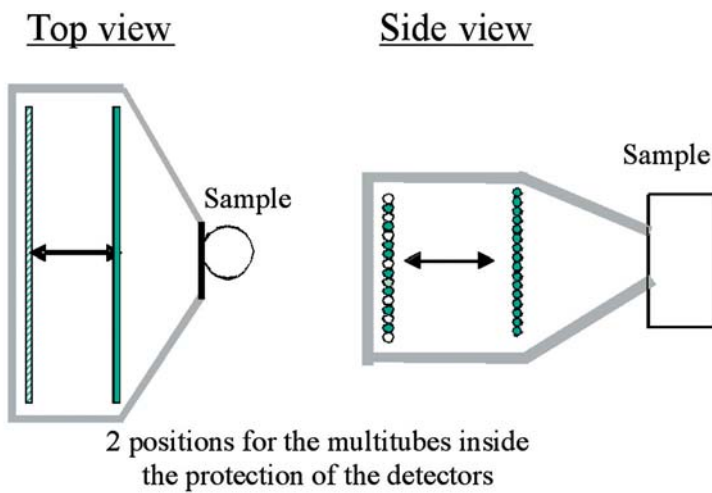


Figure 7. The new 16 tubes detector setup for G6-1.

## H3. NEW SUPERMIRROR COLLIMATORS FOR THE IN PILE COLD TRIPLE AXIS

B. HENNION, P. BOUTROUILLE

Léon Brillouin Laboratory, CEA-CNRS, CE Saclay, 91191 Gif sur Yvette, France.

Neutron optics elements are now commonly used to improve the flux on the instruments. Taking advantage of a maintenance on the 4F thimble, during the summer 2006,  $m=3$  supermirror have been installed in the collimators of the 4F1 and 4F2 beam ports which feed two cold neutron triple axis. An expected gain of intensity on the sample up to 80% for some experimental conditions is foreseen.

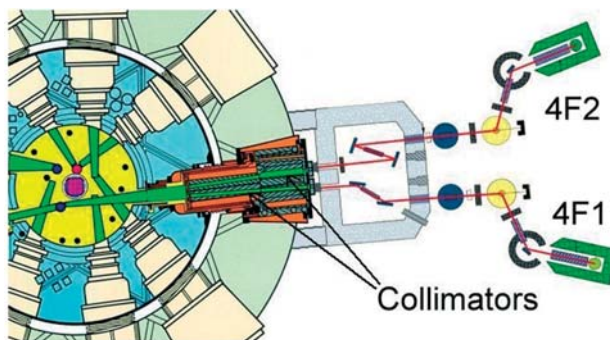


**Figure 1.** Setup of 4F1 4F2 cold triple axis spectrometers around the Orphée reactor.

Thimbles of beam ports are submitted to high radiation damages. They modify the metallurgical properties of the alloy which becomes more fragile. An important part of this effect is due to transmutation of aluminum atoms in silicon. As a consequence, thimbles have to be changed before the amount of Si in the Al alloy becomes larger than a known limit. This limit is close to be reached by the 4F thimble which has to be replaced. This is a long and delicate operation which requires the removal of 4F beam plug and the whole 4F1 and 4F2 spectrometers.

This is a unique opportunity to change the collimators inserted within this beam plug (see fig. 1) since the flux available on the 4F1 and 4F2 instruments is very dependant upon the geometry of these collimators. Such a modification has already been done in 1999 on the channel 2T [1] where an increase of the size of the beam plug collimators did provide a gain in intensity of 80%. However, an increase of

the mean gamma radiation level on the 2T area has been notice afterwards.

During these last years, tremendous progress have been done in supermirrors neutron optics elements [2]. They provide a way to transport more neutrons through the beam plug collimators without having to change their size, and hence without changing the radiation protection provided by the beam plug. Supermirrors are especially efficient with the cold neutrons used on the 4F spectrometers. This is why we have chosen to insert  $m=3$  supermirrors in the beam plug collimators without changing their size (see fig. 2).

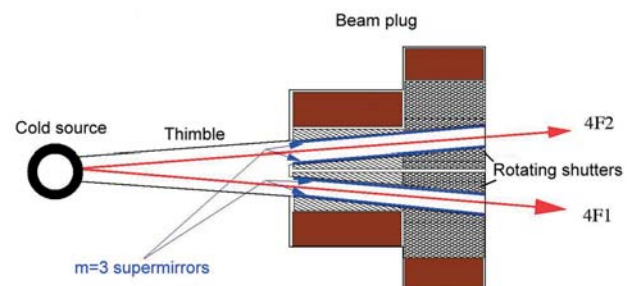


**Figure 2.** Schematic view of the cold source, thimble and beam plug assembly.

$M=3$  supermirrors enable the transmission of neutrons which hit the mirrors up to angles of  $0.3 \cdot \lambda$  degrees, ( $\lambda$  being the wavelength of the incident neutron in angstroms). Compared to collimators without guides, they allow a transmission of a larger divergence, and provide a higher flux on the monochromator.

Simple ray tracing simulations have been performed in order to obtain an estimation of the gain provided by the supermirrors. A source of equal and homogeneous intensity has been assumed. These simulations enable to obtain an estimation of the loss of angular resolution and energy resolution due to the increase of divergence of the incoming beam on the sample.

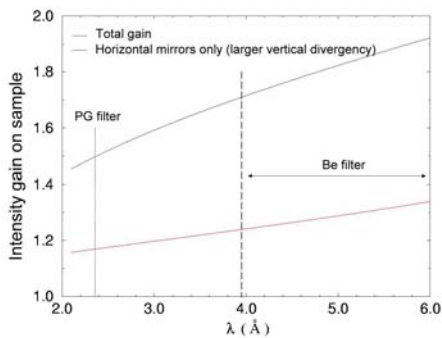


**Figure 3.** Calculated gain with supermirrors as a function of wavelength in two different configurations (see text).

Two different configurations have been taken into account :

**a.** Install only horizontal mirrors at the top and bottom part of the collimators (increase only transmitted vertical divergence).

**b.** Mirrors installed on the 4 sides of the collimators (increase transmitted vertical and horizontal divergence)

Results of the expected flux gain compare to the current collimators without mirrors are presented on Fig. 3.

It shows that horizontal mirrors (configuration **a**) bring only a gain of 20% in intensity (red curve). This comes from the fact that the current height of the beam (8 cm) provides already the transmission of a divergence of 5°. M=3 supermirrors just add an additional 0.9° at 3 Å. However, this gain is obtained with a negligible loss in resolution.

Configuration **b** with horizontal and vertical supermirrors in the beam plug is more interesting since it provides a potential gain varying from 40% at 2 Å to 90% at 6 Å. The corresponding energy resolution degradation has been calculated to be 15% at maximum. For most of the inelastic experiments performed on these spectrometers this is an acceptable degradation.

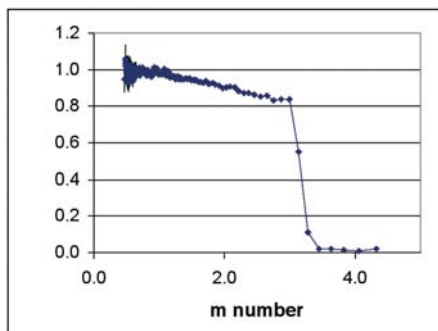


**Figure 4.** Neutron reflectivity measurement of one of the supermirrors inserted in the beam plug.

Our rotating shutters offered 3 different positions. In order to be able to perform high flux or high resolution experiments, we have chosen to install the 3 following configurations :

- High flux : Horizontal and vertical supermirrors m=3
- Intermediate : 40' collimators without mirrors
- High resolution : 15' collimators without mirrors

Supermirrors have been purchased from the Mirrotron company, and collimators from the GMI-STEEM company. Supermirrors have been deposited on float glass substrate which is known to sustain high irradiation damages without degradation. The reflection quality of each mirror has been checked before being inserted in the beam plug. A typical measurement is represented on fig. 4. They show up a reflectivity coefficient above 80% at m=3.

Mirrors have then been carefully aligned, and inserted in the

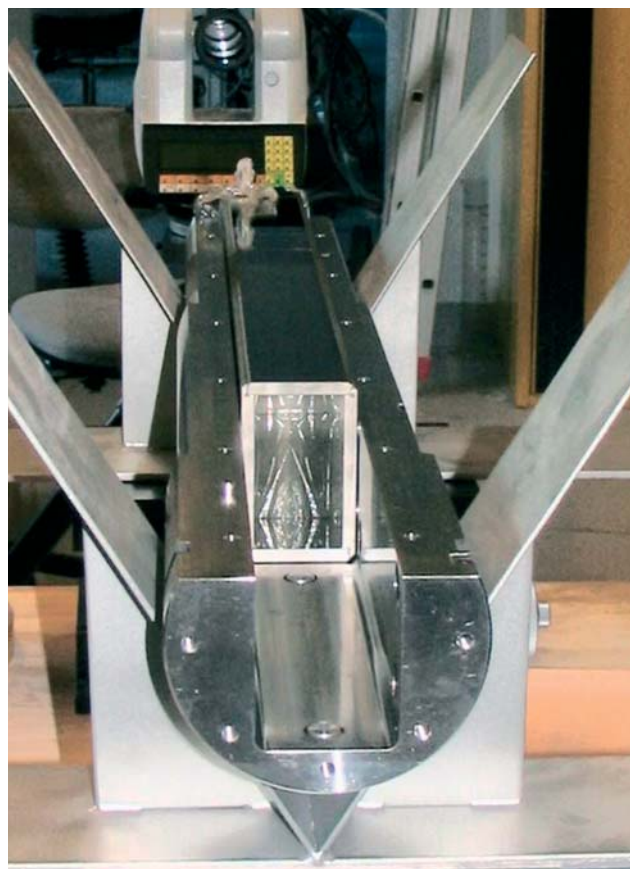


**Figure 5.** Alignment of the mirrors in the collimator

beam plug in July 2006 (fig. 5). At the restart of the reactor, test measurements will be performed. They will have to show that, no significant increase of the gamma radioactive background is present, and validate the calculated gain of flux on the sample. If deviation to the predictions will be detected, we will take the opportunity of the second part of the maintenance of 4F thimbles that will occur in summer 2007 to apply corrective actions.

[1] LLB Scientific report, 1999-2000 p.108-113

[2] O. Elsenhans, P. Boni, H.P. Friedli, et al., Thin Solid Films, 246 (1994) 110-119.

## INSTRUMENTATION

**[Cl. F. Damay] Upgrade of the 3T2 High Resolution Powder Diffractometer**

Research on novel materials of technological interest is an ever expanding area which requires fine structures determination to fully understand and tailor materials properties. Examples in ionic conductors, solid electrolytes, catalysers, high temperature superconductors or magnetic semiconductors can easily be found. Neutron powder diffraction plays a key role in these fields, because it provides an easy way to locate light atoms and to determine an existing magnetic order.

LLB proceeded mid-2005 to an important upgrade of the detection module of the 3T2 high resolution powder diffractometer. Electronics has been replaced by new LLB elements and the spectrometer is now equipped with an array of 50 new  $^3\text{He}$  large detectors and 50 new collimators made by the EuroCollimators Ltd company, which provide a resolution of  $10'$ . Tests show that a gain of 2.5 in the overall detection efficiency has been achieved compared to the previous 3T2.

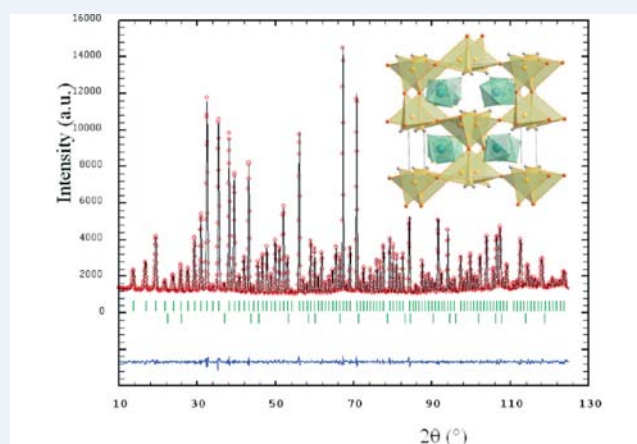
The next objective now is to reduce the background noise in order to get high quality data with smaller quantities of sample. To this purpose, additional neutron shielding has been designed and will be installed at the end of 2006.

This project has been financed partly by the "Région Aquitaine".

[Contact: F.Damay, F.Bourée, B.Rieu, LLB]



View of the new bank of 50 detectors



Na<sub>2</sub>Ca<sub>3</sub>Al<sub>2</sub>F<sub>14</sub> measured with the new 3T2

**[C2. S. Desert] A double super-mirror monochromator for the new Very Small Angle Neutron Scattering spectrometer (TPA, Très Petits Angles)**

On TPA, the very small scattering vector  $2.10^{-4}\text{\AA}^{-1}$  is accessible by using a very high resolution (pixels of  $150\ \mu\text{m}$ ) image plate detector located only 6 m far from the sample. Due to the high sensitivity to  $\gamma$  radiation of such detector, a conventional velocity selector cannot be used as monochromator because its neutron absorber, Gd, is a strong  $\gamma$  emitter. Instead, a new monochromator (figure 1) composed of two super mirror monochromators (critical angle  $m=3$ ,  $\Delta m/m=0.15$ ) is now installed on TPA. The wavelength selection is achieved with the mirrors angle  $\theta$ , according to  $\lambda = \theta / (m\theta_c)$ , where  $\theta_c$  is the critical angle for ordinary Ni. Both mirrors are mounted on rotations, the second one being also mounted on a translation stage in order to keep the outgoing monochromatic beam at a fixed position when changing the wavelength. This monochromator has a good transmission ( $\sim 70\%$ ) while avoiding the strong  $\gamma$  emission and a direct view of the guide. Figure 2 shows Time of Flight measurements of various wavelengths obtained with this new kind of monochromator. The resolution is constant:  $\Delta\lambda/\lambda=0.11$ .

[Collaboration: V. Thévenot, A. Gabriel, P. Permingeat, S. Désert, A. Brûlet, LLB; J. Oberdisse, LCVN, Montpellier]

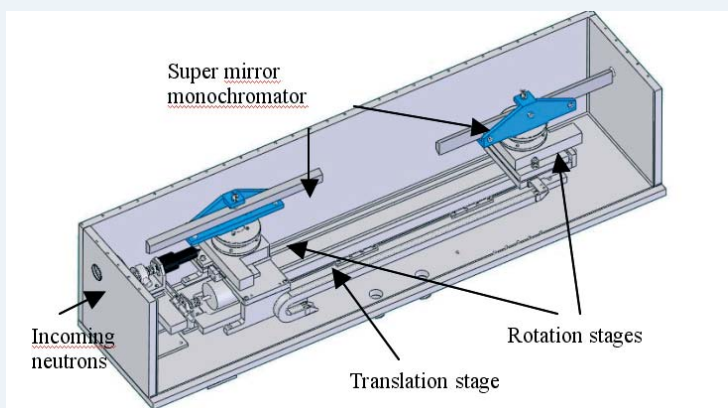


Figure 1. Drawing of the monochromator

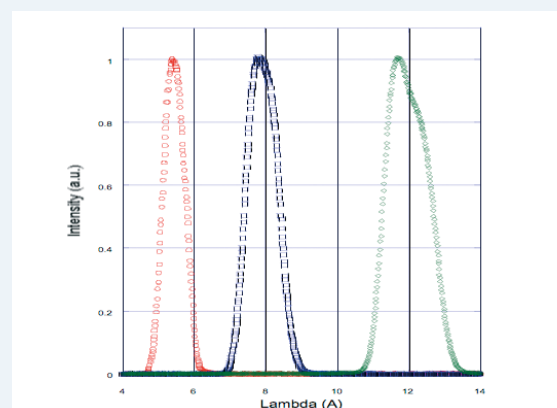


Figure 2. Raw TOF measurements of monochromated beams

**[C3. S. Desert] Multi beam collimator prototype for the new Very Small Angle Neutron Scattering spectrometer (TPA, Très Petits Angles)**

The very small scattering vector expected for TPA,  $q_{\text{min}}=2.10^{-4}\text{\AA}^{-1}$ , will be achieved by using a tiny collimation. Indeed, the collimation for TPA requires 1.8 mm and 1mm diameter pinholes at the collimator entrance and exit. The drawback of the latter is the huge loss of neutrons. In order to enhance the effective neutron beam used, a multi beam prototype collimator has been built and successfully tested. It features 7 individual masks (figure 1), made from  ${}^6\text{Li}$  in an epoxy matrix, with 51 pinholes per mask. These masks are defining 51 beams converging on the detector while absorbing the unwanted neutrons (i.e. not focusing on the detector). Measurements comparing a simple collimation and the multi beam prototype with 16 pinholes show a gain in flux of 12. The advantage of such a setup is its flexibility regarding the wavelengths. Indeed, the fall of neutron due to gravity is not negligible compared to the pinhole diameter of 1 mm at the collimator exit ( $20\ \text{\AA}$  neutrons fall 2 mm after 4m path). The masks are mounted on translation stages to take into account for the gravity and thus only one setup is required for all the wavelengths. A multi slit prototype (used for isotropic scattering samples) is currently being manufactured and should improve the gain by a factor of 60 compared to the pinhole multi beam prototype. Deconvolution should then be achieved to get the true scattering curve.

[V. Thévenot, S. Désert, A. Brûlet, LLB]



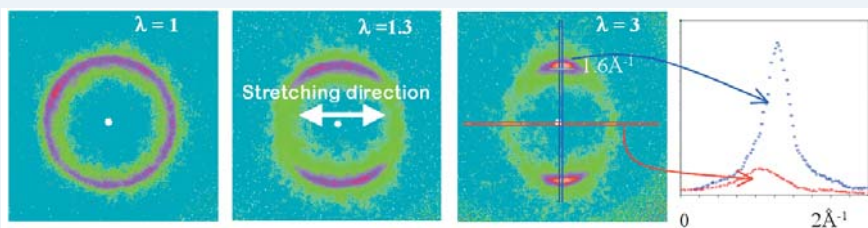
Figure 1. Picture of the prototype multi beam collimator with 7 masks

## INSTRUMENTATION

**[C4. P. Baroni] New developments for 2D High Resolution Neutron Scattering Experiments. Application case and experimental evidences from crystals to polymer science.**

We present here a new type of 2-dimensional neutron detector (CNRS CEA patent **WO2006095013** – publication date: 2006-09-14), allowing a high resolution investigation of the scattering space including both large to small angles. This new system being almost insensitive to most radiations ( $\gamma$ , X radiation and visible light) except neutron radiation, is particularly adapted to the detection of neutron scattering or neutron diffraction, without exhibiting memory effects. Combining the advantages of the high resolution and of a 2 dimensional integrating readout, this new instrumental development appears as a reliable, efficient and evolutionary setup which could extend the possibilities of time-resolved experiments in this research field. An example of illustration of structural investigations carried out using this new system is displayed below. It is an original study at two-dimensions of the effect of an uniaxial mechanical deformation (elongational stress  $\lambda = L/L_0$  where  $L_0$  is the initial sample length) on the structure of a bulky sample of polytetrafluoroethylene (PTFE). The experiment points out different effects with respect to the stress, which can be interpreted by the uncorrelated contributions of the crystalline and of the amorphous parts respectively. The experimental conditions are: wavelength=  $2.85\text{\AA}$ , sample-detector distance: 53.5mm, exposure time: 5 min, beam diameter: 3mm, 16 bits data.

[P. Baroni and L. Noirez, LLB]

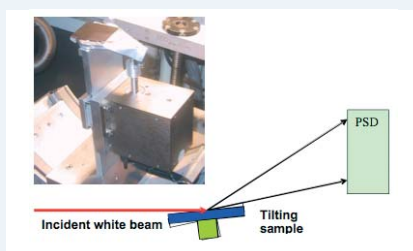


2D-Diffraction patterns displayed at 3 elongation rates ( $\lambda=1, 1.3$  and  $3$ ) by the IV phase of the PTFE, observed from  $0.05$  to  $2.2\text{\AA}^{-1}$ . The fourth figure shows the vertical (blue points) and the horizontal (red points) profiles of the anisotropic scattering corresponding to the elongation rate ( $\lambda=3$ )

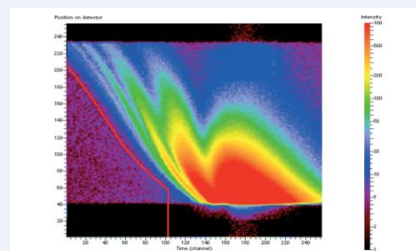
**[C5. F. Ott] TilTof a high intensity space-time reflectometer**

Being able to measure reflectivities down to  $10^{-9}$  is the challenge of neutron reflectometers for the 21<sup>st</sup> century. The use of a periodic tilt of the sample, coupled with a position sensitive detector enables to perform specular reflectivity measurements on continuous neutron sources without any monochromator or chopper and thus allows intensity gains up to 10 compared to conventional reflectometers. The implementation consists in modulating the incidence angle of the beam by a periodic **Tilt** of the sample of a few degrees at a frequency of the order of 20 Hz. At each time, the sample reflects the neutron white beam at a different angle. The reflected beam arrives at a different position on the detector. The time of flight (**Tof**) from the sample allows wavelengths separation, and as a result, the full reflectivity curve is measured in each detector cell. The duty cycle of such a reflectometer is only limited by the velocity of the sample movements and may exceed 90%. We have performed the first measurements on a simplified setup (40% duty cycle) installed on the EROS reflectometer. Results show that the expected intensity gain has been obtained. However, mechanical instabilities conduct to poor resolution. In addition, off specular scattering from the sample gives a high unexpected background. A new version of Tilttof with less vibrations and equipped with a synchronized slit after the sample to cut background is under development to solve the two problems encountered.

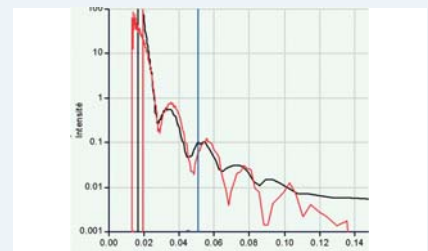
[F.Ott, A.Menelle, ICNS 2005]



Principle of TilTof and implementation on Eros



TilTof measurement of a Cu layer on silicon. X axis is time channels, Y axis is position on the detector.

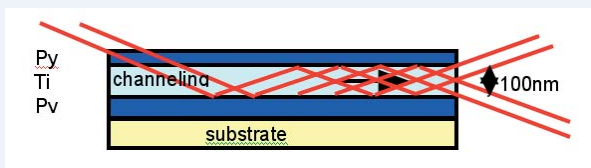


Reflectivity obtained on Eros with TilTof (black) or with the usual chopper configuration (red).

[C6. S.V. Kozhevnikov] **Magnetic neutron waveguides**

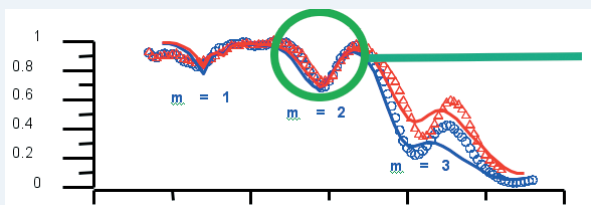
In order to produce submicron neutron beams, we are developing neutron waveguides (NWG). The large magnetic neutron cross section allows to fabricate guides in which the optical index can be dynamically modulated. We produced NWG with the tri-layer structure: Py(10-20nm)/Ti(10-70nm)/Py(10-50nm)//glass. The top Py layer acts as the coupling layer with the incident beam, the Ti layer acts as the guiding layer and the bottom layer acts as the reflecting layer (see Fig. 1). We have characterized our systems by polarized neutron reflectometry (specular and off-specular) in order to probe the effect of the different imperfections (interface roughness, magnetic non-collinearity, dispersion of the layers thickness) on the reflectivity. We show that it is possible to guide up to 30% of the incident neutrons. This corresponds to a flux density of  $10^8$  n/cm<sup>2</sup>/s at the waveguide exit.

[Collaboration: S.V. Kozhevnikov, aFrank Laboratory of Neutron Physics, Dubna, F. Ott, LLB, E. Kentzinge, , Forschungszentrum Jülich]

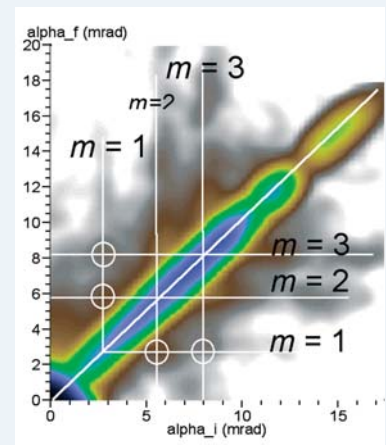


Diffuse off-specular scattering on a waveguide structure.  
The resonance modes in grey.  
(measured on HADAS)

Localization of the wavefunction in the NWG.



Specular reflectivity  
up to 30% of the incident neutrons are trapped in the guide









# THEORY

# LABORATOIRE LÉON BRILLOUIN

# THEORY

The theoretical activity at LLB for the last few years can be divided into three parts.

One activity is concerned with fundamental developments in the field of non linear physics [**C1**, **S. Aubry**] with application to different fields.

One example is the suggestion of a possible implication of polarons in the transmission of a long distance electromechanical signal in regulatory enzymes (in collaboration with enzymologist G.Hervé).

Another example is the suggestion of a new mechanism concerning the origin of sonoluminescence (in collaboration with B. Dey). In this scenario sonoluminescence is produced by the tremendously large adiabatic pressure pulse (shock wave) generated by the close to supersonic impact of the fluid on the hardcore bubble and the light flash is emitted by the fluid surrounding the bubble.

The second one is concerned with the field of strongly correlated electron systems and mainly with the fundamental development of a theory of high Tc superconductors [**C2**, **F.Onufrieva**].

The asymmetry between hole-doped and electron-doped cuprates has been explained on the basis of the existence of two different topological quantum critical points monitoring the change of Fermi surface when doping is varied. In particular one consequence is the very small q width of the antiferromagnetic dynamical spin response in electron-doped cuprates observed by neutron scattering.

For the mechanism of superconductivity the role of spin fluctuations is emphasized and quantitative calculations have been achieved which are based on the spin fluctuation spectrum obtained by neutron scattering with the presence in the superconducting state of a spin exciton mode close to the antiferromagnetic wave vector. The most interesting results obtained recently in 2006 are the rather high value of the maximum superconducting gap close to that observed experimentally and the symmetry of the order parameter which is of the d-wave type but with large deviations from the pure d-wave symmetry with an antinodal part gap quite different from the nodal part gap as seen experimentally by photoemission and Raman scattering.

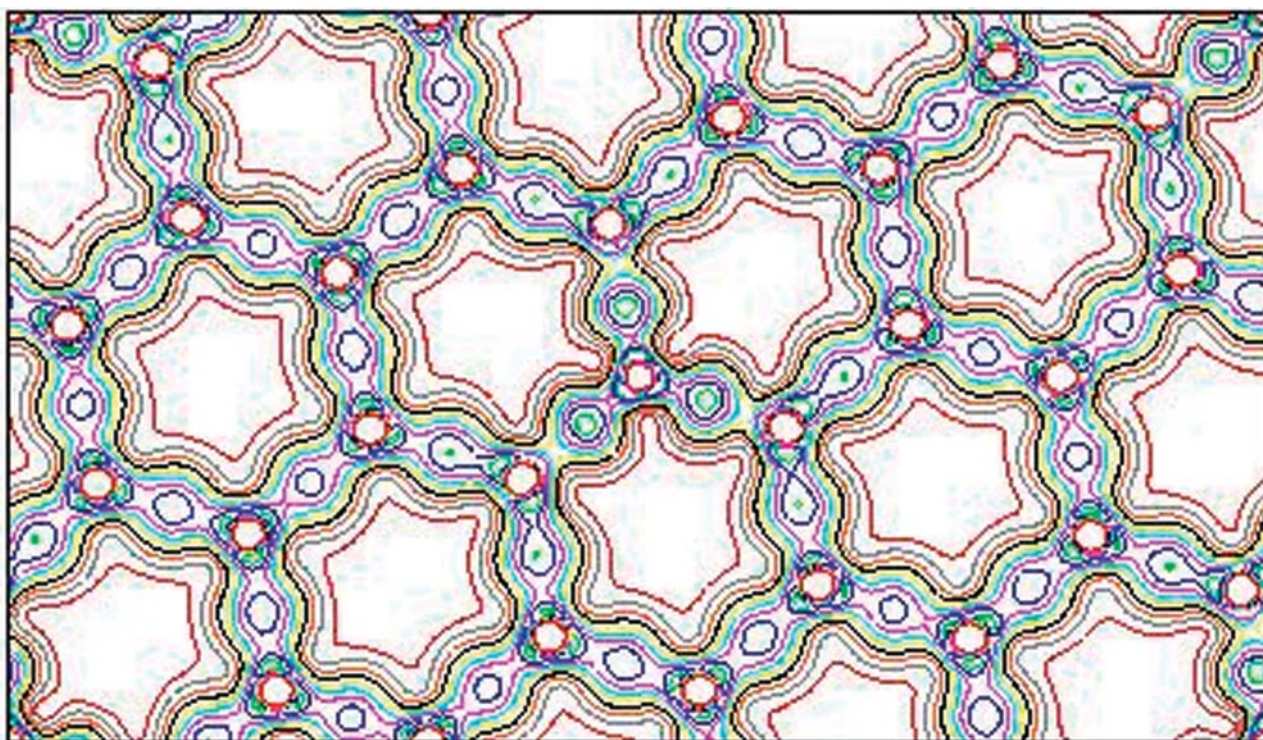
Another development by H.Moudden [**C3**, **H. Moudden**] concerns the physics of the novel superconductor MgB<sub>2</sub> with the study of the effects of carbon substitution on the superconducting properties from realistic ab initio calculations.

The third one by G.Kneller and K.Hinsen [**C4**, **G. Kneller**] is concerned with simulation studies of brownian and fractional brownian dynamics with application to the study of the dynamics of proteins in relation to quasielastic neutron scattering developed at LLB.

A new approach has been developed to describe the relaxation dynamics of proteins. A theoretical model such as the fractional brownian dynamics has been used to study the dynamics of proteins and to connect the dynamical events seen on the pico-nanosecond time scale, accessible to quasielastic neutron scattering, to the functional dynamics of proteins on much longer time scales of the order of the millisecond.

The combined simulation and neutron scattering studies of proteins in solution under hydrostatic pressure, have been started in collaboration with M.C. Bellissent in the framework of the thesis of V. Hamon and currently continued as part of the thesis work of P. Calligari

# THEORY



[C1. S. Aubry] About the Origin of Sonoluminescence

[C2. F. Onufrieva] Magnetic and Electronic properties of the High-Tc Cuprates: from electron- to hole- doping.

[C3. H. Moudén] Effects of Carbon Substitution on Magnesium Diboride : Ab Initio Study

[C4. G. Kneller] Relaxation dynamics and quasielastic neutron scattering in proteins from the model of fractional brownian dynamics

### [C1. S. Aubry] About the Origin of Sonoluminescence

Some liquids (typically water), submitted to intense ultrasounds (at typically 40 kHz), may emit broadband light (sonoluminescence) over frequencies ranging from IR to UV. It has been proven experimentally that sonoluminescence is generated by stable spherical microbubbles (of the order of  $\mu\text{m}$ ) of some insoluble gas (typically rare gas). The radius of those bubbles oscillates at the frequency of the driving ultrasound. When the pressure amplitude of the ultrasound field becomes larger than a certain threshold (typically 1B), the gas in the bubble reaches its minimum Van der Waals volume and there is a radial impact of the fluid onto the core of the bubble. This situation occurs at radial bubble velocities comparable to the sound velocity in the liquid. During this sharp impact which lasts few 100 ps, the flash of light which produces sonoluminescence, is emitted. The most frequent interpretation of this phenomena is that the energy of the shock wave generated at the impact focuses and diverges at the bubble center (in quasilinear theories) which should generate a plasma at a very high temperature emitting the light flash. It was even argued that nuclear fusion could be generated in that way. However, this interpretation is ruled out by some crucial experiments for example by the fact that near threshold, sonoluminescence becomes dim with a spectrum shifted toward IR which moreover is much more pronounced with deuterated water. Up to now the physical origin of this phenomena remains an enigma.

We suggest a new interpretation for this phenomena. Shockwaves which are generated by quasisupersonic impacts becomes tremendously nonlinear. We prove in that conditions with rigorous arguments only based on mass conservation and the existence of a Van der Waals minimum volume that energy focusing cannot occur at the bubble center. A compacted sphere appears right after the impact which includes the compacted gas of the bubble but also and mostly a part of the surrounding liquid. The pressure and temperature inside becomes very high but remains spatially rather uniform. The radius of this compacted sphere expands up to few minimum bubble radius while its pressure and temperature simultaneously drops very fast. Next the pressure profile in the liquid continues to evolve but as a standard quasi linear pressure pulse which radially propagates and decays. It is also proven that the sound velocity in the liquid of that highly compacted sphere, is enhanced by a factor  $\lambda$  near unity at weak impacts but which suddenly increases as soon the impact becomes close to supersonic. It may easily reach one or several order of magnitudes in the experimental conditions. Thus beyond a certain threshold, this Grüneisen coefficient  $\lambda$  becomes large, so that the frequency spectrum of the thermal radiation of the compacted liquid and gas is strongly dilated from IR toward UV while its temperature is (adiabatically) increased by the same factor  $\lambda$  (which correspond to a power of the thermal radiation increased by  $\lambda^4$ ). The sonoluminescent light flash is thus due to the intense thermal radiation of this compacted sphere (which is mostly composed of the liquid surrounding the bubble) during the short time of its existence.

[B. Dey and S.Aubry Physica D 216 (2006) 136-156 ]

---

### [C2. F. Onufrieva] Magnetic and Electronic properties of the High-Tc Cuprates: from electron- to hole- doping.

We have shown that a basic difference between electron- and hole- doped cuprates is their proximity to two different topological quantum critical points (QCP's), one related to saddle point electrons and relevant for hole-doped Cuprates and the other related to nodal electrons and relevant for electron-doped cuprates. This has consequences for both magnetic and electronic properties.

#### 1. Spin dynamics

We have shown [1] that the striking features observed recently in the electron-doped cuprates (neutrons), the extremely narrow  $q$  width and very low spin gap, are consequences of the proximity to the "nodal" quantum critical point while the resonance peak that is a remarkable property of the hole-doped cuprates (also observed by neutrons) is a consequence of the proximity to the "saddle point" quantum critical point.

#### 2. Electronic properties:

We have shown [2] that the presence of these QCP's imposes strong constraints on electronic properties in the cuprates. One of the consequences is the existence of the electron pseudogap of density wave origin, large pseudogap, that increases towards low doping from both sides, electron- and hole- doping. The qualitative behaviour and even absolute values of the pseudogap are in a good agreement with experiment (ARPES, optical conductivity etc.). Another effect is the existence at low doping of a second pseudogap, one order of magnitude smaller (at  $T=0$  it becomes a true gap). This small gap also increases towards zero doping and could explain the recent ARPES observation of the small gap observed for both electron and hole doping in the whole Brillouin zone. The most interesting feature is the existence at low doping of a specific insulating state different from the Mott-Hubbard (MH) insulator. It is characterized by a small chemical potential jump (much smaller than in the MH insulator), this feature is close to that observed experimentally.

[Collaboration: F.Onufrieva et P.Pfeuty, LLB]

[1] F.Onufrieva and P.Pfeuty Phys.Rev.Lett. 92 247003 (2004).

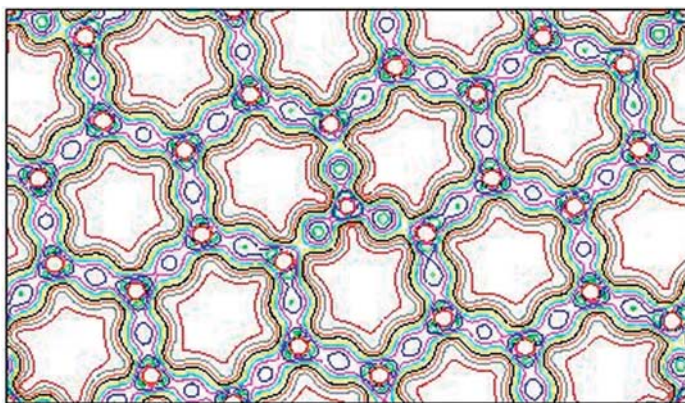
[2] F.Onufrieva and P.Pfeuty Phys.Rev.Lett. 95 207003 (2005).

## THEORY

**[C3. H. Moudden] Effects of Carbon Substitution on Magnesium Diboride : Ab Initio Study**

MgB<sub>2</sub> is now widely considered as a non-cuprate high T<sub>c</sub> superconductor for which the electron-phonon coupling is unambiguously determined as the main ingredient in the mechanism of its high T<sub>c</sub>. But many aspects such as the presence of multi-bands, low concentration of holes and two-dimensionality could be important as well. The C-substitution revealed many new features including the presence of two regimes of T<sub>c</sub> depression, and strong enhancement of the critical field. These features are currently under intense research. I made numerical simulations of the C-doping effects [A.H. Moudden, J. Phys. Chem. of Solids 67(2006)115], using super-cells method for high doping, larger than 7% (figure), and recently using the virtual crystal approximation VCA, for doping smaller than 5%. The electronic structure, the Fermi surface, the density of states and the lattice dynamics have been determined carefully within the density functional theory with all electrons and full potentials. Strong electron-phonon coupling could be determined by pseudo-potential codes only. These quantities were then used in the Eliashberg strong coupling approach of superconductivity [G.A. Umbarino et al. Phys. Rev. B.71, 134511(2005)] with some success in describing the C dependence of T<sub>c</sub>. The role of inter band scattering and Coulomb screening remain under active investigation.

[Collaboration: A.H. Moudden , LLB,G.A.Umbarino et al. Politecnico di Torino ]



Valence electron redistribution near the doped C at the centre:  
Hexagonal Super-cell  $\sqrt{7} \times \sqrt{7}$

**[C4. G. Kneller] Relaxation dynamics and quasielastic neutron scattering in proteins from the model of fractional brownian dynamics**

The non exponential relaxation in a complex system like a protein can be described by the **fractional brownian dynamics** of a single particle. Such a model describes a protein on a coarse grained scale and localised motions cannot be described within such a model. The fractional brownian dynamics which has absolutely no characteristic time scale is certainly an idealized mathematical model of a physical system which has a very broad but limited distribution of relaxation times. The simulation study that we performed for **lysosyme** revealed a signature of fractional Brownian dynamics in the collective dynamics of the protein. The concept of fractional brownian dynamics leads to the introduction of generalized lorentzians which describe empirically the very broad quasielastic neutron scattering spectrum obtained from internal protein dynamics. The study of the average mean square displacement of the atoms in **lysosyme** has shown that fractional brownian dynamics models may be used to extrapolate the dynamics in a certain way to very long time scales. In this respect these models describe the slow relaxation processes. Thus the extrapolation of the properties of these models in combination with computer simulations can help to study the slow relaxation processes in proteins in particular to establish a signature of protein function.

These type of models we have introduced help to connect the **rapid** dynamics seen by **Quasielastic Neutron Scattering** to the **slow** dynamics more characteristic of the of the protein

[G.Kneller, Phys. Chem. Chem. Phys., 2005, 7, 2641-2655]









# EXPERIMENTAL AND USERS PROGRAMS

# LABORATOIRE LÉON BRILLOUIN

We present in this section the main facts and figures related to beam statistics and users activity of the Orphée-LLB facility in 2005-2006.

### Beam statistics 2005-2006:

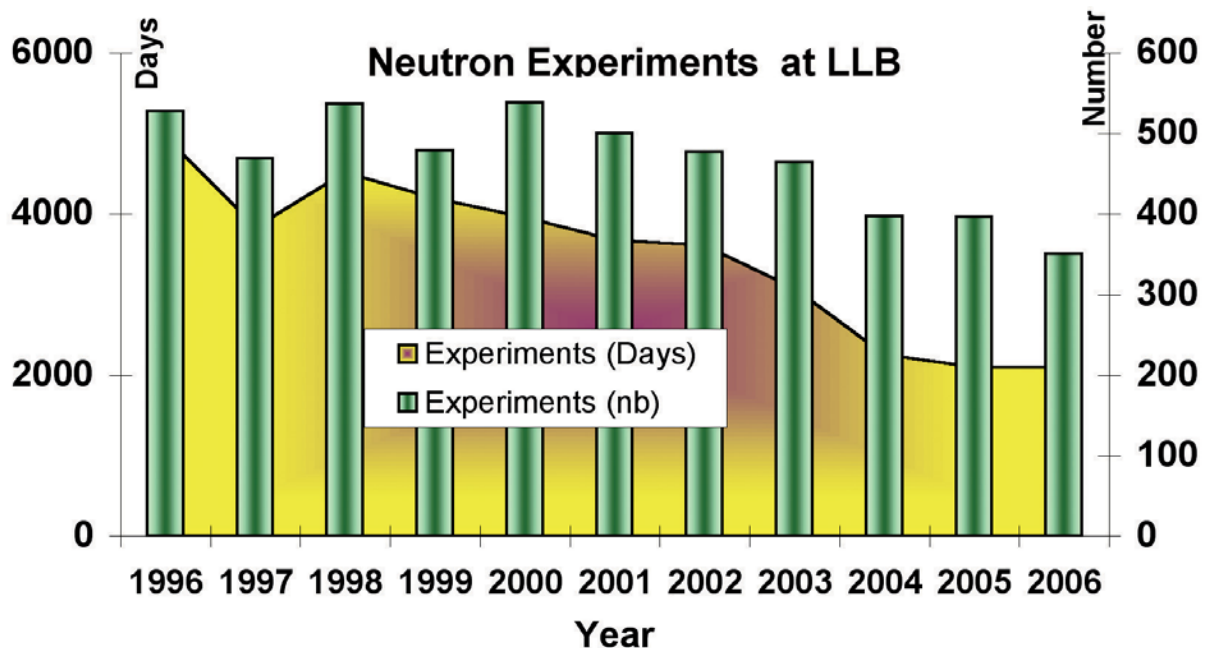
Table 1 summarizes the LLB-Orphée performance during the last 8 years. The first line shows the operation days established by the Associates Agreement (CNRS and CEA). Because of severe budget cuts, a significant reduction of the operation days took place in 2004 and 2005. Fortunately, from 2006, the situation is different: The new CEA-CNRS Agreement represents a return to normal working conditions (a minimum of 180 days per year). This agreement was effective on January 2006 for 5 years.

The second and third lines of table 1 summarize the real number of working days (FPED, Full Power

Year	1999	2000	2001	2002	2003	2004	2005	2006
CEA CNRS Agreement	210	210	180	180	180	114	114	180
Reactor Days (EFPD)	205	213	186	183	163	118	112	123
% Availability	97,6	101,4	103,3	101,7	90,6	103,5	98,2	68,3

Equivalent Days) and the availability of the facility. For 2006, the FPED will be 123 instead of 180 because a technical breakdown occurred in the Orphée reactor after the long summer shutdown.

Table 1



Operation of the LLB-Orphée facility for the last 8 years.

Figure 1

Number of experiments (green bars and right side scale) and experiments days in the LLB spectrometers (yellow curve and left side scale) performed at the facility during the last 10 years. Both curves show the same evolution than the FPED of table 1.

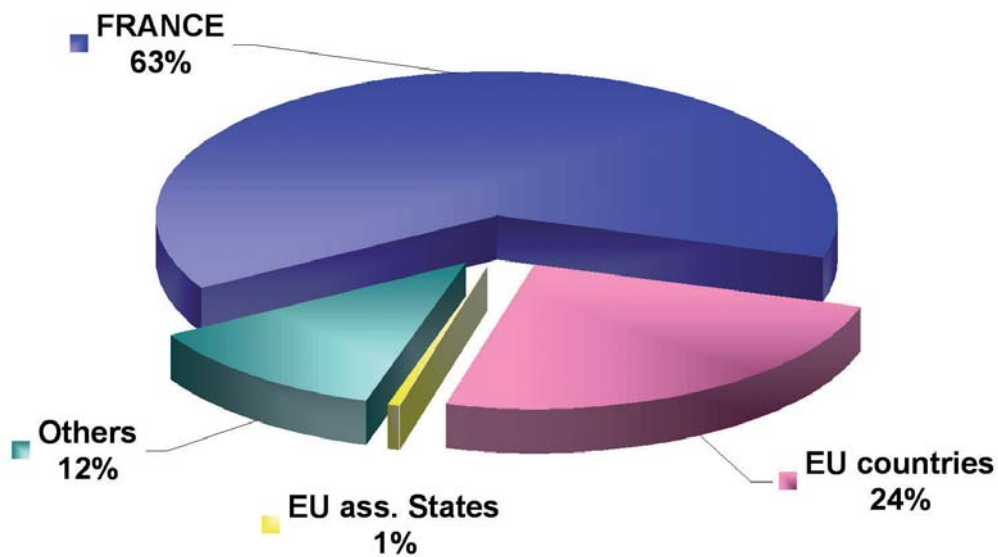
## EXPERIMENTAL AND USERS PROGRAMS

## Beam time allocation

Proposals for experiments are selected through a peer review. Selection Committees (SC) are composed by high level scientists from France and European Countries. Details are given in the subsection "Selection Committees". The SC meet twice a year (typically spring and fall). The composition of the SC which will take place the 4th and 5th December 2006, is given at the end of the section.

The following series of figures summarizes the statistics of the beamtime allocation at the LLB corresponding to the four SC previous meetings (Spring 2005 - Fall 2005 - Spring 2006 - Fall 2006). Figure 2 and table 2 summarize the distribution amongst the different countries of beamtime allocat-

### Nationalities of the beamtime allocation at LLB in 2005-2006



ed by the 4 SC meetings from Spring 2005 to Fall 2006.

Figure 2

Beam time allocated at the LLB-Orphée facility by the four SC meetings from Spring 2005 to Fall 2006, as a function of the National affiliation of the users involved in the accepted proposal.

Country	number of proposals 2005-2006	number of experiments accepted 2005-2006	beamtime requested (days)	beamtime allocated (days)	beam time requested (%)	beamtime allocated (%)
FRANCE	620	514	4811	2794,5	59,9%	63,1%
<b>FRANCE</b>	<b>620</b>	<b>514</b>	<b>4811</b>	<b>2794,5</b>	<b>59,9%</b>	<b>63,1%</b>
Germany	100	75	737	434,5	9,2%	9,8%
United Kingdom	35	27	242	135	3,0%	3,0%
Poland	32	18	266	130	3,3%	2,9%
Italy	45	29	249,5	123	3,1%	2,8%
Spain	13	10	90	50	1,1%	1,1%
Others (1)	71	46	463	207	5,8%	4,7%
<b>EU countries</b>	<b>296</b>	<b>205</b>	<b>2047,5</b>	<b>1079,5</b>	<b>25,5%</b>	<b>24,4%</b>
Israel	4	4	28	22	0,3%	0,5%
Others (2)	3	2	26	12	0,3%	0,3%
<b>EU ass. States</b>	<b>7</b>	<b>6</b>	<b>54</b>	<b>34</b>	<b>0,7%</b>	<b>0,8%</b>
Russia	31	24	288	155	3,6%	3,5%
United States	36	18	378	124	4,7%	2,8%
Japan	13	13	107	89	1,3%	2,0%
Australia	13	9	103	56	1,3%	1,3%
Others (3)	32	19	247	99,5	3,1%	2,2%
<b>Others</b>	<b>125</b>	<b>83</b>	<b>1123</b>	<b>523,5</b>	<b>14,0%</b>	<b>11,8%</b>
<b>TOTAL</b>	<b>1048</b>	<b>808</b>	<b>8035,5</b>	<b>4431,5</b>	<b>100%</b>	<b>100%</b>

(1) Belgium, Hungary, Sweden, Czech Rep., Austria, Greece, Portugal, Slovakia, Slovenia, Bulgaria, The Netherlands, Denmark, Finland, and Romania

(2) Switzerland and Norway

(3) Tunisia, China, Canada, Algeria, India, Ukraine, Brazil and Morocco

Table 2

Distribution amongst the different countries of beamtime requested and allocated by the 4 SC meetings from Spring 2005 to Fall 2006. The countries with the highest allocations are highlighted.

The LLB is the French National Facility. Consequently, the most important part of the allocated experiments rises from French teams, coming from all over the country. As in the precedent periods, the French experiments account for nearly two-thirds (2/3) of the total beam time allocated.

The research teams of European Union and EU associated states have benefitted from more than one fourth (1/4) of the total allocated beam time. A large part of the expenses of these groups (beam time costs and travel expenses) have been supported by the ACCESS program of the EU-FP6 (see below). Details of the team national affiliations are given in Figure 3. Nearly half of the European beamtime goes to German experiments, which is the result of long term collaborations and CRG agreements. 10% of the allocated beam time has been given to countries out of the EU area, mainly United States and Russia. A detailed analysis of the team national affiliations is given in Figure 4.

EXPERIMENTAL AND USERS PROGRAMS

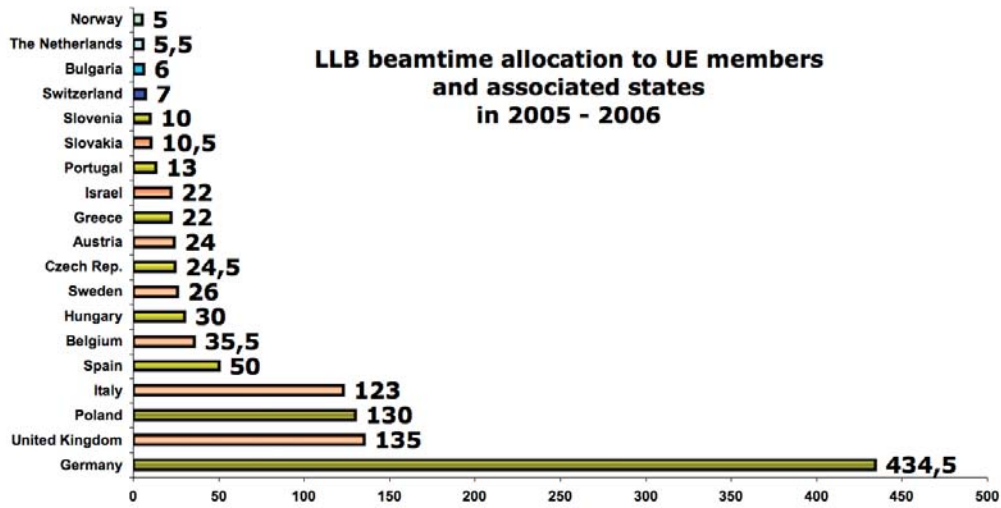
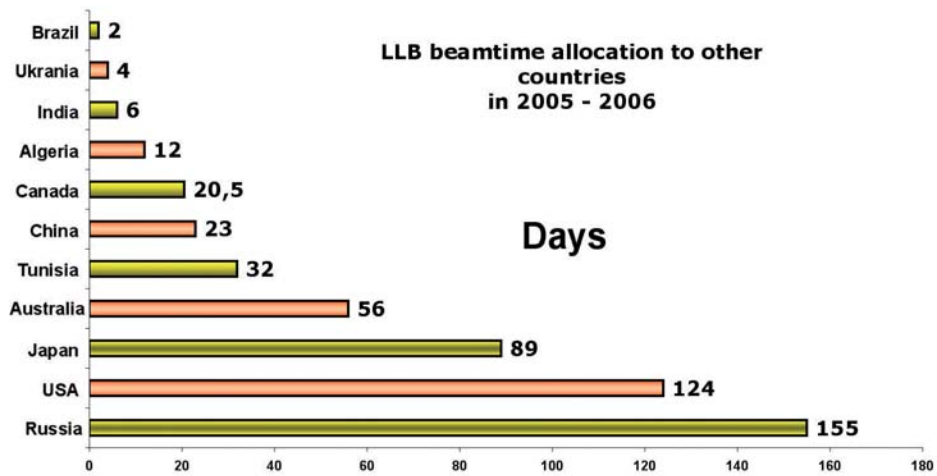


Figure 3

Beam time allocated in the period Spring 2005–Fall 2006 to UE members and associated states as function of the national affi-



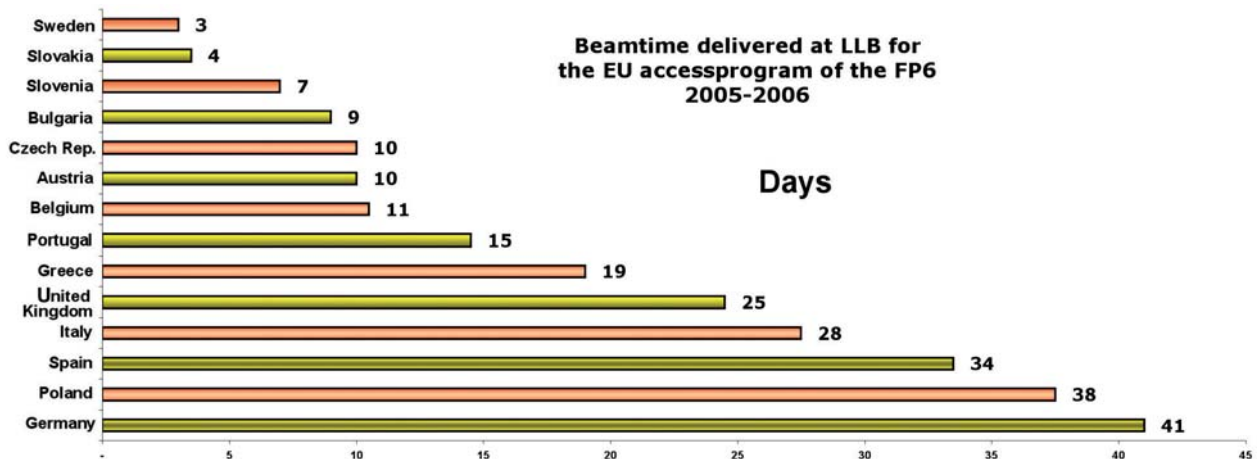
liations of the teams.

Figure 4

Beam time allocated in the period Spring 2005–Fall 2006 to other countries as function of the national affiliations of the teams.

## The ACCESS program at the LLB

The LLB successfully participates in the Transnational Access of European Users to Large Scale Facilities in the Neutron-Muon Integrated Infrastructure Initiative (NMI<sup>3</sup>, see detail in the web page <http://www.neutron-eu.net>). The LLB is particularly keen to attract new user groups from European Countries, which can apply for beamtime via the normal LLB proposal mechanism. Thanks to the Access support, the LLB funds the travel and subsistence expenses form up to two researchers of an



accepted proposal. Figure 5 gives details about the national affiliations of the teams participating in the access program in 2005 and 2006.

Figure 5

Beam time (in days) delivered by the LLB-Orphée facility in 2005 and 2006 in the framework of the Transnational Access Program supported by the European FP6 scheme, as a function of the nationality of the experimentalist invited by the LLB.

## The Selection Committees

The Selection Committee of the LLB is composed by high level scientists from France and European Countries. The meeting takes place twice a year (typically spring and fall) to review all the proposals submitted to the facility based on scientific merit and timeliness. Four subcommittees have been set up in the following research areas:

- Section A: Physical Chemistry and Biology
- Section B: Structural Studies and Phase Transitions
- Section C: Magnetism and Superconductivity
- Section D: Material Science and Disordered Systems.

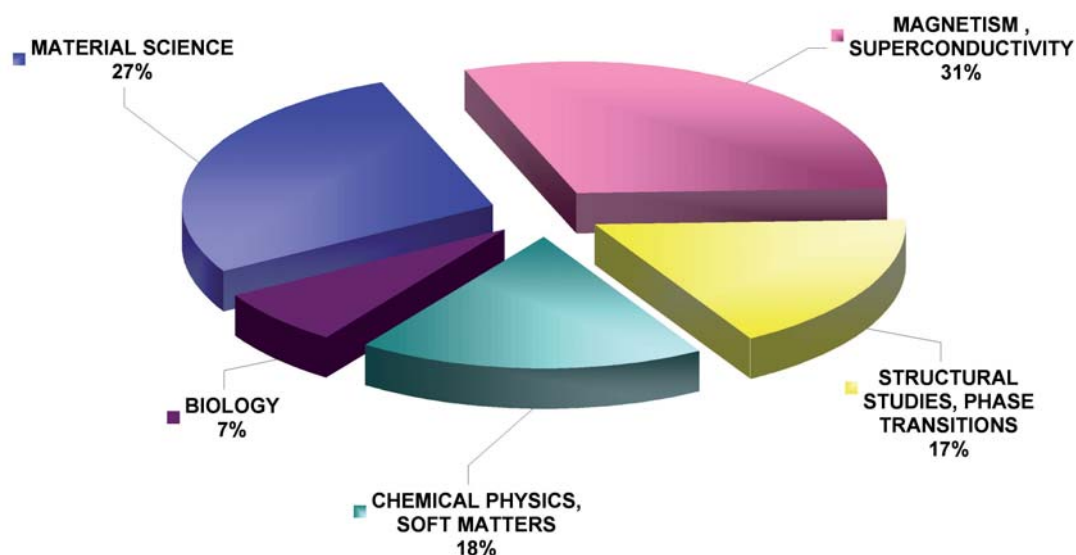
## EXPERIMENTAL AND USERS PROGRAMS

The LLB facility Scientific Committee Membership (Fall 2006 meeting) is given in table 3. The list of the LLB instruments scheduled of external users are given at the end of the section.

The relative importance of these 4 committees is depicted in Figure 6. We remark the predominance of section C "Magnetism and Superconductivity" (31%), followed by section A "Physical Chemistry and Biology" (25%), section D "Material Science and Disordered Systems" (27%) and section B "Structural Studies and Phase Transitions" (17%). In figures 7, 8, 9, 10 and 11 the research sub-fields contained in main research areas are detailed.

More information on applications for beamtime and deadlines is given in real time on the LLB web site.

### Scientific domains of the beamline allocation at LLB in 2005-2006



<http://www-llb.cea.fr>

Figure 6

Repartition of the beam time allowed amongst the 4 subcommittees with the corresponding percentage. (Spring 2005-Fall 2006)

## Chemical physics, soft matter beamtime allocated in 2005-2006

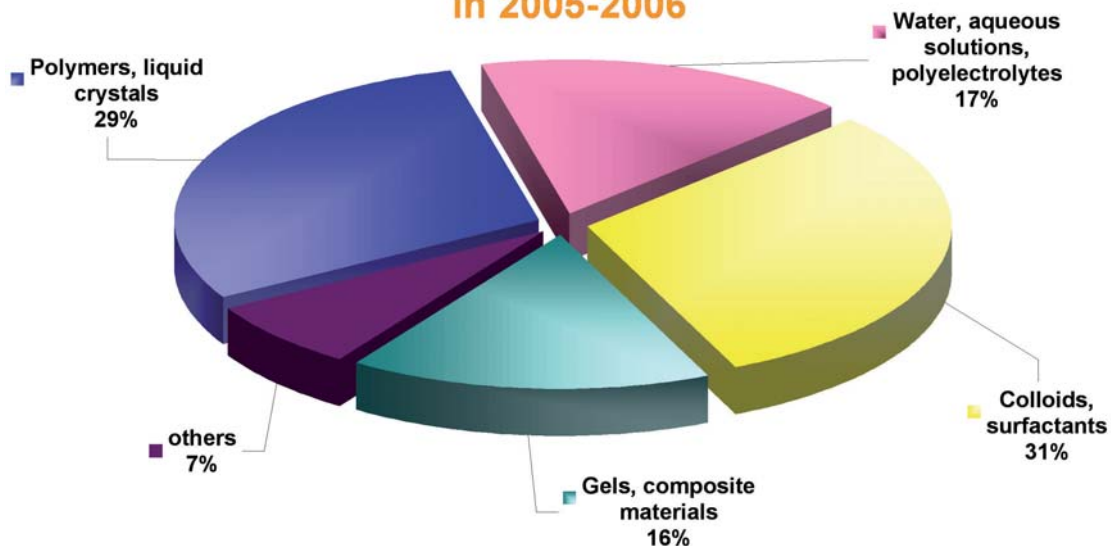


Figure 7

Beam time repartition detailed by sub-fields in the area of Chemical Physics and Soft Matter (Selection Committees from Spring 2005 to Fall 2006).

## Biology : beamtime allocated in 2005-2006

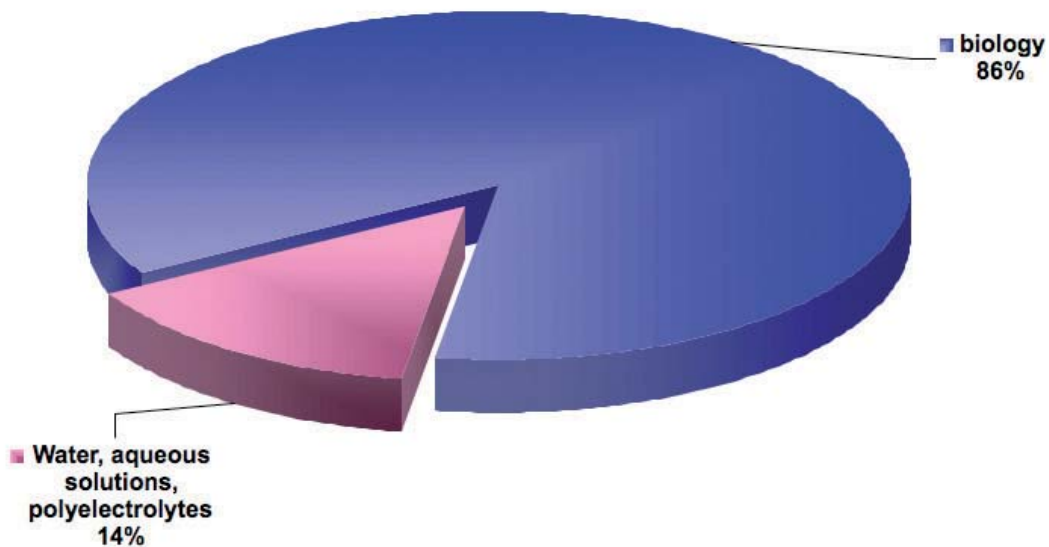


Figure 8

Beam time repartition detailed by sub-fields in the area of Biology (Selection Committees from Spring 2005 to Fall 2006).

### Structural studies, phase transition : beamtime allocated in 2005-2006

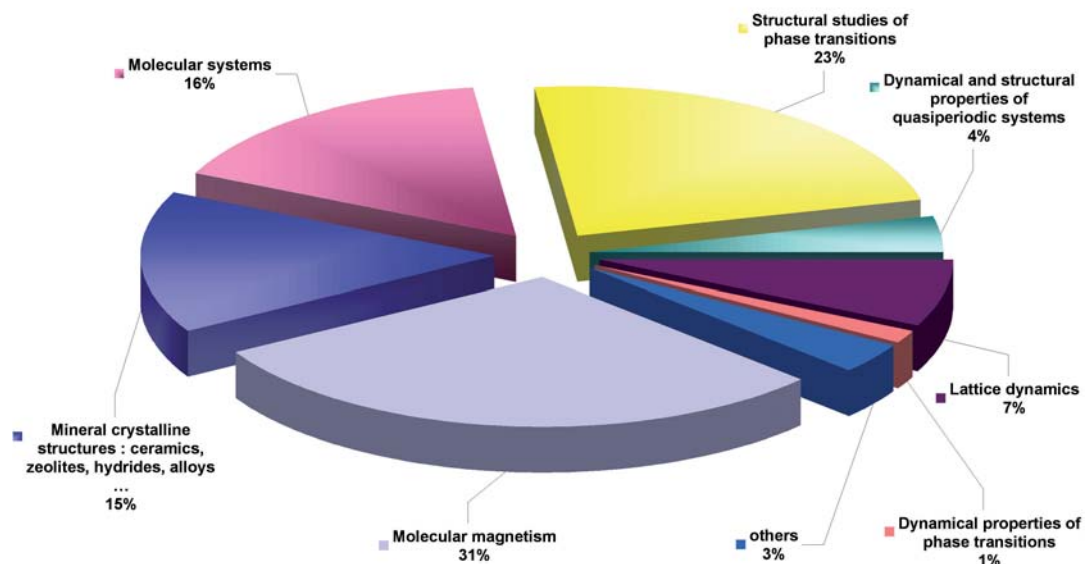


Figure 9

Beam time repartition detailed by sub-fields in the area of Structural Studies and Phase Transitions (Selection Committees from Spring 2005 to Fall 2006).

### Magnetism, superconductivity : beamtime allocated in 2005-2006

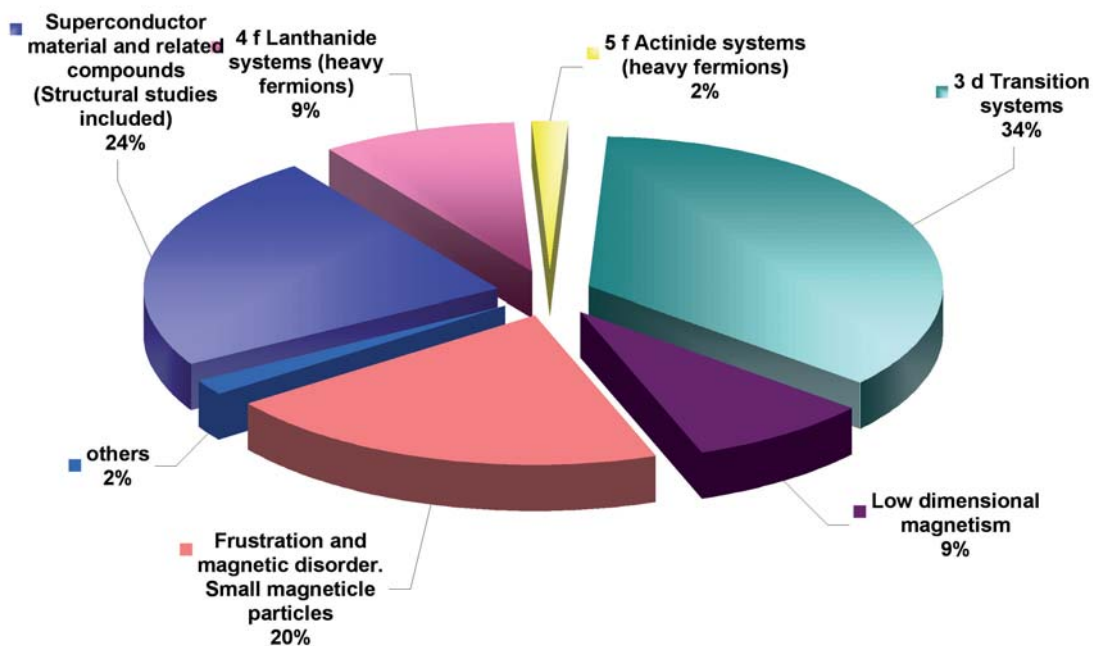


Figure 10

Beam time repartition detailed by sub-fields in the area of Magnetism and Supraconductivity (Selection Committees from Spring

## Material Science : beamtime allocated in 2005-2006

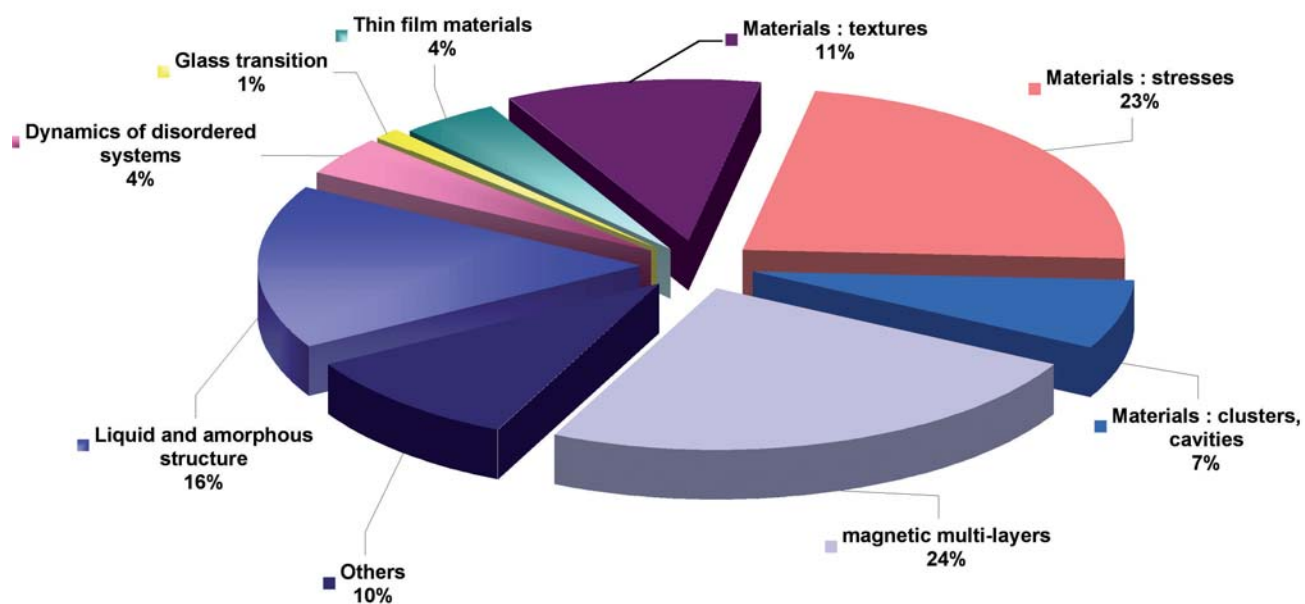


Figure 11

Beam time repartition detailed by sub-fields in the area of Material Science and Disordered Systems (Selection Committees from Spring 2005 to Fall 2006).

## EXPERIMENTAL AND USERS PROGRAMS

## Comités de Sélection - LLB Session Automne 2006

COMITE A : Physico-Chimie, Biologie Organisateurs : S. Combet, F. Cousin		
Représentants LLB	Représentants français	Représentants européens
J. Jestin J.M. Zanotti	O. Diat [Président] CEA/Grenoble P. Fontaine SOLEIL I. Grillo ILL S. Lecommandoux LCPO, Pessac	M. Geoghegan Université de Sheffield T. Hellweg Technische Univ. Berlin P. Mariani Université
COMITE B : Etudes Structurales, Transitions de Phase Organisateurs : F. Bourée, D. Petitgrand		
Représentants LLB	Représentants français	Représentants européens
J.-M. Kiat, ECP H. Moudden	N. Hansen Université Nancy M.H. Lemée-Cailleau ILL G. Rousse Université Paris	F. Frey [Président] Université Münich D. Reznik KFK, Allemagne
COMITE C : Magnétisme, Supraconductivité Organisateurs : P. Bourges, G. Chaboussant		
Représentants LLB	Représentants français	Représentants européens
B. Gillon S. Petit	M. d'Astuto Université Paris VI K. Dumesnil Université Nancy I E. Janod IMN, Nantes C. Martin CRISMAT, Caen	L. Chapon ISIS M. Enderle ILL J.-L. Garcia-Munoz [Pdt] I C M A B , Barcelone E. Kentzinger Jülich
COMITE D : Systèmes désordonnés, Matériaux Organisateurs : A. Goujon, M.H. Mathon		
Représentants LLB	Représentants français	Représentants européens
B. Beuneu	J.L. Bechade CEA/Saclay D. Morineau Université Rennes P. Vajda Ecole	I. Cabaco-Fialho [Pdte] Université de Lisbonne H.G. Priesmeyer Université de Kiel

Table 3

LLB Facility Panel Membership. The four sub-committees meet twice a year to review all proposals submitted to the facility based on scientific merit and timeliness





# PUBLICATIONS 2005 - 2006

**Abdelhedi, M.; Dammak, M.; Cousson, A.; Kolsi, A.W.**  
*Structural, calorimetric and conductivity study of the new mixed solution  $Rb_2(SO_4)_{0.5}(SeO_4)_{0.5}Te(OH)_6$*   
Journal of Alloys and Compounds 398 (2005) 55-61

**Abdelhedi, M.; Dammak, M.; Cousson, A.; Nierlich, .; Abdelwaheb, K.**  
 *$Cs-2(SO_4)_{0.57}(SeO_4)_{0.43} - Te(OH)_6$  an adduct between dicalcium sulfate selenate and telluric acid*  
Acta Crystallographica E 61 (2005) I256-I258

**Aïn, M.; Regnault, L.P.; Lorenzo, J.; Dhalenne, G.; Revcolevschi, A.**  
 *$CuGeO_3$  and  $CuO$  by respectively elastic and inelastic polarized neutrons*  
Physica B 356 (2005) 60-63

**Akbarzadeh, A.R.; Kornev, I.; Malibert, C.; Bellaiche, L.; Kiat, J.M.**  
*Combined theoretical and experimental study of the low-temperature properties of  $BaZrO_3$*   
Physical Review B 72 (2005) 205104

**Alekseev, P.A.; Mignot, J.-M.; Nefedova, E.V.; Nemkovski, K.S.; Lazukov, V. N.; Tiden, N.N.; Menushenkov, A. P.; Chernikov, R.V.; Klementiev, K. V.; Ochiai, A.; Golubkov, A.V., Bewley, R.I.; Rybina, A.V.; Sadikov, I.P.**  
*Magnetic spectral response and lattice properties in mixed-valence  $Sm_{1-x}Y_xS$  solid solutions studied with x-ray diffraction, x-ray absorption spectroscopy, and inelastic neutron scattering*  
Physical Review B 74 (2006) 035114

**Alekseev, P.A.; Mignot, J.M.; Nefedova, E.V.; Nemkovski, K.S.; Lazukov, V.N.; Ochiai, A.; Golubkov; A.V.**  
*Effects of intermediate valence and Sm-Sm interactions on magnetic excitation spectra in  $(Sm, Y)S$*   
Physica B 339 (2005) 54-56

**Alloul, H.; Mukhamedshin, I.R.; Blanchard, N.; Collin, G.**  
*Superconductivity, charge order and anomalous magnetism in sodium cobaltates*  
Journal de Physique IV 131 (2005) 27-32

**Anastassopoulos, D. L.; Spiliopoulos, N.; Vradis, A. A. ; Toprakcioglu, C.; Baker, S. M. ; Menelle, A.**  
*Shear-induced desorption in polymer brushes*  
Macromolecules 39 (2006) 8901-8904

**Andreata, G.; Lee, L.T.; Lee, F.K.; Benattar, J.J.**  
*Gas permeability in polymer- and surfactant-stabilized bubble films*  
Journal of Physical Chemistry B 110 (2006) 19537-19542

**Apetrei, A.; Mirebeau, I.; Goncharenko, I.; Andreica, D. ; Bonville, P.**  
*Microscopic study of a pressure-induced ferromagnetic - Spin-glass transition in the geometrically frustrated pyrochlore  $(Tb_{1-x}La_x)_{(2)}Mo_2O_7$*   
Physical Review Letters 97 (2006) 206401

**Appavou, M.S.**  
*Etude de l'influence de la température et de la pression sur la structure et la dynamique de l'inhibiteur de la trypsine pancréatique bovine. Une étude par diffusion de neutrons*  
Thèse soutenue à l'Université Paris XI-Orsay, le 06 avril 2005

**Appavou, M.-S.; Gibrat, G., Bellissent-Funel, M.C.**  
*Influence of pressure on structure and dynamics of bovine pancreatic trypsin inhibitor (BPTI) : small angle and quasi-elastic neutron scattering*  
Biochimica and Biophysica Acta 1764 (2006) 414-423

**Appavou, M.S.; Gibrat, G., Bellissent-Funel, M.C.; Plazanet, M.; Pieper, J.; Buchsteiner, A.; Annighofer, B.**  
*The influence of a medium pressure on the structure and dynamics of a bovine pancreatic trypsin inhibitor protein*  
Journal of Physics Condensed Matter 17 (2005) S3093-S3099

**Appell, J.; Porte, G.; Buhler, E.**  
*Self-diffusion and collective diffusion of charged colloids studied by dynamics light scattering*  
Journal of Physical Chemistry B 109 (2005) 13186-13194

**Arcos, D.; Rodriguez-Carvajal, J.; Vallet-Regi, M.**  
*Crystal-chemical characteristics of silicon - Neodymium substituted hydroxyapatites studied by combined X-ray and neutron powder diffraction*  
Chemistry of Materials 17 (2005) 57-64

**Aubry, S.**  
*Discrete breathers : Localisation and transfer of energy in discrete Hamiltonian nonlinear systems*  
Physica D 216 (2006) 1-30

**Aubry, S.; Kopidakis, G.**  
*A non adiabatic theory for ultrafast catalytic electron transfer*  
Journal of Biological Physics 31 (2005) 375-402

**Baczewski, L.T.; Pankowski, P.; Wawro, A.; Mergia, K.; Messoloras, S.; Ott, F.**  
*Induced magnetism at interfaces in ultra-thin epitaxial V/Gd bilayers*  
Physical Review B 74 (2006) 075417

**Baczanski, A.; Wierzbanski, K.; Benmarouane, A., Lodini, A.**  
*Residual stresses, dislocation density recrystallization process*  
Materials Science Forum 524-525 (2006)

**Barrier, N.; Pelloquin, D.; Nguyen, N.; Giot, M.; Bouree, F.; Raveau, B.**  
*Ferrite  $Sr_3NdFe_3O_9$ : An original intergrowth between the brownmillerite and  $K_2NiF_4$ -type structures*  
Chemistry of Materials 17 (2005) 6619-6622

## PUBLICATIONS

**Basler, R.; Sieber, A.; Chaboussant, G.; Gudel, H.U.; Chakov, N.E.; Soler, M.; Christou, G.; Desmedt, A.; Lechner, R.**

*Inelastic neutron scattering study of electron reduction in Mn-12 derivatives*

Inorganic Chemistry 44 (2005) 649-653

**Bastiat, G.; Grassl, B.; Borisov, O.; Lapp, A.; Francois, J.**  
*A small-angle neutron scattering study of sodium dodecyl sulfate-poly(propylene oxide) methacrylate mixed micelles*

Journal of Colloid and Interface Science 295 (2006) 417-426

**Baudin, T.; Etter, AL.; Gerber, P.; Samet, A.; Penelle, R.; Rey, C.**

*Influence of thermo-mechanical treatments on the stored energy simulated by FEM for two low carbon steels.*

Materials Science Forum 495-497 (2005) 1291-1296

**Bayrakci, S.P.; Mirebeau, I.; Bourges, P.; Sidis, Y.; Enderle, M.; Mesot, J.; Chen, D.P.; Lin, C.T.; Keimer, B.**

*Magnetic ordering and spin waves in  $Na_{0.82}CoO_2$*

Physical Review Letters 94 (2005) 157205

**Bazin, D.; Daudon, M.; Chevallier, P.; Rouziere, S.; Elkaim, E.; Thiaudiere, D.; Fayard, B.; Foy, E.; Albouy, PA.; Andre, G.; Matzen, G.; Veron, E.**

*Synchrotron radiation techniques for structural characterisation of biological entities: an example with renal stone analysis*

Annales de Biologie Clinique 64 (2006) 125-139

**Beaumont, E.; Fournier, B.; Stokes, D.; Hinsén, K.; Lacapere, J.J.**

*Atomic structure of a covalently phosphorylated intermediate of SERCA1  $Ca^{2+}$ -ATPase: Normal mode fits of electron densities*

Journal of General Physiology 126 (2005) 14A

**Becker P, Siebert H, Noirez L, Schmidt C.**

*Shear-induced order in nematic polymers*

Macromolecular Symposia 220 (2005) 111-122

**Bélier, G.; Roig, O.; Daugas, J.-M.; Giarmata, O.; Méot, V.; Letourneau, A.; Marie, F.; Foucher, Y.; Aupiais, J.; Abt, D.; Jutier, Ch. Le Petit, G.; Bettoni, C.; Gaudry, A.; Veysseyre Ch.**

*Thermal neutron capture cross section for the K isomer  $^{177}Lu^m$*

Physical Review C 73 (2006) 014603

**Bellissent-Funel, M.C.**

*Hydrophilic-hydrophobic interplay : from model systems to living systems*

Comptes Rendus Geoscience 337 (2005) 173-179

**Bellissent-Funel, M.C.**

*Internal diffusive and collective motions in proteins studied by neutron scattering*

Journal of Molecular Liquids 129 (2006) 44-48

**Beltran, L.M.C.; Bennett, M.V.; Kong, J.S.; Goujon, A.; Mathoniere, C.; Long, J.R.**

*Electrochemistry and photomagnetism of high-nuclearity cubic metal-cyanide clusters.*

Abstracts of papers of the American Chemical Society 229 (2005) U1079-U1079, Part 1

**Ben Salah, M.; Vilminot, S.; Andre, G.; Bouree-Vigneron, F.; Richard-Plouet, M.; Mhiri, T.; Kurmoo, M.**

*Nuclear and magnetic structures and magnetic properties of  $Co_3(OH)_2(SO_4)_2(H_2O)_2$  comparison to the Mn and Ni analogues*

Chemistry of Materials 17 (2005) 2612-2621

**Ben Salah, M.; Vilminot, S.; Andre, G.; Richard-Plouet, M.; Mhiri, T.; Takagi, S.; Kurmoo, M.**

*Nuclear and magnetic structures and magnetic properties of the layered cobalt hydroxysulfate  $Co_3(OH)_6(SO_4)_2(H_2O)_4$  and its deuterated analogue;  $Co_3(OD)_6(SO_4)_2(D_2O)_4$*

Journal of the American Chemical Society 128 (2006) 7972-7981

**Bérardan, D.; Alleno, E.; Godart, C.; Rouleau, O.; Rodriguez-Carvajal, J.**

*Preparation and chemical properties of the skutterudites  $(Ce-Yb)_3Fe_{4-x}(Co/Ni)_xSb_{12}$*

Materials Research Bulletin 40 (2005) 537-541

**Bert, F.; Mendels, P.; Olariu, A.; Blanchard, N.; Collin, G.; Amato, A.; Baines, C.; Hillier, A.D.**

*Direct evidence for a dynamical ground state in the highly frustrated  $Tb_2Sn_2O_7$  pyrochlore*

Physical Review Letters 97 (2006) 117203

**Bircher, R.; Chaboussant, G.; Dobe, C.; Gudel, H.U.; Ochsenein, S.T.; Siebe, A.; Waldmann, O.**

*Single-molecule magnets under pressure*

Advanced Functional Materials 16 (2006) 209-220

**Bircher, R.; Chaboussant, G.; Ochsenein, S.T.; Fernandez-Alonso, F.; Gudel, H.U.; Brechin, E.K.**

*Inelastic neutron scattering study of undeuterated  $[Mn_9O_7(OAc)_{11}(thme)(py)_3(H_2O)_2]$*

Polyhedron 24 (2005) 2455-2458

**Blake, G.R.; Chapon, L.C.; Radaelli PG.; Park, S.; Hur, N.; Cheong, S.W.; Rodriguez-Carvajal, J.**

*Spin structure and magnetic frustration in multiferroic  $RMn_2O_5$  ( $R=Tb, Ho, Dy$ )*

Physical Review B 71 (2005) 214402

- Bobroff, J.; Lang, G.; Alloul, H.; Blanchard, N.; Collin, G.**  
*NMR study of the magnetic and metal-insulator transitions in  $\text{Na}_{0.5}\text{CoO}_2$ : A nesting scenario*  
Physical Review Letters 96 (2006) 107201
- Bogdanova, A.N.; Irodova, A.V.; André, G.; Bouree, F.**  
*Novel superstructure in the high-concentrated hydrogen solid solutions  $\text{ZrV}_2\text{D}_{x>4}$*   
Journal of Alloys and Compounds 396 (2005) 25-28
- Bonetti, M.; Calmettes, P.**  
*Sapphire-anvil cell for small-angle neutron scattering measurements in large-volume liquid samples up to 530 MPa*  
Review of Scientific Instruments 76 (2005) 043903
- Bonini, M.; Berti, D.; Di Meglio, J.M.; Almgren, M.; Teixeira, J.; Baglioni, P.**  
*Surfactant aggregates hosting a photoresponsive amphiphile: structure and photoinduced conformational changes*  
Soft Matter 1 (2005) 444-454
- Bono, D.; Mendels, P.; Collin, G.; Blanchard, N.; Bert, F.; Amato, A.; Baines, C.; Hillier, A.D.**  
*Low-T dynamics in the highly frustrated  $S=3/2$  kagome bilayers: A phenomenological function for a spin liquid state?*  
Physica B 374 (2006) 138-141
- Bono, D.; Limot, L.; Mendels, P.; Collin, G.; Blanchard, N.**  
*Correlations; spin dynamics; defects: the highly frustrated kagome bilayer*  
Low Temperature Physics 31 (2005) 704-721
- Bouanani, F.; Bendedouch, D.; Maitre, C.; Teixeira, J.; Hemery, P.**  
*Characterization of miniemulsion polymerization by small-angle neutron scattering*  
Polymer Bulletin 55 (2005) 429-436
- Bouazizi, S.; Nasr, S.; Jaidane, N.; Bellissent-Funel, M.-C.**  
*Local order in aqueous NaCl solutions and pure water: X-ray scattering and molecular dynamics simulations study*  
Journal of Physical Chemistry B 110 (2006) 23515-23523
- Bourges, P.; Keimer, B.; Pailhes, S.; Regnault, L.P.; Sidis, Y.; Ulrich, C.**  
*The resonant magnetic mode: A common feature of high- $T_c$  superconductors*  
Physica C 424 (2005) 45-49
- Braden, M.; Pintschovius, L.; Uefuji, T.; Yamada, K.**  
*Dispersion of the high-energy phonon modes in  $\text{Nd}_{1.85}\text{Ce}_{0.15}\text{CuO}_4$*   
Physical Review B 72 (2005) 184517
- Brulet, A.; Lairez, D.; Lapp, A.; Cotton, J.P.**  
*Improvement of data treatment in SANS*  
Journal of Applied Crystallography 40 (2006) 167-177
- Brutovsky, B.; Kneller, G.R.**  
*Linear prediction of force time series to accelerate molecular dynamics simulations*  
Computer Physics Communications 169 (2005) 339-342
- Buffet, J.C.; Clergeau, J.F.; Cooper, R.G.; Darpentigny, J.; De Laulany, A.; Fermon, C.; Fetal, S.; Fraga, F.; Guerard, B.; Kampmann, R.; Kastenmueller, A.; Mc Intyre, G.J.; Manzin, G.; Meilleur, F.; Millier, F.; Rhodes, N.; Rosta, L.; Schooneveld, E.; Smith, G.C.; Takahashi, H.; Van Esch, P.; Van Vuure, T.L.; Zeitelhack, K.**  
*Advances in detectors for single crystal neutron diffraction*  
Nuclear Instruments and Methods in Physics Research 554 (2005) 392-405
- Bychkov, E.; Miloshova, M.; Price, D.L.; Benmore, C.J.; Lorriaux, A.**  
*Short intermediate and mesoscopic range order in sulphur-rich binary glasses*  
Journal of Non Crystalline Solids 352 (2006) 63-70
- Calandrini, V.; Deriu, A.; Onori, G.; Paciaroni, A.; Telling, M.T.F.**  
*Pressure effect on water dynamics in tert-butyl alcohol/water solutions*  
Journal of Physics : Condensed Matter 18 (2006) S2363-S2371
- Calandrini, V.; Sutmann, G.; Deriu, A.; Kneller, G.R.**  
*Role of effective atomic masses in memory function-based models for liquids: A simulation study of liquid water*  
Journal of Chemical Physics 125 (2006) 236102
- Cambedouzou, J.; Rols, S.; Bendiab, N.; Almairac, R.; Sauvajol, J.L.; Petit, P.; Mathis, C.; Mirebeau, I.; Johnson, M.**  
*Tunable intertube spacing in single-walled carbon nanotube bundles*  
Physical Review B 72 (2005) 041404
- Cario, L.; Lafond, A.; Tangui, M.A.; Kabbour, H.; André, G.; Palvadeau, P.**  
*Design and magnetic properties of new compounds containing iron 2D building blocks of the perovskite type*  
Solid State Sciences 7 (2005) 936-944
- Carling, S.G.; Fanucci, G.E.; Talham, D.R.; Visser, D.; Day, P.**  
*The crystal and magnetic structures of the organic-inorganic layer compound phenylphosphonato-Mn(II)-hydrate: A synchrotron X-ray and neutron powder diffraction study*  
Solid State Sciences 8 (2006) 321-325
- Carreaud, J.; Gemeiner, P.; Kiat, J.M.; Dkhil, B.; Bogicevic, C.; Rojac, T.; Malic, B.**  
*Size-driven relaxation and polar states in  $\text{PbMg}_{1/3}\text{Nb}_{2/3}\text{O}_3$ -based system*  
Physical Review B 72 (2005) 174115

## PUBLICATIONS

**Carreaud, J.; Kiat, J. M.; Dkhil, B.; Alguero, M.; Ricote, J.; Jimenez, R.; Holc, J.; Kosec, M.**

*Monoclinic morphotropic phase and grain size-induced polarization rotation in  $Pb(Mg_{1/5}Nb_{2/3})O_3$ - $PbTiO_3$*   
Applied Physics Letters 89 (2006) 252906

**Carrot, G.; Perez, H.**

*Controlled surface initiated polymerizations from inorganic nanoparticles*  
Polymer Preprint 47 (2006) 827-828

**Carrot, G.; El Harrak, A.; Oberdisse, J.; Jestin, J.; Boué F.**

*Polymerization of n-butyl methacrylate from nanosized silica particles: monitoring of the synthesis via SANS*  
Soft Matter 2 (2006) 1043-1047

**Casas-Cabanas, M.; Palacin, M.R.; Rodriguez-Carvajal, J.**

*Microstructural analysis of nickel hydroxide: Anisotropic size versus stacking faults*  
Powder Diffraction 20 (2005) 334-344

**Casas-Cabanas, M.; Rodriguez-Carvajal, J.; Canales-Vazquez, J.; Palacin, M.**

*New insights on the microstructural characterisation of nickel hydroxides and correlation with electrochemical properties*  
Journal of Materials Chemistry 16 (2006) 2925-2939

**Casas-Cabanas, M.; Rodriguez-Carvajal, J.; Palacin, M.R.**

*FAULTS: a new program for refinement of powder diffraction patterns from layered structures*  
Zeitschrift für Kristallographie 243-248 . (2006) Part 1 Suppl. 23

**Cathala, B.; Rondeau-Mouro, C.; Lairez, D.; Belval, FB.; Durand, H.; Gorrichon, L.; Touzel, J.P.; Chabbert, B.; Monties, B.**

*Model systems for the understanding of lignified plant cell wall formation*  
Plant Biosystems 139 (2005) 93-97

**Céolin, R.; Tamarit, J.L.; Barrio, M.; López, D.O.; Espeau, P.; Allouchi, H.; Papoular, R.J.**

*Solid state studies of the  $C_{60}$   $2(CH_3)CCL_3$  solvate*  
Carbon 43 (2005) 417-424

**Chaboussant, G.**

*Nanostructures magnétiques*  
Techniques de l'Ingénieur 2 (2005) 21

**Chagnault, V.; Thibaudeau, S.; Jouannetaud, M.-P.; Jacquesy, J.-C.; Cousson, A.; Bachmann, C.**

*Rearrangement and fluorination of quinidinone in superacid*  
Journal of Fluorine Chemistry 128 (2006) 55-59

**Chaieb, I.; Braham, C.; Peyre, P.; Labbe, E.; Lodini, A.**

*Neutron diffraction analysis of residual stresses induced by Shock peening*  
Materials Science Forum 490-491 (2005) 263-268

**Chakir, M., El Jazouli, A., Chaminade, JP., Bouree, F., de Waal, D.**

*New process of preparation., X-ray characterisation, structure and vibrational studies of a solid solution  $LiTiOAs_{1-x}PxO_4$  ( $0 \leq x \leq 1$ )*  
Journal of Solid State Chemistry 179 (2006) 18-28

**Chaplot, S.L.; Pintschovius, L.; Choudhury, N.; Mittal, R.**

*Phonon dispersion relations, phase transitions, and thermodynamic properties of  $ZrSiO_4$ : Inelastic neutron scattering experiments, shell model, and first-principles calculations*  
Physical Review B 73 (2006) 094308

**Chaplot, S.L.; Pintschovius, L.; Mittal, R.**

*Phonon dispersion relation measurements on zircon,  $ZrSiO_4$*   
Physica B 385 (2006) 150-152 Part 1

**Chaker, H.; Roisnel T.; Cador, O.; Amami, M.; Ben Hassen, R.**

*Neutron powder diffraction studies of  $NdSrNi_{1-x}Cu_xO_{4-\delta}$  ( $0 < x < 1$ )*  
Solid State Sciences 8 (2006) 142-148

**Checot, F.; Brulet, A.; Oberdisse, J.; Gnanou, Y.; Mondain-Monval, O.; Lecommandoux, S.**

*Structure of polypeptide-based diblock copolymers in solution: Stimuli-responsive vesicles and micelles*  
Langmuir 21 (2005) 4308-4315

**Christianson, A.D.; Llobet, A.; Bao, W.; Gardner, J.S.; Swainson, I.P.; Lynn, J.W.; Mignot, J.M.; Prokes, K.; Pagliuso, P.G.; Moreno, N.O.; Sarrao, J.L.; Thompson, J.D.; Lacerda, A.H.**

*Novel coexistence of superconductivity with two distinct magnetic orders*  
Physical Review Letters 95 (2005) 217002

**Chumakov, N.K., Tugushev, V.V.; Gudenko S.V.; Nikolaeva O.A.; Lazukov, V.N.; Goncharenko, I.N.; Alekseev P.A.**

*Effect of the spin short-range order on electron transport and neutron scattering in amorphous alloys  $Gd_xSi_{1-x}$*   
JETP Letters 81 (2005) 292-295

**Citterio-Bigot, H.; Benmarouane, A.; Jakani, S.; Millet, P.; Lodini, A.**

*Residual stress and texture evaluation by diffraction techniques in biomaterials implants*  
Journal of Neutron Research, in press (2006)

**Claiser, N.; Souhassou, M.; Lecomte, C.; Gillon, B.; Carbonera, C.; Caneschi, A.; Dei, A.; Gatteschi, D.; Bencini, A.; Pontillon, Y.; Lelievre-Berna, E.**

*Combined charge and spin density experimental study of the yttrium(III) semiquinonato complex  $Y(HBPz_{(3)})_{(2)}(DTBSQ)$  and DFT calculations*

Journal of Physical Chemistry B 109 (2005) 2723-2732

**Combet, J.; Isel, F.; Rawiso, M.; Boue, F.**

*Scattering Functions of Flexible Polyelectrolytes in the Presence of Mixed Valence Counterions: Condensation and Scaling*

Macromolecules 38 (2005) 7456-7469

**Cormier, L.; Majérus, O.; Neuville, D.R.; Calas, G.**

*Temperature-induced structural modifications between alkali borate glasses and melts*

Journal of the American Ceramic Society 89 (2006) 13-19

**Cousin, F.; Gummel, J.; Ung, D.; Boue, F.**

*Polyelectrolyte-protein complexes: structure and onformation of each specie revealed by SANS*

Langmuir 21 (2005) 9675-9688

**Cousson, A.; Nicolai, B.; Fillaux, F.**

*Melamine (1,3,5-triazine-2,4,6-triamine): a neutron diffraction study at 14 K*

Acta Crystallographica E 61 (2005) O222-O224

**Coustard, M.; Soro, Y.; Siaka, S.; Bamba F.; Cousson A.**  
*Synthesis of 6- to 10-membered ring (E)-hydroxyiminohydroazaazoniabenzocycloalkenes derivative from cyclization of 2-nitromethylene-1-( $\alpha$ -phenylalkyl)imidazolidine or 2-nitromethylene-1-( $\alpha$ -phenylalkyl)hexahydropyrimidine in trifluoromethanesulfonic acid*

Tetrahedron 62 (2006) 3320-3328

**Cruz-Gandarilla, F.; Baudin, T.; Mathon, M.H.; Penelle, R.; Mendoza-Leon, H.; Cabanas-Moreno, J.G.**

*Characterization of global and local textures in hot rolled CGO Fe3%Si*

Advanced Structural Materials II : Materials Science Forum 509 (2006) 25-30

**Cser, L.; Krexner, G.; Prem, M.; Sharkov, I.; Torok, Gy.**

*Neutron holography of metal-hydrogen systems*

Journal of Alloys and Compounds 404-406 (2005) 122-125

**Cuevas, F.; Latroche, M.; Bouree-Vigneron, F.; Percheron-Guegan, A.**

*A conjoint XRD-ND analysis of the crystal structures of austenitic and martensitic  $Ti_{0.64}Zr_{0.36}Ni$  hydrides*

Journal of Solid State Chemistry 179 (2006) 3295-3307

**Cwik, M.; Benomar, M.; Haider, M.; Lorenz, T.; Braden, M.; Sidis, Y.**

*Interplay between structure, magnetism and ordering phenomena in  $La_{2-x}Sr_xCoO_4$*

Verhandlungen der Deutschen Physikalischen Gesellschaft 40 (2005) 574

**da Silva, I.; Gonzalez-Silgo, C.; Gonzalez-Platas, J.; Rodriguez-Carvajal, J.; Martinez-Sarrion, M.L.; Mestres, L.**

*Neutron powder diffraction study of  $A_{(2)}BeF_{(4)}$  ( $A = K, Rb, Cs$ ): Structure refinement and analysis of background*

Journal of Solid State Chemistry 178 (2005) 1601-1608

**da Silva, I.; Gonzalez-Silgo, C.; Gonzalez-Platas, J.; Rodriguez-Carvajal, J.; Martinez-Sarrion, M.L.; Mestres, L.**

*Powder neutron diffraction of  $Tl_2BeF_4$  at six temperatures from room temperature to 1.5 K*

Acta Crystallographica C 61 (2005) I113-I116

**Damay, F.; Carretero-Genevri, A.; Cousson, A.; Van Beek, W.; Rodriguez-Carvajal, J.; Fillaux, F.**

*Synchrotron and neutron diffraction study of 4-methylpyridine-N-oxide at low temperature*

Acta Crystallographica B 62 (2006) 627-633

**Dammak, M.; Cousson, A.; Nierlich, M.**

*Dipotassium selenate tellurate*

Acta Crystallographica E 61 (2005) I55-I57

**Dammak, M.; Ktari, L.; Cousson, A.; Mhiri, T.**

*Structural and conductivity study of a new protonic conductor  $Cs_{0.86}(NH_4)_{1.14}SO_4 \cdot Te(OH)_6$*

Journal of Solid State Chemistry 178 (2005) 2109-2116

**Dammak, M.; Mhiri, T.; Cousson, A.**

*Neutron structural and vibrational studies of dipotassium selenate tellurate*

Journal of Alloys and Compounds 407 (2006) 176-181

**Daoud-Aladine, A.; Roessli, B.; Gvasaliya, S.N.; Perca, C.; Pinsard-Gaudart, L.; Rodriguez-Carvajal, J.; Revcolevschi, A.**

*Paramagnetic fluctuations in  $Pr_{0.65}Ca_{0.35}MnO_3$  around the charge-ordering temperature*

Journal of Physics Condensed Matter 18 (2006) 1509-1517

**Debargue, S.; Violeau, B.; Jouannetaud, M.P.; Jacquesy, J.C.; Cousson, A.**

*Reaction of quinidine acetate., epiquinidine and its acetate in superacid: formation of gem-difluoro derivatives with or without rearrangement*

Tetrahedron 62 (2006) 662-667

**Debargue, S.; Thibaudeau, S.; Violeau, B.; Martin-Mingot, A.; Jouannetaud, M.P.; Jacquesy, J.C.; Cousson, A.**

*Rearrangement or gem-difluorination of quinine and 9-epiquinine and their acetates in superacid*

Tetrahedron 61 (2005) 2065-2073

**Delacourt, C.; Rodriguez-Carvajal, J.; Schmitt, B.; Tarascon, J.M.; Masquelier, C.**

*Crystal chemistry of the olivine-type  $LixFePO_4$  system ( $0 \leq x \leq 1$ ) between 25 and 370 degrees C*

Solid State Sciences 7 (2005) 1506-1516

## PUBLICATIONS

**Delagnes, D.; Lamesle, P.; Mathon, M.H.; Mebarki, N.; Levailant, C.**

*Influence of silicon content on the precipitation of secondary carbides and fatigue properties of a 5%Cr tempered martensitic steel*

Materials Science and Engineering A 394 (2005) 435-444

**Desvergne, S.**

*Polymacropolymères, Synthèse, diffusion de neutrons aux petits angles, rhéologie. De l'architecture à la conformation : étoiles et cylindres chevelus au repos et sous écoulement*

Thèse soutenue à l'Université de Bordeaux, le 11 juillet 2005

**Devaux, C.; Cousin, F.; Beyou, E.; Chapel, JP.**

*Low swelling capacity of highly stretched polystyrene brushes*

Macromolecules 38 (2005) 4296-4300

**Dey, B.; Aubry, S.**

*New suggestion concerning the origin of sonoluminescence*

Physica D 216 (2006) 136-156

**Diaz, S.; de Brion, S.; Chouteau, G.; Strobel, P.; Canals, B.; Rodriguez-Carvajal, J.; Rakoto, H.; Broto, J.M.**

*Magnetic frustration in the spinel compounds  $GeNi_2O_4$  and  $GeCo_2O_4$*

Journal of Applied Physics 97 (2005) 10A512

**Dincer, I.; Elmali, A.; Elerman, Y.; Ehrenberg, H.; Fuess, H.; Andre, G.**

*Neutron diffraction study on  $PrMn_{2-x}Fe_xGe_2$  and general magnetic phase diagram for  $RMn_{2-x}Fe_xGe_2$  (R : La-Sm)*

Journal of Alloys and Compounds 416 (2006) 22-30

**Djurado, D.; Bée, M.; Sniechowski, M.; Howells, S.; Rannou, P.; Pron, A.; Travers, J. P. Luzny, W.**

*Counter-ions dynamics in highly plastic and conducting compounds of poly(aniline). A quasi-elastic neutron scattering study*

Physical Chemistry Chemical Physics 7 (2005) 1235-1240

**Douliez, J.P.; Barrault, J.; Jerome, F.; Heredia, A.; Navailles, L.; Nallet, F.**

*Glycerol derivatives of cutin and suberin monomers : synthesis and self-assembly*

Biomacromolecules 6 (2005) 30-34

**Doussier, C.; Andre, G.; Leone, P.; Jano, E.; Moelo, Y.**

*Magnetic study of two isotopic manganese chloro-sulfides:  $MnSbS_2Cl$  and the new compound  $MnBiS_2Cl$*

Journal of Solid State Chemistry 179 (2006) 486-491

**Dubreuil, F.; Fontaine, P.; Alba, M.; Daillant, J.; Mays, J.W.; Zalczner, G.; Guenoun, P.**

*Buckling of charged diblock copolymer monolayers at the air-water interface*

Europhysics Letters 70 (2005) 176-182

**Dufour, C.; Dumesnil, K.; Mangin, P.H.**

*Strain-induced modification of magnetic structure and new magnetic phases in rare-earth epitaxial films*

Pramana – Journal of Physics 67 (2006) 173-190

**Dul'kin, E.; Roth, M.; Dkhil, B.; Kiat, J.M.**

*Acoustic emission and nonergodic states of the electric-field-induced-phase transition of  $PbMg_{1/3}Nb_{2/3}O_3$*

Journal of Applied Physics 98 (2005) 023520

**Ebeling, W. ; Onufrieva, F.P. ; Tkachenko, I.M.**

*Non-Maxwellian velocity distribution of grains in dusty plasmas with ion flow*

Ukrayins'-kij-Fyzichnij-Zhurnal-Kiev 50 (2005) 135-136

**El Harrak, A.; Carrot, G.; Oberdisse, J. ; Jestin, J. ; Boue, F.**

*Atom transfer radical polymerization from silica nanoparticles using the 'grafting from' method and structural study via small-angle neutron scattering*

Polymer 46 (2005) 1095-1104

**El Harrak, A.**

*Nanoparticules hybrides silice/polymère : Synthèse, analyses DNPA. Applications au renforcement mécanique des polymères*

Thèse soutenue à l'Université Paris XI-Orsay, le Juin 2005

**El Harrak, A.; Carrot, G.; Oberdisse, J.; Jestin, J.; Boue, F.**

*Control of the colloidal stability of polymer-grafted-silica nanoparticles obtained by atom transfer radical polymerization*

Macromolecular Symposia 226 (2005) 263-278

**Espeau, P.; White, J.W. ; Papoular, R.J.**

*The structure of n-alkane binary mixtures adsorbed on graphite*

Applied Surface Science 252 (2005) 1350-1359

**Etrillard, J.; Axelos, MAV.; Cantat, I.; Artzner, F.; Renault, A.; Weiss, T.; Delannay, R.; Boue, F.**

*In situ investigations on organic foam films using neutron and synchrotron radiation*

Langmuir 21 (2005) 2229-2234

**Etter, A.L.; Baudin, T.; Mathon, M.H.; Swiatnicki, W.; Penelle, R.**

*Stored energy evolution in both phases of a duplex steel as a function of cold rolling reduction*

Scripta Materialia 54 (2005) 683-688

**Etxebarria, I.; Perez-Mato, J.M.; García, A.; Blaha, P.; Schwarz, K.; Rodriguez-Carvajal, J.**

*Comparison of empirical bond-valence and first-principles energy calculations for a complex structural instability*

Physical Review B 72 (2005) 174108

**Fauqué, B.; Sidis, Y.; Hinkov, V.; Pailhès, S.; Lin, C.T.; Chaud, X.; Bourges, P.**

*Magnetic order in the pseudogap phase of high- $T_c$  superconductors*

Physical Review Letters 96 (2006) 197001

**Fèvre, M.; Finel, A.; Caudron, R.**

*Local order and thermal conductivity in yttria-stabilized zirconia. I. Microstructural investigations using neutron diffuse scattering and atomic-scale simulations*

Physical Review B 72 (2005) 104117

**Fèvre, M.; Finel, A.; Caudron, R.; Mévrel, R.**

*Local order and thermal conductivity in yttria-stabilized zirconia. II. Numerical and experimental investigations of thermal conductivity*

Physical Review B 72 (2005) 104118

**Fillaux, F.; Cousson, A.; Gutmann, M.J.**

*Macroscopic quantum entanglement and 'super-rigidity' of protons in the  $\text{KHCO}_3$  crystal from 30 to 300 K*

Journal of Physics : Condensed Matter 18 (2006) 3229-3249

**Fillaux, F.; Cousson, A.; Gutmann, M.**

*Macroscopic quantum tunnelling of protons in the  $\text{KHCO}_3$  crystal*

Journal of Molecular Structure 790 (2006) 122-128

**Fitzsimmons, M.R.; Park, S.; Dumesnil, K.; Dufour, C.; Pynn, R.; Borchers, J.A.; Rhyne, J.J.; Mangin, P.**

*Vector magnetization depth profile of a Laves-phase exchange-coupled superlattice obtained using a combined approach of micromagnetic simulation and neutron reflectometry*

Physical Review B 73 (2006) 134413

**Fleury, G.; Brochon, C.; Schlatter, G.; Bonnet, G.; Lapp, A.; Hadziioannou, G.**

*Synthesis and characterization of high molecular weight polytaxanes: towards the control over a wide range of threaded alpha-cyclodextrins*

Soft Matter 1 (2005) 378-385

**Floquet, N.; Coulomb, J.P.; Dufau, N.; Andre, G.; Kahn, R.**

*Confined water in mesoporous MCM-41 and nanoporous AIPO(4)-5: Structure and dynamics Adsorption*

Journal of the International Adsorption Society 11 (2005) 139-141

**Floquet, N.; Coulomb, J.P.; Llewellyn, P.; Andre, G.; Kahn, R.**

*Growth mode of hydrogen in mesoporous MCM-41. Adsorption and neutron scattering coupled studies*

Adsorption - Journal of the International Adsorption Society 11 (2005) 679-684

**Francoval, S.; Livet, F.; de Boissieu, M.; Yakhou, F.; Bley, F.; Letoublon, A.; Caudro, R.; Gastaldi, J.; Currat, R.**

*Dynamics of long-wavelength phason fluctuations in the  $i\text{-Al-Pd-Mn}$  quasicrystal*

Physiological Magazine 86 (2006) 1029-1035

**Fratini, E.; Bonini, M.; Oasmaa, A.; Solantausta, Y.; Teixeira, J.; Baglioni, P.**

*SANS analysis of the microstructural evolution during the aging of pyrolysis oils from biomass*

Langmuir 22 (2006) 306-312

**Gambi, C.M.C.; Giordano, R.; Chittofrati, A.; Pieri, R.; Baglioni, P.; Teixeira, J.**

*Small-angle neutron scattering of ionic perfluoropolyether micellar solutions: Role of counterions and temperature*

Journal of Physical Chemistry B 109 (2005) 8592-8598

**Geoghegan, M.; Ruiz-Perez, L.; Dang, C.C.; Parnell, A.J.; Martin, S. J.; Howse, J.R.; Jones, R.A. L.; Golestanian, R.; Topham, P.D.; Crook, C.J.; Ryan, A.J.; Sivia, D.S.; Webster, J. R. P.; Menelle, A.**

*The pH-induced swelling and collapse atom transfer radical polymerization*

Soft Matter 2 (2006) 1076-1080

**Gerber, P.; Baudin, T.; Chiron, R.; Bacroix, B.**

*EBSA study of annealing twinning during recrystallization of cold rolled copper*

Materials Science Forum 495-497 (2005) 1303-1308

**Gerber, Ph.; Jakani, S.; Mathon, M.H.; Baudin, T.**

*Neutron diffraction measurements of deformation and recrystallization textures in cold wire-drawn copper*

Materials Science Forum 495-497 (2005) 919-926

**Gerber, Ph.; Tarasiuk, J.; Chiron, R.; Bacroix, B.**

*Estimation of the recrystallized volume fraction from local misorientation calculations*

Archives of Metallurgy and Materials 50 (2005) 747-755

## PUBLICATIONS

**Gillon, B.**

*The classical flipping ratio technique applied to non classical magnetic materials: Molecule-based and Photoswitchable magnetic compounds*

A paraître dans Journal de Physique IV (2006)

**Giot, M.; Beran, P.; Perez, O.; Malo, S.; Hervieu, M.; Raveau, B.; Nevrieva, M.; Knizek, K.; Roussel, P.**

*Bi<sub>1-x</sub>Ca<sub>x</sub>MnO<sub>3</sub> (x=0.4 and 0.45): X-ray single-crystal and electron microscopy study*

Chemistry of Materials 18 (2006) 3225-3236

**Giot M.**

*Etudes structurales et magnétiques de manganites Bi<sub>x</sub>Ca<sub>1-x</sub>MnO<sub>3</sub> présentant des mises en ordre complexes*

These soutenue à l'Université de Caen, le 20 novembre 2006

**Giot, M. ; Pautrat, A. ; Perez, O. ; Simon, C. ; Nevrieva, M.; Hervieu, M.**

*Critical point of the competition between different orbital- and Bi lone pair-orderings in the Bi-rich part of the Bi-Ca-Mn-O system*

Solid State Sciences 8 (2006) 1414-1421

**Golosovsky, I.V.; Mirebeau, I.; Elkaim, E.; Kurdyukov, D.A.; Kumzerov, Y.A.**

*Structure of MnO nanoparticles embedded into channel-type matrices*

European Physical Journal B 47 (2005) 55-62

**Golosovsky, I.V.; Mirebeau, I.; Sakhnenko, V.P.; Kurdyukov, D.A.; Kumzerov, Y.A.**

*Evolution of the magnetic phase transition in MnO confined to channel type matrices: Neutron diffraction study*

Physical Review B 72 (2005) 144409

**Golosovsky, I.V.; Mirebeau, I.; Fauth, F.; Kurdyukov, D.A.; Kumzerov, Y.A.**

*Low-temperature phase transition in nanostructured MnO embedded within the channels of MCM-41-type matrices*

Physical Review B 74 (2006) 054433

**Golosovsky, IV.; Tovar, M.; Hoffman, U.; Mirebeau, I.; Fauth, F.; Kurdyukov, DA.; Kumzerov, Y.A.**

*Diffraction studies of the crystalline and magnetic structures of gamma-Fe<sub>2</sub>O<sub>3</sub> iron oxide nanostructured in porous glass*

JETP Letters 83 (2006) 298-301

**Golosovsky, I. V.; Mirebeau, I.; Fauth, F.; Mazaj, M.; Kurdyukov, D. A.; Kumzerov, Yu. A.**

*High-resolution x-ray diffraction study of MnO nanostructured within a MCM-48 silica*

Physical Review B 74 (2006) 155440

**Goncharenko, I.; Loubeyre, P.**

*Neutron and X-ray diffraction study of the broken symmetry phase transition in solid deuterium*

Nature 435 (2005) 1206-1209

**Goncharenko, I.N.**

*High-pressure oxygen: a non-conventional magnet studied by means of neutron diffraction*

Journal of Physics: Condensed Matter 17 (2005) S947-S956

**Goncharenko, I.N.**

*Evidence for a magnetic collapse in the epsilon phase of solid oxygen*

Physical Review Letters 94 (2005) 205701

**Goncharenko, I.N.; Mirebeau, I.; Markosyan, A.S.; Cadavez-Peres, P.; Le Bihan T.**

*Pressure-induced magnetic transitions in the frustrated Laves compound GdMn<sub>2</sub>*

Physical Review B 72 (2005) 014420

**Gordeliy, V.I.; Cherezov, V.; Teixeira, J.**

*Strength of thermal undulations of phospholipid membranes*

Physical Review E 72 (2005) 061913

**Goujon, A.; Gillon, B.; Debede, A.; Cousson, A.; Gukasov, A.; Jeftic, J.; McIntyre, G.J.; Varret, F.**

*Neutron Laue diffraction on the spin crossover crystal [Fe(1-n-propyltetrazole)](BF<sub>4</sub>)<sub>2</sub> showing continuous photoinduced transformation*

Physical Review B 73 (2006) 104413

**Goujon, A.; Gillon, B.; Gukasov, A.; Jeftic, J.; Codjovi, E.; Varret, F.**

*Photomagnétisme de solides moléculaires étudiés par diffraction de neutrons polarisés : une approche microscopique du magnétisme photo-induit*

L'actualité Chimique n°292, (2005) 9-17

**Guegan, R.; Morineau, D.; Loverdo, C.; Beziel, W.; Guendouz, M.**

*Evidence of anisotropic quenched disorder effects on a smectic liquid crystal confined in porous silicon*

Physical Review E 73 (2006) 011707

**Gukasov, A.; Wang, F.; Anighofer, B.; He, L.; Suryanarayanan, R.; Revcolevschi, A.**

*Neutron diffraction studies under pressure of the field-induced ferromagnetic metallic state in (La<sub>0.4</sub>Pr<sub>0.6</sub>)<sub>1.2</sub>Sr<sub>1.8</sub>Mn<sub>2</sub>O<sub>7</sub>: Role of super and double exchange*

Physical Review B 72 (2005) 092402

**Gummel, J.**

*Structures et mécanismes de formation de complexes polyélectrolytes-protéines.*

Thèse soutenue le 9 octobre 2006 à l'Université de Paris XI-Orsay

**Gummel, J.; Boue, F.; Deme, B.; Cousin, F.**

*Charge stoichiometry inside polyelectrolyte-protein complexes: A direct SANS measurement for the PSSNa-lysozyme system*

Journal of Physical Chemistry B 110 (2006) 24837-24846

**Haidar, B.; Spycykerelle, O.; Ziegler, P.; Vidal, A.; Boue, F.**

*Supra-molecular structure of PDMS bimodal network as revealed by small angle neutron scattering*

Abstract Papers of the American Chemical Society 230 (2006) U3613-U3614

**Hammami, F.; Nasr S.; Bellissent-Funel, M.C.; Oumezzine, M.**

*Neutron scattering experiments on fully deuterated liquid N-methylformamide DCONDCD<sub>3</sub> at various temperatures and under pressure. Comparison to X-ray results*

Journal of Physical Chemistry B 109 (2005) 16169-16175

**Hammami, F.; Nasr, S.; Bellissent-Funel, M.C.**

*Neutron scattering study of the H-bond network in amorphous N-methylformamide*

Journal of Chemical Physics 122 (2005) 064505

**Hamon, V.; Calligari, P.; Hinsen, K.; Kneller, G.R.**

*Simulation studies of structural changes and relaxation processes in lysozyme under pressure*

Journal of Non Crystalline solids 352 (2006) 4417-4423

**Hao, L.; Iwasa, K.; Kuwahara, K.; Kohgi, M.; Sugawara, H.; Aoki, Y.; Sato, H.; Matsuda, T.D.; Mignot, J.M.; Gukasov, A.; Nishi M.**

*Neutron scattering studies of order parameters and excitations in antiferro-quadrupolar phase of PrFe<sub>4</sub>P<sub>12</sub>*

Physica B 359-361 (2005) 871-873

**Hardy, V.; Martin, C.; Martinet, G.; Andre, G.**

*Magnetism of the geometrically frustrated spin-chain compound Sr<sub>3</sub>HoCrO<sub>6</sub>: Magnetic and heat capacity measurements and neutron powder diffraction*

Physical Review B 74 (2006) 064413

**Hauet, T.; Borchers, J.A.; Mangin, P.; Henry, Y.; Mangin, S.**

*Training effect in an exchange bias system: The role of interfacial domain walls*

Physical Review Letters 96 (2006) 067207

**Haumont R, Gemeiner P, Dkhil B, Kiat JM, Bulou A.**

*Polar and chemical states at a nanometer scale in a PbSc<sub>1/2</sub>Nb<sub>1/2</sub>O<sub>3</sub>-PbTiO<sub>3</sub> system investigated by Raman spectroscopy*

Physical Review B 73 (2006) 104106

**Haumont, R.; Al-Barakaty, A.; Dkhil, B.; Kiat, J.M.; Bellaiche, L.**

*Morphotropic phase boundary of heterovalent perovskite solid solutions: Experimental and theoretical investigation of PbSc<sub>1/2</sub>Nb<sub>1/2</sub>O<sub>3</sub>-PbTiO<sub>3</sub>*

Physical Review B 71 (2005) 104106

**Haumont, R.; Carreaud, J.; Gemeiner, P.; Dkhil, B.; Malibert, C.; Al-Barakaty, A.; Bellaiche, L.; Kiat, J.M.**

*Polar and chemical order in relation with morphotropic phase boundaries and relaxor behaviour in bulk and nanostructured PSN-PT*

Phase Transitions 79 (2006) 123-134

**Haumont, R.; Malibert, C.; Dkhil, B.; Kiat, J.M.; LeMarrec, F.; Asanuma, S.; Uesu, Y.**

*Observation of rotation of polarization in thin films of Pb(Sc<sub>1/2</sub>Nb<sub>1/2</sub>)O<sub>3</sub>-PbTiO<sub>3</sub> via a monoclinic phase*

Japanese Journal of Applied Physics, 45 (2006) (part.2) L42-L4

**Hennion, M.; Moussa, F.**

*The precursor phase of the CMR metallic state probed by spin and lattice dynamics*

New Journal of Physics 7 (2005) Art. No. 84

**Hennion, M.; Moussa, F.; Lehouelleur, P.; Wang, F.; Ivanov, A.; Mukovskii, Y.M.; Shulyatev, D.**

*Confined spin waves reveal an assembly of nanosize domains in ferromagnetic La<sub>1-x</sub>Ca<sub>x</sub>MnO<sub>3</sub> (x=0.17,0.2)*

Physical Review Letters 94 (2005) 057006

**Hennion, M.; Moussa, F.; Lehouelleur, P.; Reutler, P.; evcolevschi, A.**

*Metal-insulator transition of La<sub>7/8</sub>Sr<sub>1/8</sub>MnO<sub>3</sub> probed by spin waves: Stabilization of a two-dimensional stripe structure*

Physical Review B 73 (2006) 104453

**Hervé, G.; Aubry, S.**

*Intramolecular signal transmission in regulatory enzymes : are polarons involved ?*

Soumis à Physica D 216 (2006) 235-243

**Hinkov, V.; Keimer, B.; Kulakov, A.; Lin-Chengtian, Chen-Dapeng; Bernhard, C.; Bourges, P.; Pailhes, S.; Sidis, Y.; Ivanov, A.**

*Testing stripe theories : geometry of spin excitations in the superconducting and normal state of YBa<sub>2</sub>Cu<sub>3</sub>O<sub>6+x</sub>*

Verhandlungen der Deutschen Physikalischen Gesellschaft 40 (2005) 546

**Hinsen, K.**

*Comment on: "Energy landscape of a small peptide revealed by dihedral angle principal component analysis"*

Proteins-Structure Function and Bioinformatics 64 (2006) 795-797

## PUBLICATIONS

**Hinsen, K.; Reuter, N.; Navaza, J.; Stokes, D.L.; Lacapere, J.J.**

*Normal mode-based fitting of atomic structure into electron density maps: Application to sarcoplasmic reticulum Ca-ATPase*  
Biophysical Journal 88 (2005) 818-827

**Hinsen, K.**

*Normal mode theory and harmonic potential approximations in: Normal Mode Analysis: Theory and Applications to Biological and Chemical Systems*  
Ivet Bahar & Qiang Cui eds, CRC press (2006)

**Hlinka, J.; Kempa, M.; Kulda, J.; Bourges, P.; Kania, A.; Petzelt, J.**

*Lattice dynamics of ferroelectric PbTiO<sub>3</sub> by inelastic neutron scattering*  
Physical Review B 73 (2006) 140101

**Hofmann, M.; Campbell, S. J.; Link, P.; Fiddy, S.; Goncharenko, I.**

*Valence and magnetic transitions in YbMn<sub>2</sub>Ge<sub>2</sub>-pressure and temperature*  
Physica B 385 (2006) 330-332 Part 1

**Honecker, A.; Fukushima, N.; Normand, B.; Chaboussant, G.; Gudel, H.U.**

*Exchange constants and spin dynamics in Mn-12-acetate*  
Journal of Magnetism and Magnetic Materials 290 (2005) 966-969

**Hourdet, D.; Gadgil, J.; Podhajecka, K.; Badiger, M.V.; Brûlet, A.; Wadgaonkar, P.P.**

*Thermoreversible Behavior of Associating Polymer Solutions: Thermothinning versus Thermothickening*  
Macromolecules 38 (2005) 8512-8521

**Inoubi, R.; Dagreou, S.; Lapp, A.; Billon, L.; Peyrelasse, J.**

*Nanostructure and mechanical properties of polybutylacrylate filled with grafted silica particles*  
Langmuir 22 (2006) 6683-6689

**Ivanov, A.; Petitgrand, D.**

*Critical scattering near quantum critical point in a quasi-2D antiferromagnet*  
Physica B 385 (2006) 421-424 Part 1

**Jakani, S.; Mathon, M.-H.; Benmarouane, A.; Lodini, A.**

*Neutron diffraction study of nano-hydroxyapatite coatings on titanium substrates*  
Journal of Neutron Research, sous presse (2006)

**Jean, B.; Lee, L.T.**

*Noninteracting versus interacting poly(N-isopropylacrylamide)-surfactant mixtures at the air-water interface*  
Journal of Physical Chemistry B 109 (2005) 5162-5167

**Jeanneau, F.; Junca, R.; Pancin, J.; Voytchev, M.; Andriamonje, S.; Dangendorf, V.; Espagnon, I.; Friedrich, H.; Giganon, A.; Giomataris, I.; Menelle, A.; Pluquet, A.; Rodriguez L.R.**

*Neutron Imaging with a Micromegas Detector*  
IEEE Transactions on nuclear science, Vol.53 n°2, Avril 2006

**Jimenez-Melero, E.; Gubbens, P.C.M.; Steenvoorden, M.P.; Sakarya, S.; Goosens, A.; de Reotier, P.D.; Yaouanc, A.; Rodriguez-Carvajal, J.; Beuneu, B.; Isasi, J.; Saez-Puche, R.; Zimmerman, U.; Martinez, J.L.**

*A combined study of the magnetic properties of GdCrO<sub>4</sub>*  
Journal of Physics : Condensed Matter 18 (2006) 7893-7904

**Jimenez, R.; Jimenez, B.; Carraud, J.; Kiat, J.M.; Dkhil, B.; Holc, J.; Kosec, M.; Alguero, M.**

*Transition between the ferroelectric and relaxor states in 0.8Pb(Mg<sub>0.115</sub>Nb<sub>0.23</sub>)O<sub>3</sub>-0.2PbTiO<sub>3</sub> ceramics*  
Physical Review B 74 (2006) 184106

**Joubert, J.M.**

*Crystal structure, hydrogen absorption properties and crystal structure of the deuterides of some Nb-Ni derived m phase compounds*  
Journal of Solid State Chemistry 178 (2005) 1620-1629

**Kaiser-Bischoff, I.; Boysen, H.; Scherf, C.; Hansen, T.**

*Anion diffusion in Y- and N-doped ZrO<sub>2</sub>*  
Physical Chemistry Chemical Physics 7 (2005) 2061-2067

**Kempa, M.; Hlinka, J.; Kulda, J.; Bourges, P.; Kania, A.; Petzelt, J.**

*Lattice dynamics of cubic PbTiO<sub>3</sub> by inelastic neutron scattering*  
Phase Transitions 79 (2006) 351-359

**Kaneko, K.; Metoki, N.; Matsuda, T.D.; Kuwahara, K.; Kohgi, M.; Shiina, R.; Mignot, J.M.; Gukasov, A.; Bernhoeft, N.**

*Field-induced antiferroquadrupolar order in the heavy fermion superconductor PrOS<sub>4</sub>Sb<sub>12</sub>*  
Physica B 378-380 (2006) 189-191

**Kantor, A.P.; Dubrovinsky, L.S.; Dubrovinskaia, N.A.; Kantor, I.Y.; Goncharenko, I.N.**

*Phase transitions in MnO and FeO at low temperatures: A neutron powder diffraction study*

Journal of Alloys and Compounds 402 (2005) 42-45

**Kaptas, D.; Svab, E.; Somogyvari, Z.; Andre, G.; Kiss, L.F.; Balogh, J.; Bujdoso, L.; Kemeny, T.; Vincze, I.**

*Incommensurate antiferromagnetism in FeAl<sub>2</sub>: Magnetic, Mossbauer, and neutron diffraction measurements*

Physical Review B 73 (2006) 012401

**Karlovska, J.; Uhrikova, D.; Kucerka, N.; Teixeira, J.; Devinsky, F.; Lacko, I.; Balgavy, .**

*Influence of N-dodecyl-N,N-dimethylamine N-oxide on the activity of sarcoplasmic reticulum Ca<sup>2+</sup>-transporting ATPase reconstituted into diacylphosphatidylcholine vesicles: Effects of bilayer physical parameters*

Biophysical Chemistry 119 (2006) 69-77

**Kgomo, DB.; Levendis, DC.; Gukasov, A.; Cousson, A.; Schonig L.F.R.; Venter, A.M.**

*Low-temperature (110 K) single-crystal neutron diffraction study of (+/-)-camphoric anhydride*

Acta Crystallographica E 61 (2005) O1141-O1143

**Khomchenko, V.A.; Troyanchuk, I.O.; Kurbakov, A.I.; Gamari-Seale, H.; Eremenko, V.V.; Szymczak, H.; Szymczak, R.**

*Magnetic phase transitions in the lightly doped Nd<sub>1-x</sub>Ca<sub>x</sub>MnO<sub>3</sub> manganites*

Journal of Magnetism and Magnetic Materials 288 (2005) 224-235

**Kittaka, S.; Takahara, S.; Yamaguchi, T.; Bellissent-Funel, M.C.**

*Interlayer water molecules in vanadium pentoxide hydrate. 8. Dynamic properties by quasi-elastic neutron scattering*

Langmuir 21 (2005) 1389-1397

**Klein, L.C.; Daiko, Y.; Aparicio, M.; Damay, F.**

*Methods for modifying proton exchange membranes using the sol-gel process*

Polymer 46 (2005) 4504-4509

**Kneller, G.R.**

*Quasielastic neutron scattering and relaxation processes in proteins: analytical and simulation-based models*

Physical Chemistry Chemical Physics 7 (2005) 2641-2655

**Kneller, G.R.**

*Molecular simulations and their analysis*

Journal de Physique IV 130 (2005) 155-178

**Kneller, G.R.**

*Comment on "Using quaternions to calculate RMSD" - [J. Comp. Chem. 25, 1849 (2004)]*

Journal of Computational Chemistry 26 (2005) 1660-1662

**Kneller, G.R.; Calligari, P.**

*Efficient characterization of protein secondary structure in terms of screw motions*

Acta Crystallographica D 62 (2006) 302-311 Part 3

**Kneller, G.R.**

*Hamiltonian formalism for semiflexible molecules in Cartesian coordinates.*

Journal of Chemical Physics 125 (2006) 114107

**Koepfer, I.; Bellissent-Funel, M.C.; Petry, W.**

*Dynamics to pico- to nanoseconds of trehalose in aqueous solutions as seen by quasielastic neutron scattering*

Journal of Chemical Physics 122 (2005) 024902

**Kohgi, M.; Iwasa, K.; Mignot, J.M.; Hiess, A.; Ochiai, A.; Aoki, H.**

*Quantum spin excitations in Yb<sub>4</sub>As<sub>3</sub> under magnetic field*

Physica B 359-361 (2005) 1436-1438

**Komarek, A.; Roth, H.; Lorenz, T.; Stein, W.D.; Cwik, M.; Freimuth, A.; Braden, M.; Bourée, F.**

*Structural properties of RE<sub>2</sub>TiO<sub>7</sub> and Y<sub>1-x</sub>Ca<sub>x</sub>TiO<sub>7</sub>*

Verhandlungen der Deutschen Physikalischen Gesellschaft 40 (2005) 577

**Korobko, A.V.; Jesse, W.; Lapp, A.; Egelhaaf, S.U.; van der Maarel, J.R.C.**

*Structure on strongly interacting polyelectrolyte diblock copolymer micelles*

Journal of Chemical Physics 122 (2005) 024902

**Krezhov, K.A.; Kovacheva, D.; Svab, E.; Bouree, F.**

*Neutron powder diffraction study of a system of half-hole-doped bismuth-based calcium manganites at room temperature*

Journal of Physics Condensed Matter 17 (2005) SS3139-S3147

**Kriener, M.; Steffens, P.; Baier, J.; Schumann, O.; Zabel, T.; Lorenz, T.; Friedt, O.; Muller, R.; Gukasov, A.; Radaelli, PG.; Reutler, P.; Revcolevschi, A.; Nakatsuji, S.; Maeno, Y.; Braden, M.**

*Structural aspects of metamagnetism in Ca<sub>2-x</sub>Sr<sub>x</sub>RuO<sub>4</sub>: Evidence for field tuning of orbital occupation*

Physical Review Letters 95 (2005) 267403

**Kroll, T.; Klingeler, R.; Geck, J.; Buchner, B.; Selke, W.; Hucker, M.; Gukasov, A.**

*Magnetism of low-doped spin chains in L<sub>a</sub><sub>1-x</sub>(Sr, Ca)<sub>14-x</sub>Cu<sub>24</sub>O<sub>41</sub>*

Journal of Magnetism and Magnetic Materials 290-291 (2005) 306-309

**Kusnierz, J.; Mathon, M.H.; Baudin, T.; Jasienski, Z.; Penelle, R.**

*Texture of Al-Cu alloys deformed by ECAP*

Materials Science Forum 495-497 (2005) 851-856

**Kusnierz, J.; Mathon, M.H.; Bogucka, J.; Faryna, M.; Jasienski, Z.; Penelle, R.; Baudin, T.**

*Microstructure, texture and mechanical properties of copper under ARB processing*  
Archives of Metallurgy and Materials 50 (2006) 237-243

**Kusnierz, J.; Mathon, M.H.; Dutkiewicz, J.; Baudin, T.; Jasienski, Z.; Penelle, R.**

*Microstructure and texture of ECAP processed AlCu<sub>4</sub>SiMn and AlCu<sub>5</sub>AgMgZr alloys*  
Archives of Metallurgy and Materials 50 (2005) 367-377

**Lagrené, K.; Zanotti, J.-M.**

*Dynamics of porous alumina confined polymer*  
To appear in European Physical Journal.

**Lagrené, K.; Zanotti, J.-M.**

*PEO melt dynamics in bulk and confined in nanometric cylindrical channels*  
Proceedings of the QENS 2006 conference.; To appear in MRS Symposium Proceedings

**Lairez, D.; Cathala, B.; Monties, B.; Bedos-Belval, F.; Duran, H.; Gorrichon, L.;**

*Aggregation during Coniferyl Alcohol Polymerization in Pectin Solution: A Biomimetic Approach of the First Steps of Lignification*  
Biomacromolecules 6 (2005) 763-774

**Lairez, D.; Pelta, J.**

*Diffusion of neutrons in small angles: application in the study of the biological macromolecules in solution*  
Journal de Physique IV 130 (2005) 39-62

**Lambert, S.; Vincent, A.; Bruneton, E.; Beaudet-Savignat, S.; Guillet, F.; Minot, B.; Bouree, F.**

*Structural investigation of La<sub>9,33</sub>Si<sub>6</sub>O<sub>26</sub><sup>-</sup> and La<sub>9</sub>EASi<sub>6</sub>O<sub>26+δ</sub> doped apatites-type lanthanum silicate (AE=Ba, Sr and Ca) by neutron powder diffraction*  
Journal of Solid State Chemistry 179 (2006) 2602-2608

**Lang, G.; Bobroff, J.; Alloul, H.; Mendels, P.; Blanchard, N.; Collin, G.**

*Evidence of a single nonmagnetic Co<sup>3+</sup> state in the Na<sub>1</sub>CoO<sub>2</sub> cobaltate*  
Physical Review B 72 (2005) 094404

**Le Toquin, R.; Paulus, W.; Cousson, A.; Prestipino, C.; Lamberti, C.**

*Time-resolved in situ studies of oxygen intercalation into SrCoO<sub>2.5</sub>; performed by neutron diffraction and X-ray absorption spectroscopy*  
Journal of the American Chemical Society 128 (2006) 13161-13174

**Li, C.P.; Roshchin, I.V.; Batlle, X.; Viret, M.; Ott, F.; Schuller, I.K.**

*Fabrication and structural characterization of highly ordered sub-100-nm planar magnetic nanodot arrays over 1 cm<sup>2</sup> coverage area*  
Journal of Applied Physics 100 (2006) 074318

**Litaiem, H.; Dammak, M.; Mhiri, T.; Cousson, A.**

*Structural, conductivity and dielectric studies in (NH<sub>4</sub>)<sub>2</sub>SeO<sub>4</sub> · Te(OH)<sub>6</sub>*  
Journal of Alloys and Compounds 396 (2005) 34-39

**Lodini, A.; Millet, P.**

*Les nanomatériaux : nouvelles applications en biomécanique*  
Traitement Thermique et Ingénierie des Surfaces 366 (2005) 27-34

**Loupiac C, Bonetti M, Pin S, Calmettes P**

*beta-lactoglobulin under high pressure studied by small-angle neutron scattering*  
Biochimica et Biophysica Acta 1764 (2006) 211-216

**Ludwig, K.; Livet, F.; Bley, F.; Simon, J.-P.; Caudron, R.; Le Bolloc'h, D.; Moussaid, A.**

*X-ray intensity fluctuation spectroscopy studies of ordering kinetics in a Cu-Pd alloy*  
Physical Review B 72 (2005) 144201

**Maillard P; Tessier, F.; Orhan, E.; Ceviré, F.; Marchand, R.**

*Thermal Ammonolysis study of the rare-earth translates RTaO<sub>4</sub>*  
Chemical Materials 17 (2005) 152-156

**Malik, S.; Rochas, C.; Schmutz, M.; Guenet, J.M.**

*Syndiotactic polystyrene intercalates from naphthalene derivatives*  
Macromolecules 38 (2005) 6024-6030

**Malikova, N.; Cadene, A.; Marry, V.; Dubois, E.; Turq, P.; Zanotti, J.M.; Longeville, S.**

*Diffusion of water in clays - microscopic simulation and neutron scattering*  
Chemical Physics 317 (2005) 226-235

**Maniadis, P.; Aubry, S.**

*Targeted energy transfer by Fermi resonance*  
Physica D 202 (2005) 200-217

**Maniadis, P.; Kopidakis, G.; Aubry, S.**

*Energy dissipation threshold and self-induced transparency in systems with discrete breathers*  
Physica D 216 (2006) 121-135

**Martinez-de la Cruz, A.; Amador, U.; Rodriguez-Carvajal, J.; Garcia-Alvarado, F.**

*Electrochemical zinc insertion into  $W_{18}O_{49}$ : Synthesis and characterization of new bronzes*

Journal of Solid State Chemistry 178 (2005) 2998-3003

**Mata, I.; Espinosa, E.; Molins, E.; Veintemillas, S.; Maniukiewicz, W.; Lecomte, C.; Cousson, A.; Paulus, W.**  
*Contribution to the application of the transferability principle and the multipolar modeling of H atoms : electron-density study of L-histidinium dihydrogen orthophosphate orthophosphoric acid I*

Acta Crystallographica A 62 (2006) 365-378

**Memboeuf, A.; Aubry, S.**

*Targeted energy transfer between a Morse oscillator and a Rotor : a model for selective chemical dissociation*

Physica D 207 (2005) 1-23

**Mendels, P.; Bono, D.; Bobroff, J.; Lang, G.; Collin, G.; Colson, D.; Blanchard, N.; Alloul, H.; Mukhamedshin, I.; Bert, F.; Amato, A.; Hillier, A.D.**

*Series of bulk magnetic-phase transitions in  $Na_xCoO_2$ : A mSR study*

Physica B 374 (2006) 278-281

**Mendels, P.; Bono, D.; Bobroff, J.; Collin, G.; Colson, D.; Blanchard, N.; Alloul, H.; Mukhamedshin, I.; Bert, F.; Amato, A.; Hillier, A.D.**

*Cascade of bulk magnetic phase transitions in  $Na_xCoO_2$  as studied by muon spin rotation*

Physical Review Letters 94 (2005) 136403

**Mendil, A.**

*Identification d'un comportement terminal élastique dans les fondus de polymères, de polymères cristaux liquides et analyse de la transition de phase induite par cisaillement*

Thèse soutenue le 30 septembre 2006 à l'Université Paris XI-Orsay

**Mendil, H.; Baroni, P.; Noirez, L.**

*Solid-like rheological response of non-entangled polymers in the molten state*

European Physical Journal E 19 (2006) 77-85

**Mendil, H.; Baroni, P.; Noirez, L.**

*Unexpected giant elasticity in side-chain liquid-crystal polymer melts: A new approach for the understanding of shear-induced phase transitions*

Europhysics Letters 72 (2005) 983-989

**Mendil, H.; Noirez, L.**

*Identification of gel-like behaviour in side-chain liquid crystal polymer melts*

Macromolecular Symposia 220 (2005) 143-148

**Mendil, H.; Noirez, L.; Baroni, P.**

*Reply to the "Commentary by D. Collin & P. Martinoty"*

European Physical Journal E 19 (2006) 99-100

**Mendil, H.; Noirez, L.; Baroni, P.; Grillo, I.**

*The frozen state in the liquid phase of side-chain liquid crystal polymers*

Physical Review Letters 96 (2006) 077801

**Menig, R.; Pintschovius, L.; Schulze, V.; Vohringer, O.**

*Depth profiles of macro residual stresses in thin shot peened steel plates determined by X-ray and neutron diffraction*

Scripta Materialia 45 (2006) 977-983

**Menelle, A.; Ott, F.**

*TiToF : a high intensity space-time reflectometer.*

Physica B 385-386 (2006) 985-988

**Meriguet G.; Cousin F.; Dubois E.; Boue F.; Cebers A.; Farago B.; Perzynski W.**

*What tunes the structural anisotropy of magnetic fluids under a magnetic field ?*

Journal of Physical Chemistry B 110 (2006) 4378-4386

**Michaud, C.; Teixeira, J.**

*Bac to Basic : L'eau*

La Recherche Hors Série, n°1 (2005) 52-58

**Michel, J.P.; Lacaze, E.; Goldmann, M.; Gailhanou, M.; de Boissieu, M.; Alba, M.**

*Revealing the structure of focal conics cores and their influence on the evolution with temperature: An x-ray study of ultra-thin 8CB films*

Molecular Crystals and Liquid Crystals 437 (2005) 1343-1353

**Michel, J.P.; Lacaze, E.; Goldmann, M.; Gailhanou, M.; de Boissieu, M.; Alba, M.**

*Structure of smectic defect cores: X-ray study of 8CB liquid crystal ultrathin films*

Physical Review Letters 96 (2006) 027803

**Michel, J.P.; Lacaze, E.; Goldmann, M.; Alba, M.**

*Comment on "Structure of smectic defect cores: X-ray study of 8CB liquid crystal ultrathin films" - Reply*

Physical Review Letters 97 (2006) 159802

**Mignot, J.-M.; Alekseev, P.A.; Nemkovski, K.S.; Nefeodova, E.V.; Rybina, A.V.; Regnault, L.P.; Shitsevalova, N.Yu.; Iga, F.; Takabatake, T.**

*Neutron scattering study of spin and lattice dynamics in  $YbB_{12}$*

Physica B 383 (2006) 16-19

**Mignot, J.M.; Alekseev, P.A.; Nemkovski, K.S.; Regnault, L.P.; Iga, F.; Takabatake, T.**

*Evidence for short-range antiferromagnetic fluctuations in Kondo-insulating  $YbB_{12}$*

Physical Review Letters 94 (2005) 247204

## PUBLICATIONS

**Mignot, J.M.; Goncharenko, I.N.; Matsumura, T.; Suzuki, T.**

*Magnetic phase diagram of the mixed-valence semiconductor TmSe under multi-extreme (P, H, T) conditions*  
Physica B 359-361 (2005) 105-107

**Mignot, J.M.; Sera, M.; Iga, F.**

*Magnetic phase diagram of  $Ce_{0.70}Pr_{0.30}B_6$*   
Physica B 383 (2006) 41-42

**Mirebeau, I.; Apetrei, A.; Rodriguez-Carvajal, J.; Bonville, P.; Forget, A.; Colson, D.; Glazkov, V.; Sanchez, J.P.; Isnard, O.; Suard, E.**

*Ordered spin ice state and magnetic fluctuations in  $Tb_2Sn_2O_7$*   
Physical Review Letters 94 (2005) 246402

**Mirebeau, I.; Goncharenko, I.N.**

*$Tb_2Ti_2O_7$ : a 'spin liquid' single crystal studied under high pressure and high magnetic field*  
Journal of Physics: Condensed Matter 17 (2005) S771-S782

**Mirebeau, I.; Apetrei, A.; Goncharenko, I. N.; Moessner, R.**  
*Two geometrically frustrated magnets studied by neutron diffraction*

Physica B 385 (2006) 307-312 Part 1

**Mirebeau, I.; Apetrei, A.; Goncharenko, I.; Andreica, D.; Bonville, P.; Sanchez, J. P.; Amato, A.; Suard, E.; Crichton, W. A.; Forget, A.; Colson, D.**

*Pressure-induced ferromagnet to spin-glass transition in  $Gd_2Mo_2O_7$*   
Physical Review B 74 (2006) 174414

**Monceau, P.**

*Nature of the Peierls transition in charge density wave systems: Strong coupling versus weak coupling*  
Physica D 216 (2006) 167-171

**Mondiere, R.; Goddard, J.P.; Huiban, M.; Carrot, G.; Le Gall, T.; Mioskowski, C.**

*Boron-mediated polymerization of ylides derived from allylic arsonium salts: influence of the double bond substitution on the outcome*  
Chemical Communications 7 (2006) 723-725

**Mondiere, R.; Goddard, J.P.; Carrot, G.; Le Gall, T.; Mioskowski, C.**

*Synthesis of poly(2-substituted-1-propenylene)s from allylic arsonium ylides*  
Macromolecules 38 (2005) 663-668

**Motoyama EM, Mang PK, Petitgrand D, Yu G, Vajk OP, Vishik IM, Greven M.**

*Magnetic field effect on the superconducting magnetic gap of  $Nd_{1.85}Ce_{0.15}CuO_4$*   
Physical Review Letters 96 (2006) 137002

**Moudden A.H.**

*Ab initio study of C-substituted MgB<sub>2</sub>*  
Journal of Physics and Chemistry of Solids 67 (2006) 115-119

**Mukhamedshin, I.R.; Alloul, H.; Collin, G.; Blanchard, N.**

*$^{9}Co$  NMR study of the Co states in superconducting and anhydrous cobaltates*

Physical Review Letters 94 (2005) 247602

**Mukhamedshin, I.R.; Alloul, H.; Collin, G.; Blanchard, N.**

*$^{23}Na$  NMR evidence for charge order and anomalous magnetism in  $Na_2CoO_2$*

Physical review Letters 94 (2005) 207003

**Mutka, H.; Ehlers, G.; Payen, C.; Bono, D.; Stewart, J.R.; Fouquet, P.; Mendels, P.; Mevellec, J.Y.; Blanchard, N.; Collin, G.**

*Neutron spin-echo investigation of slow spin dynamics in kagome-bilayer frustrated magnets as evidence for phonon assisted relaxation in  $SrCr_{9x}Ga_{12-9x}O_{19}$*   
Physical Review Letters 97 (2006) 047203

**Nagasawa, M.; Nad, F.; Monceau, P.; Fabre, J.M.**

*Modification of the charge ordering transition in the quasi-one-dimensional conductor  $(TMTTF)_{(2)}SbF_6$  under pressure*  
Solid State Communications 136 (2005) 262-267

**Nefeodova, E.V.; Alekseev, P.A.; Mignot, J.M.; Nemkovski, K.S.; Lazukov, V.N.; Sadikov I.P.; Paderno Y.B.; Shitsevalova N.Y.; Bewley R.I.**

*Spin-gap magnetic response in  $(Yb.; Lu)B-12$*   
Journal of Solid State Chemistry 179 (2006): 2858-2861

**Nemkovski, K.S.; Alekseev, P.A.; Mignot, J.M.; Rybina, A.V.; Iga, F.; Takabatake, T.; Shitsevalova, N.Y.; Paderno, Y.B.; Lazukov, V.N.; Nefeodova, E.V.; Tiden N.N.; Sadikov I.P.**

*Lattice dynamics in the kondo insulator  $YbB12$*   
Journal of Solid State Chemistry 179 (2006) 2895-2899

**Nguyen Xuan HN, Galez P, Pisch A, Bertrand C, Beauquis S, Soubeyroux JL, Bouree-Vigneron F.**

*High resolution and in situ neutron powder diffraction study of the crystal structure and the stability of  $Ba_4CaCu_3O_{8+\delta}$*   
Journal of Solid State Chemistry 178 (2005) 3207-3217

**Noirez, L.**

*Origin of shear-induced phase transitions in melts of liquid-crystal polymers*

Physical Review E 72 (2005) 051701

**Noirez, L.; Pépy, G.; Baroni, P.**

*Structural investigation of the pressure induced effects in liquid crystal*

Journal of Physics Condensed Matter 17 (2005) 53155-53164

**Noirez, L.**

*Complex Melts under Extreme Conditions: from Liquid Crystal to Polymers. The Key-role of the Scattering methods for flow and pressure investigations.*

"Neutron and X-Ray Scattering" du livre "Soft Matter: Scattering, Imaging and Manipulation" Volume 3/4 Ed. R. Pecora & R. Borsali, Kluwer Academic Publishers (2006).

**Nunes, C.A.; Kaczorowski, D.; Rogl, P.; Baldissera, M.R.; Suzuki, P.A.; Coelho, G.C.; Grytsiv, A.; Andre, G.; Bouree, F.; Okada, S.**

*The NbB<sub>2</sub>-phase revisited: Homogeneity range, defect structure, superconductivity*

Acta Materialia 53 (2005) 3679-3687

**Oberdisse, J.; El Harrak, A.; Carrot, G.; Jestin, J.; Boue, F.**

*Structure and rheological properties of soft-hard nanocomposites: influence of aggregation and interfacial modification*

Polymer 46 (2005): 6695-6705

**Onufrieva, F.; Pfeuty, P.**

*Doping Evolution of the Electronic Properties of Hole- and Electron-Doped High-T<sub>c</sub> Cuprates: Role of Density Wave Correlations*

Physical Review Letters 95 (2005) 207003

**Ostoréro, J.; Paul-Boncour, V.; Bourée, F.; André G.**

*Neutron diffraction study of Ho<sub>5</sub>YFe<sub>23</sub> and Ho<sub>5</sub>YFe<sub>23</sub>D<sub>16</sub> deuteride*

Journal of Alloys and Compounds 404-406 (2005) 191-194

**Ouazi, S.; Bobroff, J.; Alloul, H.; Le Tacon, M.; Blanchard, N.; Collin, G.; Julien, M.H.; Horvatic, M.; Berthier, C.**

*Impurity-induced local magnetism and density of states in the superconducting state of YBa<sub>2</sub>Cu<sub>3</sub>O<sub>7</sub>*

Physical Review Letters 96 (2006) 127005

**Pailhes, S.; Bourges, P.; Sidis, Y.; Bernhard, C.; Keimer, B.; Lin, C.T.; Tallon, J.L.**

*Absence of an isotope effect in the magnetic resonance in high-T<sub>c</sub> superconductors*

Physical Review B 71 (2005) 220507

**Pailhes, S.; Ulrich, C.; Fauque, B.; Hinkov, V.; Sidis, Y.; Ivanov, A.; Lin, C.T.; Keimer, B.; Bourges, P.**

*Doping dependence of bilayer resonant spin excitations in (Y;Ca)Ba<sub>2</sub>Cu<sub>3</sub>O<sub>6+x</sub>*

Physical Review Letters 96 (2006) 257001

**Palancher, H.; Hodeau, J.L.; Pichon, C.; Berar, J.F.; Lynch, J.; Rebours, B.; Rodriguez-Carvajal, J.**

*Direct localization of atoms in mixed-occupancy powders by resonant contrast diffraction*

Angewandte Chemie-International Edition 44 (2005) 1725-1729

**Palancher, H.; Pichon, C.; Hodeau, J.L.; Berar, J.F.; Lynch, J.; Rebours, B.; Rodriguez-Carvajal, J.**

*Cation distributions in fully hydrated Sr- and Rb- bicationic zeolites: an X-ray anomalous powder diffraction study*

Zeitschrift für Kristallographie 487-492 Part 2 Suppl. 23.: 2006

**Papavassiliou, G.; Pissas, M.; Diamantopoulos, G.; Belesi, M.; Fardis, M.; Stamopoulos, D.; A. Kontos, A.; Hennion, M.; Dolinsek, J.; Ansermet, J-Ph.; Dimitropoulos, C.**

*Charge and orbital textures in La<sub>1-x</sub>Sr<sub>x</sub>MnO<sub>3</sub> (x= 0.075, 0.125, and 0.2)*

Physical Review Letters 96 (2006) 097201

**Papoular, R.J.; Allouchi, H.; Chagnes, A.; Dzyabchenko, A.; Carre, B.; Lemordant, D.; Agafonov, V.**

*X-ray powder diffraction structure determination of gamma-butyrolactone at 180 K: phase-problem solution from the lattice energy minimization with two independent molecules*

Acta Crystallographica 61 (2005) 312-320

**Papoular, R.J.; Allouchi, H.; Dzyabchenko, A.V.; Davydov, V.A.; Rakhmanina, A.V.; Boltalina, O.V.; Seppelt, K.; Agafonov, V.**

*High-resolution X-ray powder diffraction structure determination of C60F48*

Fullerenes nanotubes and carbon nanostructures 14 (2006) 279-285

**Pasturel, M.; Weill, F.; Bouree, F.; Bobet, J.L.; Chevalier, B.**

*Hydrogenation of the ternary silicides RENiSi (RE = Ce, Nd) crystallizing in the tetragonal LaPtSi-type structure*

Journal of Alloys and Compounds 397 (2005) 17-22

**Patrascu, C.; Gauffre, F.; Nallet, F.; Bordes, R.; Oberdisse, J.; de Lauth-Vigueri, N.; Mingotaud, C.**

*Micelles in ionic liquids: Aggregation behavior of alkyl poly(ethyleneglycol)-ethers in 1-butyl-3-methyl-imidazolium type ionic liquids*

Chemphyschem 7 (2006) 99-101

## PUBLICATIONS

- Paul-Boncour, V.; Guillot, M.; Wiesinger, G.; André, G.**  
*Giant isotope effect on the itinerant-electron metamagnetism in  $YFe_2(HyD_{1-y})_{(4.2)}$*   
Physical Review B 72 (2005) 174430
- Paul-Boncour V.; Filipek, S.M.; Andre, G.; Bouree, F.; Guillot, M.; Wierzbicki, R.; Marchuk, I.; Liu, R.S.; Villeroy, B.; Percheron-Guegan, A.; Yang, H.D.; Pin, S.C.**  
*Structural, thermal and magnetic properties of  $ErMn_2D_6$  synthesized under high deuterium pressure*  
Journal of Physics-Condensed Matter 18 (2006) 6409-6420
- Paul-Boncour, V.; Filipek, S.M.; Dorogova, M.; Bouree, F.; Andre, G.; Marchuk, I.; Percheron-Guegan A.; Liu R.S.**  
*Neutron diffraction study, magnetic properties and thermal stability of  $YMn_2D_6$  synthesized under high deuterium pressure*  
Journal of Solid State Chemistry 178 (2005) 356-362
- Paul-Boncour, V.; Guillot, M.; André G.; Bourée, F.; Wiesinger, G.; Percheron-Guégan, A.**  
*Origin of the first order magnetostructural transition in  $YFe_2D_{4.2}$*   
Journal of Alloys and Compounds 404-406 (2005) 355-359
- Pautrat, A.; Scola, J.; Simon, C.; Mathieu, P.; Brulet, A.; Goupil, C.; Higgins, M.J.; Bhattacharya, S.**  
*Metastable states of a flux-line lattice studied by transport and small-angle neutron scattering*  
Physical Review B 71 (2005) 064517
- Pépy, G.**  
*Neutron beam. Analysis of traces, imaging and medicine*  
Techniques de l'Ingénieur, Génie Nucléaire (2006) 59
- Perca, C.; Pinsard-Gaudart, L.; Daoud-Aladine, A.; Fernandez-Diaz, M.T.; Rodriguez-Carvajal, J.**  
*Crystal and magnetic structures of the  $Mn^{3+}$  orbital ordered manganite  $YBaMn_2O_{5.5}$*   
Chemistry of Materials 17 (2005) 1835-1843
- Perreur, C., Habas, J.P., Lapp, A., Peyrelasse, J.**  
*Salt influence upon the structure of aqueous solutions of branched PEO-PPO-PEO copolymers*  
Polymer 47 (2006) 841-848
- Phelippeau, A.; Pommier, S.; Zakharchenko, I.; Levy-Tubiana, R.; Tsakalakos, T.; Clavel, M.; Croft, M.; Zhong, Z.; Prioul, C.**  
*Cold drawn steel wires-processing, residual stresses and ductility- Part II: Synchrotron and neutron diffraction*  
Fatigue & Fracture of Engineering Materials & Structures 29 (2006) 255-265
- Pintschovius, L.; Reznik, D.; Yamada, K.**  
*Oxygen phonon branches in overdoped  $La^{1.7}Sr_{0.3}Cu_3O_4$*   
Physical Review B 74 (2006) 174514
- Piekos, K.; Tarasiuk, J.; Wierzbowski, K.; Gerber, P.; Bacroix, B.**  
*Monte-Carlo version of vertex model applied to recrystallization modelling*  
Materials Science Forum 495-497 (2005) 1183-1188
- Plentz-Meneghetti, S.; Kress, J.; Peruch, F.; Lapp, A.; Duval, M.; Muller, R.; Lutz, P.J.**  
*Solution and bulk rheological behavior of poly(ethylenes) based on VERSIPOLTM catalysts*  
Polymer 46 (2005) 8913-8925
- Pouget, J.P.; Foury-Leylekian, P.; Le Bolloc'h, A.; Hennion, B.; Ravy, S.; Coulon, C.; Cardoso, V.; Moradpour, A.**  
*Neutron-scattering evidence for a spin-peierls ground state in  $(TMTTF)_2PF_6$*   
Journal of Low Temperature Physics 142 (2006): 147-152
- Prem, M.; Krystian, M.; Pichl, W.; Krexner, G.; Klotz, S.**  
*Neutron scattering investigation of pressure-induced phase transitions in Li and Ba*  
Journal of Physics : Condensed Matter 17 (2005) S3165-S3171
- Quintana, I.; Arbe, A.; Colmenero, J.; Frick, B.**  
*Dynamics of polyethersulfone phenylene rings: a quasielastic neutron scattering study*  
Macromolecules 38 (2005) 3999-4013
- Reznik, D.; Pintschoviu, L.; Endoh, Y.; Bourges, P.; Sidis, Y.; Masui, T.; Tajima, S.**  
*Spin gap in optimally-doped YBCO*  
Journal of Physics and Chemistry of Solids 67 (2006) 509-510
- Reznik, D.; Pintschovius, L.; Ito, M.; Iikubo, S.; Sato, M.; Goka, H.; Fujita, M.; Yamada, K.; Gu, G.D.; Tranquada, J.M.**  
*Electron-phonon coupling reflecting dynamic charge inhomogeneity in copper oxide superconductors*  
Nature 440 (2006) 1170-1173
- Reznik, D.; Reichardt, W.**  
*Bond-bending and bond-stretching phonons in ferromagnetic  $La_{0.7}Sr_{0.3}MnO_3$*   
Physical Review B 71 (2005) 092301

- Rippel, M.M.; Leite, C.A.; Lee, L.T.; Galembeck, F.**  
*Formation of calcium crystallites in dry natural rubber particles*  
Journal of Colloid and Interface Science 288 (2005) 449-456
- Rippel, M.M.; Leite, C.A.P.; Lee, L.T.; Galembeck, F.**  
*Direct imaging and elemental mapping of microgels in natural rubber particles*  
Colloid and Polymer Science 283 (2005) 570-574
- Ristori, S.; Obserdisse, J.; Grillo, I.; Donati, A.; Spalla, O.**  
*Structural characterization of cationic liposomes loaded with sugar-based carboranes*  
Biophysical Journal 88 (2005) 535-547
- Roth, H.; Kordonis, K.; Komarek, A.; Cwik, M.; Schittner, N.; Baier, J.; Kriener, M.; Lorenz, T.; Zabel, T.; El Filali, A.; Braden, M.; Freimuth, A.; Andre, G.**  
*Relevance of structural distortions to the metal insulator transition of doped  $LaTiO_3$*   
Verhandlungen der Deutschen Physikalischen Gesellschaft 40 (2005) 542
- Rotter, M.; Lindbaum, A.; Barcza, A.; El Massalami, M.; Doerr, M.; Loewenhaupt, M.; Michor, H.; Beuneu, B.**  
*Magnetoelastic paradox: Absence of symmetry-breaking distortions below  $T-N$  in antiferromagnetic systems without orbital moment*  
Europhysics Letters 76 (2006) 160-166
- Rousse, G.; Klotz, S.; Saitta, AM.; Rodriguez-Carvajal, J.; McMahan, M.I.; Couzinet, B.; Mezouar, M.**  
*Structure of the intermediate phase of  $PbTe$  at high pressure*  
Physical Review B 71 (2005) 224116
- Rouxel, T.; Dely, N.; Sangleboeuf, J.C.; Deriano, S.; LeFloch, M.; Beuneu, B.; Hampshire, S.**  
*Structure-property correlations in  $Y-Ca-Mg$ -sialon glasses: Physical and mechanical properties*  
Journal of the American Ceramic Society 88 (2005) 889-896
- Ruegg, C.; Norman, B.; Matsumoto, M.; Niedermayer, C.; Furrer, A.; Kramer, K.W.; Gudel, H.U.; Bourges, P.; Sidis, Y.; Mutka, H.**  
*Quantum statistics of interacting dimer spin systems*  
Physical Review Letters 95 (2005) 267201
- Ruiz, E.; Rajaraman, G.; Alvarez, S.; Gillon, B.; Stride, J.; Clerac, R.; Larionova, J.; Decurtins, S.**  
*Symmetry and topology determine the  $Mo-V-CN-Mn-II$  exchange interactions in high-spin molecules*  
Angewandte Chemie-International Edition 44 (2005) 1725-1729
- Rule, K.C.; Ruff, J.P.C.; Gaulin, B.D.; Dunsiger, S.R.; Gardner, J.S.; Clancy, J.P.; Lewis, M.J.; Dabkowska, H.A.; Mirebeau, I.; Manuel, P.; Qiu, Y.; Copley, J.R.D.**  
*Field-induced order and spin waves in the pyrochlore antiferromagnet  $Tb_2Ti_2O_7$*   
Physical Review Letters 96 (2006) 177201
- Runov, V.V. Chernenkov, Yu.P., Runova, M.K., Gavrilyuk, V.G., Glavatska, N.I., Goukasov, A.G., Koledov, V.V., Shavrov, V.G., Khova\_lo, V.V.**  
*Spin correlations and a mesoscopic structure in  $Ni-Mn-Ga$*   
Journal of Experimental and theoretical Physics 102 (2006) 102-113
- Ryan, A.J.; Crook, C.J.; Howse, J.R.; Topham, P.; Jones, R.A.L.; Geoghegan, M.; Parnell, A.J.; Ruiz-Pérez, L.; Martin, S.J.; Cadby, A.; Menelle, A.; Gleeson, A.J.; Bras, W.**  
*Responsive brushes and gels as components of soft nanotechnology*  
Faraday Discussion, 128 (2005) 55-74
- Ryan, A.J.; Crook, C.J.; Howse, J.R.; Topham, P.; Geoghegan, M.; Martin, S.J.; Parnell, A.J.; Ruiz-Pérez, L.; Jones, R.A.L.**  
*Mechanical actuation by responsive polyelectrolyte brushes and triblock gels*  
Journal of Macromolecular Science B 44 (2005) 1103-1121
- Saurel D, Brulet A, Heinemann A, Martin C, Mercone S, Simon C**  
*Magnetic field dependence of the magnetic phase separation in  $Pr_{1-x}Ca_xMnO_3$  manganites studied by small-angle neutron scattering*  
Physical Review B 73 (2006) 094438
- Saurel, D.**  
*Etude de la séparation de phase magnétique dans les manganites à effet CMR par diffusion de neutrons aux petits angles*  
Thèse soutenue à l'Université Caen-Basse Normandie, le 7 décembre 2005
- Schenker, R.; Leuenberger, M.N.; Chaboussant, G.; Loss, D.; Gudel, H.U.**  
*Phonon bottleneck effect leads to observation of quantum tunneling of the magnetization and butterfly hysteresis loops in  $(Et_4N)_3Fe_2F_9$*   
Physical Review B 72 (2005) 184403
- Schobinger-Papamantellos P, Rodriguez-Carvajal J, Andre G, Buschow KHJ**  
*Magneto structural phase transitions of  $DyFe_4Ge_2$ ; Part II - Neutron diffraction*  
Journal of Magnetism and Magnetic Materials 300 (2006) 333-350

Schobinger-Papamantellos, P.; Rodriguez-Carvajal, J.; Buschow, K.H.J.; Dooryhee, E.; Fitch, A.N.

*Magneto structural phase transitions of DyFe<sub>4</sub>Ge<sub>2</sub>: Part I - By XRPD*

Journal of Magnetism and Magnetic Materials 300 (2006) 315-332

Schumann, O.; Steffens, P.; Muller, R.; Braden, M.; Andre, G.; Radaelli, P.G.; Andelmann, P.; Nakatsuj, S.; Maen, Y.

*Structural properties of Ca<sub>2-x</sub>Sr<sub>x</sub>RuO<sub>4</sub>*

Verhandlungen der Deutschen Physikalischen Gesellschaft 40 (2005) 591

Schussler-Langeheine, C.; Schlappa, J.; Tanaka, A.; Hu, Z.; Chang, C.F.; Schierle, E.; Benomar, M.; Ott, H.; Weschke, E.; Kaindl, G.; Friedt, O.; Sawatzky, G.A.; Lin, H.J.; Chen, C.T.; Braden, M.; Tjeng, L.H.

*Spectroscopy of stripe order in La<sub>1.8</sub>Sr<sub>0.2</sub>NiO<sub>4</sub> using resonant soft X-ray diffraction*

Physical review Letters 95 (2005) 156402

Senff, D.; Kruger, F.; Scheidl, S.; Benomar, M.; Sidis, Y.; Demmel, F.; Braden, M.

*Spin-wave dispersion in orbitally ordered La<sub>1/2</sub>Sr<sub>3/2</sub>MnO<sub>4</sub>*

Physical Review Letters 96 (2006) 257201

Senff, D.; Reutler, P.; Braden, M.; Friedt, O.; Bruns, D.; Cousson, A.; Bouree, F.; Merz, M.; Buchner, B.; Revcolevschi, A.

*Crystal and magnetic structure of La<sub>1-x</sub>Sr<sub>1+x</sub>MnO<sub>4</sub>: Role of the orbital degree of freedom*

Physical Review B 71 (2005) 024425

Serban, F.; Baczmanski, A.; Labbe, K.; Wierzbanski, K.; Lodini, A.

*Effect of graphite inclusions on mechanical properties and thermal stresses in austempered ductile iron*

Materials Science Forum 490-491 (2005) 73-78

Sieber, A.; Bircher, R.; Waldmann, O.; Carver, G.; Chaboussant, G.; Mutka, H.; Gudel, H.U.

*Effect of pressure on the magnetic anisotropy in the single-molecule magnet Mn-12-acetate: An inelastic neutron scattering study*

Angewandte Chemie-International Edition 44 (2005) 4239-4242

Sieber, A.; Boskovic, C.; Bircher, R.; Waldmann, O.; Ochsenein, S.T.; Chaboussant, G.; Gudel, H.U.; Kirchner, N.; van Slageren, J.; Wernsdorfer, W.; Neels, A.; Stoekli-Evans, H.; Janssen, S.; Juranyi, F.; Mutka, H.

*Synthesis and spectroscopic characterization of a new family of Ni-4 spin clusters*

Inorganic Chemistry 44 (2005) 4315-4325

Simon, Ch.; Pautrat, A.; Goupil, C.; Scola, J.; Mathieu, P.; Brûlet, A.; Ruyter, A.; Higgins, M.J.; Bhattacharya, S.; Plessis, D.

*Why pinning by surface irregularities can explain the peak effect in transport properties and neutron diffraction results in NbSe<sub>2</sub> and Bi-2212 crystals.*

Pramana 66 (2006) 83

Simonet, V., Hippert F., Brand, R.A., Calvayrac, Y., Rodriguez-Carvajal, J., Sadoc, A.

*Chemical decoration in cubic approximant and quasicrystal in the Al-Cu-Fe system*

Philosophical Magazine 86 (2006) 573-579

Simonet, V.; Hippert, F.; Brand, R.A.; Calvayrac, Y.; Rodriguez-Carvajal, J.; Sadoc, A.

*Chemical order in 1/1 Al(Si)-Cu-Fe approximant phases*

Physical Review B 72 (2005) 024214

Soriano, S.; Dumesnil, K.; Dufour, C.; Hennion, M.; Borchers, J.A.; Mangin, P.

*Clamping effect on the magnetic behavior of europium epitaxial thin films*

Journal of Applied Physics 97 (2005) 10K111

Sotiropoulou, M.; Oberdisse, J.; Staikos, G

*Soluble hydrogen-bonding interpolymer complexes in water: A small-angle neutron scattering study*

Macromolecules 39 (2006) 3065-3070

Steffens, P.; Friedt, O.; Alireza, P.; Marshall, W.G.; Schmidt, W.; Nakamura, F.; Nakatsuji, S.; Maeno, Y.; Lengsdorf, R.; Abd-Elmeguid, M.M.; Braden, M.

*High-pressure diffraction studies on Ca<sub>2</sub>RuO<sub>4</sub>*

Physical Review B 72 (2005) 094104

Steffens, P.; Schumann, O.; Fried, O.; Braden, M.

*Competing magnetic instabilities in 214-ruthenates*

Verhandlungen der Deutschen Physikalischen Gesellschaft 40 (2005) 591

**Stein, W.D.; Braden, M.**

*Structure and lattice dynamics in bismuth triborate, BiB<sub>3</sub>O<sub>6</sub>*  
Verhandlungen der Deutschen Physikalischen Gesellschaft  
40 (2005) 143

**Stepanek, P.; Tuzar, Z.; Nallet, F.; Noirez, L.**

*Small-angle neutron scattering from solutions of diblock copolymers in partially miscible solvents*  
Macromolecules 38 (2005) 3426-3431

**Strassle, T.; Klotz, S.; Loveday, J.S.; Braden, M.**

*Equation of state of ordinary ice Ih at 145 K under true hydrostatic pressure up to 5 kbar*  
Journal of Physics Condensed Matter 17 (2005) S3029-S3033

**Stride J.A.; Jayasooriya U.A.; Zanotti J.M.; Kahn R.**

*Molecular dynamics of the self-organising strong hydrogen bonded 3,5-dimethylpyrazole*  
New Journal of Chemistry 30 (2006) 425-429

**Swenson, J.; Jansso, H.; Howells, W.S.; Longeville, S.**

*Reply to 'Comment on 'Dynamics of water in a molecular sieve by quasielastic neutron scattering''*  
Journal of Chemical Physics 125 (2006) 077102

**Swenson, J.; Jansson, H.; Howells, W.S.; Longeville, S.**

*Dynamics of water in a molecular sieve by quasielastic neutron scattering*  
Journal of Magnetism and Magnetic Materials 122 (2005) 084505

**Szuskiewicz, W.; Dynowska, E.; Witkowska, B.; Hennion, B.**

*Spin-wave measurements on hexagonal MnTe of NiAs-type structure by inelastic neutron scattering*  
Physical Review B 73 (2006) 104403

**Szuskiewicz, W.; Fronc, K.; Hennion, B.; Ott, F.; Aleszkiewicz, M.**

*Magnetic stripe domains in Fe/Fe-N multilayers*  
Journal of Alloys and Compounds 423 (2006) 172-175

**Takahara, S.; Kittaka, S.; Mori, T.; Kuroda, Y.; Yamaguchi, T.; Bellissent-Funel, M.C.**

*Neutron scattering study on dynamics of water molecules confined in MCM-41*  
Adsorption - Journal of the International Adsorption Society 11 (2005) 479-483

**Takahara, S.; Sumiyama, N.; Kittaka, S.; Yamaguchi, T.; Bellissent-Funel M.C.**

*Neutron scattering study on dynamics of water molecules in MCM-41. 2. Determination of translational diffusion coefficient*  
Journal of Physical Chemistry B 109 (2005) 11231-11239

**Teixeira, J.**

*As anomalias da agua a baixa temperatura*  
Gazeta de Fisica 28 (2005) 10-16

**Teixeira, J.**

*Les mystères de l'eau*  
Techniques de l'Ingénieur 53 (2006) 1-8

**Teixeira, J.; Luzar, A.; Longeville, S.**

*Dynamics of hydrogen bonds: how to probe their role in the unusual properties of liquid water*  
Journal of Physics : Condensed Matter 18 (2006) S2353-S2362

**Terada, N.; Mitsuda, S.; Gukasov, A.**

*Impurity-induced orthogonal double sinusoidal magnetic structure in the triangular lattice antiferromagnet CuFe<sub>1-x</sub>Al<sub>x</sub>O<sub>2</sub>*  
Physical Review B 73 (2006) 014419

**Toudic, B.; Aubert, F.; Ecolivet, C.; Bourges, P.; Brezczewski, T.**

*Pressure-induced lock-in in an aperiodic nanoporous crystal*  
Physical Review Letters 96 (2006) 145503

**Trabelsi, S.; Guillot, S.; Raspaud, E.; Delsanti, M.; Langevin, D.; Boue, F.**

*New nano- and microparticles with a liquid-crystal-like interior*  
Advanced Materials 18 (2006) 2403

**Tran, V.H.; Rog, P.; Andre, G.; Bouree, F.**

*Electron correlation effects and ferromagnetic order in b-UB2C*  
Journal of Physics : Condensed Matter 18 (2006) 703-718

**Tseggai, M.; Mathieu, R.; Nordblad, P.; Tellgren, R.; Bau, L.V.; Nam, D.N.H.; Phuc, N.X.; Khiem, N.V.; Andre, G.; Bouree, F.**

*Effects of magnesium substitution on the magnetic properties of Nd<sub>0.7</sub>Sr<sub>0.3</sub>MnO<sub>3</sub>*  
Journal of Solid State Chemistry 178 (2005) 1203-1211

**Ummarino, G.A.; Daghero, D.; Gonnelli, R.S.; Moudden, A.H.**

*Carbon substitutions in MgB<sub>2</sub> within the two-band Eliashberg theory*  
Physical Review B 71 (2005) 134511

**Vajda, P.; Andre, G.; Udovic, T.J.; Erwin, R.W.; Huang, Q.**

*Magnetic structure of beta-ErD<sub>2</sub>: Long-range and short-range order from powder neutron diffraction*  
Physical Review B 71 (2005) 054419

**Vangeyte P.; Leyh B.; Rojas O.J.; Claesson P.M.; Heinrich M.; Auvray L.; Willet N.; Jerome R.**

*Adsorption of poly(ethylene oxide)-b-poly(is an element of caprolactone) copolymers at the silica-water interface*  
Langmuir 21 (2005) 2930-2940

## PUBLICATIONS

**Vangeyte, P.; Leyh, B.; De Clercq, C.; Auvray, L.; Misselyn-Bauduin, A.M.; Jerome, R.**

*Concomitant adsorption of poly(ethylene oxide)-b-poly(epsilon-caprolactone) copolymers and sodium dodecyl sulfate at the silica-water interface*

Langmuir 21 (2005) 7710-7716

**Vilminot, S.; Richard-Plouet, M.; Andre, G.; Swierczynski, D.; Bouree-Vigneron, F.; Kurmoo, M.**

*Nuclear and magnetic structures and magnetic properties of synthetic brochantite,  $Cu_4(OH)_6SO_4$*

Dalton Transactions 11 (2006) 1455-1462

**Vilminot, S.; Andre, G.; Richard-Plouet, M.; Bouree-Vigneron, F.; Kurmoo, M.**

*Magnetic structure and magnetic properties of synthetic lindgrenite,  $Cu_3(OH)_2(MoO_4)_2$*

Inorganic Chemistry 45 (2006) 10938-10946

**Viret, M.; Gabureac, M.; Ott, F.; Fermon, C.; Barreteau, C.; Autes, G.; Guirado-Lopez, R.**

*Giant anisotropic magneto-resistance in ferromagnetic atomic contacts*

European Physical Journal B 51 (2006) 1-4

**Viret, M.; Vanhaverbeke, A.; Ott, F.; Jacquinet, J.F.**

*Current induced pressure on a tilted magnetic domain wall*

Physical Review B 72 (2005) 140403

**Volovitch, P.; Caley, F.; Baudin, T.; Gerber, P.; Penelle, R.; Rey, C.**

*Monte Carlo modeling of low carbon steel recrystallization: Role of thermo-mechanical treatment and chemical composition*

Materials Science Forum 495-497 (2005) 507-512

**Wang, X.; Mainville, J.; Ludwig, K.; Flament, X.; Finel, A.; Caudron, R.**

*Ordering kinetics in the long-period superlattice alloy  $Cu_{0.79}Pd_{0.21}$*

Physical Review B 72 (2005) 024215

**Wang, F.; Kurbakov, A.; Wang, G.J.; Hu, F.H.; Shen, B.G.; Cheng, Z.H.**

*Strong interplay between structure and magnetism in  $LaFe_{11.5}Co_{0.6}Si_{1.1}$ : A neutron diffraction study*

Physica B 385 (2006) 343-345

**Weigel, C.; Cormier, L.; Galois, L.; Calas, G.; Bowron, D.; Beuneu, B.**

*Determination of  $Fe^{3+}$  sites in a  $NaFeSi_2O_6$  glass by neutron diffraction with isotopic substitution coupled with numerical simulation*

Applied Physics Letters 89 (2006) 141911

**Wierzbowski, K.; Baczmanski, A.; Wawszczak, R.; Tarasiuk, J.; Gerber, P.H.; Bacroix, B.; Lodini, A.**

*Internal stress and stored energy in recrystallized copper*

Archives of Metallurgy and Materials 50 (2005) 201-208

**Wierzbowski, K.; Baczmanski, A.; Wawszczak, R.; Tarasiuk, J.; Gerber, P.H.; Bacroix, B.; Lodini, A.**

*Residual stress and stored energy during recrystallisation in polycrystalline copper*

Journal of Materials Science and Technology 21 (2005) 46-52

**Wierzbowski, K.; Baczmanski, A.; Wronski, S.; Braham, C.; Lodini, A.**

*Tuning of deformation models by residual stress measurements*

Archives of Metallurgy and Materials 50 (2005) 201-208

**Wierzbowski, K.; Wronski, S.; Baczmanski, A.; Wrobel, M.; Braham, C.; Fitzpatrick, M.; Lodini, A.**

*Residual stresses induced by cross-rolling*

Materials Science Forum 524-525 (2006) 63-68

**Winkler, B.; Kahle, A.; Hennion, B.**

*Neutron radiography of rocks and melts*

Physica B 385-86 (2006) 933-934 Part 2

**Yaicle, C.; Frontera, C.; Garcia-Munoz, J. L.; Martin, C.; Maignan, A.; Andre, G.; Bouree, F.; Ritter, C.; Margiolaki, I.**

*Avalanches, irreversibility, and phase separation in Co-substituted  $Pr_{0.50}Ca_{0.50}Mn_{1-x}Co_xO_3$*

Physical Review B 74 (2006) 144406

**Yamazaki, D.; Soyama, K.; Ebisawa, T.; Takeda, M.; Torikai, N.; Tasaki, S.; Matsuoka, H.**

*Resonance spin-echo option on neutron reflectometers for the study of dynamics of surfaces and interfaces*

Physica B 356 (2005) 229-333

**Yusuf, S. M.; De Teresa, J. M.; Algarabel, P. A.; Mukadam, M. D.; Mirebeau, I.; Mignot, J. -M.; Marquina, C.; Ibarra, M. R.**

*Two- and three-dimensional magnetic ordering in the bilayer manganite  $Ca_{2.5}Sr_{0.5}GaMn_2O_8$*

Physical Review B 74 (2006) 184409

**Zanotti, J.M.**

*Vibrations and relaxations in biological molecules. Provisions of inelastic incoherent broadcasting of neutrons*

Journal de Physique IV 130 (2005) 87-113

**Zanotti, J.M.; Bellissent-Funel, M.C.; Chen, S.H.**  
*Experimental evidence of a liquid-liquid transition in interfacial water*  
Europhysics Letters 70 (2005) 91-97

**Zanotti, J.M.; Smith, L.J.; Price, D.L.; Saboungi, M.L.;**  
*Inelastic neutron scattering as a probe of dynamics under confinement. The case of a PEO polymer melt*  
Annales de Chimie - Science des Matériaux 30 (2005) 353-364

**Zanotti, J.M.; Bellissent-Funel, M.C.; Chen, S.H.; Kolesnikov, A.I**  
*Further evidence of a liquid-liquid transition in interfacial water*  
Journal of Physics : Condensed Matter 18 (2006) S2299-S2304

**Zanotti, J.M.; Smith, L.J.; Price, D.L.; Saboungi M.L.**  
*A unified approach to the dynamics of a polymer melt*  
Journal of Physics : Condensed Matter 18 (2006) S2391-S2402

**Zanotti, J. -M.; Herve, G. ; Bellissent-Funel, M. -C.**  
*Picosecond dynamics of T and R forms of aspartate transcarbamylase: A neutron scattering study*  
Biochemica et Biophysica Acta 1764 (2006) 1527-1535

**Zhang, C.H.; Arrighi, V.; Gagliardi, S.; McEwen, IJ.; Tanchawanich, J.; Telling, M.T.F.; Zanotti, J.M.**  
*Quasielastic neutron scattering measurements of fast process and methyl group dynamics in glassy poly(vinyl acetate)*  
Chemical Physics 328 (2006) 53-63

**Zhao, X.; Yu, C.; Cho, Y.-C.; Chabot-Couture, G.; Barisic, N.; Bourges, P.; Kaneko, N.; Li, Y.; Lu, L.; Motoyama, .; Vajk, O.P.; Greven, M.**  
*Crystal growth and characterization of the model high-temperature superconductor  $HgBa_2CuO_{4+\delta}$*   
Advanced Materials 18 (2006) 3243

Dépôt de brevet:

**1. "DéTECTEUR 2-D pour Rayonnement Neutrons."**

P. Baroni & L. Noirez, n°0502379 du 24/03/2005.

**2. "Méthode de détermination des propriétés dynamiques d'un matériau fluide ou solide déformable."**

P. Baroni, H. Mendil & L. Noirez, n°0510988 du 27/11/2005.



